SEDIMENTATION, CLIMATE CHANGE AND TECTONICS: DYNAMIC STRATIGRAPHY OF THE PLIOCENE-PLEISTOCENE PALM SPRING GROUP, FISH CREEK-VALLECITO BASIN, CALIFORNIA

by

THOMAS CHARLES PERYAM

A DISSERTATION

Presented to the Department of Geological Sciences
and the Graduate School of the University of Oregon
in partial fulfillment of the requirements
for the degree of
Doctor of Philosophy

September 2012

DISSERTATION APPROVAL PAGE

Student: Thomas Charles Peryam

Title: Sedimentation, Climate Change and Tectonics: Dynamic Stratigraphy in the Pliocene-Pleistocene Palm Spring Group, Fish Creek-Vallecito Basin, California

This dissertation has been accepted and approved in partial fulfillment of the requirements for the Doctor of Philosophy degree in the Department of Geological Sciences by:

Rebecca Dorsey	Chair
Ilya Bindeman	Member
Gregory Retallack	Member
Patrick Bartlein	Outside Member

and

Kimberly Andrews Espy	Vice President for Research & Innovation/Dean of the Graduate School

Original approval signatures are on file with the University of Oregon Graduate School.

Degree awarded September 2012

DISSERTATION ABSTRACT

Thomas Charles Peryam

Doctor of Philosophy

Department of Geological Sciences

September 2012

Title: Sedimentation, Climate Change and Tectonics: Dynamic Stratigraphy of the Pliocene-Pleistocene Palm Spring Group, Fish Creek-Vallecito Basin, California

In order to better understand the interactions between climate change, landscape erosion and sedimentation, a detailed study was conducted on Plio-Pleistocene non-marine deposits of the Palm Spring Group in the Fish Creek-Vallecito basin, California, USA. Three inter-related studies focused on (1) local response to global climate change in late Pliocene-early Pleistocene time, (2) large-scale evolution of lithofacies architecture, and (3) climate modulation of late Pliocene sediment flux on Milankovitch time scales.

Stable isotopes and paleosol classification reveal that between ~4.0 and 0.75 Ma, aridity increased in the study area concurrent with a shift towards a less intense and more winter-dominated precipitation regime. These changes are interpreted to reflect the long-term waning of summer monsoon precipitation in southern California.

A dramatic and enigmatic reorganization of basin strata occurred at 2.9 Ma. Detailed basin analysis shows that locally-derived sediment was supplied by the predecessors of two modern drainages, Vallecito and Carrizo creeks. Initial progradation of alluvial deposits from these two sources across the Colorado River delta plain began

between 4.0-3.4 Ma. At 2.9 Ma, rapid progradation of these two deposystems was coeval with emplacement of a megabreccia and transgression of Borrego Lake. My data indicate that tectonic realignments at both local and regional scales drove this reorganization.

Time series analysis of rock magnetic data from a densely-sampled stratigraphic section of the lacustrine Tapiado Formation reveals that between 2.9 and ~2.75 Ma landscape denudation in the Carrizo Creek catchment was partly modulated by orbital obliquity. Peaks in landscape denudation implied by my data correspond to obliquity highs. More frequent high intensity precipitation events (i.e. monsoons and tropical storms) probably drove increased erosion during these time periods relative to obliquity lows. The breakdown of this relationship at around 2.75 Ma corresponds to a dramatic increase in northern hemisphere glaciation and may reveal a reduction in monsoonal influence in southern California.

A geologic map of the Fish Creek-Vallecito basin is included as a supplemental file to this dissertation.

This dissertation contains previously published and unpublished coauthored material.

CURRICULUM VITAE

NAME OF AUTHOR: Thomas Charles Peryam

GRADUATE AND UNDERGRADUATE SCHOOLS ATTENDED:

University of Oregon, Eugene
New Mexico State University, Las Cruces

DEGREES AWARDED:

Doctor of Philosopy, 2012, University of Oregon
Master of Science, 2006, New Mexico State University
Bachelor of Science, 2004, University of Oregon

AREAS OF SPECIAL INTEREST:

Influence of Global Climate Change on Sedimentary Basins
Stratigraphic Record of Tectonism

PROFESSIONAL EXPERIENCE:

Geoscience Intern, Devon Energy, Western Division, Oklahoma City, Oklahoma 2011

Geoscience Intern, Devon Energy, Southern Division, Houston, Texas, 2010

GRANTS, AWARDS, AND HONORS:

Graduate Student Research Grant, Geological Society of America, 2008

Baldwin Fellowship, University of Oregon Department of Geological Sciences, 2007

PUBLICATIONS:

Dorsey, R.J., Axen, G., Peryam, T.C., 2012, Initiation of the Southern Elsinore Fault at ~1.2 Ma: Evidence from the Fish Creek - Vallecito Basin, southern California: Tectonics, v. 31, doi:10.1029/2011TC003009.

Peryam, T.C., Lawton, T.F., Amato, J.M., González-León, C.M., and Mauel, D.J., 2012, Lower Cretaceous strata of the Sonora Bisbee basin: a record of the tectonomagmatic evolution of northwestern Mexico: Geological Society of America Bulletin, doi:10.1130/B30456.1.

Peryam, T.C., Dorsey, R.J., and Bindeman, I., 2011, Plio-Pleistocene climate change and timing of Peninsular Ranges uplift in southern California: evidence from paleosols and stable isotopes in the Fish Creek-Vallecito basin: Palaeogeography, Palaeoclimatology, Palaeoecology, v. 305, no. 1-4, p. 65-74. doi:10.1016/j.palaeo.2011.02.014.

ACKNOWLEDGMENTS

I wish to thank Rebecca Dorsey for her enthusiastic support through all the stages of this research. I wish to express sincere appreciation to Pat Bartlein, Ilya Bindeman and Greg Retallack for their service on my committee and the many helpful conversations which helped in crafting this manuscript. In addition, special thanks are due to my collaborators and sometime co-authors Max Bezada of the University of Oregon, Bernie Housen, Russ Burmester, and Chris Deboer at Western Washington University, and Kim Blisniuk, Nicole Longinotti, and Mike Oskin at the University of California, Davis. Logistical support and discussions with George Jefferson were essential to completing this work. Many people provided valuable reviews and discussions of this work including Mike Darin, Todd Lamaskin, Paul Heller, Gene Humphreys, Leland O'Driscoll, Jay Quade, Josh Roering and an anonymous reviewer.

Molly Keogh assisted with collection of voluminous stratigraphic data. Field assistance was also provided by volunteers from the Anza-Borrego Desert State Park Paleontology Society. Jim Palandri and Kathryn Watts provided laboratory assistance. Unparalleled hospitality was provided by Karen and Burnie Burnworth, Eric Mustonen and Jim and Judy Smith. The investigation was supported in part by Geological Society of America Graduate Student Research Grant 8750-08 to me, National Science Foundation grants EAR-0838119 and EAR-0711293 to R.J. Dorsey and EAR-0844772 to I. Bindeman.

Gratitude will always be felt towards all of my family and the support they have provided.

For Marilee, with love.

TABLE OF CONTENTS

Chapter Page

Chapter Page

Chapter Page

LIST OF FIGURES

Figure Page

Figure Page

LIST OF TABLES

Table Page

CHAPTER I

INTRODUCTION

A major focus of contemporary Earth science research is the study of how environmental perturbations affect surficial processes. This involves coming to understand the complex interactions between climate, ecology, landscape evolution and sedimentary basins. Surface processes dictate not only the physical appearance of a landscape, but also directly control the location of arable land, distribution and quality of reservoirs in sedimentary basins, and the sites of potential natural hazards. Deconvolving the impact of climate change on surficial processes, then, is crucially important to society, particularly in light of projected future climate changes.

The Palm Spring Group in the Fish Creek-Vallecito basin, southern California, USA, contains a high-resolution record of continuous non-marine sedimentation between 4.2 and ~1.0 Ma. This unit was deposited during a period of dramatic global climate change, when Pliocene warmth gave way to global cooling and orbitally-modulated periods of glaciation and deglaciation in the northern hemisphere during late Pliocene and Pleistocene time. Excellent surface exposure of this unit makes it a superb natural laboratory for investigating complex feedbacks between global climate change, tectonics and local surficial processes.

In order to understand the impact of global climate change on local landscapes, it is necessary to understand how the local climate of the study area responded to global climate forcing during Plio-Pleistocene time. For this reason, Chapter II documents an investigation of abundant paleosols exposed in the Palm Spring Group. Qualitative analysis of paleosol characteristics and quantitative study of stable isotopes of pedogenic

carbonate nodules provide a record of long-term aridification and decrease in high-intensity summer precipitation the study area. The local climate during middle Pliocene time was significantly more moist than modern hyper-aridity and also experienced more abundant summer monsoonal precipitation. A combination of northward tectonic transport of the study area along and the end of near-permanent middle Pliocene El Niño conditions in the eastern Pacific Ocean resulted in a decrease in summer monsoonal precipitation, a shift to a coole growing season, and long-term aridification. Chapter II was published in the journal *Palaeogeography, Palaeoclimatology, Palaeoecology* in February, 2011, volume 305, page 65-74, and co-authored with Rebecca Dorsey and Ilya Bindeman.

Chapter III documents and interprets a major reorganization of stratigraphic architecture in the Fish Creek-Vallecito basin. This reorganization involved abrupt progradation of locally-derived coarse sediment and simultaneous transgression of a regionally-extensive lake at 2.9 Ma. Simultaneous sediment progradation and lacustrine transgression defies explanation using existing models of stratigraphic evolution in tectonically-controlled basins. The possibility that late Pliocene climate-driven increases in erosion rate and sediment flux may have played a part in this enigmatic basin reorganization led me to investigate the timing and nature of this event. In Chapter III I present a detailed basin analysis of the Palm Spring Group in which I subdivide and date the unit using new magnetostratigraphic data, define sediment source areas, and map lithofacies distribution. I conclude that abrupt basin reorganization at 2.9 Ma was driven by tectonism at both local and regional scales, and that global climate change had no

discernible effect at the basin scale. Chapter III was coauthored with Rebecca Dorsey, Chris DeBoer and Bernie Housen.

Having established the primacy of tectonic over climatic controls on the basin-scale architecture of the Fish Creek-Vallecito basin, Chapter IV presents a more focused investigation of climatic controls on landscape evolution. I present a detailed magnetic susceptibility record from a stratigraphic interval in the lower part of the Tapiado Formation, which records lacustrine deposition between 2.9 and ~2.52. Rock magnetic analysis indicates that magnetic susceptibility in the Tapiado Formation is provided primarily by magnetite derived from local catchments, and that magnetic susceptibility fluctuations therefore record relative variation in the rate of catchment erosion and sediment flux. Frequency analysis of magnetic susceptibility data indicate that, between 2.9 and ~2.75 Ma, erosion in one local catchment (Carrizo Creek) was modulated by climate fluctuations driven by ca. 41 k.y. orbital obliquity cycles. This finding represents one of the first well documented linkages between global climate cyclicity and erosion rates, and has implications for understanding both hypothesized global landscape response to climate change and local paleoclimate reconstructions. Chapter IV was coauthored with Max Bezada, Rebecca Dorsey, Russ Burmester and Bernie Housen.

CHAPTER II

PLIO-PLEISTOCENE CLIMATE CHANGE AND TIMING OF PENINSULAR RANGES UPLIFT IN SOUTHERN CALIFORNIA: EVIDENCE FROM PALEOSOLS AND STABLE ISOTOPES IN THE FISH CREEK-VALLECITO BASIN

This work was published in volume 305 of the journal 'Palaeogeography, Palaeoclimatology, Palaeoecology," in February, 2011. This paper is co-authored with Rebecca Dorsey, who provided funding and advisorial help. Stable-isotope analysis was conducted in the laboratory and under the supervision of Dr. Bindeman, who also provided editorial support.

1. Introduction

One of the most recent large climate changes in Earth's history took place during Pliocene to Pleistocene time, when early Pliocene warmth was replaced by a cooler and strongly variable late Pliocene to Pleistocene climate regime marked by the onset of Northern Hemisphere glaciation (e.g., Haug et al., 2001; Zachos et al., 2001; Haug et al., 2005; Ravelo et al., 2004; Lisiecki and Raymo, 2005). The Pliocene warm period is the most recent period of sustained global warmth and is considered a potential analogue for future climate (IPCC, 2007). Thus studies of Plio-Pleistocene climate change and its effects on local weather patterns can provide useful insights that aid in predicting future climate change. Despite previous work that reconstructed Late Tertiary climate change in

the western U.S. (Smith, 1984; Smith et al., 1993), there is little information about this period due to poor exposure and limited age controls in Plio-Pleistocene deposits.

Paleosols exposed in deposits of the Fish Creek-Vallecito Basin of southern California provide a unique terrestrial record of continental climate conditions during the transition from early Pliocene warmth to Plio-Pleistocene glaciation. There, a 5.5 km thick Miocene to Pleistocene sedimentary section has been uplifted, tilted and exposed as a result of motion on young strike-slip faults (Dorsey et al., 2011). Rapid sedimentation and recently-published magnetostratigraphic dating enable high-resolution age determination of abundant paleosol horizons. Useful paleoclimatic and paleoecological information can be extracted from paleosol characteristics and stable isotope values of pedogenic carbonate (e.g., Cerling, 1984; Cerling et al., 1989; Quade et al., 1995). An abundance of vertebrate and invertebrate fossils has drawn researchers to the Fish Creek-Vallecito basin for over a century (e.g., Vaughan, 1904; Marrs, 2006), but until now there has been no detailed study of the climate proxies preserved in the paleosols of this area.

The Peninsular Ranges of southern California form the faulted western margin of the Salton Trough and currently produce a strong rain shadow affecting the Salton Trough lowlands and Imperial Valley (Fig. 2.1a; Minnich et al., 2000; Cerezo-Mota et al., 2006.). Understanding the evolution of this mountain range is important for reconstructing both Plio-Pleistocene climate change and the history of the Pacific-North America plate boundary. Recent work suggests that lower crustal or upper mantle processes may contribute to high topography in the Peninsular Ranges (Yang and Forsyth, 2006; Mueller et al., 2009), yet the timing of uplift is not known.

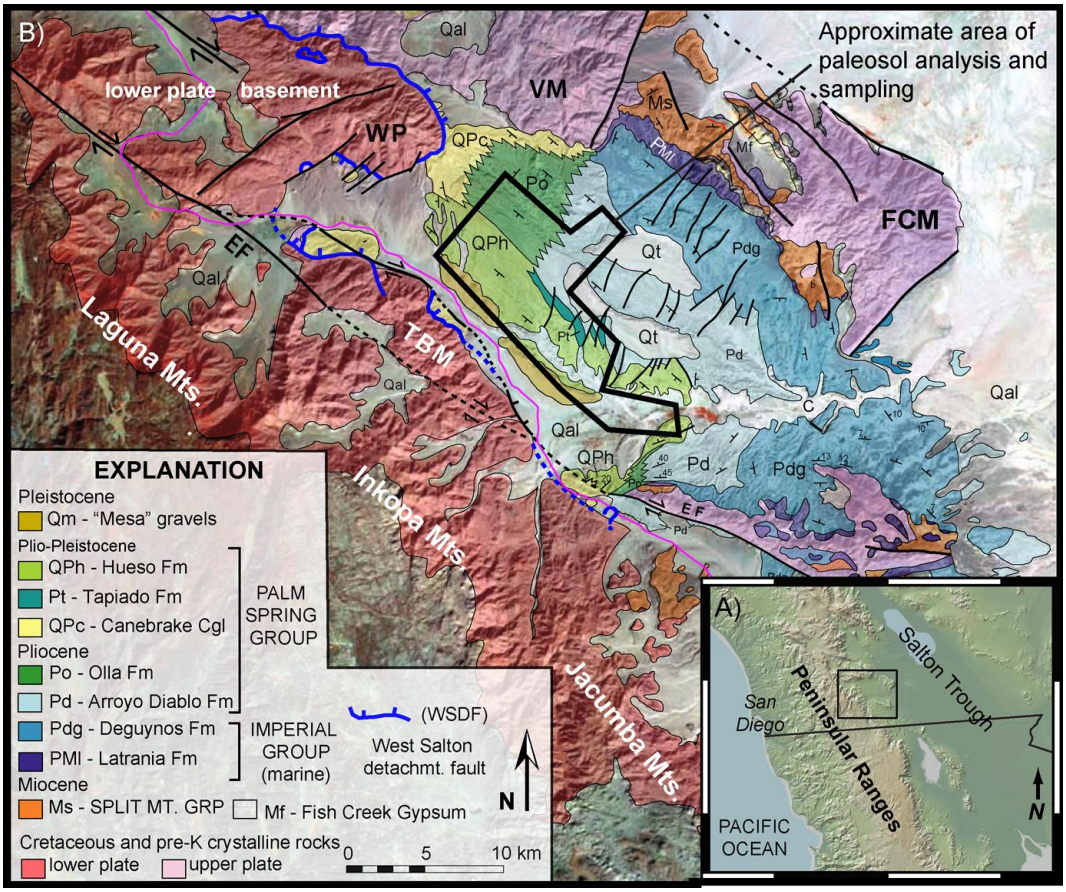

Figure 2.1: A (inset) Shaded color relief map of southern California and NW Mexico showing location of map B. B) Geologic map of the Fish Creek-Vallecito Basin and surrounding area. Southwest-dipping Plio-Pleistocene strata which are the focus of this study are well exposed in badlands in Anza-Borrego Desert State Park, California. Polygon shows approximate area of paleosol analysis and sampling. Modified from Dorsey et al. (2011).

This paper presents an integrated study of proxies used to interpret changes in Pliocene to Pleistocene paleoclimate. We use paleosol data and stable-isotope analyses from a well-exposed stratigraphic section to document changes in soil moisture regime and soil carbonate composition through time. We then compare this record to a previous paleoclimate study in the same section, and use these data to test hypotheses for the timing of Peninsular Ranges uplift and global climatic controls on evolution of local climate patterns in southern California.

2. Background

The Fish Creek-Vallecito basin contains a well-exposed stratigraphic record of late Miocene to early Pleistocene sedimentation along the obliquely diverging Pacific-North American plate boundary. Deposits of the Fish Creek-Vallecito basin accumulated in a supradetachment basin in the hanging wall of the West Salton detachment fault (Fig. 2.1b; Axen and Fletcher, 1998). A major tectonic reorganization at 1.3-1.0 Ma terminated slip on the detachment fault, initiated the San Felipe, San Jacinto and Elsinore strike-slip faults, and initiated uplift and erosion of basinal deposits (Lutz et al., 2006; Kirby et al., 2007; Steely et al., 2009). In the present-day Fish Creek-Vallecito basin a thick section (>5 km) of strata is well exposed in southwest-dipping beds along a series of dry washes and badlands.

A rich fossil record in the Fish Creek-Vallecito basin has provided evidence of large-magnitude climatic shifts in the region since mid-Pliocene time. The study area presently lies along the western margin of the Colorado Desert and averages 8-15 cm of precipitation annually. The flora of the study area in the modern interglacial period is dominated by creosote bush, saltbush and cactus scrub (Schoenherr and Burk, 2007). During Late Pleistocene glacial periods, the region had widespread Juniper scrub (Van Devender, 1990). These xeric floras are in contrast to fossil floral assemblages from the Pliocene Arroyo Diablo Formation that contain abundant hardwoods, palms and conifers, suggesting a wet and temperate climate in mid-Pliocene time with rainfall of 38-62 cm (Remeika, 2006). Plant fossils are absent in the Plio-Pleistocene deposits of the Tapiado and Hueso formations (Fig. 2.2), but faunal evidence suggests a shift to a cooler

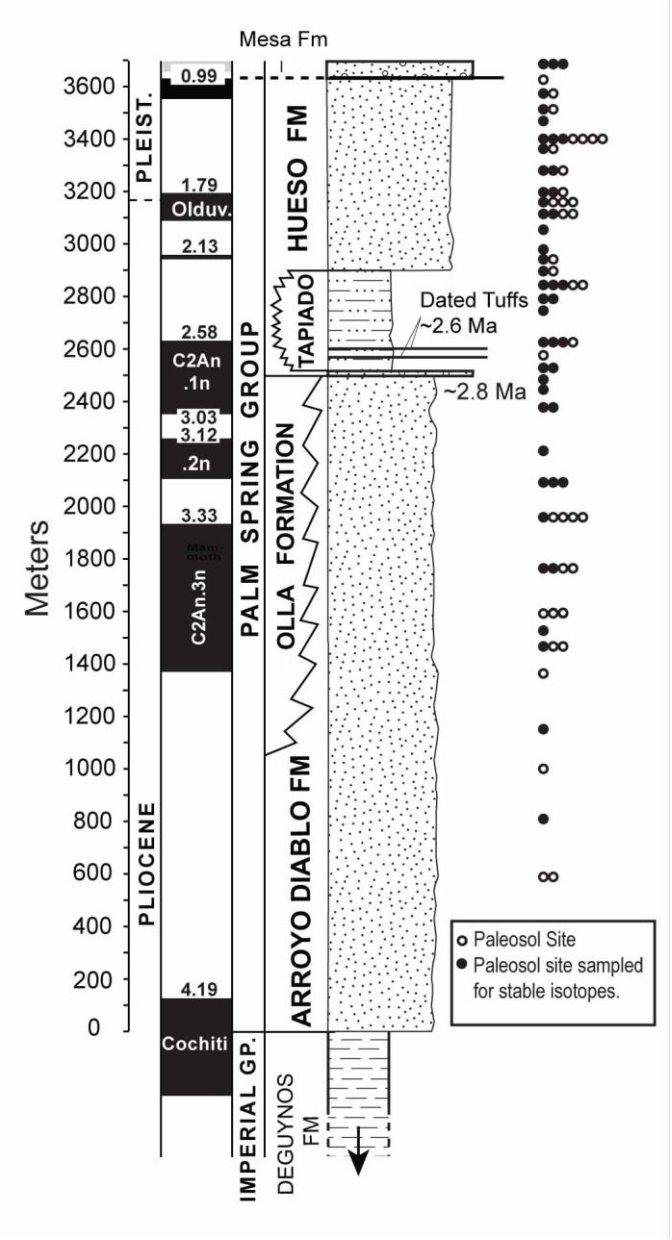

Figure 2.2: Generalized stratigraphic column of the Palm Spring Group in the Fish Creek-Vallecito Basin, modified from Dorsey et al. (2011), showing approximate stratigraphic position of paleosols analyzed for this study.

but still wet environment during late Pliocene to early Pleistocene time (Howard, 1963; Cassiliano, 1994; Jolly, 2000; Gensler et al., 2006; White et al., 2006). In contrast, ostracode assemblages from lacustrine deposits in the Tapiado Formation suggest that the

region was warm with tropically influenced precipitation throughout most of the late Pliocene, with an increase in aridity circa 2.0 Ma (Cosma, 2002a). Brogenski (2001) interpreted enrichment in $\delta^{18}O$ in fossil horse teeth at circa 2.3 Ma to record a change from a cool and wet climate to one that was warmer and drier, possibly due to increased Pacific Ocean upwelling along the coast of California (Brogenski, 2001; Spero et al., 2003).

In addition to uncertainty about paleoclimate evolution, the timing of uplift in the Peninsular Ranges uplift is not well understood. The current configuration of the Peninsular Ranges as a topographic boundary must post-date Eocene deposition of the Sonora-derived Poway Conglomerate along coastal California (Abbot and Smith, 1989). Late Miocene initiation of the West Salton detachment fault likely resulted in uplift of the footwall, including the Peninsular Ranges (Axen and Fletcher, 1998). Recent work indicates that high topography in the Peninsular Ranges is not supported by a crustal root (Lewis et al., 2000; 2001), and is instead supported by mantle buoyancy due to either delamination of the lower crust (Yang and Forsyth, 2006) or removal of the mantle lithosphere beneath the area (Mueller et al., 2009). Mueller et al. (2009) suggested that at least some Peninsular Ranges uplift is Quaternary in age, based on modeling of uplifted marine terraces along the Pacific Coast. Cosma (2002b) interpreted changes in lacustrine ostracodes in the Fish Creek-Vallecito basin to suggest that uplift of the Peninsular Ranges and concurrent rain shadow enhancement was ongoing throughout Pliocene time, and that the range achieved something close to its current elevation by 2 Ma.

3. Approach

This paper presents and analyses three data sets: (1) paleosol morphology, (2) carbon isotopes and (3) oxygen isotopes from pedogenic carbonate. The paleoclimatic evolution of the study area is evaluated using all three of these data sets. In addition, we use oxygen isotope data to test hypotheses for Plio-Pleistocene uplift of the Peninsular Ranges and production of a rain shadow during this time.

Paleosols provide useful proxies for paleoclimatic conditions. Soil characteristics such as horizon types, stage of soil development and type of ped structures reveal significant information about the climate, precipitation and vegetation regime in which paleosols formed (e.g., Mack, 1994; Retallack, 1999; Retallack, 2005; Sheldon and Tabor, 2009). Paleosol investigations are made even more powerful when they are incorporated into larger paleoclimatic investigations (e.g., Quade et al., 1995; Kleinert and Strecker, 2001).

Pedogenic carbonate preserves useful paleoecological information, as it precipitates in equilibrium with soil CO_2, which is itself a product of decaying vegetative material and diffusive exchange with the atmosphere (Cerling, 1984; Cerling et al., 1989; Quade et al., 1989; Fox and Koch, 2003). Trees, shrubs and cool-season grasses utilize the C3 photosynthetic pathway and had an average, preindustrial $\delta^{13}C$ value of -25.5‰ VPDB (Fox and Koch, 2003). In relatively arid habitats (<1000 mm mean annual precipitation) C3 organic matter can be less negative, with an average $\delta^{13}C$ value of -24.6‰ VPDB (Fox and Koch, 2003). Grasses that require a warm growing season generally utilize the C4 photosynthetic pathway and had a mean, preindustrial $\delta^{13}C$ value of -11.5‰. In the late Pliocene/Early Pleistocene time period of this study, atmospheric

$\delta^{13}C$ for the late Pliocene/early Pleistocene did not vary more than +/- .25‰ from the preindustrial value of -6.5‰ (Tipple et al., 2010), and thus the C3/C4 end-member values presented by Fox and Koch (2003) are used when discussing paleoecological interpretations. CAM (crasulacean acid metabolism) plants include many desert succulents, and have a $\delta^{13}C$ value intermediate between C3 and C4 plants (Farquhar et al., 1989). Diffusion kinetic effects and fractionation during calcite precipitation enrich soil carbonate by 14-17‰, but the difference in values between C3 and C4 biotas is preserved. Pedogenic carbonate in soils dominated by C4 grasses therefore has a $\delta^{13}C$ of around +2‰, while carbonate in soils dominated by C3 plants has a typical $\delta^{13}C$ of -12 to -9‰, with lighter values typical of more arid environments (Cerling, 1984; Cerling et al., 1989; Fox and Koch, 2003).

Oxygen isotopes in pedogenic carbonate provide a valuable tool for detecting ancient tectonic uplifts due to their tendency to record the effects of orographic rain shadows. Oxygen isotopes in pedogenic carbonate are well correlated with the isotopic composition of local precipitation, despite differences in temperature and pedogenic processes of carbonate formation (Cerling, 1984; Cerling and Quade, 1993). Pedogenic carbonate has been used by numerous workers to detect the timing and extent of ancient orographic events, since atmospheric water vapor becomes depleted in ^{18}O as it passes over mountain ranges (Cerling et al., 1989; Chamberlain and Poage, 2000; Kent-Corson et al., 2006; Kleinert and Strecker, 2001; Quade et al., 2007). This orographic fractionation is reflected both in soils formed at elevation and in soils formed in lee-side sedimentary basins.

The Fish Creek-Vallecito basin, located on the leeward side of the Peninsular Ranges, presently lies in a hyper-arid orographic rain shadow (mean annual precipitation = 10-15 cm). Complications related to below-cloud-base evaporation and/or mixing of water vapor sources can obscure the isotopic record of an orographic rain shadow, especially in arid environments (Blisniuk and Stern, 2005). Most modern precipitation in the study area comes from winter storms originating in the Pacific Ocean (Woodhouse, 1997; Minnich, 2000). The Peninsular Ranges are oriented perpendicular to winds carrying this water vapor, and thus are a potential source of an isotopic rain shadow (Blisniuk and Stern, 2005). There is a paucity of data on the isotopic composition of meteoric precipitation in the western Salton Trough, but water vapor passing over the Peninsular Ranges is known to be isotopically depleted due to orographic effects, and groundwater in the Imperial Valley shows depleted $\delta^{18}O$ values, although these values are complicated by irrigation with water from the Colorado River (Williams and Rodoni, 1997). If significant uplift of the Peninsular Ranges occurred during late Pliocene to early Pleistocene time, the resultant creation or enhancement of a rain shadow could be reflected in $\delta^{18}O$ values from pedogenic carbonate analyzed in this study.

4. Methods

A total of 82 paleosols were surveyed in the upper non-marine ~3.2 km of the stratigraphic section in the Fish Creek-Vallecito basin (Fig. 2.2). Paleosols ages were assigned using the results of a new, high-resolution magnetostratigraphic study (Dorsey et al., 2011). Ages of each isotopic sample site are shown in Table 2.1, and the ages of each described paleosol are listed in Appendix A. Field mapping and satellite photos were used to project individual sites into the stratigraphic section of Dorsey et al. (2011),

Table 2.1. Age and isotopic value of pedogenic carbonate samples

				UTM (NAD 83)						UTM (NAD 83)	
Sample	Age (Ma)	δ13C ‰	δ18O ‰	Northing	Easting	Sample	Age (Ma)	δ13C ‰	δ18O ‰	Northing	Easting
P09-AB-35	0.70 ± 0.25	-4.77 ± 0.04	-8.43 ± 0.08	576493	3637260	P09-AB-29	2.32 ± 0.03	-7.16 ± 0.05	-9.19 ± 0.07	572418	3645994
P08-AB-23	0.70 ± 0.25	-5.27 ± 0.13	-8.6 ± 0.13	569852	3645422	P09-AB-25	2.34 ± 0.02	-6.52 ± 0.09	-8.87 ± 0.09	572995	3645404
P08-AB-22b	0.70 ± 0.25	-6.74 ± 0.14	-8.34 ± 0.24	569749	3645364	P08-AB-7	2.39 ± 0.02	-6.2 ± 0.13	-9.15 ± 0.27	572797	3645966
P08-AB-19	1.10 ± 0.06	-3.65 ± 0.06*	-8.24 ± 0.07*	571549	3643778	P09-AB-12	2.61 ± 0.1	-8.42 ± 0.07	-9.66 ± 0.12	572626	3646605
P08-AB-18	1.21 ± 0.07	-6.03 ± 0.12	-8.92 ± 0.11	571644	3644022	P09-AB-11	2.62 ± 0.1	-7.15 ± 0.15	-9.03 ± 0.06	572580	3646685
P08-AB-25	1.27 ± 0.06	-6.37 ± 0.08	-8.69 ± 0.069	571586	3644233	P08-AB-6	2.62 ± 0.1	-10.4 ± 0.12	-12.35 ± 0.15	572580	3646685
P08-AB-17	1.42 ± 0.05	-7.27 ± 0.13	-10.73 ± 0.25	571920	3644180	P08-AB-5	2.76 ± 0.07	-5.6 ± 0.11	-10.61 ± 0.13	572614	3646874
P09-AB-13	1.43 ± 0.06	-6.39 ± 0.06	-8.57 ± 0.08	571897	3644397	P09-AB-22	2.80 ± 0.2	-5.7 ± 0.1	-8.31 ± 0.11	577710	3641466
P09-AB-14	1.46 ± 0.06	-2.38 ± 0.04	-8.71 ± 0.08	571785	3644605	P09-AB-9	2.85 ± 0.04	-4.35 ± 0.1	-9.8 ± 0.23	572629	3647017
P08-AB-15	1.50 ± 0.05	-4.68 ± 0.13	-9.33 ± 0.29	571959	3644440	P09-AB-41	2.90 ± 0.1	-4.79 ± 0.07	-8.51 ± 0.11	578324	3640106
P08-AB-16	1.68 ± 0.05	-3.46 ± 0.12*	-9.84 ± 0.13*	572034	3644696	P09-AB-23	3.00 ± 0.2	-8.35 ± 0.11	-9.54 ± 0.05	578194	3640979
P09-AB-42	1.69 ± 0.04	-6.25 ± 0.07	-8.86 ± 0.11	573375	3643289	P09-AB-20	3.00 ± 0.2	-7.01 ± 0.05	-8.73 ± 0.04	582077	3635946
P08-AB-13	1.79 ± 0.03	-7.99 ± 0.13	-10.68 ± 0.16	572768	3644227	P08-AB-31	3.18 ± 0.06	-3.27 ± 0.07*	-9.6 ± 0.9*	573630	3646976
P09-AB-38	1.80 ± 0.03	-6.9 ± 0.06	-9.22 ± 0.06	573501	3643351	P08-AB-4	3.23 ± 0.05	-5.03 ± 0.09	-10.3 ± 0.15	573029	3647519
P08-AB-14	1.84 ± 0.03	-6.77 ± 0.1	-9.55 ± 0.21	572048	3644953	P09-AB-6	3.25 ± 0.03	-5.19 ± 0.07	-8.72 ± 0.1	572859	3647816
P08-AB-12	1.92 ± 0.06	-7.4 ± 0.08	-7.96 ± 0.13	573178	3644118	P09-AB-7	3.25 ± 0.03	-4.96 ± 0.07	-8.53 ± 0.11	572859	3647816
P08-AB-11	1.94 ± 0.03	-4.08 ± 0.1	-9.37 ± 0.02	573660	3643494	P09-AB-31	3.30 ± 0.01	-9.33 ± 0.08	-9.84 ± 0.07	572287	364883
P09-AB-32	2.03 ± 0.04	-8.94 ± 0.12	-9.75 ± 0.1	570453	3647406	P09-AB-37	3.40 ± 0.15	-4.11 ± 0.05	-9.37 ± 0.1	572195	3649457
P09-AB-34	2.11 ± 0.09	-7.11 ± 0.1	-8.47 ± 0.05	574750	3642488	P08-AB-3	3.41 ± 0.01	-9.04 ± 0.13*	-10.19 ± 0.16*	573266	3648186
P09-AB-28	2.15 ± 0.04	-9.03 ± 0.07	-9.89 ± 0.12	572446	3645522	P08-AB-28	3.53 ± 0.01	-6.14 ± 0.14	-10.39 ± 0.26	573613	3648535
P09-AB-33	2.19 ± 0.06	-6 ± 0.09	-8.41 ± 0.06	575075	3642367	P09-AB-39	3.55 ± 0.15	-7.2 ± 0.11	-9.94 ± 0.07	570253	3651313
P08-AB-9	2.25 ± 0.04	-8.07 ± 0.1	-10.16 ± 0.26	572616	3645624	P08-AB-26	3.70 ± 0.01	-4.23 ± 0.1	-11.02 ± 0.13	574286	3649029
P09-AB-26	2.28 ± 0.04	-5.25 ± 0.07	-7.98 ± 0.07	572570	3645740	P09-AB-40	3.83 ± 0.01	-2.78 ± 0.07	-10.48 ± 0.08	576716	3647197
P09-AB-27	2.28 ± 0.04	-6.91 ± 0.12	-8.03 ± 0.09	572570	3645740	*Isotope value averaged from multiple analyses of the same sample					

and site ages were calculated using the stratigraphic height above or below a magnetic reversal divided by the sediment accumulation rate in that part of the section. Sites situated in poorly constrained magnetic chrons or further from the paleomagnetic sampling transect are assigned higher age uncertainties than paleosols within well-constrained chrons and/or co-located with the paleomagnetic transect. The average uncertainty of sampled paleosols dated with this method is +/- 0.06 m.y. Paleosols separated from the magnetostratigraphic section by faults cannot be dated using this method and were assigned ages through stratigraphic inference with a much larger uncertainty (usually +/- 0.1-0.2 m.y.). The average sample age uncertainty for the entire dataset is +/- 0.07 m.y.

Pedogenic carbonate nodules were collected from the carbonate-accumulation (Bk) horizon of 47 paleosols. The Bk horizon is defined as the interval in which nodules or other forms of carbonate dominate the fabric of the soil profile (Soil Survey Staff, 1999). Sampled nodules range in size from 0.5 cm to 3 cm in diameter. Nodules that contain more than 5% sparry calcite as seen in thin section were not included in this study due to probable recrystallization and diagenetic contamination of isotope values. Nodules were cleaned, crushed, weighed and loaded into beakers. Beakers were flushed with helium gas in a Gasbench and then dissolved in phosphoric acid. The resulting carbon dioxide was analyzed in a MAT253 mass spectrometer at the University of Oregon Stable Isotope Lab, along with the NBS-19 carbonate standard ($\delta^{13}C$ = 1.95‰ and $\delta^{18}O$ = -2.2‰). Stable isotope ratios are reported relative to the Vienna PeeDee Belemnite (VPDB) scale. Analytical errors in Table 2.1 are reported as two standard deviations of repeated measurements of the same gas. The mean sample uncertainties are ±0.09‰ for

$\delta^{13}C$, and ±0.12‰ for $\delta^{18}O$. In order to test for reproducibility, a subset of five nodules were subsampled and analyzed separately. The resulting values showed an average range of 0.26‰ for $\delta^{13}C$ and 0.44‰ for $\delta^{18}O$ (Appendix B), far smaller than the overall range of isotope ratios in those two systems. These multiple analyses are reported as averaged values and are marked with an asterisk in Table 2.1.

5. Results

5.1. Paleosols

Paleosols in the Fish Creek-Vallecito basin are divided into two primary populations: vertic and calcic. Vertic paleosols are found exclusively in deposits older than 2.8 Ma whereas calcic paleosols are found throughout the studied section (Fig. 2.3). Vertic paleosols are the dominant paleosol type in deposits between 4.0 and 3.0 Ma and decrease in abundance over time before vanishing from the stratigraphic record at about 2.8 Ma (Fig. 2.3). Calcic paleosols are nearly the only paleosol type present in strata younger than 2.8 Ma.

Vertic paleosols contain many features produced by shrinking and swelling of clay minerals during soil formation. Vertic paleosols in the studied section exhibit deeply-penetrating soil cracks, lenticular to angular peds with clay cutans, and well-developed slickensides (Fig. 2.4). Vertic paleosols in this section are relatively thin (<1 m thick) and lack some of the features commonly associated with true Vertisols, such as gilgai microrelief (Dudal and Eswaran, 1988; Soil Survey Staff, 1999), and are best understood as Vertic Inceptisols rather than true Vertisols. Variations of vertic paleosols include clayey paleosols with slickensides and angular peds but no soil cracks, as well as clayey cracked paleosols with a surface gleyed horizon. Dispersed, thin (3-7 cm thick) zones of

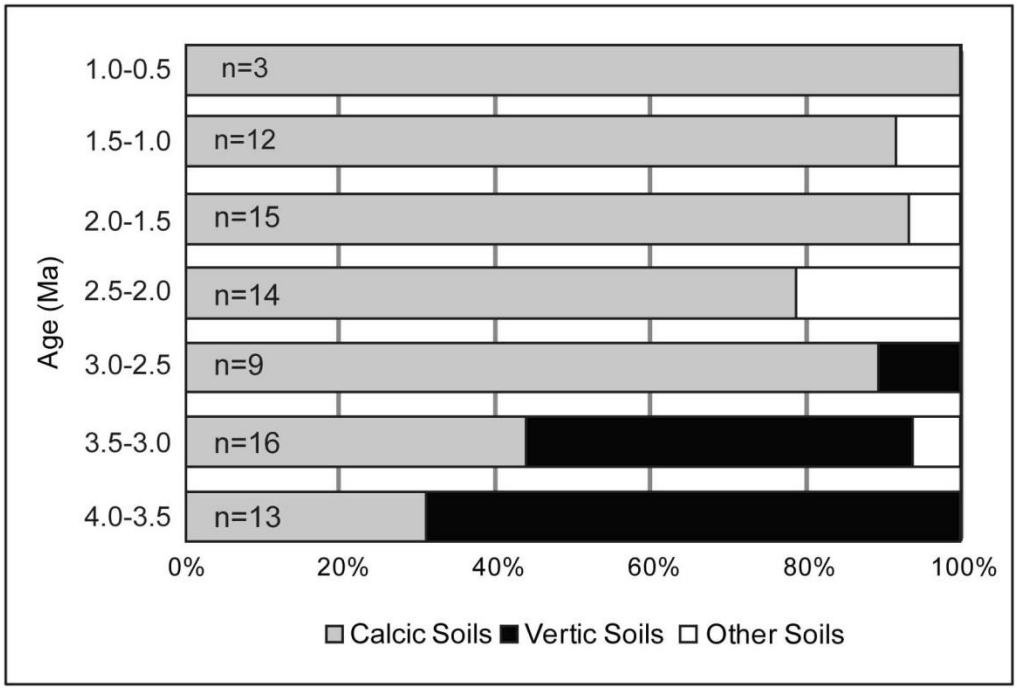

Figure 2.3: Relative abundance of paleosol types as a function of age, grouped into 0.5-m.y. bins. Vertic soils, which are dominant in the interval 4.0 to 3.0 Ma, decrease in abundance before disappearing from the stratigraphic record by about 2.8 Ma.

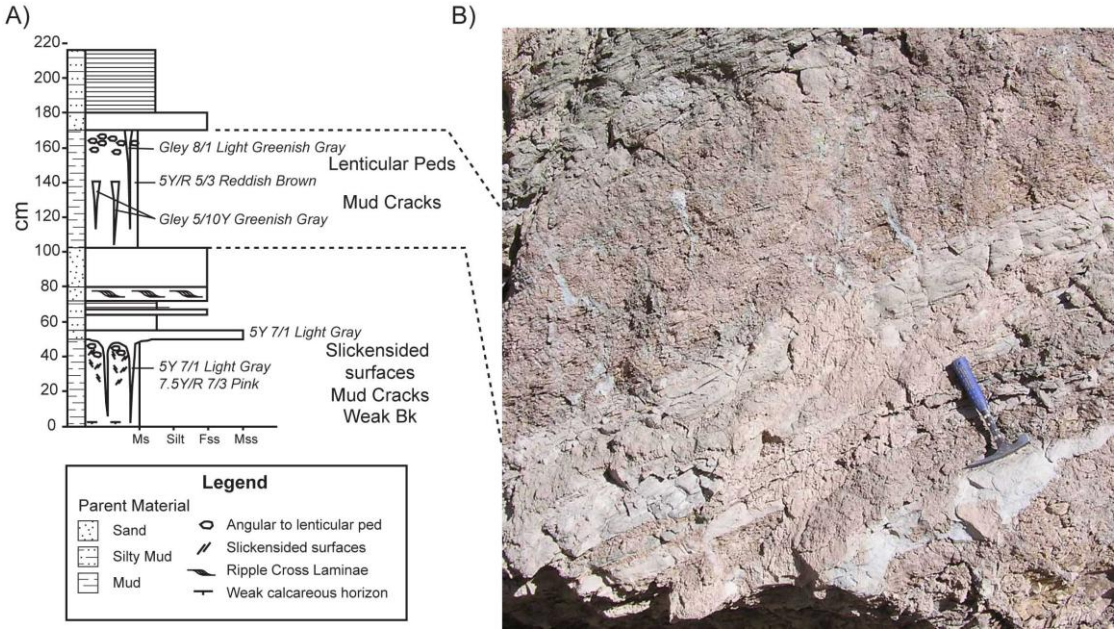

Figure 2.4: A) Soil profile of two representative vertic paleosols in the Arroyo Diablo Formation showing deep mud cracks. B) Photograph of the upper vertic paleosol in A. Paleosols in this group are interpreted as Vertic Inceptisols.

calcite enrichment are present near the base of some vertic paleosols (Fig. 2.4). These horizons may represent very weakly-developed soil carbonate (Bk) horizons (Stage I of Machette, 1985), although their very thin nature suggests that the calcite enrichment may be non-pedogenic. Calcite from these zones was not included in the stable isotope analyses.

Calcic paleosols are characterized by the presence of a prominent Bk horizon (Fig. 2.5). Calcic paleosols in the Fish Creek-Vallecito basin have thin to non-existent A horizons and shallow Bk horizons. Some A horizons contain visible root traces and small, 1-2 cm diameter burrows. Bk horizons range from a very faint horizon of calcite enrichment to a well-developed zone of intergrown pedogenic carbonate nodules (stage I to stage III calcic soils of Machette (1985), with most calcic paleosols exhibiting 0.5-4 cm diameter carbonate nodules in a non-calcareous matrix (stage II calcic soils). Carbonate nodules have displacive, calciasepic fabrics and range from orthic to disorthic (e.g., Wieder and Yaalon, 1974). Framework grains are present in nodules to varying degrees, with embayed quartz grains most common. Feldspar and biotite are present within nodules, and are more pervasively replaced than quartz. Evidence for scouring and erosion of surface horizons is common in calcic paleosols, and in some cases all material overlying the Bk has been removed prior to deposition of overlying sediment. In other paleosols, multiple Bk horizons overlie each other due to soil overprinting (Fig. 2.5a). In the small subset of paleosols (n=19) where depth to the Bk horizon can be measured with confidence Bk horizons are typically shallow, with an average undecompacted depth of 31 cm (Fig. 2.6). Most calcic paleosols lack identifiable peds, although poorly-developed

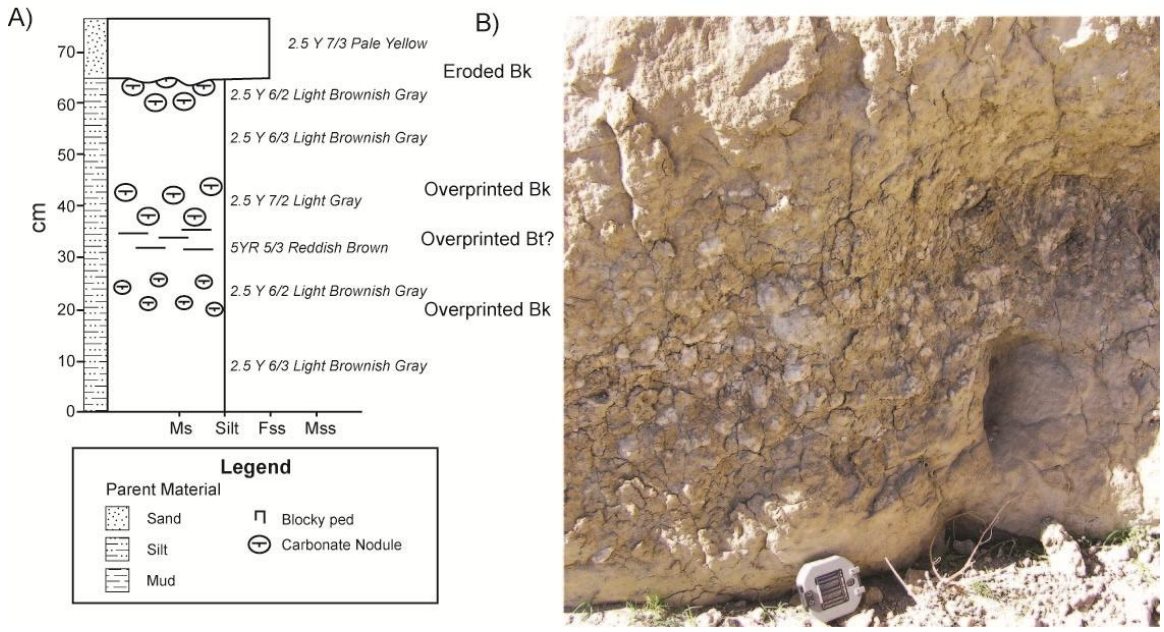

Figure 2.5: Soil profiles of calcic soils showing (A) typical profile and (B) photograph of a nodular Bk horizon as commonly exposed in the Hueso Fm. Paleosols in this group are interpreted as calcic Aridisols.

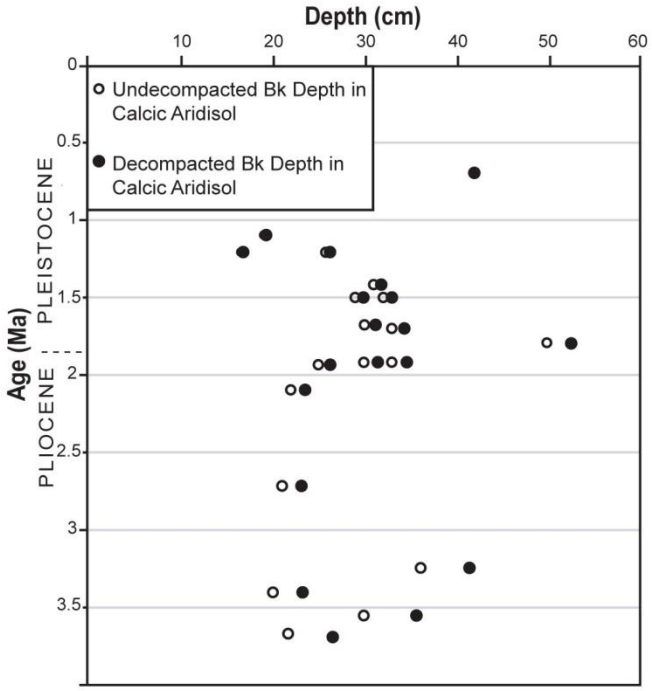

Figure 2.6: Depth to calcic enrichment (Bk) horizon in calcic Aridisols as a function of age. Data shown represent subset of 19 paleosols with identifiable, un-eroded surface horizons. Decompacted depths to Bk calculated using the methodology of Sheldon and Retallack (2001).

blocky peds are sometimes present. Calcic paleosols are interpreted as Calcids (i.e. Calcic Aridisols; Soil Survey Staff, 1999). Variations among calcic paleosols include paleosols with substantially thicker and deeper Bk horizons as well as calcic paleosols with a surface gley horizon.

Other paleosol types present in the studied section include poorly developed Inceptisols and deep calcic paleosols developed on lacustrine limestone. Inceptisols are identified by the presence of root traces as well as weakly developed cambic horizons. These paleosols are uncommon and are found throughout the stratigraphic column.

5.2. Stable Isotopes from Pedogenic Carbonate

The results of analyses of 47 pedogenic carbonate horizons are listed in Table 2.1 and plotted against age in Figure 2.7. The data show large scatter with an overall depletion in $\delta^{13}C$ of about 2‰ between 3.9 and 2.0 Ma, from an average of -5.08‰ between 3.9 and 3.5 Ma to -7.34‰ between 2.75 and 2.25 Ma (Fig. 2.7a). After 2.5 Ma there is a minor enrichment in $\delta^{13}C$ of about 1.5‰ by the interval 1.5-1.0 Ma. Oxygen isotope values show less scatter and display a coherent slight enrichment in $\delta^{18}O$ from an average of -10.5‰ between3.9 and 3.5 Ma to -8.4‰ between 1.0 and 0.7 Ma (Fig. 2.7b).

6. Discussion

6.1. Paleosol Evolution

The shift from vertic to calcic paleosols is roughly coincident with progradation of the locally derived Hueso and Tapiado formations (Fig. 2.3), although the abrupt change in sediment provenance is not itself a satisfactory explanation for the disappearance of vertic paleosols. Locally derived deposits appear suddenly in the section

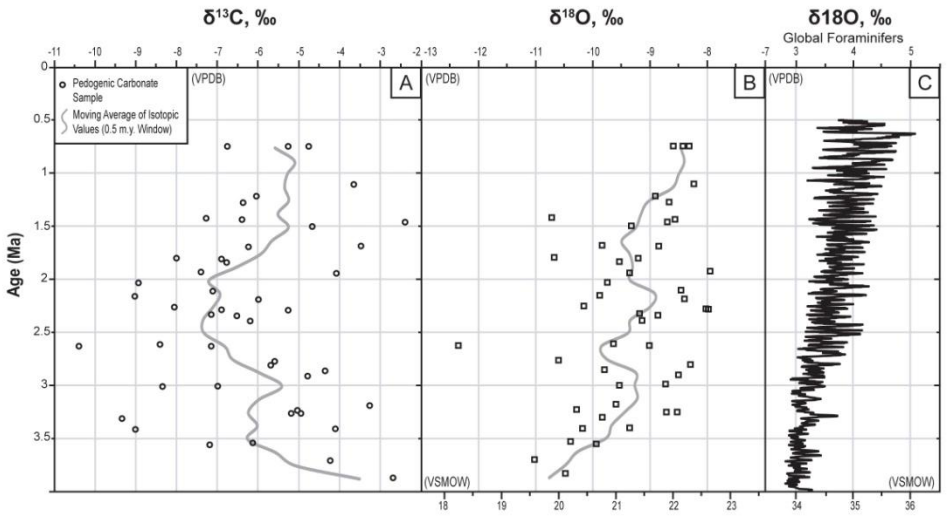

Figure 2.7. (A) Carbon and (B) oxygen isotope ratios of pedogenic carbonate as a function of age. Open circles show data for individual samples. Line shows 0.5 m.y. moving average of isotopic values. (C) $\delta^{18}O$ values for global benthic foraminifers compiled by Lisiecki and Raymo (2005).

(Dorsey et al., 2011), whereas the disappearance of vertic paleosols was preceded by a gradual decrease spanning roughly 1 m.y. Locally-derived sediment also contains abundant swelling clays, in spite of the overall coarser nature of these deposits (Carey, 1976). We infer that the decrease and demise of vertic paleosols and their replacement by calcic paleosols was driven by a decrease in overall seasonality of rainfall. Vertic soils form in areas where seasonal rainfall leads to repeated cycles of water–saturation and desiccation (Dudal and Eswaran, 1988; Driese and Mora, 1993; Caudill et al., 1996). Soils that are either continually moist or never water-saturated will not undergo the shrinking and swelling of clay minerals that create the features associated with vertic soils (Soil Survey Staff, 1999).

Calcic Aridisols with shallow Bk horizons form in areas of low to moderate precipitation (Soil Survey Staff, 1999; Retallack, 2005), whereas vertic soils are found in sub-humid to semiarid climate zones (Caudill et al., 1996). We infer that a climate regime dominated by highly seasonal precipitation caused periodic water-logging and vertic soil formation during middle to late Pliocene time. The cessation or weakening of seasonal precipitation from 3.7 to 2.8 Ma likely caused the decrease and end of vertic paleosol formation by 2.8 Ma. Concurrent with and possibly resulting from this reduction in seasonality, the increased abundance and eventual dominance of calcic Aridisols shows that aridity increased over time and became the dominant climate condition by about 2.5-3.0 Ma. The average decompacted depth to Bk horizon of 31 cm (Fig. 2.6) corresponds to a mean annual precipitation of 359±147 mm in modern soils (Retallack, 2005).

6.2. Carbon Isotopes

A reduction in seasonality of precipitation is also suggested by the carbon-isotope data, which show a depletion in $\delta^{13}C$ values from about 3.9 to 2.5 Ma (Fig. 2.7a). This trend suggests a possible increase in abundance of C3 plants at the expense of C4 grasses. Because C4 grasses tend to grow in areas with abundant warm-season precipitation (Sage et al., 1999), our data suggest a decrease in summer precipitation and a shift toward a Mediterranean-type climate with winter precipitation and summer drought. This shift does not necessarily require cooling of the area; it instead suggests that more vegetation growth took place during the cool season rather than the warm season, consistent with a reduction in summer precipitation and overall decrease in seasonality. This finding is consistent with paleobotanical evidence from fossil assemblages, which suggest that the present-day winter-wet Mediterranean-type climate conditions developed in southern California between middle Pliocene and early Pleistocene time (Axelrod, 1973; Graham, 1999). Regional cooling is a possible additional cause of this proposed vegetation shift, as the timing of the $\delta^{13}C$ depletion generally corresponds with global cooling at the onset of northern hemisphere glaciations (Raymo, 1994; Zachos et al., 2001; Ravelo et al., 2004).

An enrichment in $\delta^{13}C$ of about 1.5‰ from ca. 2.5 to 1.0 Ma probably reflects increasing aridity and a decrease in soil productivity. Ongoing aridification, as suggested by the paleosol record, likely led to an overall decrease in soil productivity. Low rates of soil productivity can result in infiltration of atmospheric CO_2 into the soil, which has the effect of enriching soil CO_2 in $\delta^{13}C$ (Amundson et al., 1988; Stevenson et al., 2005;

Breecker et al., 2009). Enrichment of $\delta^{13}C$ between 2.5 and 1.0 Ma may also reflect an increase in the abundance of desert succulents using the CAM photosynthetic pathway.

It is possible that all observed variations in pedogenic carbonate $\delta^{13}C$ reported here were solely driven by changes in soil productivity. This possibility must be considered in light of observed shallow Bk formation in paleosols in the study area (Fig. 2.6). In this interpretation, depletion of $\delta^{13}C$ in paleosol carbonate between ~3.8 and 2.5 Ma would reflect increasing soil productivity, probably related to increasing precipitation and a corresponding decreasing atmospheric input. This possibility is inconsistent with changes in paleosol morphology documented in this study. While we favor the interpretation that $\delta^{13}C$ depletion between 3.9 and 2.5 Ma was driven by vegetative changes, any explanation for the observed variation in carbon-isotope data is at this time non-unique.

6.3. Oxygen Isotopes

Large scatter in measured $\delta^{18}O$ ratios (Fig. 2.7b) suggests large variation in both precipitation and local evaporation regime. Milankovitch-scale climate variations (e.g., Lisiecki and Raymo, 2005; Fig 2.7c) likely affected local isotopic $\delta^{18}O$ ratios of meteoric precipitation through temperature effects on fractionation. Shifts in the $\delta^{18}O$ composition of the oceanic source of meteoric precipitation may have varied by as much as 1‰ between glacial and interglacial periods (Schrag et al., 1996). Similarly, alternating periods of relative humidity and aridity may have altered the evaporative regime of soil water, driving variation in pedogenic carbonate $\delta^{18}O$ (Cerling and Quade, 1993; Hsieh et al., 1998). Glacial-interglacial scale variation in pedogenic carbonate $\delta^{18}O$ can be up to 4‰ (Retallack et al., 2004). The pedogenic carbonate nodules studied here took 100's to

1,000's of years to form (Machette, 1985). This time-averaging in the carbonate isotopic record and the ±70 k.y. sample age uncertainty make correlation of individual paleosol profiles to specific glacial or interglacial periods impossible. Long-term trends are, however, significant despite the scatter in the isotopic record. In particular, oxygen isotopes from pedogenic carbonate in the Fish Creek-Vallecito basin record a systematic long-term enrichment in soil waters during late Pliocene and early Pleistocene time.

Enrichment of oxygen isotopes in the study area (Fig. 2.7b) was likely driven by long-term aridification. Aridification drives evaporation of soil water, resulting in increased fractionation and an increase in $\delta^{18}O$ (Cerling and Quade, 1993; Hsieh et al., 1997). This interpretation is consistent with and supported by similar indications of gradual aridification from paleosol characteristics. The enrichment in oxygen isotopes reported here corresponds to a long-term enrichment of global seawater $\delta^{18}O$ of ~1‰ (Fig. 2.7c; Lisiecki and Raymo, 2005). However, $\delta^{18}O$ in pedogenic carbonate in the section increased by a greater amount (2-3‰) during the same time interval, further suggesting a local climate influence.

Alternatively, it is possible that the enrichment in $\delta^{18}O$ values could record a shift to a warmer, more tropically derived water vapor source. We do not favor this alternative. Climate conditions that create warmer water vapor sources in southern California precipitation, such as warm El Niño Southern Oscillation (ENSO) events, are thought to have decreased after 2.8 Ma (Molnar and Cane, 2002; Wara et al., 2005).

6.4. Paleoclimate Evolution of Southern California

Weakening of the North American monsoon is the most likely mechanism to explain reduced seasonality and increased aridity in the Fish Creek-Vallecito basin from

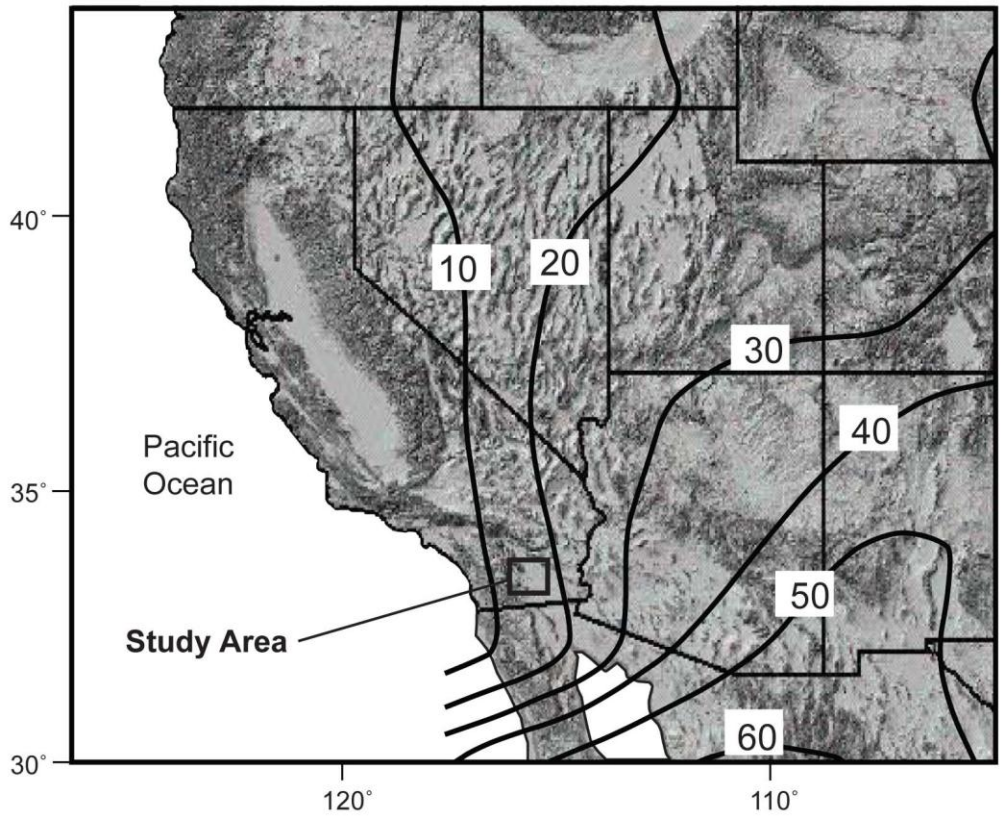

Figure 2.8. Map showing the distribution of monsoonal precipitation across southwestern North America (modified from Higgins et al., 1999). Contour lines show the percentage of annual precipitation provided by the North American monsoon in July, August and September for the period 1963-1988.

middle Pliocene to early Pleistocene time. Summer precipitation in southwestern North America comes primarily in the form of the North American monsoon (Adams and Comrie, 1997). The monsoon in this region originates when water vapor advected from the Gulf of California is drawn eastward and northward by a thermal low over the southern Cordillera (Higgins et al., 1997). The study area presently lies near the northwestern limit of the present-day North American monsoon (Fig. 2.8; Mitchell, 1976; Higgins et al.,1999). Higher global temperatures during Pliocene time (Raymo et al.,

1996; Haywood and Valdes, 2004) likely contributed to higher-than-modern sea surface temperatures in the Gulf of California, which have been shown to increase advection of moisture into the North American Monsoon (Mitchell et al., 2002). Higher-than-modern middle Pliocene temperatures may have also created a larger than present-day summer thermal low in southwestern North America, drawing more large storms into the area. Large storms would have brought higher-than-modern annual precipitation, greater seasonal water-logging of soils and resultant vertic paleosol formation, and would have contributed to a summer growing season of warm-season grasses. The combination of late Pliocene cooling of the coastal Pacific Ocean (Dekens et al., 2007) and southward deflection of the westerly jet stream due to global cooling and growth of the Laurentide Ice Sheet (Spaulding, 1991) likely caused a decrease in summer precipitation in the study area. Dextral motion on the San Andreas fault system has transl357ated the study area ~200 km NNW since 4 Ma (Oskin and Stock, 2003). This tectonic transport could also have contributed to decreasing seasonality by moving the study area away from the area of maximum monsoon influence. The remaining winter precipitation maintained a cool winter growing season, but precipitation was of insufficient concentration and/or abundance to fully waterlog soils and contribute to vertic paleosol formation.

Several workers have suggested that a virtually permanent ENSO condition existed prior to roughly 2.8 Ma (Molnar and Cane, 2002; Wara et al., 2005). In this case, southern California would have experienced abundant winter precipitation during early to mid-Pliocene time (Woodhouse, 1997; Cayan et al., 1998; Mo and Higgins, 1998). We suggest that a decrease in monsoonal precipitation from 3.8 to 2.5 Ma was coupled with a decrease in winter precipitation due to the end of persistent ENSO conditions. The data

presented above support a hypothesis in which an increase in the relative abundance of winter precipitation was coupled with an overall decrease in mean annual precipitation. The data record progressive climate change from 3.8 to 0.75 Ma. This finding is consistent with recent paleoclimate studies that document gradual, long-term global cooling and climate reorganization beginning as early as 4.0 to 3.6 Ma (Ravelo et al., 2004 ; Mundelsee and Raymo, 2005; Dekens et al., 2007).

6.5. Comparison with Previous Studies

The results of this study are broadly consistent with those of previous paleoclimatic investigations of the Fish Creek-Vallecito basin area. The middle Pliocene Carrizo Local Flora was wet-adapted (Remeika, 2006), consistent with our interpretation of a relatively wet paleoclimate during that time interval. A stable-isotope study of fossil horse teeth in the same stratigraphic section analyzed for this study found that $\delta^{13}C$ values in horse teeth became depleted over the time interval 3-0.8 Ma, while $\delta^{18}O$ was enriched over the same interval (Brogenski, 2001; Spero et al., 2003). Increasing aridity in the latest Pliocene is supported by faunal evidence from lacustrine ostracodes (Cosma, 2002a). Microfossils of small reptiles and mammals in the Hueso and Tapiado formations support the interpretation of a warm, wet middle Pliocene climate that gradually became dryer post-2.8 Ma (Gensler et al., 2006; White et al., 2006). Because prior paleoclimatic studies of the Fish Creek-Vallecito basin predate a recent high-precision magnetostratigraphic study (Dorsey et al., 2011), previous interpretations will need to be re-evaluated in light of the new age controls.

6.6. Timing of Peninsular Ranges Uplift

Our results show that the Peninsular Ranges of southern California likely did not undergo significant uplift between 0.75 and 3.8 Ma. In fact, our finding of enrichment in $\delta^{18}O$ through time is opposite of the change that would be produced by the onset of a rain shadow in the study area. The data therefore imply that significant uplift of the Peninsular Ranges probably occurred before 3.7 Ma or after 1 Ma, or perhaps took place in two stages before 3.7 Ma *and* after 1 Ma. This finding does not rule out regional uplift driven by progressive removal of the mantle lithosphere under the Peninsular Ranges, as hypothesized by Mueller et al. (2009). As noted by these authors, mantle-driven uplift may have raised the crest of the Peninsular Ranges by only 30 to several hundred meters, an amount that is too small to be reliably detected using oxygen isotopes.

We considered the possibility that the long-term aridification trend documented above resulted not from global climate change, as we propose, but rather was produced by the progressive growth of an orographic rain shadow created by uplift of the Peninsular Ranges, as has been suggested by previous workers (e.g., Cosma, 2002a; Sussman et al., 2005). In this scenario, we would infer that the observed increase in $\delta^{18}O$ which we credit to *in situ* evaporative enrichment of soil water was large enough to offset any depletion of $\delta^{18}O$ in meteoric water due to orographic isotope fractionation. We do not favor this interpretation because there is no mechanism associated with Peninsular Ranges uplift that could explain the observed decrease in seasonality. The Gulf of California is the primary source of water vapor for monsoonal precipitation in the region (Adams and Comrie, 1997). Advection from the Gulf of California, located south of the

study area, would not be affected or diminished by uplift of mountains to the west of the basin.

7. Conclusions

The results of this study show that seasonality of precipitation in the Fish Creek-Vallecito basin decreased from middle Pliocene to early Pleistocene time (~3.8 to ~0.75 Ma). This change occurred in concert with an increase in aridity and most likely resulted from a decrease in summer monsoonal precipitation across southwestern North America due to global climate change during this time interval. Decreasing seasonality produced a relative decrease in C4 vegetation and a corresponding increase in C3 vegetation. A new equilibrium in the biota was established by 2.0 to 1.5 Ma, although the region probably experienced continued aridification that drove an increase in $\delta^{18}O$ in soil and surface waters from ~2.0 to 0.75 Ma. The decrease in seasonality of precipitation and increase in aridity affected soil processes in the basin and created a landscape dominated by calcic Aridisols. Increased aridity also produced a marked decrease in overall soil productivity. Data presented here are consistent with previous workers' interpretation that persistent ENSO conditions ended during late Pliocene time. Oxygen isotope ratios from the Fish Creek-Vallecito basin are incompatible with significant uplift of the Peninsular Ranges of southern California during late Pliocene and early Pleistocene time.

This paper presents a new data set that can be used to improve our understanding of how Plio-Pleistocene global climate change affected local climates in southern California. We conclude that the climate trends reported here resulted from progressive long-term global cooling, an end of persistent ENSO conditions in the Pacific Ocean, and shifts in the westerly jet stream due to growing ice masses over the northern hemisphere.

8. Bridge

In this chapter I described a long-term trend in the climate in the region of the Fish Creek-Vallecito basin during the interval ~4.0-0.75 Ma. This local trend was the local manifestation of global climate reorganization in late Pliocene time. The Palm Spring Group was deposited during this same time interval, and records an enigmatic stratigraphic reorganization at ~2.9 Ma. The following chapter presents an investigation of this basin reorganization, with reference to both the effects of climate change (i.e. the contents of this chapter) and the impact of local and regional tectonism.

CHAPTER III

TECTONIC CONTROLS ON PLIOCENE SEDIMENTATION AND BASIN REORGANIZATION IN THE FISH CREEK-VALLECITO BASIN, SOUTHERN CALIFORNIA

This chapter was co-authored with Rebecca Dorsey, who provided funding, field and advisorial support. Chris DeBoer and Bernie Housen helped to collect magnetostratigraphic samples, and were responsible for paleomagnetic analysis.

INTRODUCTION

Decades of field, experimental, and theoretical investigations have established a strong conceptual framework for understanding climatic and tectonic controls on the distribution of coarse- and fine-grained facies in tectonically active sedimentary basins. For example, it is widely accepted that upward-coarsening progradational trends may be driven by an increase in sediment supply, decrease in subsidence rate, or lowering of base level (e.g. Leeder and Gawthorpe, 1987; Blair and Bilodeau, 1988; Heller and Paola, 1992; Horton et al., 2004; Koltermann and Gorelick, 1992; Mack and Leeder, 1999; Marr et al., 2000; Aschoff and Steel, 2011). Similarly, upward-fining retrogradational trends are understood to result from decreased rate of sediment input, increased subsidence rate, or rising base level. Hypotheses for sedimentary response to changing boundary conditions can be quantified with numerical models and tested with field data and flume experiments (e.g. Paola et al., 1992; Allen and Densmore, 2000; Densmore et al., 2007;

Marr et al., 2000; Armitage et al., 2011). Application of such concepts and hypothesis tests improve our ability to interpret past changes in regional climate, tectonics and landscape evolution.

Modern stratigraphic models can be used to interpret relatively simple monotonic trends such as overall progradation or retrogradation (e.g. Paola et al., 1992). However, they often cannot explain highly complex or internally inconsistent stratigraphic signals, such examples of coarse sediment progradation during increased subsidence rate (e.g. Brozović and Burbank, 2000; Marzo and Steel, 2000; Parra et al., 2010), or in cases where transgression occurs independent of predicted or known base-level trends (e.g. Mack and Stout, 2005). Often, parameters that are difficult to measure directly from the stratigraphic record, such as changes in sediment flux (e.g. Marzo and Steel, 2000; Parra et al., 2010) or base-level changes independent of global eustacy (e.g. Martinsen et al., 1999), are invoked to reconcile observed relationships with theoretical models. In highly complex settings, then, existing models of stratigraphic evolution can only act as a starting point in the interpretation of complicated tectonic and climatic histories.

The Late Cenozoic Fish Creek-Vallecito basin in southern California preserves a unique stratigraphic boundary across which abrupt changes in grain size, composition, and depositional environment are internally inconsistent and seemingly incompatible with current basin models. In this basin, a thick Late Cenozoic basin-fill succession is broadly tilted and well-exposed, allowing for high-precision magnetostratigraphic dating and detailed lithofacies mapping. Sharp contrasts in stratigraphic architecture and composition across this boundary record abrupt changes in sedimentary provenance and facies distribution at ~2.9 Ma, at the boundary between the lower and upper parts

(subgroups) of the Pliocene Palm Spring Group. This stratigraphic transition records rapid progradation of gravel into the basin from nearby sources at the same time as initial rapid transgression of a large regional lake. This pronounced change has been described in previous studies but its origin remains unexplained (Winker, 1987; Dorsey et al., 2011).

Synchronous gravel progradation and lacustrine transgression is particularly enigmatic because, in most basin models, gravel progradation and lake transgression are mutually exclusive and opposite in sign. Gravel progradation occurs when the rate of sediment input exceeds the rate of production of accommodation space, whereas lacustrine transgression takes place when the rate of production of accommodation space exceeds the rate of sediment influx (e.g. Blair and Bilodeau, 1988; Heller and Paola, 1992; Carroll and Bohacs, 1999; Mack and Leeder, 1999). The example analyzed in this study, in which both of these conditions were met at the same time in the same place, has not previously received detailed treatment in the geologic literature.

This paper describes a study of the abrupt, enigmatic boundary between the lower and upper subgroups of the Palm Spring Group in the Fish Creek – Vallecito basin. We integrate analyses of stratigraphic architecture, age, provenance, and sedimentology to document the nature and timing of this change. We then use the results to interpret regional controls on Pliocene basin reorganization. The results of our analysis show that simultaneous gravel progradation and lacustrine transgression at ca. 2.9 Ma resulted from local and regional changes in tectonic boundary conditions, and that late Pliocene climate change was not responsible for the observed stratigraphic transition. This analysis provides new insight into the kinematic evolution of the San Andreas fault system during

Pliocene-Pleistocene time, and may help to constrain the timing of a previously documented tectonic reorganization in the northern Gulf of California and southern Salton Trough (e.g. Aragon and Martín, 2007).

BACKGROUND

The Fish Creek-Vallecito basin is part of a large supradetachment basin that formed in the Salton Trough region of southern California, in the hanging wall of the West Salton detachment fault. Previous studies have shown that, during subsidence and basin filling, this basin was bounded on the southwest by the detachment fault and on the northeast by the San Andreas fault (Fig. 2.1; Axen and Fletcher, 1998; Dorsey et al., 2011). Transtensional deformation in the western Salton Trough began at ca. 8.0 Ma in late Miocene time, though the age of initiation of the detachment fault remains uncertain. Basin subsidence due to slip on the detachment fault continued until ca. 1.0 Ma (Johnson et al., 1983; Dorsey et al., 2011), and resulted in accumulation of ~5.5 km of basin-fill deposits (Woodard, 1963; Dibblee, 1996; Winker and Kidwell, 1996; Dorsey et al., 2011). A major tectonic reorganization ~1.2 Ma initiated the modern San Jacinto, San Felipe and Elsinore strike-slip faults, ended displacement along the West Salton detachment fault, and initiated uplift and erosion along the southwestern margin of the western Salton Trough (Fig. 3.1 ; Lutz et al., 2006; Kirby et al., 2007; Steely et al., 2009; Janecke et al., 2010; Dorsey et al., 2012). In the area of the Fish Creek-Vallecito basin, post-1.2 Ma strike-slip related deformation resulted in uplift of the Vallecito and Fish Creek mountains and dissection and deformation the late Miocene-Pleistocene basin fill (Fig. 3.2; Dorsey et al., 2012). A fanning-dip interval near the top of the basin-fill

stratigraphic section spans 1.2-1.0 Ma and records initial tilting due to this regional tectonic reorganization (Dorsey et al., 2012).

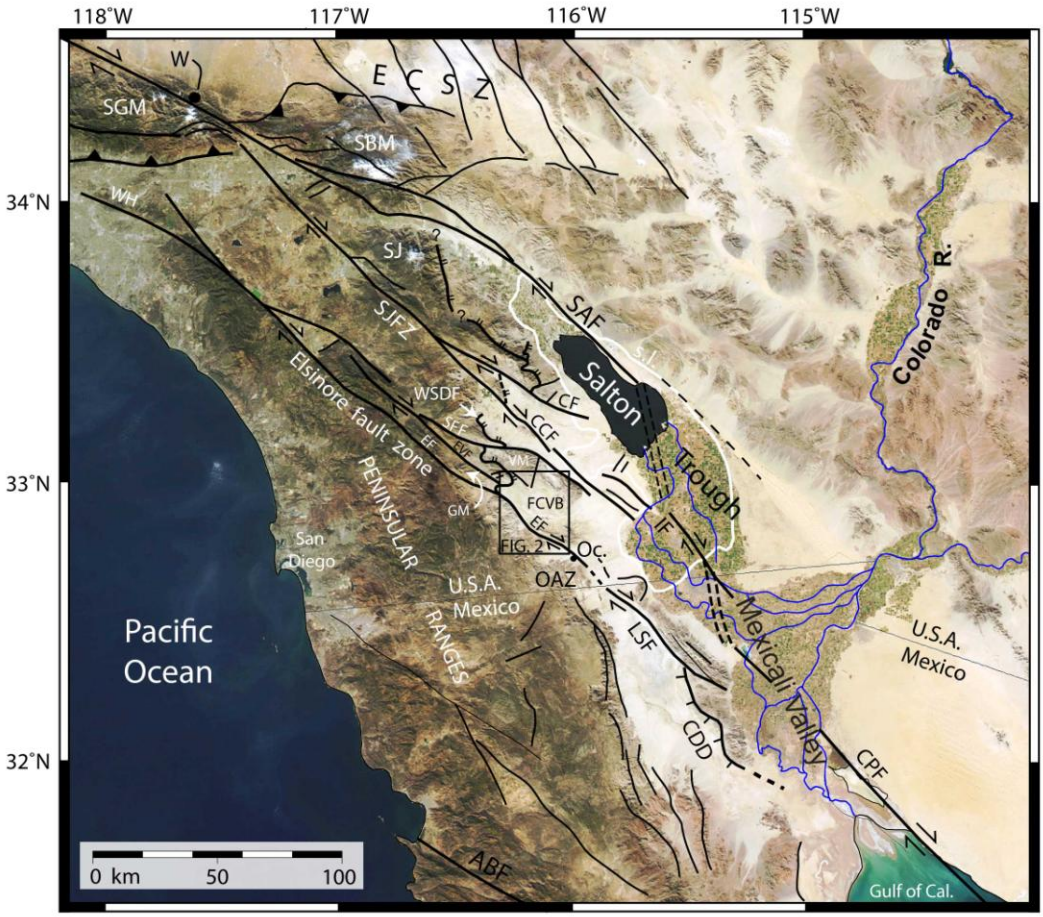

Figure 3.1. Map showing location of the study area and major regional faults. ABF, Agua Blanca Fault; CCF, Coyote Creek Fault; CDD, Canada David detachment; CF, Clark Fault; CPF, Cerro Prieto Fault; ECSZ, Eastern California Shear Zone; EF, Elsinore fault; EVF, Earthquake Valley fault; FCVB, Fish Creek-Vallecito basin; GM, Granite Mountain; IF, Imperial fault; LSF, Laguna Salada fault; OAZ, Ocotillo accommodation zone; Oc., Ocotillo, SAF, San Andreas fault; SBM, San Bernadino Mountains; SFF, San Felipe fault; SGM, San Gabriel Mountains; SJ, San Jacinto Peak; SJFZ, San Jacinto fault zone; VM, Vallecito Mountains; WH, Whittier Hills; WSDF, West Salton detachment fault.

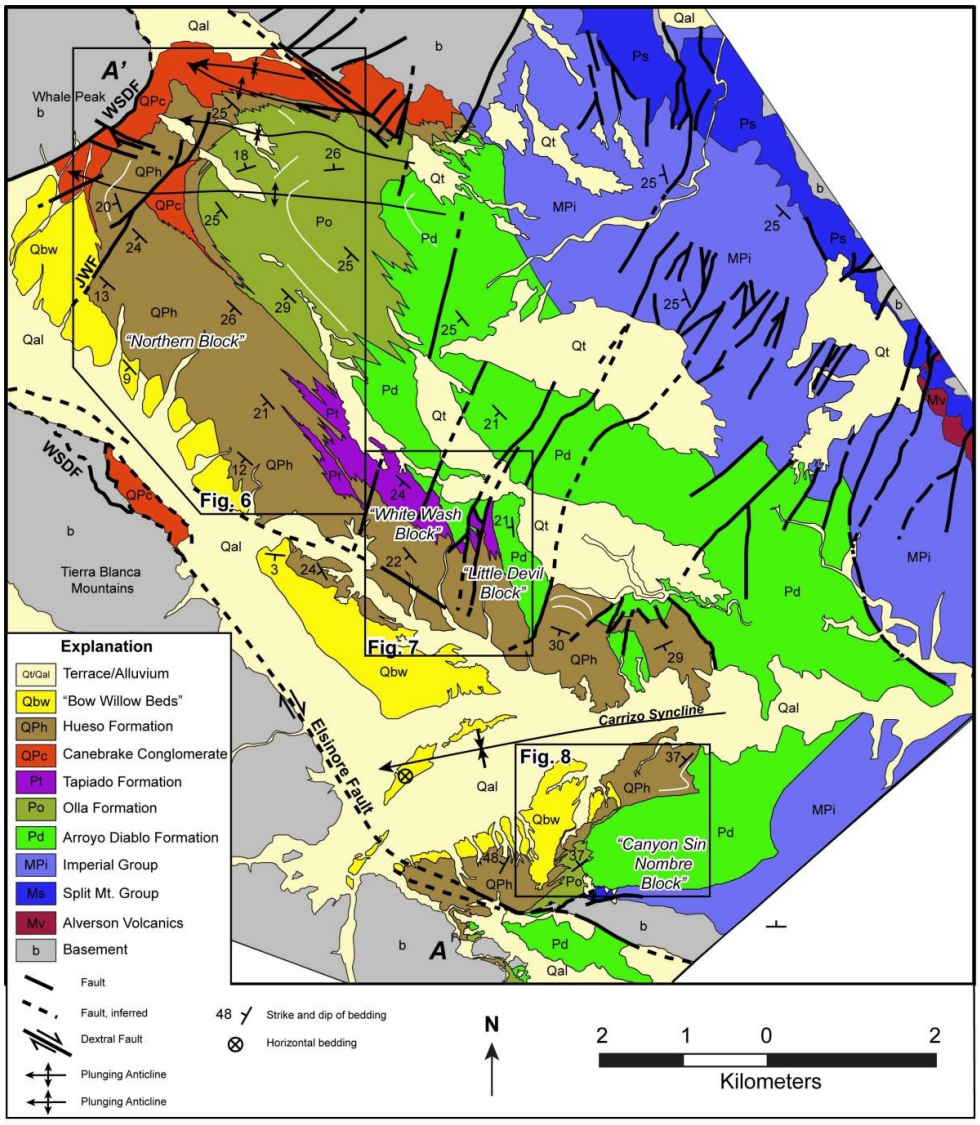

Figure 3.2. Simplified geologic map of the Fish Creek-Vallecito basin. *A* and *A'* designate the end points of facies panel illustrated in Figure3.4. Based on both detailed 1:10,000-scale geologic mapping and adaptations from Dorsey et al. (2011) and Winker (1986). JWF, June Wash fault; WSDF, West Salton detachment fault.

A complex basin-filling history is recorded in upper Miocene to Pleistocene sedimentary rocks in the Fish Creek-Vallecito basin (Fig. 3.3). Marine incursion at ca. 6.3 Ma resulted in latest Miocene to early Pliocene deposition of the marine Imperial Group (Axen and Fletcher, 1998; Dorsey et al., 2007; Dorsey et al., 2011). Establishment of the

Colorado River catchment led to earliest influx of Colorado River-derived sediment ca. 5.3 Ma, which later was followed by progradation of the Colorado River delta into and across the basin (Dorsey et al., 2007, 2011). The transition from marine to fluvial deposition is recorded by the ca. 4.2 Ma base of the Palm Spring Group (Fig. 3.3; Winker and Kidwell, 1986, 1996; Dorsey et al., 2007).

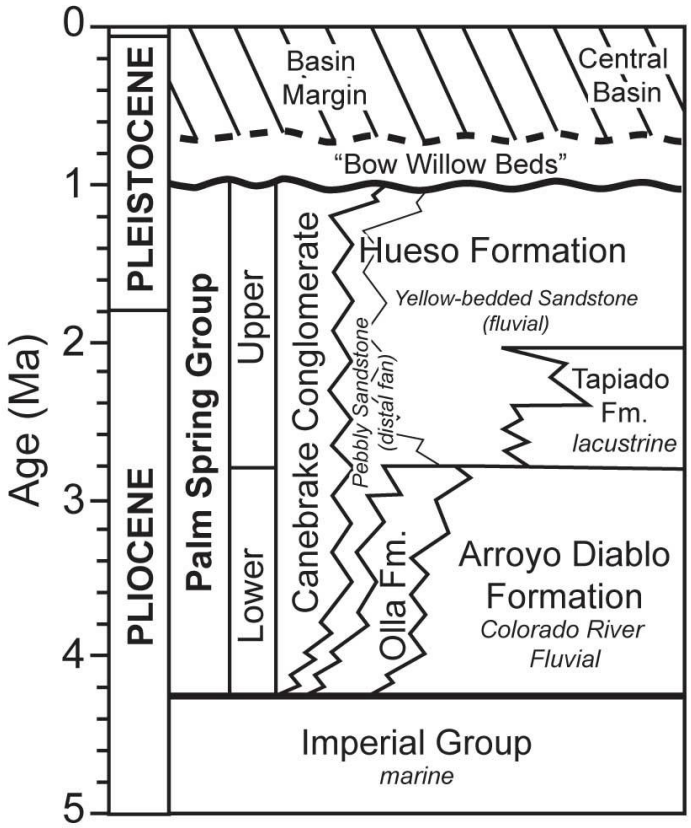

Figure 3.3. Generalized stratigraphy, distribution, and age of Palm Spring Group in the Fish Creek-Vallecito basin. The base of the Tapiado Formation marks the base of the upper Palm Spring Subgroup. The Arroyo Diablo and Olla formations are confined to the lower Palm Spring Subgroup. The Canebrake Conglomerate and Hueso Formation are time-transgressive.

Plio-Pleistocene sedimentary rocks of the Palm Spring Group include nonmarine deposits of the Colorado River fluvio-deltaic system in the Salton Trough, and locally derived equivalents around the margins of the basin (Winker and Kidwell, 1996). This

study focuses on an important transition at the boundary between the lower and upper parts (subgroups) of the Palm Spring Group (Figs. 3.3, 3.4). This stratigraphic transition records a major basin reorganization at ca. 2.9 Ma that has received little attention in previous studies. During accumulation of the lower Palm Spring Subgroup (ca. 4.2-2.9 Ma), the Fish Creek Vallecito basin was dominated by fluvial sedimentation in distributory channels and interdistributary floodplains of the lower Colorado River and delta system (Winker, 1987; Winker and Kidwell, 1986, 1996). These Colorado River-derived sediments (Arroyo Diablo Formation) interfinger with locally-derived deposits of limited areal extent (Canebrake Conglomerate, Hueso, Olla formations) (Figs. 3.3, 3.4; Winker, 1987; Winker and Kidwell, 1996; Dorsey et al., 2011).

The well-dated (2.9 Ma), abrupt change at the boundary between the lower and upper Palm Spring subgroups (Fig. 3.3) records rapid progradation of locally-derived coarse-grained alluvial fans outward from the western basin margin over a large area of the basin. At the same time, the oldest fine-grained lacustrine facies of the Tapiado Formation record abrupt appearance and transgression of a large lake in the central part of the basin (Fig. 3.4). This late Pliocene basin reorganization was initially attributed to tectonic controls such as intra-basinal uplift or fault segmentation (Winker, 1987; Dorsey et al., 2005). Subsequent work showed that the regional, contiguous supradetachment basin was not structurally segmented until initiation of modern strike-slip faults at ca. 1.2-1.0 Ma (Lutz et al., 2006 ; Kirby et al., 2007; Steely et al., 2009; Janecke et al., 2010; Dorsey et al., 2011; 2012;). Thus the driver of major changes in basin architecture at 2.9 Ma has remained unexplained until now.

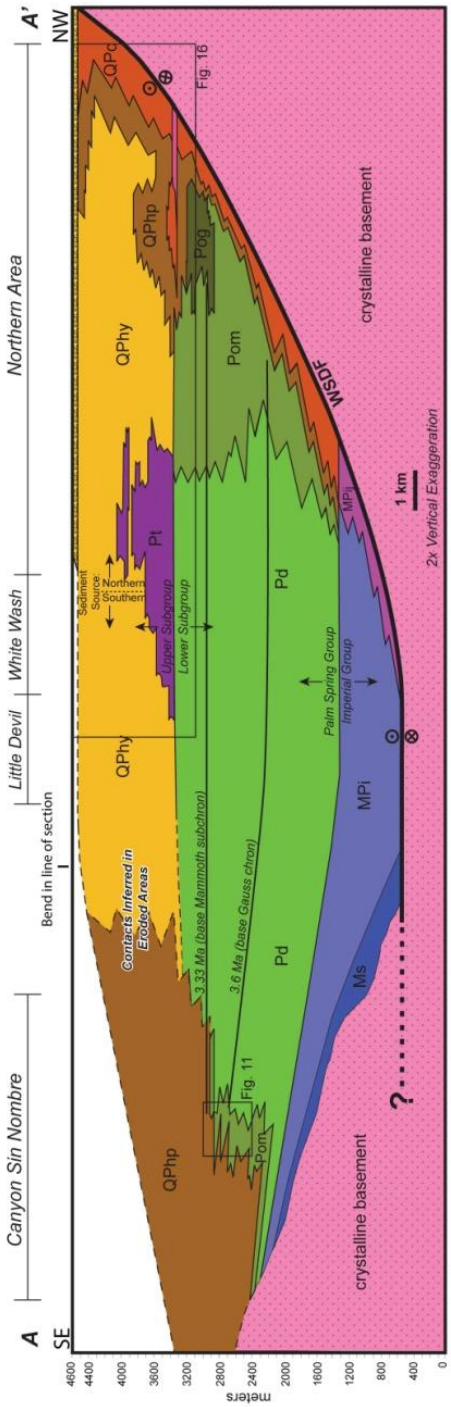

Figure 3.4. Reconstructed stratigraphic architecture of the Fish Creek-Vallecito basin in the study area, with emphasis on the Palm Spring Group, prior to dissection by strike-slip faulting ca. 1.2 Ma. Section end points are designated as *A* and *A'* in Figure 3.2. This section follows strike along the base of the upper Palm Spring Subgroup across the hinge of the Carrizo syncline. Structural relationships and unit thicknesses from this study and Dorsey et al. (2011, 2012).

It would be difficult or impossible to confidently test hypotheses for the underlying controls on this complex stratigraphic transition if we could not control for different plausible forcing mechanisms. Recent and ongoing studies of the Fish Creek – Vallecito basin provide new insights into tectonic subsidence rates and structural evolution (Dorsey et al., 2011; 2012), regional paleoclimate (Peryam et al., 2011) and local paleo-erosion rates (Longinotti et al., 2011; Peryam et al., 2010;). These studies improve our understanding of climatic and tectonic boundary conditions that existed during basin formation, and permit direct comparison between the results of our basin analysis and quantitative models of basin filling.

METHODS

We carried out detailed structural and lithofacies mapping at scales of 1:10,000 and 1:20,000 integrated with high-resolution satellite imagery. Careful identification of depositional contacts and faults allowed us to correlate magnetostratigraphic transects and reconstruct facies architecture. Stratigraphic thicknesses were measured in the field using a Jacob's staff (Compton, 1985). Conglomerate clast counts were conducted at 23 sites in the Olla and Hueso formations and the Canebrake Conglomerate (Table 3.1). At each site, all clasts larger than 1 cm were recorded along a 5 cm by 5 cm grid until a minimum of 100 clasts was counted. Paleocurrent data were collected primarily from measurements of clast imbrication planes, but locally include trough cross-bedding axes and current lineation trends. Corrections for bedding dip were made using stereographic software. Paleocurrent directions were back-rotated by 18° counterclockwise to correct for post 1.2 Ma vertical axis rotation of the basin (Deboer et al., 2012).

Table 3.1. Conglomerate clast counts

	Formation	Easting	Northing	Granite Mt. Tonalite	La Posta Tonalite	Meta-plutonic	Meta-sedimentary	Meta-volcanic	Volcanic	Other	Total n
Northern Samples											
1	Hueso	576534	3632908	0	37	55	11	1	0	10	114
2	Hueso	582524	3639728	0	32	44	14	15	1	7	113
3	Hueso	579176	3634349	0	19	52	25	8	3	7	114
4	Hueso	579142	3633642	0	18	44	30		9	5	106
5	Hueso	574861	3642329	0	21	42	29	17	3	6	118
6	Hueso	575173	3641649	0	8	48	26	19	4	6	111
7	Hueso	578203	3634072	0	30	44	24	4	6	4	112
8	Hueso	577447	3634505	0	23	42	18	14	6	5	108
9	Hueso	574859	3634869	0	11	41	22	16	4	9	103
Southern Samples											
1	Heuso	572019	3644764	4	18	55	20	0	0	14	111
2	Hueso	571627	3643767	6	23	45	27	0	0	17	118
3	Olla	571512	3648593	14	25	60	3	0	0	0	102
4	Canebrake	570312	3649355	6	35	58	16	0	0	2	117
5	Hueso	571075	3648389	15	28	48	16	0	0	5	112
6	Hueso	570164	3648812	19	37	36	16	0	0	1	109
7	Hueso	570164	3648812	10	19	55	10	0	0	7	101
8	Hueso	570236	3648515	10	22	67	5	0	0	4	108
9	Hueso	570705	3647622	14	21	58	10	0	0	3	106
10	Hueso	570468	3647532	13	12	54	20	0	0	3	102
11	Hueso	570485	3646914	4	17	43	21	0	0	14	99
12	Hueso	571450	3643764	25	11	42	10	0	0	28	116
13	Hueso	570872	3643445	10	17	51	20	0	0	8	106

Paleomagnetic samples were collected in the field using a water-cooled gasoline-powered diamond core drill. Three to seven samples were collected at each site. Site locations were spaced stratigraphically close together (5-30 m) in each transect. In total, 183 new polarity determinations constrain the ages of deposits in 4 partially overlapping transects. All laboratory measurements were conducted at the Western Washington University paleomagnetism laboratory using a 2-G 755-R cryogenic magnetometer. Specimens were subjected to stepwise thermal or alternating-field demagnetization (in some cases both). Polarity of paleomagnetic samples was determined from orthogonal vector and equal angle projections of demagnetization data (Fig. 3.5). Sites are assigned to classes for polarity determination. Polarity is interpreted from the inclination of the second removed component (C2) for Class 1 and 2 sites (Fig. 3.5a,b). Polarity for class 3 sites is inferred from a combination of demagnetization trends and equal angle projections (Fig. 3.5c). Polarity of Class 4 sites is inferred from a combination of demagnetization trends and equal angle projections with less well organized but decipherable trends (Fig. 3.5d). Site polarities are detailed in the online appendix (details tba). Magnetochron boundaries were placed at obvious reversals of polarity intervals, and compared to results of Dorsey et al. (2011).

RESULTS

Age of Basin Deposits

Because of structural segmentation of Plio-Pleistocene rocks in the Fish Creek-Vallecito basin, our magnetostratigraphic analysis of basin-fill deposits is divided into four domains, or areas: (1) northern, (2) White Wash, (3) Little Devil and (4) Canyon Sin Nombre areas (Fig. 3.2). In the northern area, deformed deposits of the Palm Spring

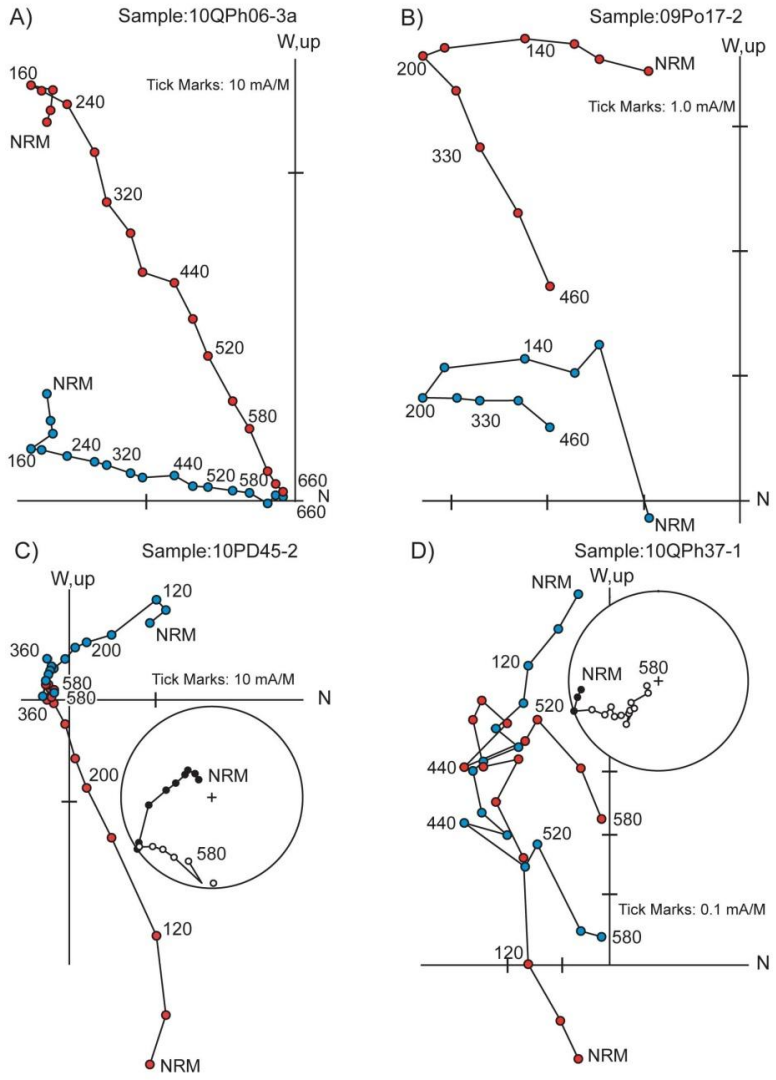

Figure 3.5. Representative orthogonal vector and equal angle projections of demagnetization data. Blue circles plot the horizontal vector projection. Red circles plot the vertical vector projection. Closed circles plot on the lower hemisphere and open circles plot on the upper hemisphere of equal angle projections. Demagnetization steps are in degrees Celsius. (A) Sites where the majority of specimens demagnetize with a second removed component (C2)of magnetization that decays linearly to the origin are categorized Class 1. (B) Sites where specimens catastrophically failed during heating but show a clear polarity based on the inclination of the C2 are labeled Class 2. (C) Sites where the majority of specimens demagnetize with a well-defined first removed component (C1) and a C2 that clusters near the origin are categorized Class 3. (D) Sites where C2 decays in a curvilinear trend and/or has variance in the measurements that prevent component estimation are classified as Class 4. NRM, natural remanent magnetization.

Group are exposed southeast and east of Whale Peak, and in a southwest-dipping homocline southeast of the June Wash fault (Fig. 3.6). The White Wash area is bracketed by the West Mesa, Salt Springs and Mesquite Oasis faults (Fig. 3.7). Sedimentary rocks in this area are exposed in steep-walled canyons along Arroyo Tapiado, and in hilly topography near White Wash.

The Little Devil area is separated from the White Wash area by a complex fault zone defined by the Salt Springs and Little Devil faults, and is bracketed to the southeast by the East Mesa fault (Fig. 3.7). The Palm Spring Group in this area is exposed in slot canyons and steep washes along Arroyo Seco del Diablo and Little Devil Wash. The Canyon Sin Nombre area contains exposures of lower Palm Spring Subgroup on the southern limb of the Carrizo syncline (Fig. 3.8). These deposits are separated from equivalent deposits to the north by Carrizo Creek and a zone of complexly-faulted, poorly exposed rocks north of Carrizo Creek (Fig. 3.2).

Northern, White Wash and Little Devil Areas

Sedimentary rocks in the Northern, White Wash and Little Devil areas were dated using new magnetostratigraphic results presented here, and through correlation to a previously published magnetostratigraphic transect (Fig. 3.9; Dorsey et al., 2011). Stratigraphic units in the Northern area correlate directly to the section of Dorsey et al. (2011), so the ages of these deposits are known. Faulting and lateral facies changes, however, prevent a direct correlation of deposits in the White Wash and Little Devil areas to those of the northern area.

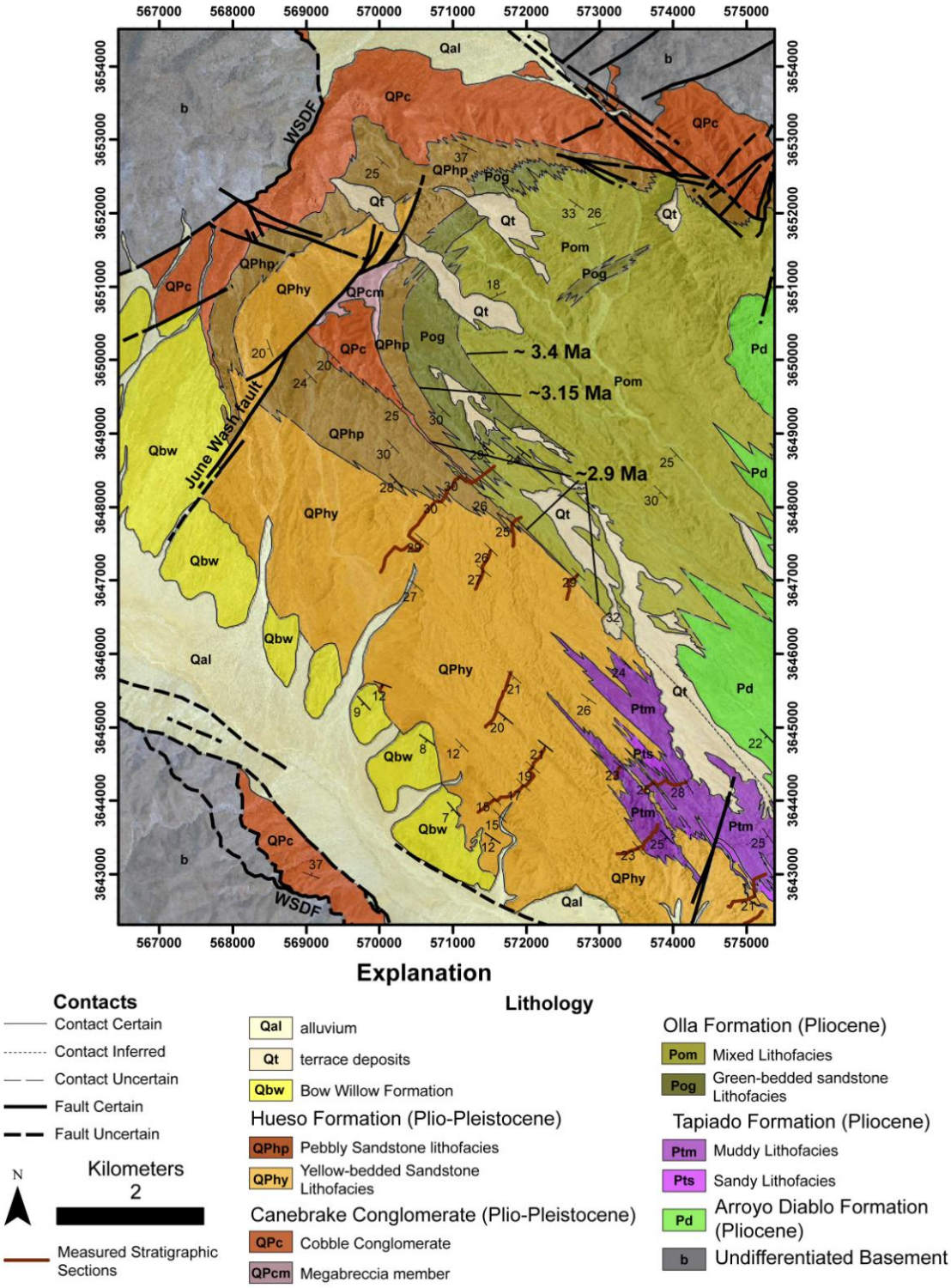

Figure 3.6. Map of Northern area showing location of measured sections and age of three datums discussed in the text.

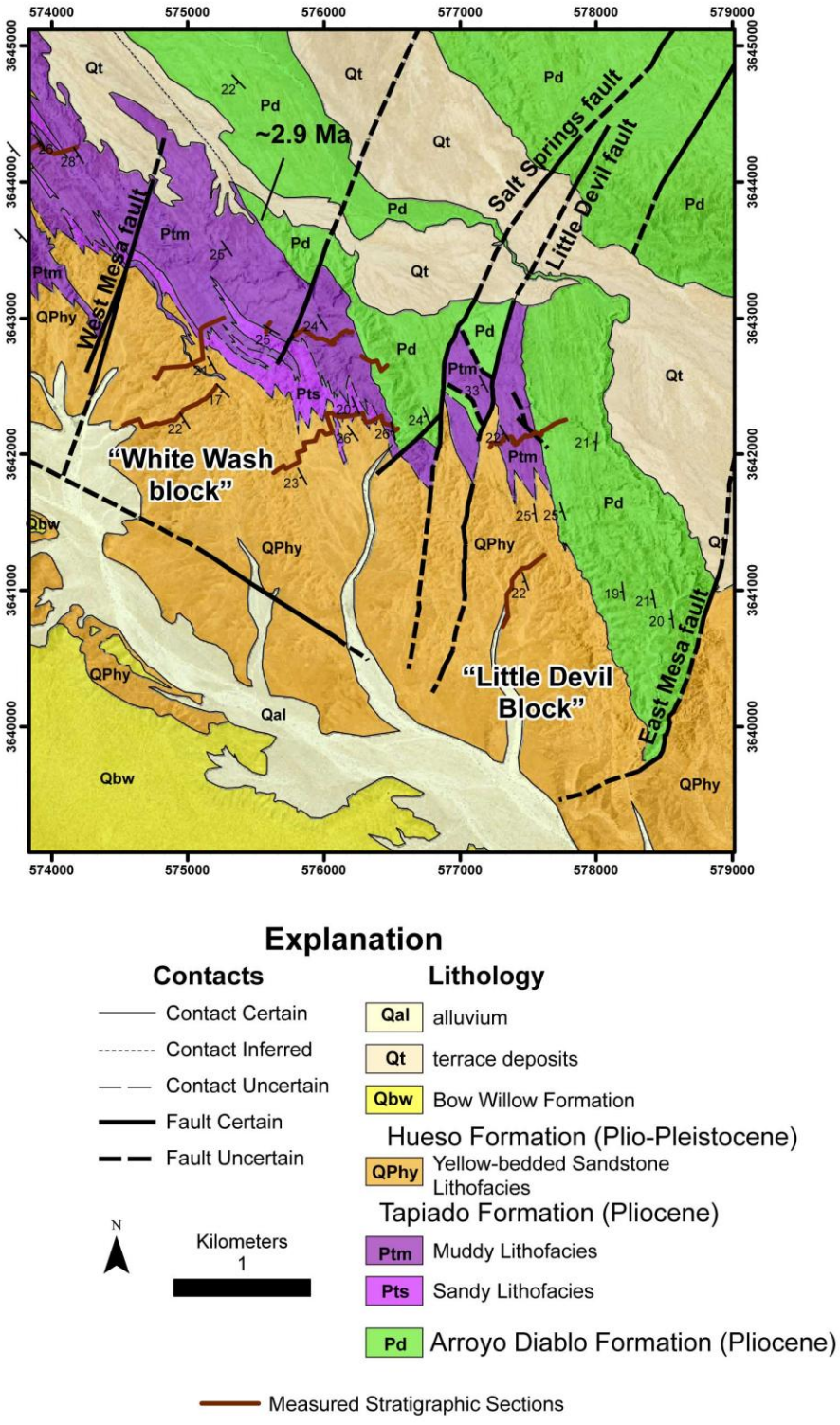

Figure 3.7. Map of White Wash and Little Devil areas showing location of measured sections.

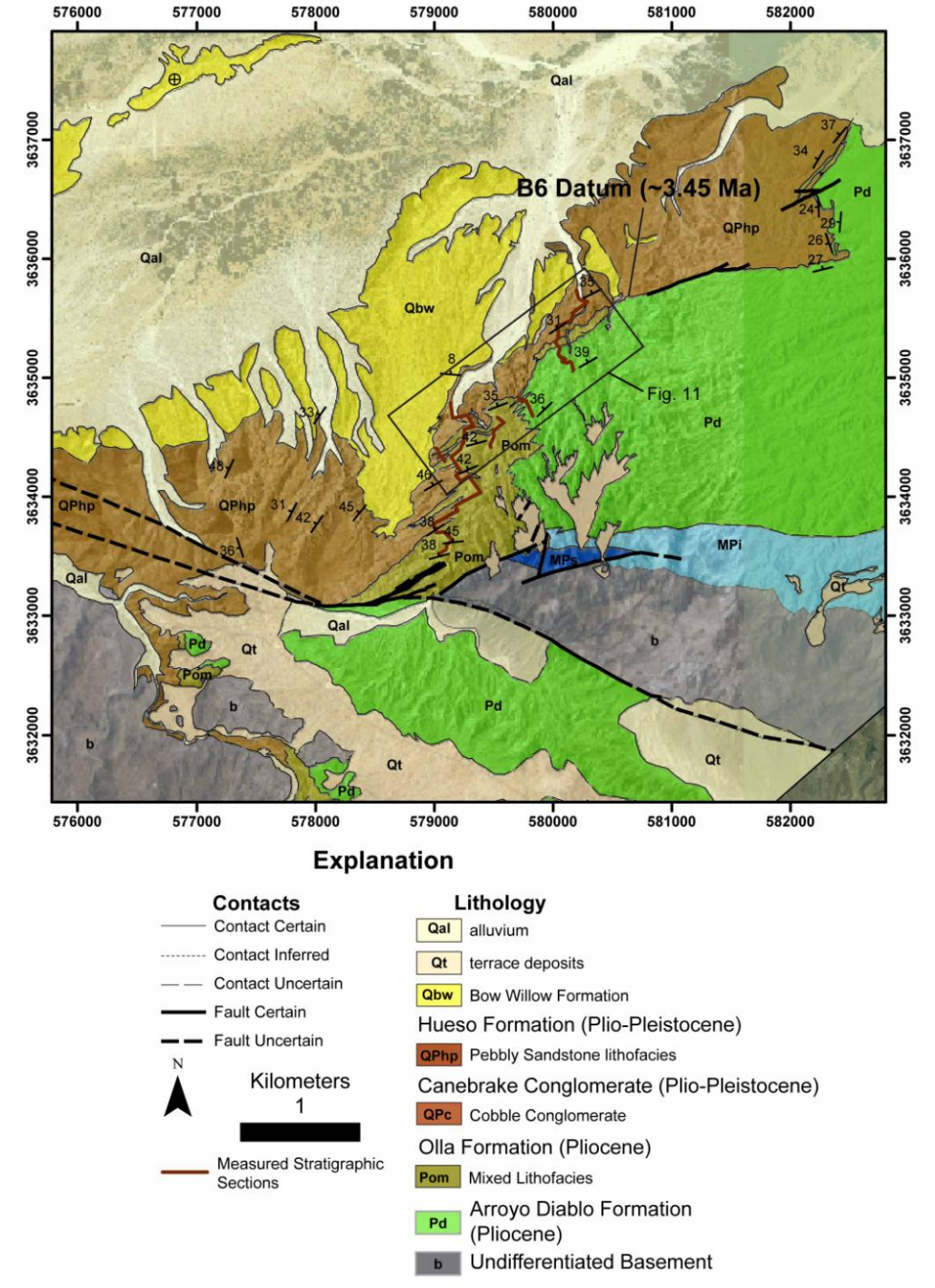

Figure 3.8. Geologic map of the Canyon Sin Nombre area showing location of measured sections and the B6 datum which records rapid progradation of the Hueso Formation ca. 3.45 Ma.

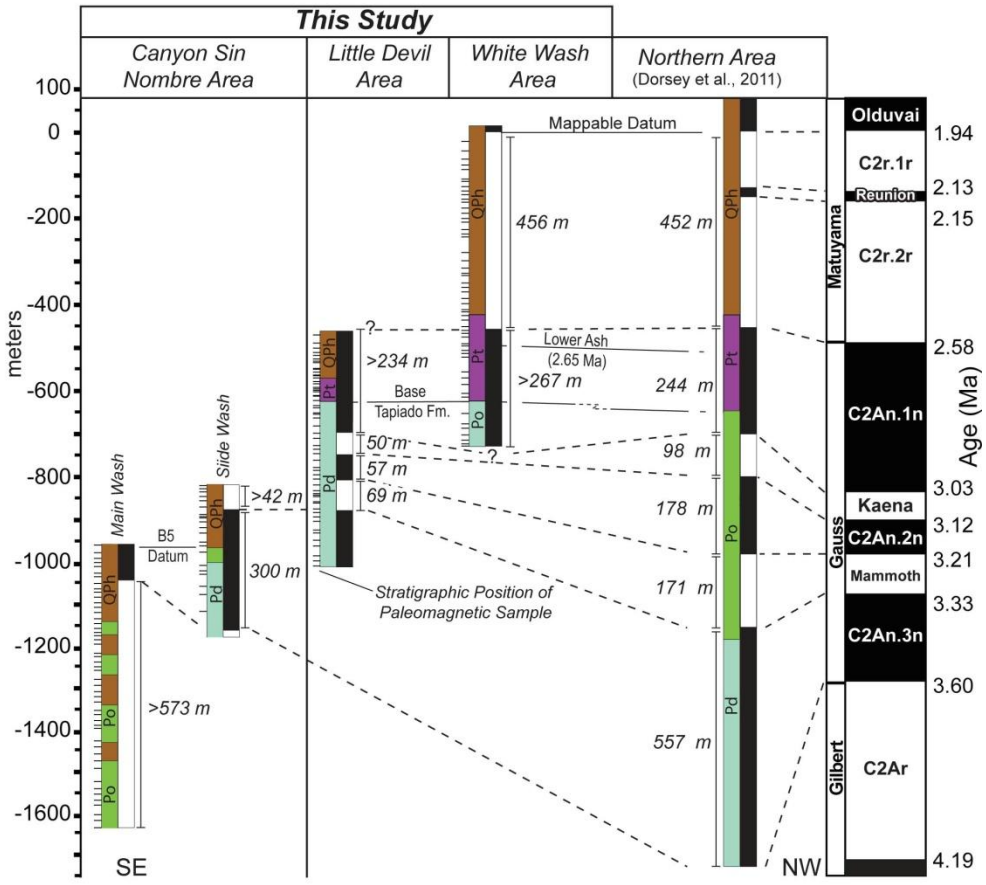

Figure 3.9. Simplified stratigraphic columns showing stratigraphic thickness, stratigraphic position of sampling sites (small tick marks) and polarity of paleomagnetic sampling transects conducted as part of this and one previous study.

In the White Wash area, 56 paleomagnetic samples define one magnetic polarity reversal in a 699 m thick section (Fig. 3.9). The lower normal interval contains a tuff dated at 2.65 ± 0.05 Ma (Dorsey et al. 2011), so the lower normal interval in the White Wash area is the C2An.1n subchron (3.03-2.58). Its base is not exposed in this area. The upper 456 m of the White Wash section consists of reversed-polarity samples that we correlate to the largely reversed part of the lower Matayama chron, below the base of the Olduvai subchron (2.58-1.94 Ma). We did not capture the short-lived Reunion paleomagnetic excursion at ca. 2.14 Ma. The top of this subchron in the White Wash area

is unconstrained with paleomagnetic sampling due to poorly-consolidated surface exposures. It was, however, identified through detailed mapping and correlation of a reference datum at the base of the Olduvai subchron in the Northern area, which allowed us to identify the top of the upper reversed interval within 10 meters (Fig. 3.9).

A composite magnetostratigraphic sampling transect in the Little Devil area contains 58 samples collected through 536.5 m of stratigraphic section (Fig. 3.9). These samples record four magnetic polarity reversals. A 234 m thick reversed polarity interval at the top of the section is interpreted to be part of the C2An.1n subchron based on the sharp contact between the Tapiado and Arroyo Diablo formations in this interval (Fig. 3.9). In descending order, the three lower intervals of 50, 57, and 69 m are interpreted to be the Kaena, C2An.2n and Mammoth subchrons, respectively (Fig. 3.9).

Canyon Sin Nombre Area

We collected 69 paleomagnetic samples from two overlapping stratigraphic sections to determine the age of deposits in the Canyon Sin Nombre area (Figs 3.10, 3.11). Our 945 m-thick sampled interval records two magnetic polarity reversals and portions of three subchrons. The thickness of our lower reversed polarity interval is unconstrained in the main Canyon Sin Nombre wash transect, but is at least 573 m thick. A normal polarity interval is partly recorded in both sections. Its full thickness was not recorded in either section, but correlation of datums between the two sections permit the thickness of this interval to be estimated at 300-310 m (Fig. 3.10). An upper reversed interval is at least 42 m thick.

Detailed analysis of the Canyon Sin Nombre area permits correlation of our section to the GPTS. We find that stratigraphic intervals thicken by almost 95% over a

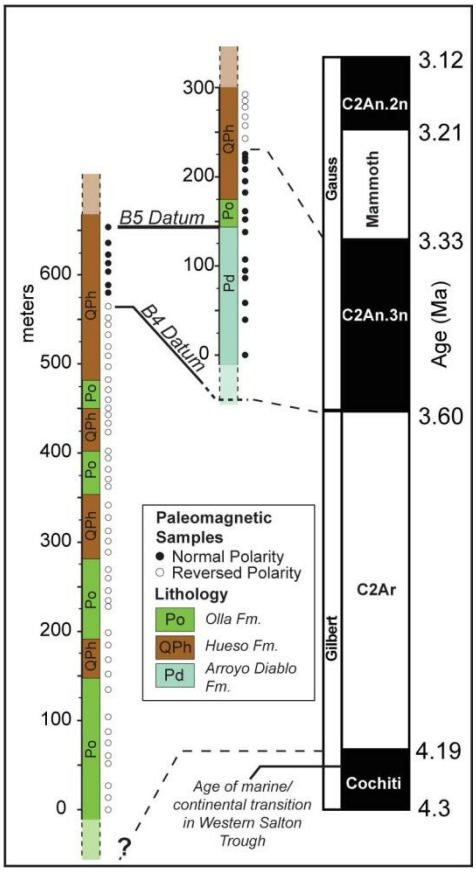

Figure 3.10. Simplified stratigraphic columns showing magnetostratigraphic correlation of two stratigraphic sections in the Canyon Sin Nombre area, the stratigraphic position and polarity of paleomagnetic samples, and our preferred correlation to the Global Paleomagnetic Time Scale (GPTS).

distance of around 1 km between the main Canyon Sin Nombre wash and the side wash transect, likely reflecting growth of folds or faults during deposition (Fig. 3.11). Despite local variations in unit thicknesses, analysis of sediment accumulation rates can aid in comparing alternative correlations to the GPTS. Figure 3.12 shows four alternative correlations of the Canyon Sin Nombre section to the GPTS. Correlation of the thick lower reversed interval to the Mammoth or Kaena subchrons produces unrealistically fast sediment accumulation rates in the two youngest alternatives (Fig. 3.12). Because the

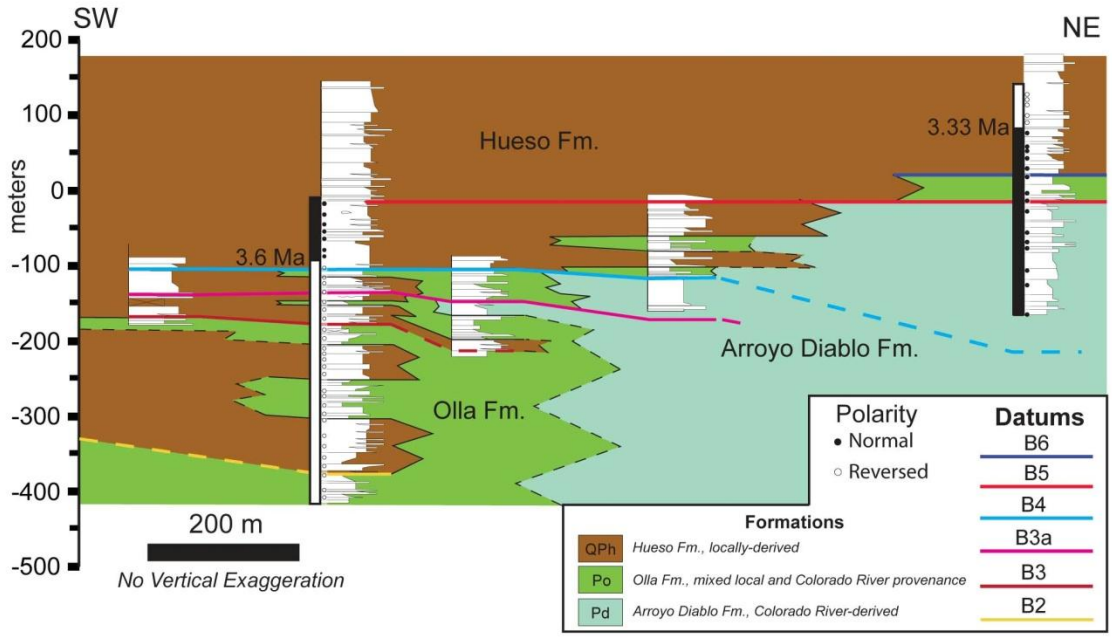

Figure 3.11. Facies panel showing correlation of five measured sections, stratigraphic position of mappable datums and position and polarity of paleomagnetic sample sites. Panel shows step-wise nature of progradation of the Hueso Formation and significant eastward stratigraphic thickening within this interval.

marine-nonmarine transition in this basin is dated at ca. 4.2 Ma (Dorsey et al., 2011), and all deposits sampled in the Canyon Sin Nombre area belong to the nonmarine Palm Spring Group, the oldest age model can be ruled out. We therefore conclude that deposits in the Canyon Sin Nombre area were deposited during the C2Ar, C2An.3n and C2An.2r subchrons of the Gilbert and Gauss magnetochrons (ca. 4.19-3.21 Ma; Figs. 3.9-3.12).

Sedimentary Lithofacies

Five formations of the Palm Spring Group in the study area are subdivided into eight lithofacies based on grain size, sedimentary structures and composition (Fig. 3.13; Table 3.2). Sedimentary deposits are grouped into two broad compositional categories:

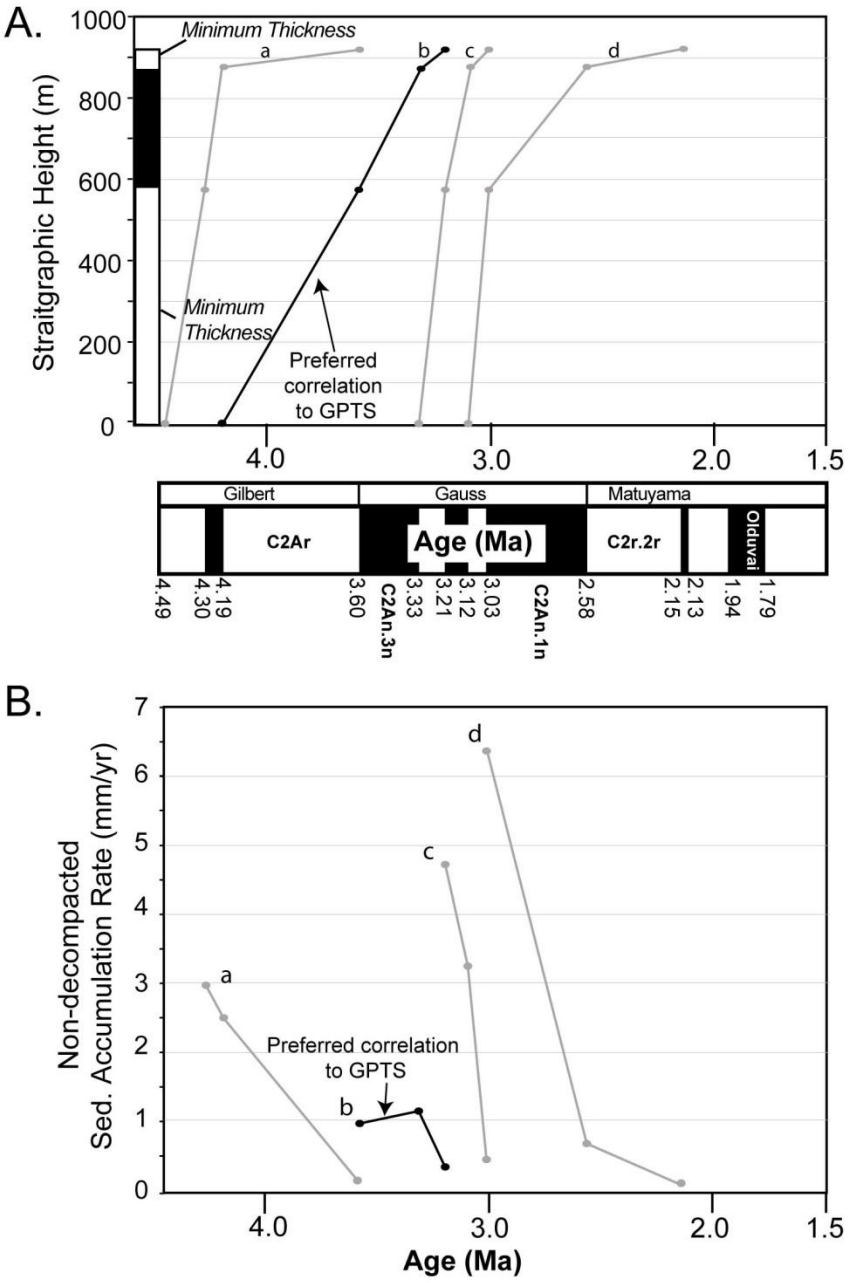

Figure 3.12. Comparison of our preferred correlation of reversal chronology in the Canyon Sin Nombre area to the Geomagnetic Polarity Time Scale (GPTS) with three alternative correlations. Stratigraphic height and thickness of polarity intervals is a composite of the two Canyon Sin Nombre paleomagnetic sampling transects. (A) Present-day stratigraphic height versus age, (B) Sediment accumulation rates (using modern-day thicknesses) versus age. The alternative correlations either yield unreasonably high sediment accumulation rates, or place non-marine Palm Spring Group strata within the time period of marine deposition in the western Salton Trough (Dorsey et al., 2011).

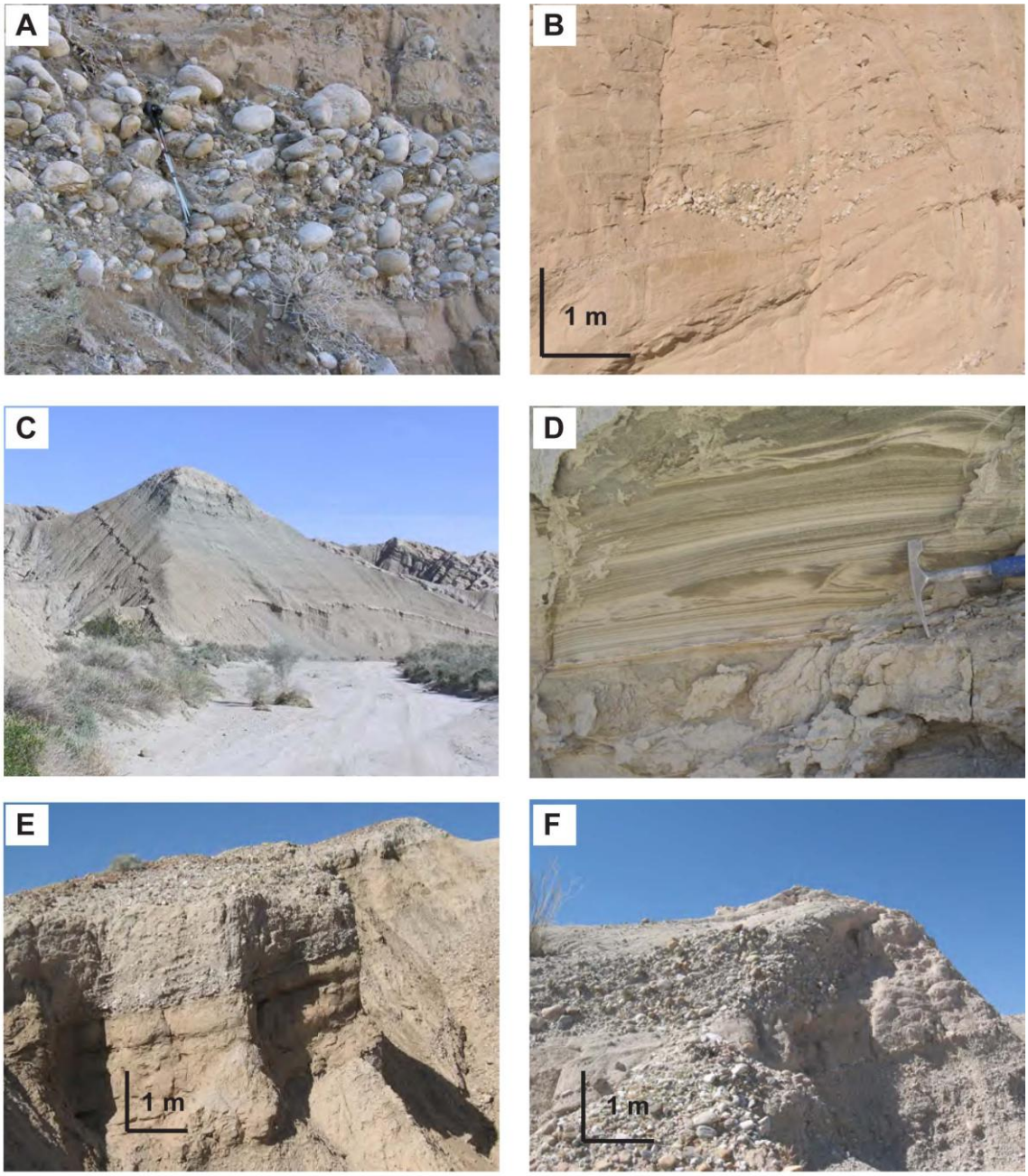

Figure 3.13. Representative field photographs of selected Palm Spring Group lithofacies. (A) Cobble to small boulder conglomerate of the clast-supported conglomerate lithofacies of the Canebrake Conglomerate. (B) Weakly stratified pebbly sandstone and interbedded lenticular imbricated cobble conglomerate in the pebbly sandstone lithofacies of the Hueso Formation. (C) Interbedded lacustrine mudstone and siltstone in the mudstone lithofacies of the Tapiado Formation. (D) Laminated fine silty sandstone in the sandstone lithofacies of the Tapiado Formation. (E) Interbedded fine, pedogenically-altered siltstone and pebbly fluvial sandstone in the yellow-bedded sandstone lithofacies of the Hueso Formation. (F) Amalgamated fluvial pebbly sandstone body in the yellow-bedded sandstone lithofacies of the Hueso Formation.

Table 3.2. Palm Spring Group Lithofacies

Lithic Designator	Lithofacies	Description	Interpretation
Qphy	Hueso Fm., Yellow-bedded sandstone lithofacies	Interbedded: (1) 20-80 cm thick fining-upward tabular beds of moderately-sorted yellow L-suite siltstone to medium-grained sandstone with well-developed calcic pedogenic horizons and(2) Trough cross-bedded to horizontally-stratified moderately-sorted local-suite pebbly sandstone to pebble conglomerate. Pebbly deposits are present in isolated, lenticular beds 0.5-1 m thick as well as in amalgamated intervals 3-10 m thick which are laterally-continuous over several kilometers. Pebbly deposits grade upwards to finer-grained units.	Deposition in channel belts and flooplains by a migrating fluvial system with frequent overbank sheet floods.
Pts	Tapiado Fm., sandstone lithofacies	Moderately- to well-sorted fine to mediugm grained biotite-rich laminated to ripple cross laminated sandstone in beds 10-30 cm thick. Climbing ripple cross-laminae transition to planar laminae. Interbeds of well-sorted massive to trough cross-bedded medium-grained to granular coarse sandstone in beds 20-200 cm thick. Rarely contains poorly-devloped pedogenic horizons. Subordinate thin beds of red, highly-oxidized sandy siltsone.	Deltaic deposition in a marginal lacustrine setting.
Ptm	Tapiado Fm., mudstone lithofacies	Laminated green to brown laminated silty local-suite claystone and argillaceous marlstone interbedded with thin beds of massive siltstone in sharp-based ungraded to upward-coarsening packages 3-20 m thick. Abundant secondary gypsum. Color transition from brown low in each mudstone package to green high. Marlstone concentrated in green intervals. Freshwater ostracode fossils (Cosma, 2002). Distinctive convolute "rolls" within siltstone bedsets.	Suspension settling of fine-grained material in a lacustrine setting. Siltstone interbeds record intermittent weak density underflow currents along lake bottom. Up-section change from brown to green color records transition from oxic to anoxic conditions.
Qpcx	Canebrake Cgl., megabreccia lithofacies	Single 0-50 m thick package of clast-supported, cobble to large boulder (>5 m diameter) breccia exposed in the hinge of the Diablo Anticline southeast of the June Wash Fault. 100% La Posta-type tonalite clast population.	Rock Avalanche

Table 3.2. continued.

Lithic Designator	Lithofacies	Description	Interpretation
Qpcc	Canebrake Cgl., clast-supported conglomerate lithofacies	Ungraded, massive to horizontally-stratified moderately-sorted clast-supported local-suite pebble to boulder conglomerate in beds 0.2-2 m thick. Uncommon inversely-graded, well-sorted small boulder conglomerate in beds 2-3 m thick. Present along basin margins near the West Salton Detachment Fault. Laterally-gradational with QPhp lithofacies.	Sheet flood and uncommon debris flow deposition in the proximal part of alluvial fan systems.
QPhp	Hueso Fm., pebbly sandstone lithofacies	Crudely horizontally-stratified, poorly-sorted medium- to coarse-grained local-suite pebbly sandstone in tabular beds 20-80 cm thick. Present in amalgamated units 2-15 m thick with sharp, erosional bases and fining-upwards profiles. Interbedded with lenticular beds of imbricated pebble/cobble conglomerate. Rare boulder conglomerate.	Sheet flood deposition in medial to distal alluvial fans. Uncommon channelized flows on sheet surfaces. Amalgamated fining-upward packages record autocyclic migration of fan lobes.
Pog	Olla Fm., green-bedded sandstone lithofacies	Tabular beds of moderately-sorted green local-suite fine-grained sandstone and green-gray mudstone. interbedded with lenticular beds of pebbly L-suite sandstone. Both calcic and vertic pedogenic features in fine-grained strata. Finer-grained than the yellow-bedded lithofacies of the Hueso Fm.	Deposition from traction transport and suspension settling in channels and low-gradient floodplains. Green color reflects early diagenesis in a water-logged setting.
Pom	Olla Fm., mixed lithofacies	Interbedding of C-suite and L-suite detritus. Pd-type lithofacies incorporate abundant re-worked local-suite material (>20% of total). Interbedding of mixed-provenance Pd and 100% L-suite Pog and Qphp lithofacies.	Interaction between Colorado River delta fluvial channels and marginal basin localsuite depositional systems.
Pd	Diablo Fm.	Fining-upward successions 5-10 m thick of fine-grained Colorado-suite sandstone and interbedded red mudstone. Sandstones are cross-laminated to cross-bedded and have sharp, erosional bases and channel-form geometry. Mudstones contain abundant pedogenic features. Sandstones contain <20% reworked L-suite detritus.	Meandering fluvial deposition on the Colorado River delta plain.

Colorado River-derived and locally-derived (e.g. Winker, 1987). Colorado-suite deposits are dominated by well-rounded fine-grained sand with pink-stained quartz and interbedded red clay and silt, whereas local-suite deposits contain metamorphic and plutonic clasts, angular grains of plutonic quartz and plagioclase, and distinctive abundant small flakes of detrital biotite.

Locally-Derived Deposits

Analysis of conglomerate clast composition and paleocurrent trends, and comparison to regional geology, reveals three distinctive sub-populations of local-suite detritus in the Palm Spring Group: (1) a monomict tonalite-clast population in fault-proximal conglomerate along the basin margins, derived from the footwall of the West Salton Detachment fault; (2) a northern suite of polymict clast conglomerate derived from the ancestral Vallecito Creek; and (3) a southern suite of polymict clast conglomerate derived from the ancestral Carrizo Creek (Table 3.2; Fig. 3.14). Tonalite clasts in monomict fault-proximal conglomerates are leucocratic with abundant quartz and plagioclase grains and are interpreted to be derived from the Late Cretaceous La Posta tonalite, which makes up the footwall of the West Salton detachment fault in the Vallecito Mountains north of the basin (Todd, 2004). Deposits containing this population include fault-proximal alluvial fan facies of the Canebrake Conglomerate and Hueso Formation, and the tonalitic megabreccia of the Canebrake Conglomerate (Fig. 3.6). Polymict conglomeratic facies in the northern part of the study area show overall transport to the east-southeast and are distinguished by abundance of Granite Mountain-

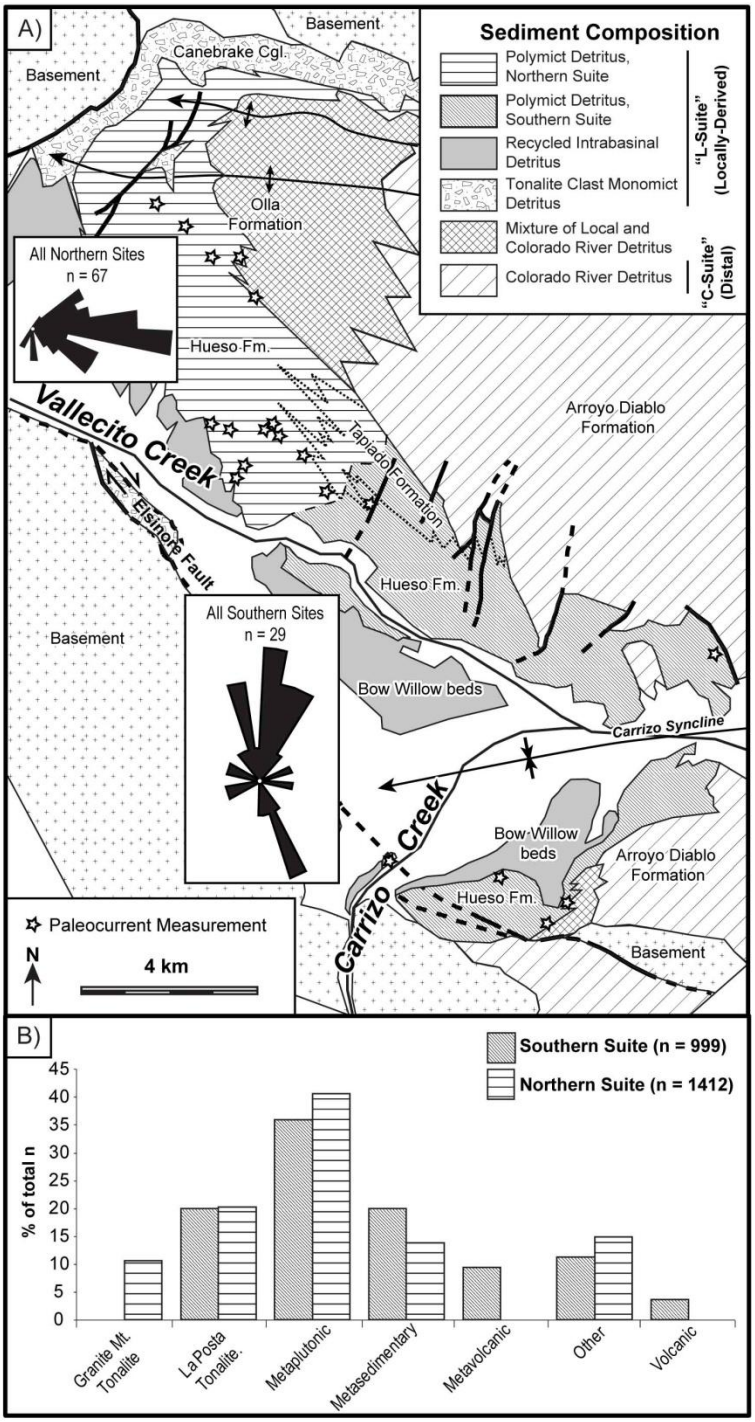

Figure 3.14. (A) Map showing distribution of sediment composition types in strata within the Fish Creek-Vallecito basin. (B) Graph of normalized abundances of conglomerate clast populations from the northern and southern suites of polymict conglomerate.

type tonalite and lack of volcanic and metavolcanic clasts (Fig. 3.14). This population was derived from a source that was similar to the modern catchment of Vallecito Creek (Fig. 3.15). Polymict conglomeratic deposits in the southern part of the study area display sediment transport toward the north-northwest. They lack clasts of Granite Mountain-type tonalite, and contain distinctive black vesicular basalt, basaltic andesite, and well-indurated porphyritic rhyolite (metavolcanics). We suggest that the vesicular basalt and basaltic andesite clasts in the southern suite were derived from the Miocene Alverson Andesite and Jacumba Volcanics, which are presently exposed south of the study area within the drainage of Carrizo Creek (Fig. 3.15; Dibblee, 1954; Gastil, 1979). Well-indurated metavolcanic rhyolite clasts are likely recycled from the Eocene Poway Conglomerate, which is currently exposed in a southwest-trending belt just south of the U.S.-Mexico border (Fig. 3.15; Abbott, 1978; Kies, 1983). This clast population includes rare reworked marine bivalve fossils that are likely reworked out of the marine Imperial Group. Exposures of metamorphic rock and La Posta-type tonalite are widespread across the study region (Fig. 3.15), as is reflected by ubiquitous quartzite, schist, gneiss, amphibolite and metaplutonic clasts in both the northern and southern suites of polymict conglomerate (Fig. 3.14).

Physical Stratigraphy and Basin Architecture

Lower Palm Spring Subgroup

The lower Palm Spring Subgroup is dominated by fluvial deposits of the Arroyo Diablo Formation, which accumulated in meandering channels and floodplains of the lower Colorado River fluvio-deltaic system (Winker, 1987). In most of the basin these

deposits conformably overlie the marine Imperial Group. The contact between the Imperial and Palm Spring groups is well dated at ~4.2 Ma (Dorsey et al., 2011). Near Canyon Sin Nombre, the Olla and Arroyo Diablo formations are in depositional contact with metamorphic basement (Figs. 3.4, 3.8).

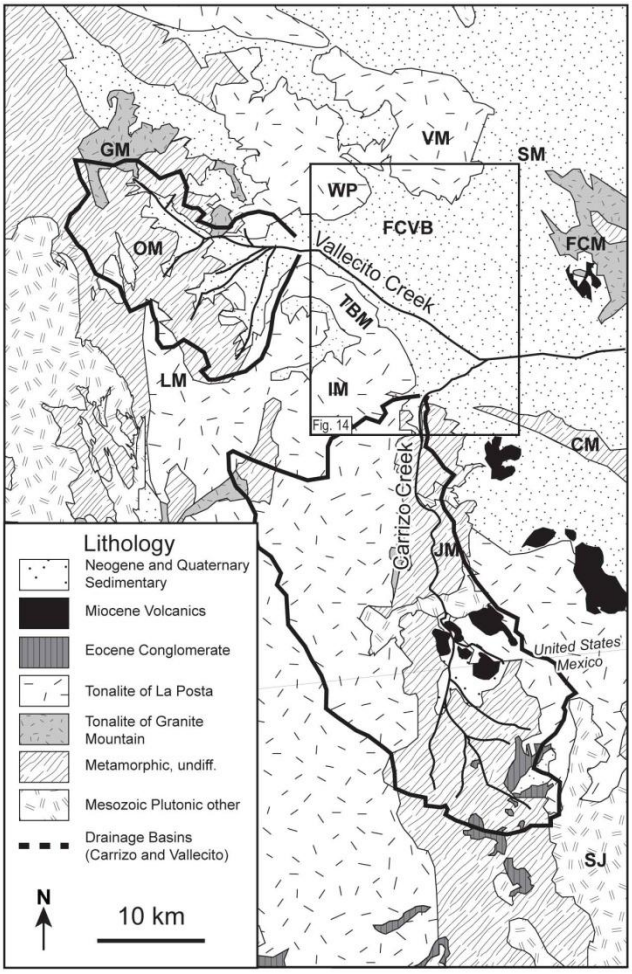

Figure 3.15. Geologic map showing bedrock types and drainages for Carrizo and Vallecito creeks. CM: Coyote Mountains; FCM: Fish Creek Mountains; FCVB: Fish Creek-Vallecito Basin; GM: Granite Mountain; IM: In Ko Pah Mountains; JM: Jacumba Mountains; LM: Laguna Mountains; OM: Oriflamme Mountain; SJ: Sierra Juarez; TBM: Tierra Blanca Mountains; WP: Whale Peak. Adapted from (Gastil, 1971; Grove, 2003; Kairouz, 2005; Rogers, 1966; Strand, 1962; Todd, 2004).

Locally-derived facies of the lower Palm Spring Subgroup make up three distinct clast populations: (1) monolithologic tonalite, (2) northern suite polymict, and (3) southern suite polymict (see above). Monolithologic tonalite-clast deposits make up a thick, areally restricted belt proximal to the West Salton detachment fault along the northern basin margin. These deposits are found in both the lower and upper Palm Spring subgroups and define a persistent retrogradational relationship relative to other basin-fill deposits (Fig. 3.4).

In the northern part of the study area, polymict detritus from the ancestral Vallecito Creek catchment is present in the Olla and Hueso formations. A change from fluvial to distal fan lithofacies is recorded in these deposits at ~3.15 Ma. In the southern part of the study area, polymict detritus from the ancestral Carrizo Creek drainage is present in distal fan facies of the Hueso Formation. About 5 km of northwestward progradation is recorded in this Carrizo Creek deposystem, and occurred in two phases: (1) moderate, step-wise progradation between ~4.0 and 3.45 Ma; and (2) abrupt basinward progradation of the Hueso Formation at about 3.45 Ma along the B6 datum (Figs. 3.8, 3.11).

Contact between Lower and Upper Palm Spring Subgroups

The contact between the lower and upper Palm Spring subgroups marks a dramatic change in stratal architecture. This contact is dated here at 2.9 Ma, and is defined by the sharp base of the Tapiado Formation and equivalent contact between the Arroyo Diablo Formation and overlying Hueso Formation (Fig. 3.4, 3.16). Above this contact, Colorado River-derived sediment is absent from deposits in the study area.

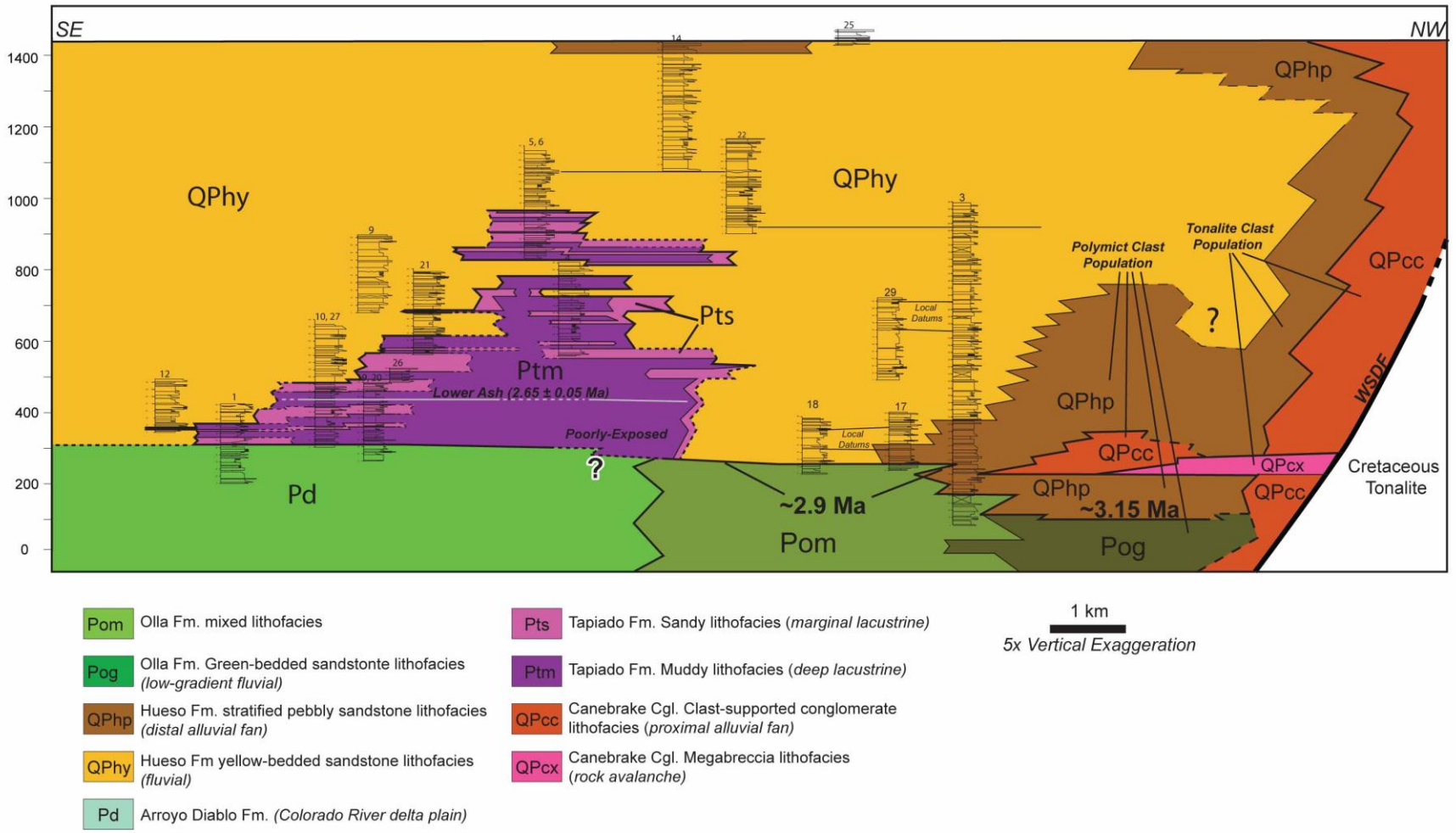

Figure 3.16. Panel showing stratigraphic thicknesses, relative position, correlation and interpreted lithofacies of fifteen measured sections the in the Little Devil, Northern and White Wash areas.

Sedimentary rocks in the Canyon Sin Nombre area are older than this contact (Fig. 3.4) and therefore do not record the transition at 2.9 Ma.

Lacustrine deposits of the Tapiado Formation directly overlie the Arroyo Diablo Formation in the central part of the basin. These strata contain thick (5-20 m) intervals of marly, laminated, ostracode-bearing mudstone and siltstone (Cosma, 2002). Interbedded with these deep lacustrine deposits are rippled fine to medium-grained sandstones recording marginal lacustrine deposition in small deltas (Fig. 3.16).

The base of the upper Palm Spring Subgroup records major expansion of locally-derived clastic deposits from both northern and southern sources. In the northern area, a thick interval (~120 m) of cobble conglomerate directly overlies this contact (Fig. 3.16). The conglomerate contains polymict clasts with Vallecito Creek affinities and onlaps the upper surface of a 40-60 m thick monolithologic, tonalite-clast megabreccia. Where alluvial fan and lacustrine lithofacies are absent, sandy fluvial deposits of the Hueso Formation make up the base of the upper Palm Spring Subgroup (Fig. 3.16). These deposits contain northern suite polymict clast populations in the northern area, and southern suite clast populations in the White Wash and Little Devil areas.

Upper Palm Spring Subgroup

The upper Palm Spring Subgroup is dominated locally derived deposits that display an upsection decrease of fanglomerates in the northern basin, with complex interfingering of lacustrine, marginal lacustrine and fluvial lithofacies in the central area (Figs. 3.4, 3.16). Above the base of the upper Palm Spring Subgroup, Vallecito Creek-derived cobble conglomerate deposits step backwards to the northwest (Figs. 3.6, 3.16)

and fine up-section. In the uppermost Palm Spring Group, deposits derived from Vallecito Creek are exclusively fluvial sandstone of the Hueso Formation.

The maximum along-strike extent of lacustrine facies is seen near the base of the Tapiado Formation, in deposits ranging from about 2.9 to 2.5 Ma. In deposits dated between ~ 2.2 and 2.05 Ma, lacustrine facies are areally restricted to absent. An upper interval of lacustrine deposits is centered slightly north of the lower interval, and ranges in age from ~2.05 to 1.85 Ma. Lacustrine facies are absent in deposits younger than ~1.85 Ma, (Fig. 3.16). The upper Palm Spring Subgroup in the northern area is overlain along a progressive unconformity by the Bow Willow beds, an informal unit that contains sandstone clasts recycled from the Palm Spring Group and is dated at about 1.0 Ma (Dorsey et al., 2012).

DISCUSSION

Lower Palm Spring Subgroup

The lower Palm Spring Subgroup in the Fish Creek-Vallecito basin records interaction between three depositional systems: (1) fine-grained deposits of the lower Colorado River in the Salton Trough; (2) steep, monomictic gravelly alluvial fans derived from the uplifting lower plate of the west Salton detachment fault at Whale Peak; and (3) polymictic, sand-rich alluvial-fan and fluvial systems sourced in the Peninsular Ranges highlands that prograded into the basin from the north and south (Fig. 3.17). The persistent retrogradational relationship of fault-proximal alluvial fan deposits along the northern basin margin (Fig. 3.4, 3.16), reflects long-term slip on the detachment fault, which caused the sediment source to shift progressively west relative to the basin through

time. The absence of an analogous fanglomerate belt along the southern basin margin reflects subdued topography in the footwall in the south during deposition of the lower Palm Spring Subgroup, likely due to reduced offset on the detachment fault toward its southern termination (Fig. 3.17). The ancestral Carrizo Creek in the south and Vallecito Creek in the north delivered alluvial fans that, along with their downstream fluvial equivalents, prograded across basin margins during the time interval ~4.0 to 2.9 Ma.

Vallecito Fan

Paleocurrent data in the northern part of the study area show that the ancestral Vallecito Creek entered the basin south of Whale Peak, near the present day course of Vallecito Creek (Figure 3.17). This suggests that the Vallecito Creek drainage has not changed significantly since the end of Palm Spring Group deposition at ca. 1 Ma, in spite of a major tectonic reorganization in basin-bounding faults beginning ~1.2 Ma (Dorsey et al., 2012). The ca. 3.4-Ma base of fluvial green-bedded sandstone in the Olla Formation records the earliest input from the Vallecito Creek deposystem. The transition from these fluvial deposits to distal alluvial fan facies of the Hueso Formation records the emergence of the Vallecito fan at about 3.15 Ma. Vallecito Creek enters the Fish Creek-Vallecito basin along the axis of an east-trending synformal corrugation in the trace of the West Salton detachment (Dorsey et al., 2012). Late Pliocene east-directed drainage in the nortehrn area likely was controlled by development of this synform, as seen in other supradetachment basins (e.g. Friedmann and Burbank, 1995; Friedman et al., 1996).

Progradation of the northern (Vallecito) deposystem is best explained by slowing of tectonic subsidence in the basin. The first appearance of distal pebbly sandstone facies,

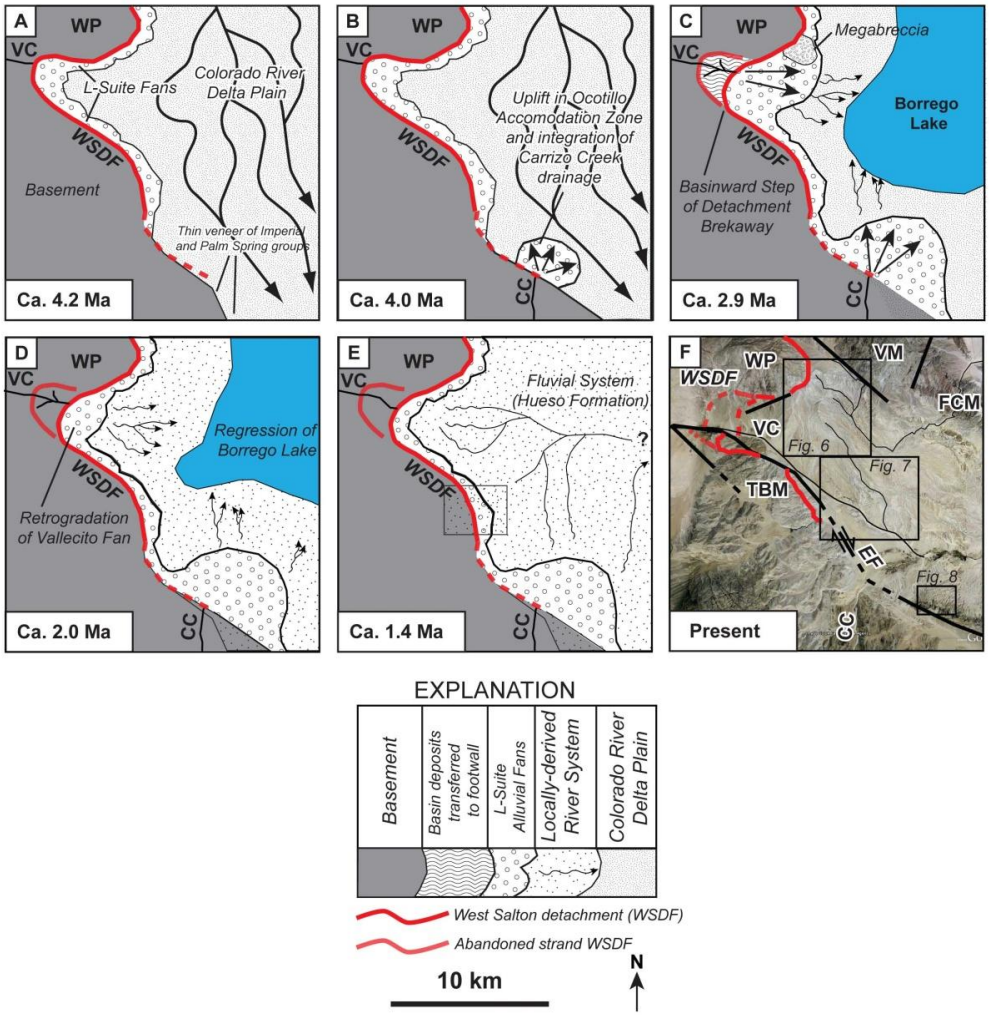

Figure 3.17. Paleogeographic reconstructions illustrating the evolution of the Fish Creek-Vallecito basin. (A) Map showing the configuration of the basin ca. 4.2 Ma, just after the progradation of the Colorado River delta across the western Salton Trough and above the contact between the marine Imperial Group and non-marine Palm Spring Group. (B) Map showing the configuration of the basin ca. 3.4 Ma showing the development of a fluvial system fed by the ancestral Vallecito Creek and rapid progradation of an alluvial fan fed by ancestral Carrizo Creek. (C) Map showing the configuration immediately following basin reorganization ca. 2.9 Ma. (D) Map showing the configuration of the basin ca. 2.0 Ma showing retrogradation of Vallecito alluvial fan and regression of Borrego Lake. (E) Map showing the configuration of the basin ca. 1.4 Ma. By this time, regression of Borrego Lake was complete and fluvial systems fed by ancestral Vallecito and Carrizo creeks deposited sediment across the basin. (E) Present configuration of the Fish Creek-Vallecito area, showing major post-1.2 Ma faults. CC, Carrizo Creek; EF, Elsinore fault; FCM, Fish Creek Mountains; TBM, Tierra Blanca Mountains; VC, Vallecito Creek; WP, Whale Peak; WSDF, West Salton detachment fault.

dated at 3.15 ± 0.03 Ma (Fig. 3.6, 3.16), coincides with a recently documented decrease in subsidence rate from 2.1 to 0.4 mm/yr at ca. 3.1 Ma (Dorsey et al., 2011). Previous studies have shown that slowing of subsidence can drive progradation of coarse sediment through reduction in the rate of production of accommodation space (e.g. Blair and Bilodeau, 1988; Heller and Paola, 1992; Paola et al., 1992). Because the up-section *increase* in grain size coincides with a *decrease* in subsidence rate, and based on principles of mass balance and sediment continuity (Paola et al., 1992), we conclude that this progradational trend resulted from slowing of tectonic subsidence rate at ca. 3.1 Ma. Following 3.1 Ma, distal fan facies of the Hueso Formation coarsen upward and expand to the southeast, indicating continued progradation for ~ 200 k.y. in response to the decrease in rate of production of accommodation space.

Carrizo Fan

The apex of the Carrizo fan was located near the mouth of the present-day Carrizo Canyon (Fig. 3.17). The oldest exposures of conglomerate derived from this source presently lie ~4 km ESE of the mouth of Carrizo Canyon (Figs. 3.2, 3.8). Restoring 1-2 km of dextral offset from the Elsinore Fault (Lampe, 1988; Grove *et al.*, 2003; Dorsey *et al.*, 2012) places these deposits NNE of the mouth of the canyon, consistent with north-northeast directed paleocurrents and modern geography. The oldest deposits of progradational Carrizo Creek-derived alluvial fans are ~575 m below the base of the Gauss chron (3.6 Ma) (Fig. 3.10). South of the Elsinore Fault, Carrizo Creek-derived detritus is absent, and deposits of the Arroyo Diablo Formation lie in depositional contact on metamorphic basement. This indicates that the southern basin was starved of locally-derived sediment for some time after 4.2 Ma (end of marine deposition). The age for

onset of Carrizo fan growth is thus conservatively estimated to be 4.0 ± .2 Ma. Stepwise progradation and up-section increase in grain size in the Hueso Formation record the continued growth of the Carrizo fan through the entire time recorded in Canyon Sin Nombre deposits (~4.0 to 3.2 Ma), with a large basinward step at ca. 3.45 Ma (Figs. 3.4, 3.8).

In contrast to the northern part of the study area, slowing of subsidence rate cannot explain progradation of sand and gravel seen in the southerly-derived Carrizo alluvial fan. In the Canyon Sin Nombre area, progradation of the Carrizo fan pre-dates the 3.1-Ma decrease in subsidence rate by ~350-900 k.y. Deposits are thinner at Canyon Sin Nombre than equivalent strata in the northern area, suggesting that subsidence rates were overall slower in this area. This likely reflects the location of Canyon Sin Nombre near the southern termination of the West Salton detachment fault (Axen and Fletcher, 1998; Dorsey *et al.*, 2012). While slowly subsiding basins are expected to have comparatively larger alluvial fans than those formed in rapidly subsiding basins (Leeder and Gawthorpe, 1987; Whipple and Trayler, 1996; Allen and Hovius, 1998; Allen and Densmore, 2000), an actual *change* to slower subsidence rate is required to drive progradation of coarse facies across finer-grained deposits in a subsidence-driven sytem (Paola *et al.*, 1992).

Progradation of sand and gravel in the Canyon Sin Nombre area during a time of constant subsidence must have been driven instead by an increase in sediment flux from the Carrizo Creek drainage. The timing of coarse sediment progradation (ca. 4.0 to 3.2 Ma) corresponds to a hypothesized global increase in sediment flux between 4 and 2 Ma (Zhang *et al.*, 2001; Molnar, 2004; Huntington *et al.*, 2006). If progradation of the

Carrizo fan was caused by increased sediment discharge due to global climate change, bedrock erosion rates in the ancestral Carrizo and Vallecito creek catchments should have increased between 4 and 2 Ma. However, recent analysis of cosmogenic radionuclides in the same section, reveals no increase in bedrock erosion during this time interval in either of the paleo-drainages, and a net decrease in paleo- erosion rates in the ancestral Vallecito Creek drainage between ca. 3.5-2.5 Ma (Longinotti *et al.*, 2011; Peryam *et al.*, 2010).

We therefore suggest that increasing sediment flux from Carrizo Creek resulted from an increase in the *area* of the Carrizo Creek catchment in the Peninsular Ranges highland, likely in response to early Pliocene uplift and regional tilting in the Ocotillo accommodation zone. The Ocotillo accommodation zone is a little-studied tectonic domain that separates the northern Peninsular Ranges, where the basin-bounding West Salton detachment fault dips east beneath the Salton Trough, from the Sierra Juarez region where the Cañada David detachment fault dips west beneath Laguna Salada and the southern Peninsular Ranges (Fig. 3.1; Axen, 1995; Axen and Fletcher, 1998). Our data suggest that uplift and/or tilting in the Ocotillo accommodation zone likely caused expansion of the ancestral Carrizo Creek drainage, thus increasing the rate of sediment delivery to the southwestern Fish Creek-Vallecito basin. Tectonic adjustments in this area resulted in uplift and erosion of fossiliferous deposits in the Imperial Group. Abrupt progradation of the Carrizo Creek alluvial fan at 3.45 Ma may record capture and redirection of an upland stream, resulting in an abrupt, one-time increase in sediment flux. Deposits of the Hueso Formation coarsen up-section above that horizon, and record

continued growth of the Carrizo fan through the stratigraphic interval exposed in the Canyon Sin Nombre area (Fig. 3.17).

Basin Reorganization at 2.9 Ma

The sharp contact between the lower and upper Palm Spring subgroups records a major reorganization of lithofacies and depositional systems in the Fish Creek – Vallecito basin at 2.9 Ma. This singular event in the basin history resulted from simultaneous transgression of a large regional lake, abrupt progradation of Vallecito and Carrizo creek deposystems, and emplacement of a megabreccia derived from the footwall of the West Salton detachment fault at Whale Peak.

Transgression of Borrego Lake

Fine-grained lake deposits of the Tapiado Formation in the Fish Creek-Vallecito basin record transgression of a large regional lake at ca. 2.9 Ma (Fig. 3.17). The first appearance of lake facies in the study area corresponds in time with the 2.9-Ma base of the lacustrine Borrego Formation in the Borrego Badlands (Housen and Dorsey, 2010). In contrast to the Tapiado Formation, the Borrego Formation is gradational with the underlying Arroyo Diablo Formation and is dominated by C-suite red mudstone (Dibblee, 1984; Reitz, 1977; Lutz *et al.*, 2006; Kirby *et al.*, 2007). These differences led Winker (1987) to suggest that the Tapiado Formation accumulated in a lake that was isolated within the Fish Creek-Vallecito sub-basin. More recently, however, workers have found that the western Salton Trough was a large contiguous supradetachment basin until ca. 1.2-1.0 Ma (Steely *et al.*, 2009; Janecke *et al.*, 2010; Dorsey *et al.*, 2012). Thick (30-150 m) intervals of deep lacustrine to prodelta deposits in the Tapiado Formation (Fig. 3.13) imply that the lake had relatively deep water and was perennial over long time

periods (10^4 yrs). We therefore conclude that similar-age lacustrine deposits in the Borrego and Fish Creek-Vallecito basins were deposited in a single, regionally-extensive lake that we call Borrego Lake. Our analysis suggests that rapid formation of Borrego Lake produced an immediate and dramatic increase in accommodation space in the Salton Trough that resulted in trapping of Colorado River sediment north or northeast of the study area. The Carrizo and Vallecito Creek drainages delivered locally derived sediment into a newly formed lake margin that was starved of Colorado River sediment due to its position on the far western side of the Salton Trough depocenter, far from the mouth of the Colorado River (Fig. 3.1). Rapid lake transgression thus created the sharp contact between Colorado-derived fluvial deposits of the Arroyo Diablo Formation and locally-derived lacustrine deposits of the Tapiado Formation.

We infer that this large, regional lake likely resulted from tectonically controlled creation of a dam somewhere in the southern Salton Trough. An increase in river water discharge could not have impounded water in the Salton Trough because of its connection to the northern Gulf of California. Facies relationships and paleocurrent data show that the mouth of the Colorado River was located northeast of the modern Salton Sea around 3-4 Ma (Winker and Kidwell, 1986; Dorsey *et al.*, 2005), and therefore the Colorado River delta itself could not have created a low topographic barrier in the southeast as seen in the modern setting (Fig. 3.1). Lake transgression at 2.9 Ma due to an increase in subsidence rate (e.g. Blair and Bilodeau, 1988) is incompatible with known basin-subsidence trends, which show stable subsidence rates in the study area during the interval 3.1 to 0.95 Ma (Dorsey *et al.*, 2011). Thus, unlike the modern setting, we infer that Borrego Lake was separated from the northern Gulf of California by a low

topographic barrier that was created by tectonic uplift in the Mexicali Valley, southeast of the modern Salton Sea (Fig. 3.1).

A structural control on damming of Borrego Lake waters is conjectural, but consistent with data from northern Mexico. Pliocene-Pleistocene (post-Imperial Formation) conglomerate exposed in the (now uplifted) Lopez Mateos basin in the Sierra El Mayor, NE of Laguna Salada (Fig. 3.1), records transport of volcanic- and crystalline-clast gravel to the west and WSW (Axen and Fletcher, 1998) from an easterly source. This requires the presence of basement exposures in a topographic highland that was located east of the Sierra El Mayor, likely in the area now occupied by the Mexicali Valley, during conglomerate deposition (which is bracketed between ~4.2 and 1.2 Ma). A 1.4-Ma andesite encountered at 3.7 km depth in a well in the Mexicali valley (Pacheco *et al.*, 2006), if it was emplaced as a surface flow, would imply subsidence and sediment accumulation at rates of ~2-4 mm/yr. Such rapid subsidence rates are documented elsewhere in the Salton Trough region (e.g. Herzig et al., 1988; Schmitt and Hulen, 2008; Dorsey et al., 2011) and could have quickly buried older low-lying topography in the Mexical Valley. Deposition of the Borrego Formation continued until the supradetachment basin was dissected by strike-slip faults at ca. 1.1-1.2 Ma (Kirby *et al.*, 2007), suggesting that the inferred topographic high lasted from about 2.9 to 1.2 Ma. The lack of evaporite facies in the Tapiado and Borrego formations suggests that Borrego Lake was an open (exorheic) lake. This suggests that tectonic uplift in the Mexicali valley may have continued until ~1.2 Ma in order to balance likely erosion at the lake outlet and maintain the inferred structural dam.

Rapid Progradation of Gravel and Sand

Synchronous with regional lake transgression in the Salton Trough, the northerly-derived Vallecito fan prograded rapidly to its most basinward position (Fig. 3.17C) at 2.9 Ma. The base of the monomictic, Whale Peak-derived megabreccia also coincides with this stratigraphic horizon. Southerly-derived fluvial deposits in the White Wash and Little Devil areas are the downstream equivalents of Carrizo fan deposits exposed in Canyon Sin Nombre. In Little Devil Wash, the contact between the Arroyo Diablo Formation and the Tapiado/Hueso formations is sharp, laterally-continuous along strike for ~4 km, and is dated at ca. 2.9 Ma (Fig. 3.7, 3.16). Thus, abrupt basinward progradation of coarse locally-derived sediment from Carrizo Creek in the south was synchronous with progradation of gravel from Vallecito Creek in the north. An increase in depositional gradient along this progradational contact is evident in the transition from a water-logged floodplain in the Arroyo Diablo and Olla formations to a well-drained, highly oxidized floodplain in the Hueso Formation.

The close relationship between emplacement of the megabreccia and abrupt progradation of coarse alluvial-fan and fluvial deposits at 2.9 Ma suggests a related origin for both events. Since these events post-date the ~3.1 Ma slowing of subsidence rate, progradation was likely driven by an increase in sediment flux. Presence of a catastrophically emplaced megabreccia suggests a tectonic driver for these synchronous processes. We therefore infer that increased sediment flux was driven by reorganization of the breakaway of the West Salton detachment fault. We hypothesize that the detachment breakaway stepped ~3 km east where it crosses the east-trending synformal corrugation between Whale Peak and the Tierra Blanca Mountains at 2.9 Ma, and

transferred an ~ 3 km wide belt of proximal basin deposits into the footwall of the fault (Fig. 3.17C). We infer that basinward migration of the breakaway caused uplift and erosion of unconsolidated coarse-grained proximal deposits in this belt and led to an immediate increase in the rate of sediment delivery to the Vallecito Creek deposystem. An eastward step in the location of footwall uplift would have produced an immediate ~3 km eastward step in the apex of the Vallecito Creek alluvial fan. We infer that these related processes – increased erosion of unconsolidated sediment and abrupt shift in the apex of the Vallecito fan – drove rapid expansion of the Vallecito Creek deposystem into the basin at 2.9 Ma. Structural adjustment along the West Salton detachment may have also resulted in temporary over steepening of the detachment fault surface near Whale Peak, resulting in emplacement of the megabreccia. This local structural adjustment is similar to other examples of basinward migration of detachment breakaway zones (e.g. Dorsey and Becker, 1995; Friedman *et al.*, 1996; Dorsey and Martín, 1999).

Regional Tectonic Reorganization at 2.9 Ma

Stratigraphic relationships described above provide evidence for a significant tectonic reorganization at 2.9 Ma that may have affected the entire Salton Trough region. Synchronous formation of Borrego Lake, likely due to tectonic uplift in the Mexicali Valley, and reorientation and basinward migration of the West Salton detachment breakaway suggests a genetic relationship between these two events. Previous studies have documented a discrete westward shift in deformation, transform faulting, and locus of oblique rifting in the northern Gulf of California and southern Salton Trough at about 2.0-3.3 Ma (Aragon and Martin, 2007; Nagy and Stock, 2000; Stock, 2000). Reorganization of transtension in this general time frame provides a plausible mechanism

for structural adjustments in the southern and western Salton Trough. Data presented here may help to refine the timing of this poorly-dated reorganization of the Pacific-North American plate boundary in the northern Gulf of California and Salton Trough (Aragon and Martin, 2007).

Upper Palm Spring Subgroup

The stratigraphic architecture in the upper Palm Spring subgroup is dominated by retrogradation of alluvial fan lithofacies in the north and fluctuations in the lateral extent of lake deposition in the central part of the basin. Coarse-grained deposits with northern (Vallecito Creek) source affinities shrink in areal extent above the base of the upper Palm Spring Subgroup, recording retrogradation of the Vallecito Fan to the west-northwest (Fig. 3.17D,E). Above the lowest 400-450 m of the Hueso Formation, distal deposits of the Vallecito fan are absent, and the section is dominated by fluvial sandstone of the Hueso Formation (Fig. 3.16). The documented retrogradation of the Vallecito fan probably resulted from a decrease in the rate of sediment delivery due to both depletion in the supply of newly exposed unconsolidated coarse-sediment, and long-term regional aridification during late Pliocene to early Pleistocene time (Peryam *et al.*, 2011)

While the transgression of Borrego Lake was likely tectonically-controlled, linkages between regional climate records and local apparent lake levels suggest that long-term fluctuations in lake level were controlled by climate conditions in the upper Colorado River watershed, which is the source of the majority of water volume in the river in the present (Gangopadhyay and McCabe, 2010). The areal restriction to absence of lacustrine strata between ~2.4-2.05 Ma broadly corresponds to a period of arid, "modern-like" climate regime in the southwestern United States (Smith, 1984; Forester,

1991; Thompson, 1991). The younger phase of Tapiado Formation deposition (2.05-1.85 Ma) likewise corresponds to records of a return to a more moist climate regime throughout the western United States (Thomson, 1991).

CONCLUSIONS

A pronounced stratigraphic boundary between the lower and upper subgroups of the Palm Spring Group in the Fish Creek-Vallecito basin records abrupt basin reorganization at 2.9 Ma. This stratigraphic boundary records simultaneous rapid lake transgression and progradation of coarse sediment from nearby drainages in the footwall of the West Salton detachment fault. The co-occurrence of lake transgression and rapid progradation is inconsistent with the predictions of most models for the behavior of tectonically active basins. In this study, we find that only a confluence of tectonic changes at both local and regional scales can explain the contradictory stratigraphic signals.

In the northern part of the basin, initial progradation of coarse detritus from Vallecito Creek resulted from a previously documented decrease in basin subsidence rate at ca. 3.1 Ma. At the southern basin margin, progradation of the Carrizo fan started at ca. 4.2 Ma, significantly earlier than slowing of basin subsidence. A companion study of ^{10}Be concentrations in sand (Longinotti *et al.*, 2011) finds that paleo-erosion rates were constant during this time, and progradation in this area cannot be explained by a climate-driven increase in erosion rate. We therefore conclude that progradation of the Carrizo fan starting at ~4.2 Ma likely resulted from increased sediment flux driven by expansion

of the Carrizo Creek catchment as a result of long-term uplift and topographic adjustments in the Ocotillo accommodation zone.

Lake transgression at 2.9 Ma likely resulted from structural segmentation of the southern Salton Trough. Rapid transgression of a regional lake is recorded by a synchronous change to lacustrine conditions in the Tapiado Formation (this study) and the Borrego Formation east of the study area. This regional lake was open (exorheic), perennial, and filled most of the northern Salton Trough from ~ 2.9 to 1.1 Ma. We conclude that rapid transgression of Borrego Lake over a large region at 2.9 Ma resulted from structurally induced uplift in the Mexicali Valley, which segmented the Salton Trough and trapped a large volume of Colorado River water north of a low topographic barrier.

Rapid progradation of locally-derived coarse sediment at 2.9 Ma was caused by local reorganization of the basin-bounding West Salton detachment fault. A basinward step in the breakaway fault south of Whale Peak likely produced an immediate eastward shift in the apex of the Vallecito Creek alluvial fan, and thus increased sediment flux by remobilizing fault-proximal gravel deposits. Seismicity and destabilization of the footwall during this tectonic adjustment may also explain deposition of a unique, catastrophically emplaced megabreccia that marks the base of the upper Palm Spring subgroup and Vallecito Creek deposits. Thus we conclude that multiple observed stratigraphic changes at 2.9 Ma resulted from tectonic mechanisms, and were not the result of Late Pliocene climate change.

The synchronous timing of lake transgression and basinward step in the detachment breakaway at 2.9 Ma indicates that the two events are genetically related, and

probably were controlled by tectonic reorganization of regional basin-bounding faults. We suggest that these regional tectonic adjustments occurred during proposed westward migration of transtensional faults and basins in the northern Gulf of California, an event that was previously bracketed in time between ~ 2.0 and 3.3 Ma (e.g. Aragon and Martin, 2007). If so, then the stratigraphic reorganization documented here may provide a new constraint on the timing of this regional event. Our results thus highlight the importance of tectonically-driven modifications to landscapes and drainages in controlling the distribution of sedimentary facies in tectonically-active basins.

BRIDGE

In this chapter I described the Palm Spring Group in the Fish Creek-Vallecito basin and conclude that tectonic adjustments at both local and regional scales were responsible for enigmatic stratigraphic reorganization at 2.9 Ma. By extension, I find that late Pliocene global climate had a negligible impact on basin-scale stratigraphic architecture, in contrast to hypothesized accelerated landscape erosion and sediment flux during this climate transition. The next chapter will presents the results of an investigation designed to determine if global climate cyclicity had an impact on landscape evolution at a level below that capable of impacting gross basin architecture.

CHAPTER IV

EVIDENCE OF LATE PLIOCENE ORBITAL MODULATION OF EROSION RATES IN SOUTHERN CALIFORNIA

This chapter was co-authored with Max Bezada, who assisted with computer programming and time-series analysis. Rebecca Dorsey provided funding and advisorial support. Russ Burmester and Bernie Housen helped to collect and interpret rock magnetic data.

INTRODUCTION

A dramatic shift in the Earth's climate occurred during the transition from Pliocene to Pleistocene time, when stable early Pliocene warmth was replaced by a cooler late Pliocene to Pleistocene climate marked by orbitally-modulated glacial-interglacial cycles (e.g., Haug et al., 2001; Zachos et al., 2001; Ravelo et al., 2004; Haug et al., 2005; Lisiecki and Raymo, 2005). This reorganization of the Earth's climate system resulted in the onset of northern hemisphere glaciation and may have had profound effects on landscapes worldwide. Periods of climatic transition are known to result in persistent disequilibrium of landscapes and high rates of denudation due to shifts in both precipitation and vegetative regime (e.g. Bull and Schick, 1979; Tucker and Slingerland, 1997; Leeder et al., 1998; McDonald et al., 2003). As a consequence of the onset of a rapidly cyclical glacial-interglacial climate regime in late Pliocene time, global bedrock erosion rates and sediment fluxes are hypothesized to have dramatically increased between ~4 and 2 Ma (e.g. Pederson et al., 2001; Zhang et al., 2001; Molnar, 2004,

Huntington et al., 2006). While basic aspects of this hypothesis are still under dispute (e.g. Clift, 2006; Willinbring and von Blanckenburg, 2010), it makes specific predictions that can be tested in appropriate geologic settings. Specifically, the hypothesis predicts that rate of sediment flux from actively eroding catchments should fluctuate at the same frequency as orbitally-modulated global climate transitions.

Magnetic susceptibility is a useful proxy for the rate of sediment influx into lakes from surrounding drainages. Ferrimagnetic mineral species such as magnetite and titanomagnetite are present in many crystalline rock types and are common in soil horizons (Dearing, 1999; Maher and Taylor, 1988). Numerous studies have linked increases in magnetic susceptibility in lacustrine sediments to landscape disturbance and soil denudation (e.g. Thompson et al., 1975; Bloumendal et al., 1979; Higgitt et al., 1991; Kodama et al., 1997; Rhoujjati et al., 2010). In Holocene lakes, strongly magnetic stratigraphic intervals have been linked to anthropogenic land use, such as deforestation and farming (e.g. Thompson et al., 1975; Kodama et al., 1997). In older deposits, climate appears to be the dominant driver of variations in flux of magnetic minerals (e.g. late Pleistocene, Rhoujjati et al., 2010). Detailed analysis of magnetic components in sediment, when coupled with bulk magnetic susceptibility, can provide insight into the sources of magnetism and linkages between sources and observed fluxes in susceptibility records (e.g. Thompson et al., 1975; Dearing, 1999; Oldfield, 2007). While magnetic susceptibility records have proven useful in understanding Holocene and late Pleistocene landscape and ecological evolution, no analysis of this kind has been published on pre-Quaternary lacustrine deposits, perhaps due to a paucity of well-dated and readily sampled outcrops of this age.

Lacustrine deposits in the Fish Creek-Vallecito basin of southern California provide a unique, well exposed and well dated record of lacustrine deposition in the western part a large lake during late Pliocene to early Pleistocene time (Peryam et al., 2012). Deposits of the Tapiado Formation contain about 600 m of deep to marginal lacustrine sediments deposited between ca. 2.9-1.85 Ma. These deposits have been uplifted, tilted and exposed as a result of motion on younger strike-slip faults (Dorsey et al., 2012). Rapid sedimentation and extensive magnetostratigraphic and geochronologic dating enable high-precision age determination of stratigraphic horizons within the lacustrine section (Dorsey et al., 2011; Peryam et al., 2012). Sediments in the Tapiado Formation were derived from two local catchments west of the basin, in the eastern Peninsular Ranges (Peryam et al., 2012). The combination of well-constrained sediment sources and a high-fidelity chronostratigraphic framework make the Tapiado Formation well suited for a study of the linkages between climate change, landscape evolution and sediment flux during late Pliocene to early Pleistocene climate transitions.

This paper presents an analysis of magnetic susceptibility in the Tapiado Formation of the Fish Creek-Vallecito basin. We use rock magnetic data from a well-exposed late Pliocene to early Pleistocene stratigraphic section in the lower part of the Tapiado Formation (~2.9-2.5 Ma) to document changes in relative rates of denudation in the ancestral Carrizo Creek catchment. We then present a time-series analysis of these data and compare the results with global climate reconstructions to test hypotheses for the effect of orbital climate modulation on erosion rates and sediment fluxes in southern California.

BACKGROUND

The Fish Creek-Vallecito basin contains a well-exposed stratigraphic record of late Miocene to early Pleistocene sedimentation in the hanging wall of the West Salton detachment fault (Fig. 4.1; Axen and Fletcher, 1998; Dorsey et al., 2011). An early Pliocene phase of marine sedimentation was followed, beginning at 4.2 Ma, by non-marine deposition as the Colorado River delta prograded across the Salton Trough (Dorsey et al., 2007; Dorsey et al., 2011). The Palm Spring Group, of which the Tapiado Formation is a part, records fluvial, alluvial fan and lacustrine deposition between 4.2 Ma and ~1 Ma, when a regional tectonic reorganization ended deposition of the Palm Spring Group (Dorsey et al., 2012). In the present-day Fish Creek-Vallecito basin a thick (>5 km) southwest-dipping section is well exposed in a series of dry washes and eroding badlands.

Fine-grained mudstone, siltstone and marlstone of the widespread Borrego Formation, and more locally preserved Tapiado Formation, record deposition in a large lake that filled much of the western Salton Trough during late Pliocene to early Pleistocene time (Dibblee, 1954; Kirby et al., 2007; Peryam et al., 2012). Borrego Lake formed by regional transgression at 2.9 Ma, when structural segmentation of the the Salton Trough resulted in damming of the Colorado River north of the modern Mexicali Valley (Housen and Dorsey, 2010; Peryam et al., 2012). Microfossils in the Borrego Formation include ostracodes, micromollusks, diatoms, fish bone fragments, charophytes, and rare planktonic foraminifers that record deposition in a large, perennial fresh-water to occasionally brackish-saline lake (Tarbet and Holman, 1944; Dibblee, 1954; Kirby et al., 2007). Ostracode faunas in the Tapiado Formation (focus of this study) are dominated by

Candona patzcuaro var. mexico, indicating that the western part of Borrego Lake was also filled with fresh water (Cosma, 2002a).

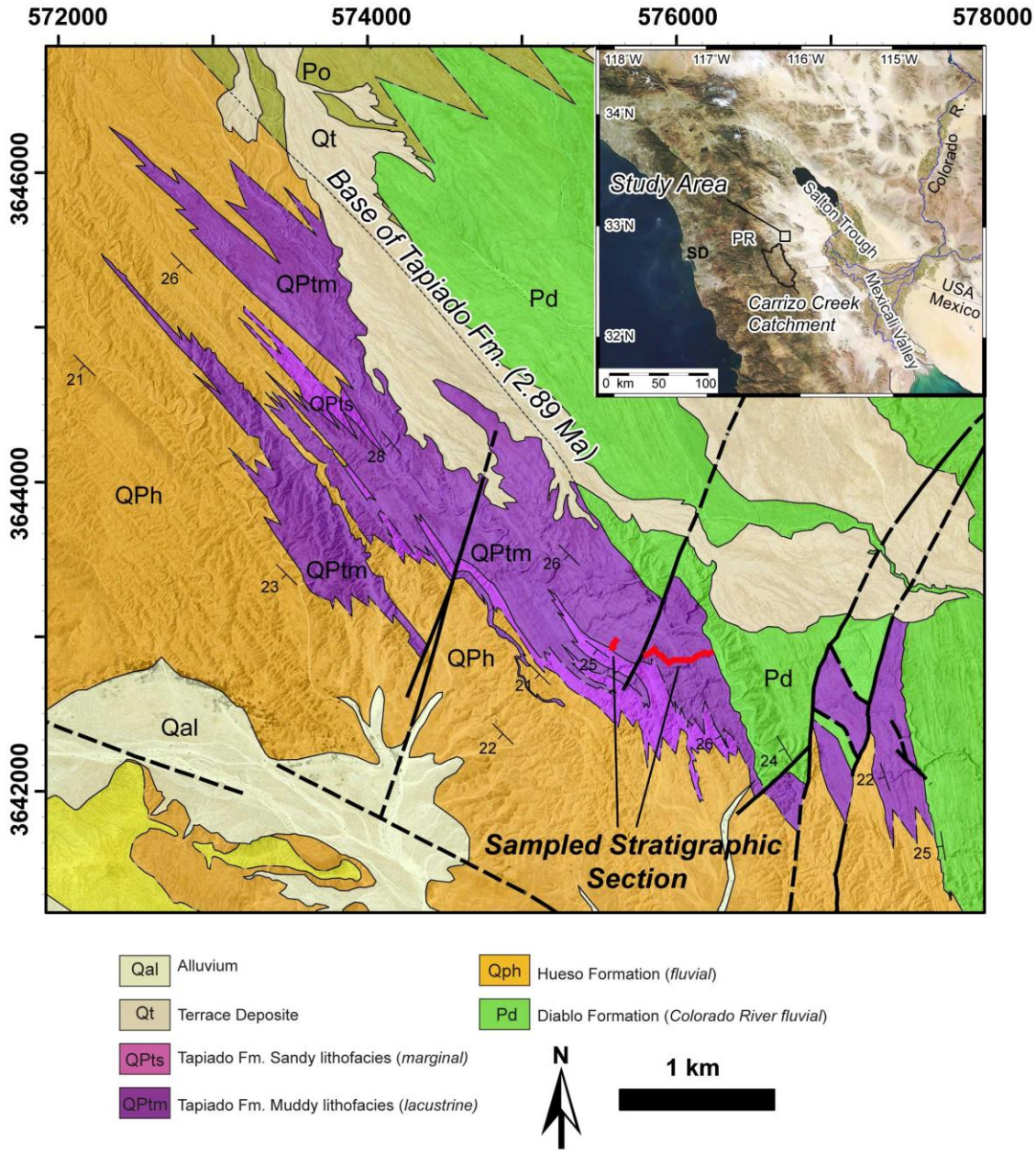

Figure 4.1: Maps showing location of the study area and measured section in the lacustrine Tapiado Formation in the Fish Creek-Vallecito Basin, California. PR, Peninsular Ranges; SD, San Diego.

While lacustrine sedimentation in the western Salton Trough is known to have continued until around 1.1 Ma (Kirby et al., 2007), the youngest Borrego Lake deposits in the Fish Creek-Vallecito basin are about 1.85 Ma (Peryam et al., 2012). The Tapiado Formation in the Fish Creek-Vallecito basin contains sediment derived from two local drainages, with no input from the Colorado River during Pliocene time (Dorsey et al., 2005; Peryam et al., 2012). The local sediment sources have been identified as the precursors of the modern Vallecito and Carrizo creeks which presently drain the eastern Peninsular Ranges (Fig. 4.1; Peryam et al., 2012).

The late Pliocene to earliest Pleistocene (2.890-2.52 Ma) rocks that are the focus of this study were deposited during a period of global climate transition. A stable, warm climate in middle Pliocene time gave way, gradually, to a cooler and highly-cyclical climate in the latest Pliocene (e.g. Maslin et al., 1998; Ravelo et al., 2004, Lisiecki and Raymo, 2005; Mundelsee and Raymo, 2005, Dekens et al., 2007). Locally, the middle Pliocene climate in the Fish Creek-Vallecito basin was more humid than at present, with a significant monsoonal component of yearly precipitation (Cosma, 2002a; Remeika, 2006; Peryam et al., 2011). Late Pleistocene global cooling resulted in a gradual but steady increase in local aridity and a shift to winter-dominated precipitation (Brogenski, 2001; Cosma, 2002a, Gensler et al., 2006; White et al., 2006; Peryam et al., 2011). Peryam et al. (2011) proposed that these long term changes resulted from the gradual extinction of permanent El Niño conditions in the Pacific Ocean during late Pliocene time (e.g. Molnar and Cane, 2002; Wara et al., 2005; Federov et al., 2006).

METHODS

Sampling and Age Modeling

A total of 183 rock samples were collected at 1 m spacing in a stratigraphic section through the lower part of the Tapiado Formation (Fig. 4.2). Samples were collected only from fresh bedrock exposures. Careful map tracing of marker beds and of an interbedded volcanic ash allowed us to correlate the section across a small fault (Fig. 4.1). Present-day 185 m thickness of the stratigraphic section restores to 244 m after decompaction, using the method of Angevine et al. (1990). Original burial depths were calculated using thicknesses reported in Dorsey et al. (2011), yielding restored, decompacted sampling intervals that range from 1.44 to 1.17 m.

The age of the stratigraphic succession was determined by linear interpolation of three independent age controls (Fig. 4.3): the base of the Tapiado Formation (2.89 ± 0.1 Ma; Peryam et al., 2012), U-Pb dating of the ash bed (2.65 ± 0.5 Ma; Dorsey et al., 2011), and the base of the Matuyama magnetochron (2.58 ± 0.1 Ma; Peryam et al., 2012). The age of sampled section is determined by this method to range from 2.89 to 2.52 Ma. We resolved decompacted sedimentation rates separately for "fine" (mudstone) or "coarse" (silt and sandstone) intervals, to account for possible variations in sedimentation rate due to different depositional settings (lake bottom or prodelta, respectively). Assuming that the accumulation rate for each lithology is constant, and given that we have three independent age controls, we can constrain the decompacted sedimentation rates to unique values of 0.64 mm/yr for mudstone intervals and 0.67 mm/yr for coarse units. These values are very near the overall average decompacted sediment accumulation rate of the section of 0.65 mm/yr. Based on the up-section decrease in burial depth,

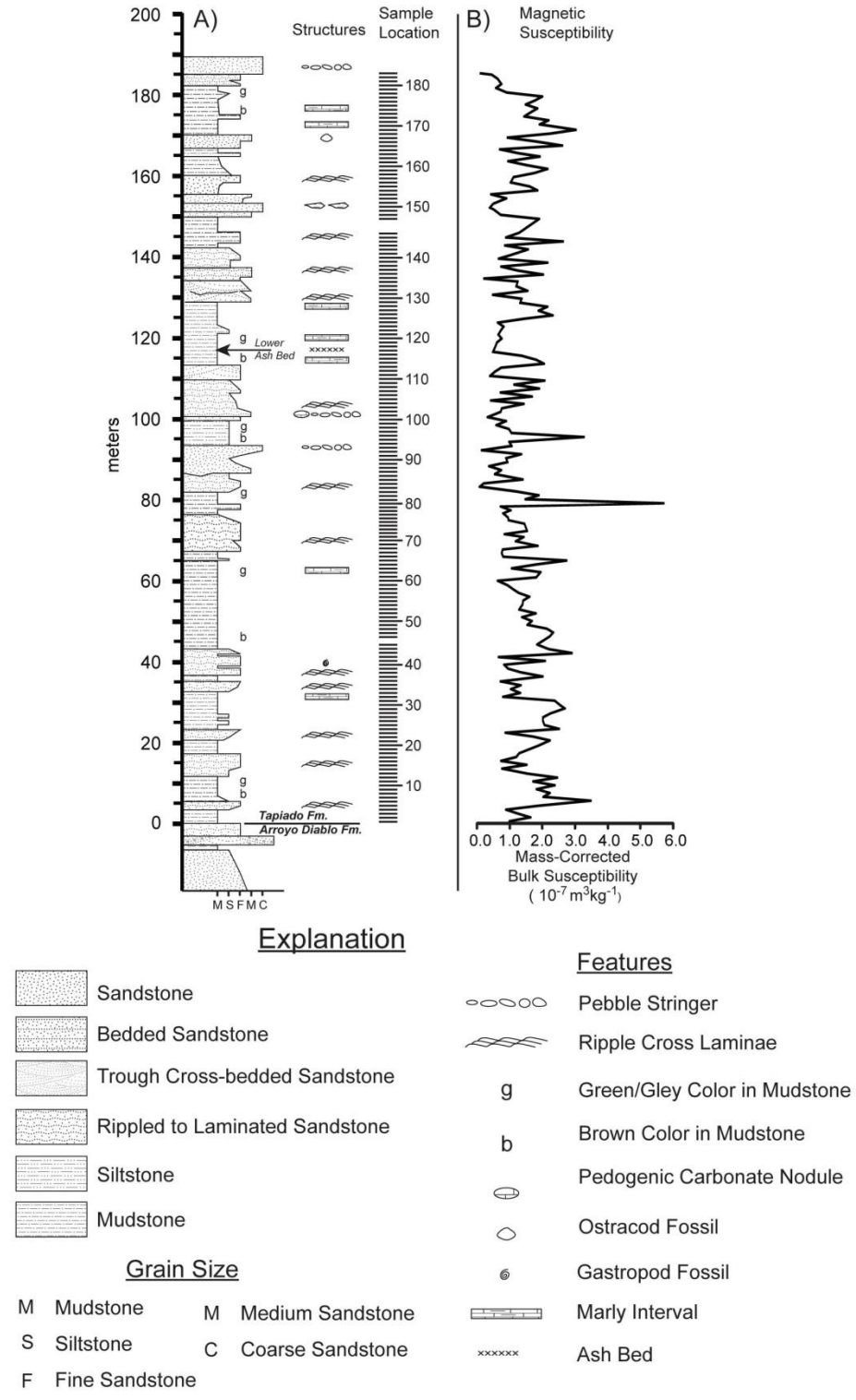

Figure 4.2: (A) Measured section in the lower part of the Tapiado Formation showing lithology, sedimentary features, and location of rock magnetic samples. (B) Curve showing mass-corrected magnetic susceptibility curve for 183 samples.

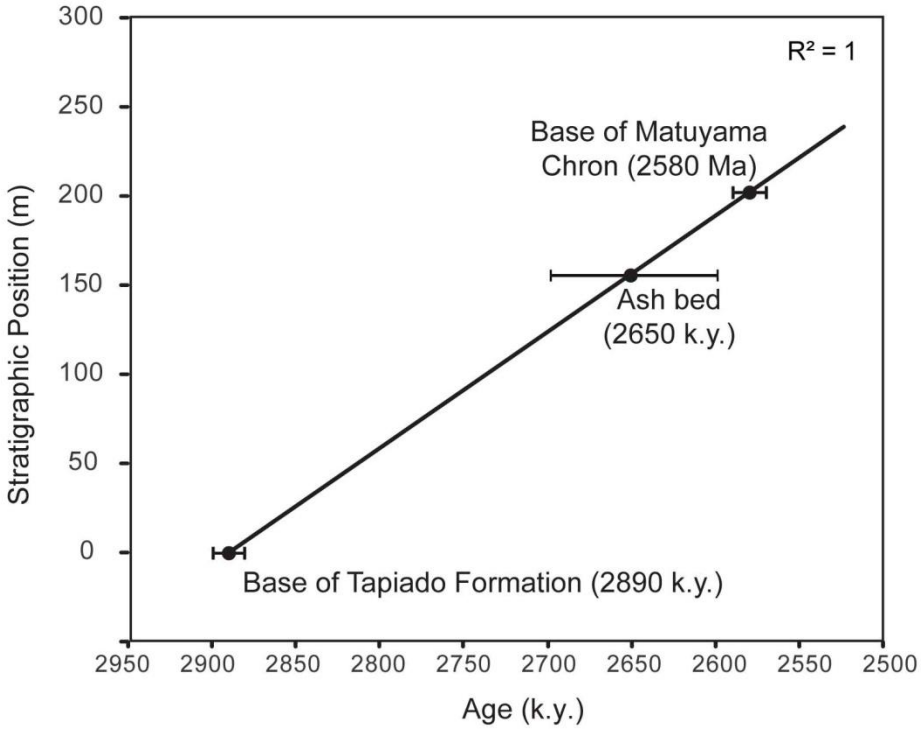

Figure 4.3: Age model of the Tapiado Formation section sampled for magnetic susceptibility analysis.

effects of decompaction, and lithologic variations, the time interval between samples varies from 2.25 to 1.74 k.y. with an average sampling interval of 2.05 k.y.

Rock Magnetic Analysis

Rock magnetic analysis was conducted at the Pacific Northwest Paleomagnetic Laboratory at the Geology Department of Western Washington University using an Agico KLY3-S magnetic susceptibility bridge (kappabridge) and a Princeton Measurements MicroMag model 3900 vibrating sample magnetometer (VSM). Bulk magnetic susceptibility was measured at room temperature on 5 cm^3 sediment samples at room temperature. Between 100 and 500 mg of material were repacked into gel capsules and analyzed for magnetic hysteresis properties and isothermal remanent magnetization

(IRM) acquisition. VSM experiments used an initial maximum field of 500 mT. Where hematite was believed to be present, samples were re-analyzed using a maximum field of 1500 mT. Coercivity component decomposition of IRM acquisition curves was conducted using the method of Kruiver et al. (2001).

Time Series Analysis

Magnetic susceptibility data were linearly resampled at 2 k.y. intervals in order to generate a regularly-spaced time series near the mean spacing of the original samples (e.g. Weedon, 2003). An outlier (sample 80) and a low-power linear trend were removed from the time series prior to spectral analysis (Percival and Walden, 1993; Weedon, 2003). Spectral analysis was conducted using the "multitaper method (MTM)" originally formulated by Thompson (1982), because of that technique's practical success in analyzing climate time series that frequently contain both purely harmonic as well as quasi-periodic frequencies (e.g. Percival and Walden, 1993; Weedon, 2003; Meyers et al., 2008). To evaluate the robustness of MTM results, one thousand iterations of bootstrap resampling and reanalysis were conducted. For each analysis 10% of samples were randomly selected from the data and discarded, the time series was resampled at 2 k.y intervals, and a 3 taper MTM was conducted on the decimated time series. Confidence intervals for MTM power spectra were calculated using the robust statistical tests of Mann and Lees (1996).

Spectral frequency estimation and spectral decomposition were also conducted using singular spectrum analysis (SSA). SSA offers a nonparametric complement to the MTM method, and is particularly useful for small, noisy data sets (Elsner and Tsnonis, 1991; Ghil et al., 2002; Hudson and Keatley, 2010). This approach is essentially a

decomposition of a data set in terms of empirical orthogonal function (EOFs) which are determined by estimating the eigenvalues and eigenvectors of a covariance matrix involving a time series and lagged copies thereof. Because SSA is not dependent upon simple harmonics, it can effectively identify non-linear oscillations (i.e. trends) as well as periodic frequency components (Ghil et al., 2002). A window length (M) of 30 was selected in order to investigate orbital cycles on the scale of 10's of k.y. while keeping under the maximum M/N ratio of 1/5, where N is the total number of data points in the time series (Vautard et al., 1992).

In order to assess the evolution of climate forcing through time, a wavelet analysis was conducted using the technique of Torrence and Compo (1998). Wavelet analysis involves shifting a fully scalable, modulated window along the time series and calculating spectrum at every position. This method is an improvement over a traditional "windowed Fourier transform" for localizing frequency variation in a time series, especially for time series that contain nonstationary power at several different frequencies (Daubechies, 1990; Kaiser, 1994).

RESULTS

Measured Section in the Lower Tapiado Formation

Distal to marginal lacustrine deposition is recorded throughout the sampled stratigraphic section (Fig. 4.2; Peryam et al., 2012). Laminated, intermittently marly, clayey silt and mudstone dominate fine-grained distal lacustrine intervals. Carey (1975) reported clay contents between 2% and 54% in mudstone exposures laterally-equivalent to those sampled in this study. Increasing gley coloration in the upper part of fine-grained intervals may reflect incorporation of lake-margin organic material into mudstones and

subsequent “burial gleyzation” related to anaerobic decomposition during early diagenesis (e.g. Retallack, 1991). Ripple cross-laminated fine sandstone, which comprises the majority of coarser-grained intervals, contains rare gastropod and/or ostracode fossils and was deposited subaqeuously near the front of small lacustrine deltas (Peryam et al., 2012). Uncommon cross-bedded and pebbly sandstone record deposition in delta channels. With the exception of one calcic paleosol at ~101 m, the sampled stratigraphic interval records continuous deposition under lacustrine prodeltaic conditions (e.g. Johnson and Graham, 2004) with no evidence of subaerial exposure.

Rock Magnetic Properties

Hysteresis properties measured on a subset of samples (Table 4.1) suggest that magnetic susceptibility in the Tapiado Formation is primarily provided by magnetite in the pseudo-single domain size range. Samples were chosen for hysteresis analysis in order to reflect the full range of rock types present in the measured section, as well as a range of bulk magnetic susceptibility values. Sediment samples uniformly plot within the pseudo-single domain field of a Day Plot, although this could also represent mixing of single and multiple-domain magnetite (Fig. 4.4; Day et al., 1977; Dunlop, 2002). Hysteresis loops have a narrow geometry typical for pseudo-single domain magnetite (Fig. 4.5; e.g. Tauxe et al., 1996, 2002). Hysteresis properties of samples are uncorrelated with bulk susceptibility, dominant sediment grain size or apparent diagenetic reduction of certain deposits (Table 4.1).

Acquisition curves of isothermal remanent magnetization (IRM) confirm that magnetite is the dominant magnetic carrier in the Tapiado Formation samples. Four

Table 4.1. Hysteresis Parameters for Tapiado Formation Samples

Sample	Lithology	Mass-Corrected Magnetic Susceptibility 10^{-7} m^3kg^{-1}	Mass-Corrected Ms, 10^4 A/m	Mass-Corrected Mr, 10^4 A/m	Mrs/Ms	Hc, mT	Hcr, mT	Hcr/ Hc
1	Mudstone (brown)	0.97	1.46	0.16	0.115	100.9	360.9	3.58
2	Mudstone (brown)	1.61	2.41	0.28	0.111	81.4	256.2	3.15
3	Mudstone (brown)	1.21	1.93	0.17	0.089	78.0	355.9	4.56
4	Fine Sandstone	0.86	1.86	0.20	0.113	81.5	229.7	2.82
5	Fine Sandstone	1.85	3.11	0.43	0.130	92.9	291.3	3.14
6	Mudstone (brown)	3.47	7.96	0.88	0.113	86.8	307.0	3.54
7	Mudstone (brown)	2.01	3.79	0.52	0.143	98.7	304.2	3.08
8	Mudstone (brown)	2.20	4.18	0.52	0.130	92.4	307.8	3.33
9	Mudstone (brown)	1.80	3.61	0.46	0.130	84.2	297.3	3.53
10	Mudstone (gleyed)	2.36	4.03	0.51	0.133	92.1	285.4	3.10
11	Mudstone (gleyed)	1.70	2.54	0.38	0.158	106.4	280.4	2.64
12	Mudstone (gleyed)	2.43	4.99	0.59	0.123	92.8	307.5	3.32
13	Mudstone (gleyed)	1.54	2.59	0.30	0.126	91.0	297.5	3.27
14	Fine Sandstone	0.73	1.69	0.16	0.111	52.7	154.8	2.94
15	Fine Sandstone	1.48	2.60	0.15	0.091	29.7	91.8	3.09
16	Fine Sandstone	0.71	1.14	0.12	0.108	75.4	256.9	3.41
17	Fine Sandstone	1.17	1.73	0.23	0.131	96.3	292.0	3.03
24	Mudstone (brown)	2.48	71.20	9.99	0.147	106.4	323.7	3.04
29	Mudstone (brown)	2.67	46.00	7.73	0.175	110.0	292.4	2.66
45	Mudstone (brown)	1.81	44.40	5.69	0.133	105.3	322.4	3.06
62	Mudstone (gleyed)	1.92	51.60	7.66	0.154	118.9	353.9	2.98
80	Mudstone (gleyed)	5.71	74.92	0.74	0.103	83.7	290.0	3.47
84	Fine Sandstone	0.07	0.11	0.18	0.189	139.8	349.6	2.50
114	Mudstone (brown)	0.45	59.00	7.25	0.128	97.9	306.4	3.13
117	Mudstone (brown)	0.58	0.18	0.22	0.135	115.3	324.1	2.81
119	Mudstone (gleyed)	0.58	8.57	0.57	0.071	72.5	400.0	5.52
120	Mudstone (gleyed)	0.73	16.30	1.33	0.083	89.4	473.5	5.30
135	Medium Sandstone	0.18	7.03	0.89	0.131	118.3	271.7	2.30
144	Siltstone (brown)	2.61	105.00	10.10	0.099	71.2	270.2	3.79
150	Coarse Sandstone	0.38	12.60	0.11	0.093	76.7	266.2	3.47

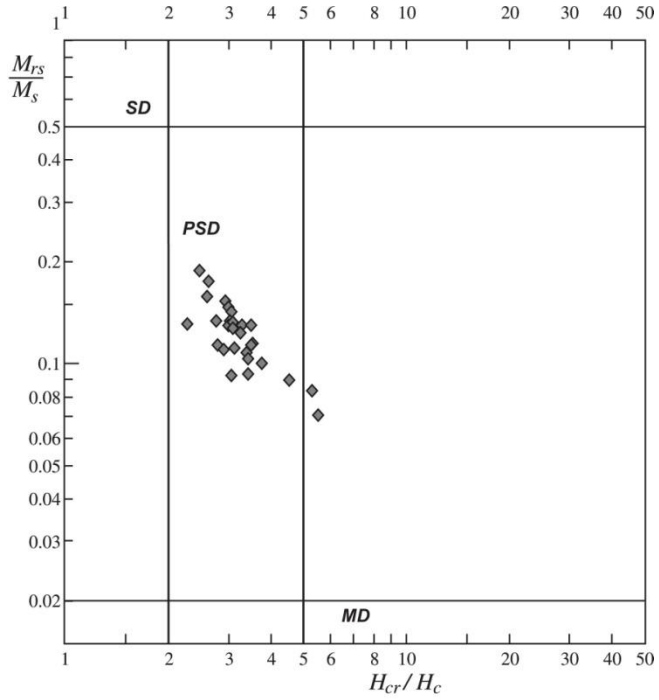

Figure 4.4: Day plot of a subset of lacustrine sediment samples. Data are shown in Table 4.1. Hc, coercive force, Hcr, remanent coercive force; Mrs, saturation remanence; Ms saturation magnetization. Domain state fields after Day (1977).

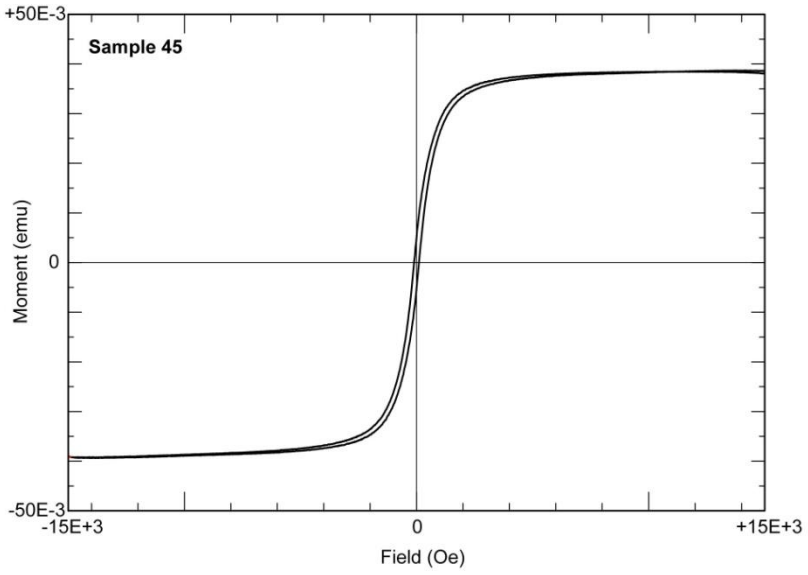

Figure 4.5: Hysteresis loop for sample 45, which is typical for the Tapiado Formation data set.

Table 4.2. Magnetic Components from IRM Acquisition

		Component 1				Component 2				Component 3				Component 4		
Sample	**Lithology**	**%**	**LogB1/2**	**B1/2**	**DP**	**%**	**LogB1/2**	**B1/2**	**DP**	**%**	**LogB1/2**	**B1/2**	**DP**	**%**	**LogB1/2**	**B1/2**
24	Mudstone (brown)	82.7	1.55	35.5	0.36	14.1	2.3	199.5	0.37	2.3	3	1000	0.42	0.9	0.45	2.8
29	Mudstone (brown)	83.2	1.54	34.7	0.32	9.4	2.32	206.5	0.31	5.5	3.00	1000.0	0.35	2.0	0.55	3.5
45	Mudstone (brown)	81.3	1.57	37.2	0.35	13.5	2.24	173.8	0.34	3.5	3.00	1000.0	0.30	1.8	0.55	3.5
62	Mudstone (gleyed)	80.8	1.60	39.8	0.35	12.4	2.12	131.8	0.32	5.7	2.85	707.9	0.32	1.2	0.50	3.2
114	Mudstone (brown)	80.1	1.54	34.9	0.35	13.2	2.20	158.5	0.33	5.3	3.00	1000.0	0.33	1.5	0.55	3.5
119	Mudstone (gleyed)	73.9	1.55	35.5	0.40	18.1	2.22	166.0	0.33	6.4	2.75	562.3	0.33	1.6	0.55	3.5
120	Mudstone (gleyed)	86.2	1.70	50.1	0.45	13.7	2.68	478.6	0.37	-	-	-	-	0.1	0.55	3.5
135	Medium Sandstone	85.4	1.60	39.8	0.35	13.6	2.20	158.5	0.34	-	-	-	-	1.0	0.54	3.5
144	Siltstone (brown)	93.2	1.55	35.5	0.41	3.8	2.21	162.2	0.32	1.0	3.00	1000.0	0.40	2.0	0.60	4.0
150	Coarse Sandstone	83.1	1.52	33.1	0.32	12.5	2.20	158.5	0.37	0.8	3.00	1000.0	0.30	3.5	0.60	4.0

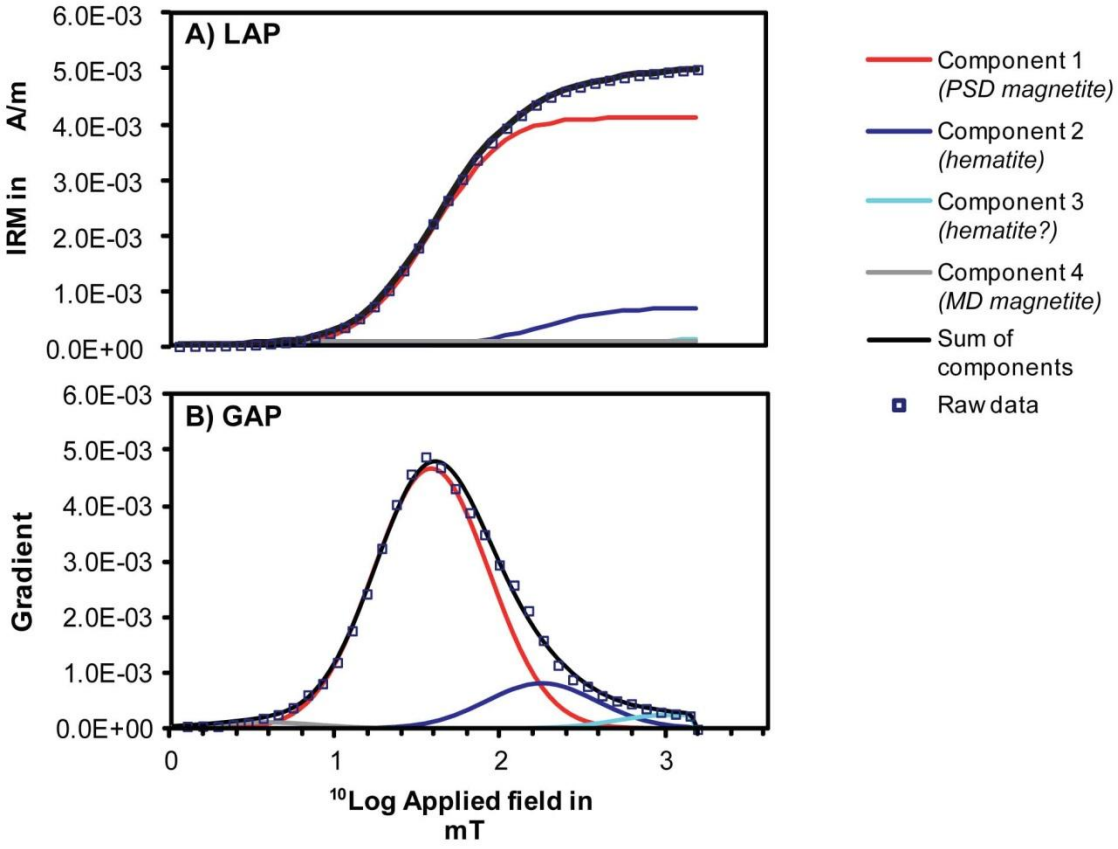

Figure 4.6: Results and component isothermal remanent magnetization (IRM) acquisition for sample 45. (A) Linear acquisition plot (LAP). (B) The gradient of acquisition plot (GAP). Details of individual IRM acquisition components are shown in Table 4.2.

primary components are identified by analyzing IRM coercivity spectra (Table 4.2; Fig. 4.6). The dominant component has a low coercivity ($B_{1/2}$ = ~35 mT), accounts for between 74% and 93% of total remanence of each sample, and is interpreted as pseudo-single domain magnetite (e.g. Robertson and France, 1994; Kruiver et al., 2001). Components 2 and 3 account for around 14% and 5% of the total remanence,

respectively, and have relatively higher mean coercivities ($B_{1/2}$ = ~150 and 1000 mT, respectively), and may represent two populations of hematite (Fig. 4.6). Component 4 has a very low coercivity and is probably multi-domain magnetite. Magnetic component abundances are consistent in all samples analyzed by IRM decomposition (Table 4.2). Analysis of correlative strata by Deboer (2012) revealed the presence of single to multiple-domain magnetite and two populations of hematite, broadly agreeing with the results of our IRM analysis.

Time Series Analysis

MTM Analysis

Analysis of magnetic susceptibility time-series identifies no highly significant spectral peaks (Fig. 4.7). A quasi-periodic signal at around 0.21 cycles per thousand years (4.7-4.8 k.y.) is observed to be significant above the 95% red noise confidence level. This spectral peak is below the Nyquist frequency of 0.22 cycles per thousand years (~4.5

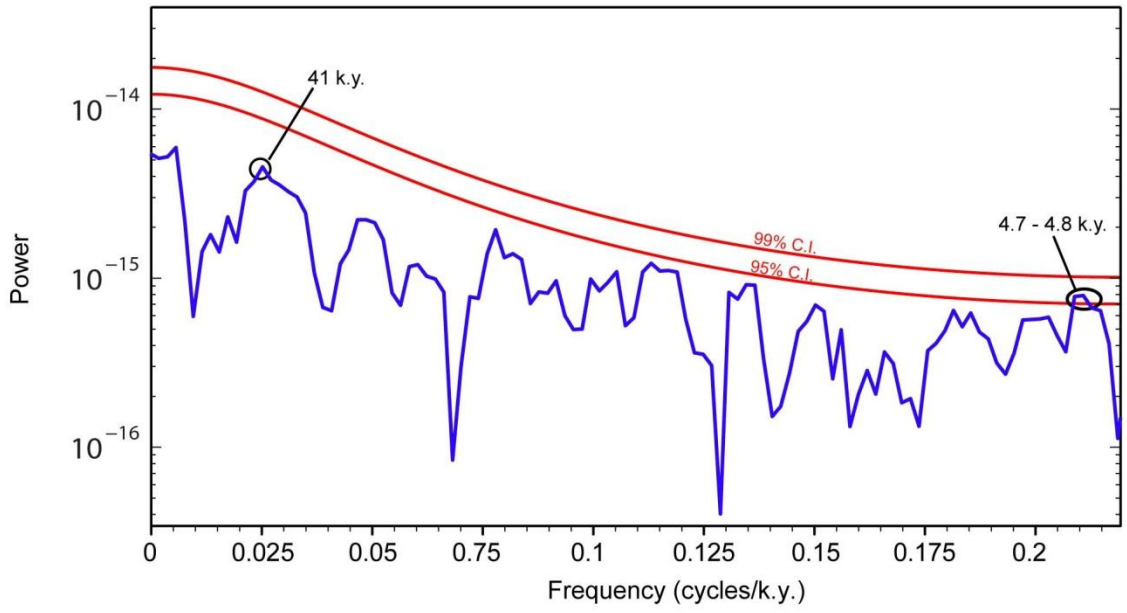

Figure 4.7: Multitaper method (MTM) power spectrum estimate for Tapiado Formation bulk magnetic susceptibility time-series. Power spectrum calculated using linearly-

detrended data and three 2π data tapers. Confidence levels calculated using the robust AR(1) red noise model of Mann and Lees (1996). Note that these results do not utilize spectrum reshaping, in contrast to Mann and Lees (1996).

k.y.), and therefore should be considered a possible periodic component in the data.

Bootstrap analysis of the time series reveals that the high frequency spectral peak is likely spurious but that other frequencies, while weak, may be present in the time series. At ~4.7 k.y. (~0.22 cycles/k.y.) the mean of 1000 iterations of the bootstrap analysis lays more than one standard deviation below the 95% confidence interval (Fig. 4.8), which implies that the apparent significance of this frequency is highly dependent on a relatively small subset of samples and is likely an artifact. In contrast, a very low standard deviation of the bootstrap population at ~40 k.y. (~0.025 cycles/k.y.) suggests that a signal at this frequency is robust in the time series, even though it is relatively weak in comparison to background noise (Fig. 4.8b).

Singular Spectral Analysis (SSA)

Principal component decomposition of the time series by SSA confirms the presence of a ~40 k.y. signal in the time series. The magnetic susceptibility time series was decomposed into 30 empirical orthogonal functions (EOFs). A scree diagram (Fig. 4.9) shows the eigenvalue power of these components. The first 4 EOFs plot to the left of a break in slope in the scree diagram, and are interpreted as "signal," while rest of the EOFs define a "noise floor." (e.g. Vautard and Ghil, 1989; Elsner and Tsonis, 1991; Shun and Duffy, 1999; Hudson and Keatley, 2010).

Figure 4.10 shows a reconstructed time series based upon the first four EOFs. The first reconstructed component (RC1), which accounts for 16.2% of the variance, is a very

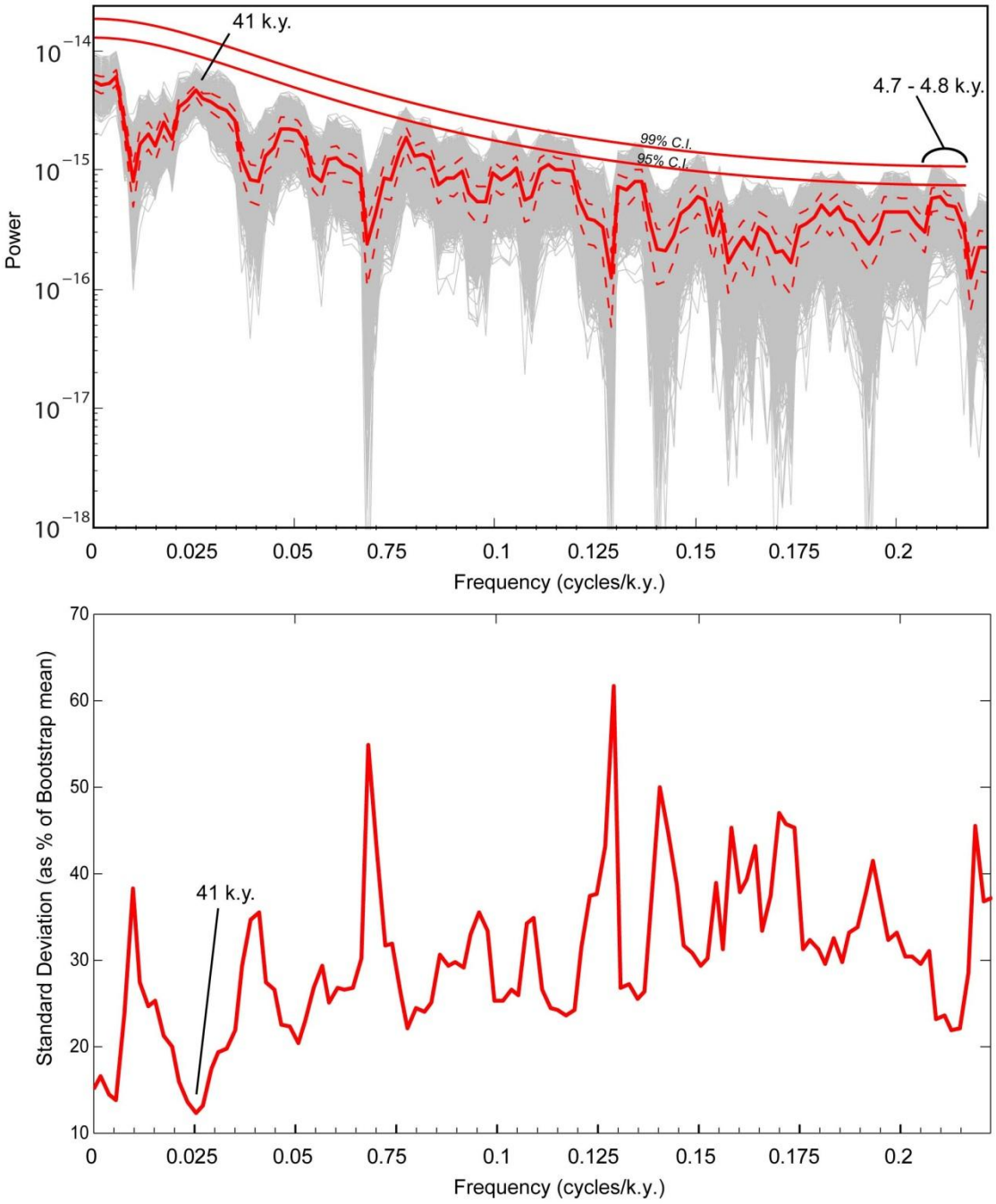

Figure 4.8: Results of bootstrapping and multitaper method (MTM) re-analysis of the magnetic susceptibility time series. (A) Shows results of one thousand iterations of bootstrap resampling with superimposed robust AR(1) confidence levels. Thin grey lines show results of individual bootstrap iterations. Solid red line shows mean spectral power of all iterations. Dashed red line shows the standard deviation of the mean. (B) Relative values of standard deviation of the mean at all frequencies.

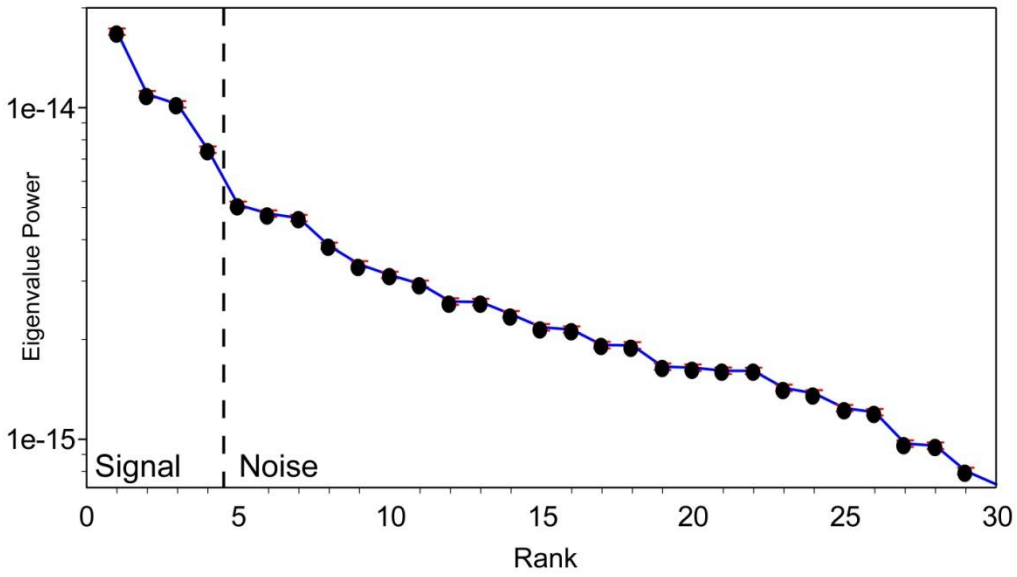

Figure 4.9: Eigenvalue power for 30 principal components of the magnetic susceptibility time series (scree diagram). Component 2 and 3 are interpreted to be an oscillatory pair (see text).

low frequency (300-300 k.y.), anharmonic or quasi-periodic oscillation and is interpreted as a non-linear trend. The fourth reconstructed component (RC4) is similarly anharmonic and accounts for 7.2% of the total variance, and may also record a trend in the data set (Fig. 4.10). The second and third components (RC2 and RC3) account for 20.3% of the time series variance and reconstruct to clearly oscillatory signals with a wavelength of ca. 40 k.y. (Fig. 4.10). The two EOFs that underlie RC 2 and 3 are of similar eignevalue power (Fig. 4.9), are in phase quadrature, and are interpreted as an oscillatory pair that defines a single periodic component in the time series (Ghil et al., 2002). Together, the four "significant" reconstructed components account for only ~44% of the total variance of the time series, indicating that the time series is dominated by noise.

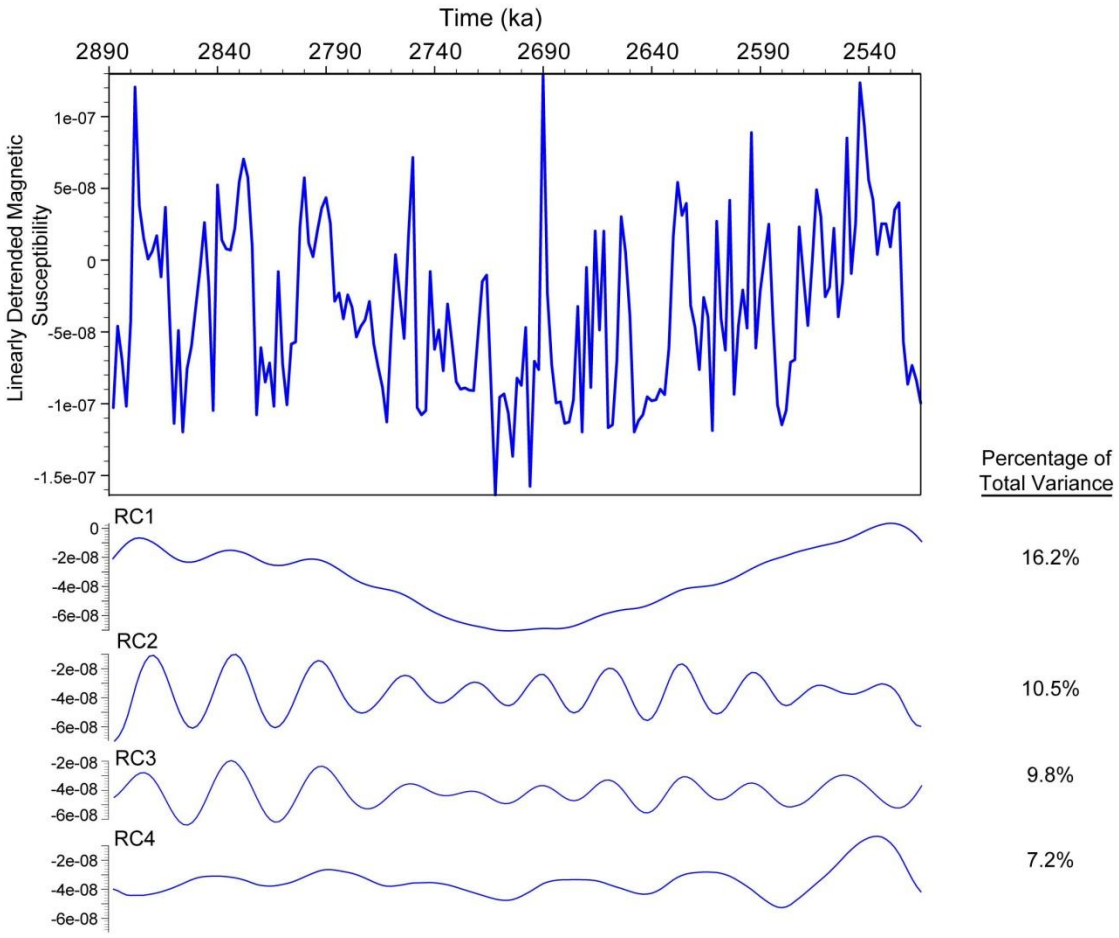

Figure 4.10: (A) Decompacted and linearly-detrended magnetic susceptibility time series. (B) The first reconstructed component (RC1) is a long-wavelength quasiharmonic trend. Reconstructed components RC2 (C) and RC3 (D) are harmonic, have similar powers and frequencies, and are an oscillatory pair that define a ~40 k.y. period signal. (E) The fourth reconstructed component (RC4) is a second non-linear trend.

Wavelet Analysis

Wavelet analysis shows that the ~40 k.y. periodic signal decreases in power through time (Fig. 4.11). The Morlet wavelet spectrum in Figure 4.11 shows that the ~40 k.y. frequency contains the most power in the oldest part of the time series (2.9-2.75 Ma).

This finding is consistent with the observation that both the second and third reconstructed SSA components (Fig. 4.10) are strongest in deposits older than ~2.75 Ma The non-stationary nature of the ~40 k.y. signal explains the apparent non-significance of this frequency in MTM analysis. A powerful low-frequency signal detected by the wavelet analysis may record the quasiharmonic, long wavelength non-linear trend detected as the first principal component in the SSA (Fig. 4.10). There are several brief time periods where high-frequency (5-12 k.y.) signals are apparently significant. These high-frequency components are highly non-stationary in both time and frequency, and are either spurious or record highly quasiperiodic forcing mechanisms.

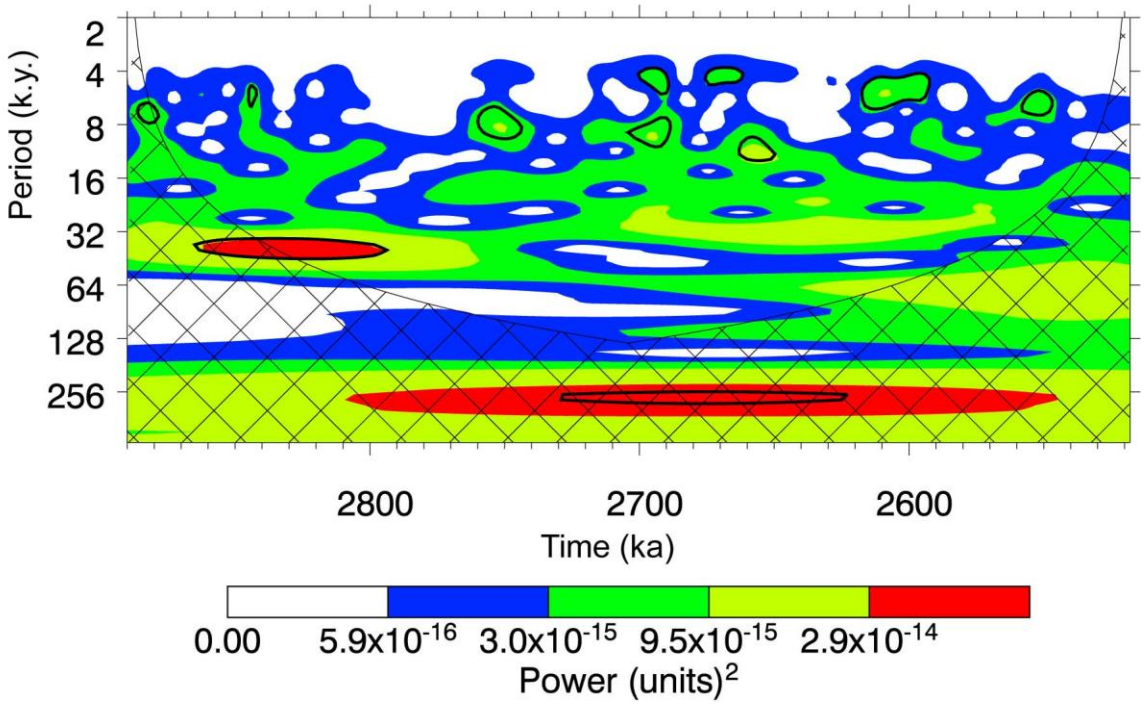

Figure 4.11: Results of wavelet power spectrum showing frequency power as a function of period and time. Wavelet constructed using a six parameter Morlet wavelet using the technique of Torrence and Campo (1998). Contour levels are chosen so that 75%, 50% 25% and 5% of the wavelet power is above each level, respectively. Black contour is the 5% significance level, using a red-noise (autoregressive) background spectrum. Cross-hatched region shows region where power is underestimated due to the effects of zero-padding.

DISCUSSION

Source and Significance of Magnetic Minerals

Magnetite in the Tapiado Formation is interpreted to be detrital in origin, supplied to the western part of regional Borrego Lake by the ancestral Carrizo Creek catchment. Magnetite in the pseudo-single domain (PSD) size range is too large to be a record of genesis from magnetotactic bacteria in the lake itself (Maher and Taylor, 1988; Dearing, 1999; Oldfield, 2007). Similarly, there is little or no record of pedogenesis in the lacustrine deposits of this study, and pedogenic magnetic enhancement (e.g. Geiss and Zanner, 2006) is unlikely. Magnetite grains in the Tapiado Formation are therefore interpreted to be detrital. Sediment in the study area was derived from the ancestral Carrizo Creek watershed, which today drains the Jacumba Mountains in the eastern Peninsular Ranges (Fig. 4.1; Peryam et al., 2012). Detrital magnetite likely was derived from Miocene intermediate to basaltic volcanic rocks and Triassic to Jurassic metamorphosed mafic to ultramafic rocks. The Late Cretaceous La Posta tonalite, also found in the modern Carrizo Creek watershed, is magnetite-free (Clinkenbeard and Walawender, 1989; Todd, 2004; Peryam et al., 2012).

Variations in our magnetic susceptibility time series are interpreted as a record of relative changes in rate of bedrock erosion in the Carrizo Creek catchment. Bulk magnetic susceptibility, hysteresis parameters, and IRM acquisition curves show no significant dependence on grain size or depositional environment (Fig. 4.12a; Tables 4.1 and 4.2). The abundance of magnetic grains is therefore independent of hydrologic regime, and must be controlled by allogenic forcing. Variations in supply of magnetic material probably reflect-fluctuations in the rate of regolith stripping in the Carrizo Creek

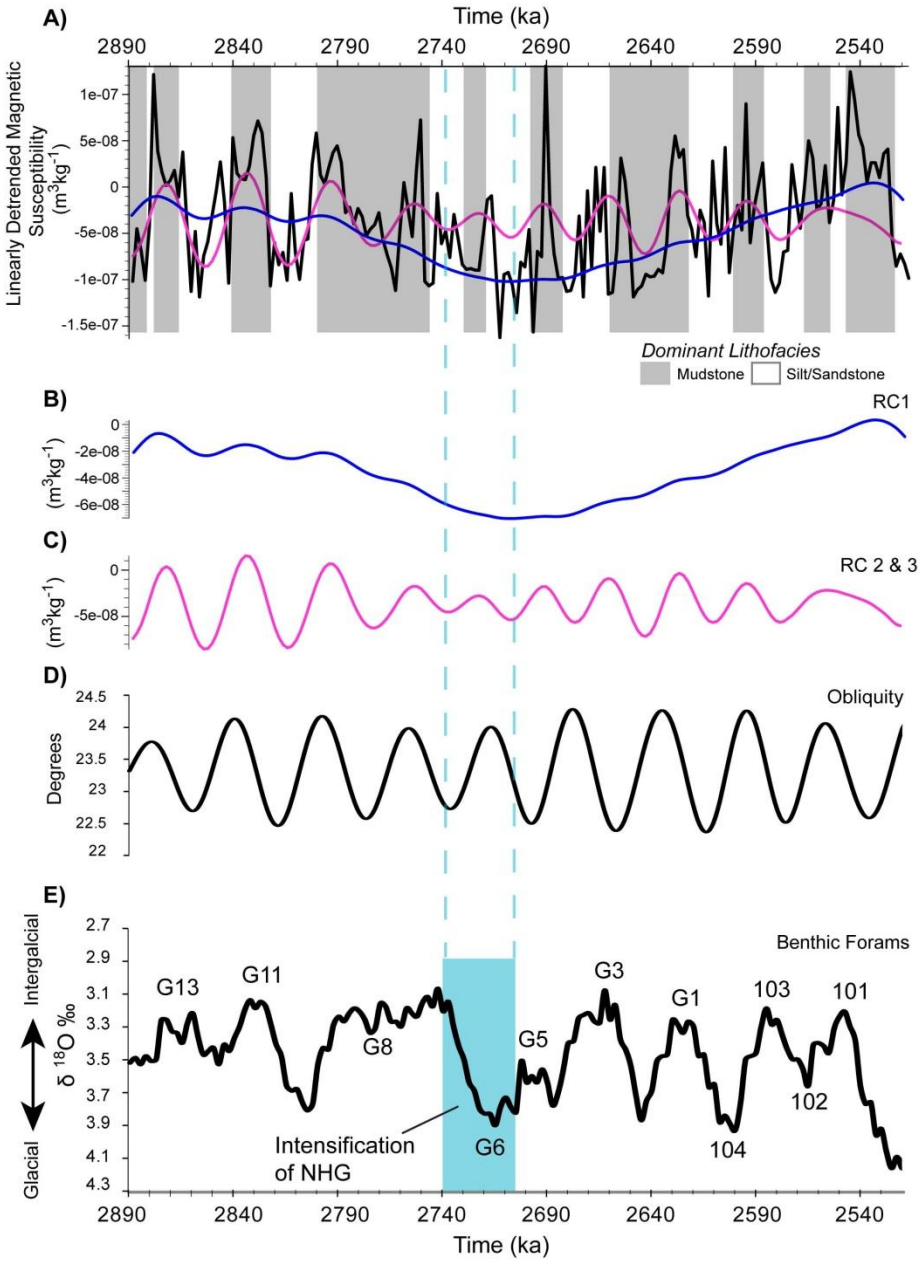

Figure 4.12: Comparison of data, time-series analysis, and global records. (A) Linearly detrended magnetic susceptibility with the first (blue line) and 2nd and 3rd (pink line) reconstructed components defined by singular spectrum analysis. (B) The first reconstructed component (RC1) interpreted as a long-wavelength non-linear trend. (C) The oscillatory ~40 k.y. period signal defined by the second and third reconstructed components (RC2 and RC3). (D) Reconstructed degree of orbital obliquity by Berger and Loutre (1991). (E) Globally-stacked, reconstructed $\delta^{18}O$ record of benthic foraminifers showing marine isotope stages and periods of relative global warmth and coolness, and intensification of northern hemisphere glaciation (NHG) glaciation at ~2.74 Ma (from Lisiecki and Raymo, 2005).

catchment and sediment flux to the lake margin. In this regard our interpretation of magnetic susceptibility is consistent with interpretations of Holocene lake records (e.g. Thompson et al., 1975; Bloumendal et al., 1979; Higgitt et al., 1991; Kodama et al., 1997). While no attempt has been made in this study to translate magnetic susceptibility to quantitative rates of hillslope denudation, erosional fluxes implied by the magnetic susceptibility record probably record fluctuations within the 0.03-0.06 mm/yr range of late Pliocene erosion rates calculated for the Carrizo Creek catchment by Longinotti et al. (2011).

In the pro-delta setting of the studied stratigraphic interval, water depth and distribution of sediment were controlled primarily by delta-lobe switching. We infer that changes in sedimentation rate and water depth, which might be expected to accompany allocyclic denudation-driven variations in sediment flux, were buffered by locally-controlled, autocyclic processes of delta lobe-switching. As a consequence, relative changes in the rate of catchment denudation that are implied by our magnetic susceptibility record do not correlate to grain size or water depth (Fig. 4.12a).

Driving Mechanisms of Time Series Variation

The abundance of noise in the magnetic susceptibility record suggests that denudation was driven by events that were either highly stochastic in nature or oscillating at frequencies below our sampling interval. Due to the amagnetic nature of much of the Carrizo Creek catchment, individual large mass-wasting events involving magnetite-bearing rocks could have had an impact on sediment magnetic mineral abundances out of proportion to the actual volume of mobilized material. The existence of long-wavelength trends and oscillations within the time series, however, strongly suggest that denudation

in the Carrizo Creek drainage was at least partly modulated by allocyclic forcing mechanisms in late Pliocene time.

Long-Term Trend

A low-frequency, quasiharmonic trend with a wavelength of between 300 to 320 k.y. in the magnetic susceptibility time series (Figs. 4.10-4.12) does not correspond to any known climate cycles and records a non-orbital, likely tectonic influence on catchment denudation rates. The primary control on late Pliocene uplift of the area encompassing the Carrizo Creek drainage was tectonism within the Ocotillo accommodation zone (Peryam et al., 2012). Intermittent uplift in this little-studied area may be responsible for the background trend detected by our spectral analysis.

Obliquity-Modulated Erosional Flux

Between ~2.9 and ~2.75 Ma a harmonic signal with a wavelength of ~40 k.y. is recorded in the magnetic susceptibility time series (Fig. 4.11). This signal is near the same frequency and is largely in phase with orbital obliquity during this time interval (Fig. 4.12a, c, d). The correspondence of magnetic susceptibility and Milankovitch orbital parameters strongly implies that hillslope denudation in the Carrizo Creek drainage was at least partly modulated by climate cyclicity during late Pliocene time.

Peaks in denudation rate reconstructed from our magnetic susceptibility time series (Fig. 4.12c) correspond closely to orbital obliquity maxima calculated by Berger and Loutre, 1991 (Fig. 4.12d). Obliquity maxima are strongly associated with longer summers, higher insolation at high latitudes, and reduced polar temperature gradients, especially during late Pliocene and early Pleistocene time (e.g. Raymo and Nisancioglu, 2003; Ravelo et al., 2004). While the Earth's climate during late Pliocene time was

transitioning away from the permanent El Niño conditions of the early and middle Pliocene (Wara et al., 2005; Federov et al., 2006), high obliquity periods in the late Pliocene have been attributed to periods of El Niño-like conditions in the Pacific Ocean basin (Lawrence et al., 2006). Modern El Niño-Southern Oscillation (ENSO) events produce marked increases in winter precipitation in southern California, and an increase in the abundance of tropical storms and hurricanes in the eastern Pacific Ocean (e.g. Cayan et al., 1998; Mo and Higgins, 1998; Minnich et al., 2000; Trenberth, 2005). Increases in summer monsoonal precipitation in northwest Mexico has also been associated with ENSO conditions (Reyes and Mejía-Trejo, 1991). In contrast, periods of low orbital obliquity are associated with glacial periods, which, in southwestern North America, are defined by a cool, dry climate with dominant winter precipitation and few large storms (Van Devender and Spaulding, 1979).

We therefore infer that cyclic variations in denudation rate between ca. 2.9 and 2.75 Ma record obliquity-driven variations in the frequency of large storms during this time interval. Extreme storm events have been shown to drive increases in erosion and sediment discharge in many geologic settings and models (e.g. Tucker and Slingerland, 1997; McDonald et al., 2003; Enzel et al., 2012). We propose that interglacial, ENSO-like conditions during obliquity highs led to more frequent high-intensity precipitation events in the study area (i.e. summer monsoonal storms and east Pacific hurricanes). These climate changes produced cyclic increases in rate of hillslope denudation and transport of sediment to Borrego Lake. Modeling by Tucker and Slingerland (1997) suggests that the denudation rate in eroding catchments responds immediately to an increase in runoff intensity. This contrasts with our data which, between 2.9 and 2.75

Ma., reveal a time lag of ca. 5-8 k.y. between peaks in the ~40 k.y. frequency component (Fig. 4.12c) and reconstructed peaks in orbital obliquity (Fig. 4.12d). The inferred time lag may record the average duration of sediment transport from hillslopes to the Borrego Lake margin. If this interpretation is correct, sediment storage may have buffered the 40 k.y. component of the time series and resulted in an underestimation of the impact of climate cyclicity on denudation rates.

Breakdown of Obliquity Modulation ca. 2.75 Ma

The termination of a significant ~40 k.y. signal in the magnetic susceptibility record at ca. 2.75 Ma (Fig. 4.11) corresponds to intensification of northern hemisphere glaciation, and likely records local climate reorganization in response to long-term global change. The obliquity-frequency (~40 k.y.) signal in the magnetic susceptibility time series weakens after 2.8 Ma and largely vanishes around 2.75 Ma (Figs. 4.11, 4.12). Marine isotope stage G6 (beginning ca. 2.74 Ma) is associated with a dramatic increase in northern hemisphere glaciation and the onset of globally significant, orbitally-controlled glacial/interglacial cycles seen in marine oxygen-isotope records (Raymo, 1994; Maslin et al., 1998; Kleiven et al., 2002; Ravelo et al., 2004; Haug et al., 2005; Mundelsee and Raymo, 2005). We propose that the end of obliquity-modulated erosion cycles in the Carrizo Creek catchment was the local manifestation of this dramatic change in the global climate system. El Niño conditions, which had persisted during obliquity highs during early to middle Pliocene time, became rare to absent as upwelling reduced sea surface temperatures in the eastern Pacific Ocean (Federov et al., 2006; Dekens, 2007). The onset of northern hemisphere glaciation at ca. 2.74 Ma, and corresponding end of strongly cyclic variations in hillslope erosion in the Carrizo Creek catchment (this study),

culminated a long-term gradual increase in aridity and decrease in high-intensity summer precipitation events in southern California (Peryam et al., 2011).

CONCLUSIONS

Time series analysis of magnetic susceptibility shows that, between ~2.9 and 2.75 Ma influx of magnetic minerals to Borrego Lake was modulated by cyclic variations in orbital obliquity. High rates of erosional denudation in the Carrizo Creek catchment correspond to previously published obliquity maxima, and are interpreted to record high intensity precipitation events (i.e. summer monsoons and tropical storms) during prolonged high-obliquity El Niño periods. The effect of orbital obliquity on denudation rates disappears around 2.75 Ma, which corresponds in time with a dramatic increase in northern hemisphere glaciation. We propose that this well documented global climate shift accelerated the waning of prolonged El Niño conditions in the eastern Pacific Ocean. After ~2.75 Ma, obliquity highs, while still associated with interglacial periods, no longer caused marked increases in high-intensity storms in the study area. Our finding that erosion rates in southern California became less responsive to orbital obliquity after ca. 2.74 Ma contrasts with global reconstructions which show that high-latitude climates became much more responsive to obliquity forcing after this time (e.g. Ravelo et al., 2004). This apparent contradiction reflects the weakening of monsoonal precipitation in southern California during mid to late Pliocene time, and highlights the importance of reconstructing region-specific responses to past global climate change.

APPENDIX A

PALEOSOL LOCATIONS AND SAMPLE AGES

	UTM (NAD 83)				
Paleosol	**Northing**	**Easting**	**Sample #**	**Type**	**Age (Ma)**
2009-18	576493	3637260	P09-AB-35	Calcic	0.7 ± 0.25
D-63	569852	3645422	P08-AB-23,24	Calcic	0.7 ± 0.25
D-61	569749	3645364	P08-AB-22a,b	Calcic	0.7 ± 0.25
D-62	571418	3643527		Calcic	1 ± 0.15
D-59	571549	3643778	P08-AB-19	Calcic	1.1 ± 0.06
D-65	570712	3644980		Calcic	1.1 ± 0.1
D-58	571560	3644076		Calcic	1.2 ± 0.1
D-57	571644	3644022	P08-AB-18	Calcic	1.21 ± 0.07
D-64	571586	3644233	P08-AB-25	Calcic	1.27 ± 0.06
D-55	571920	3644180	P08-AB-17	Calcic	1.42 ± 0.05
2009-5	571897	3644397	P09-AB-13	Other	1.43 ± 0.06
D-54	571500	3644817		Calcic	1.45 ± 0.1
D-51	571785	3644605	P09-AB-14	Calcic	1.46 ± 0.06
D-52	571785	3644605		Calcic	1.46 ± 0.06
D-53	571785	3644605		Calcic	1.46 ± 0.06
D-47	571959	3644440	P08-AB-15	Calcic	1.5 ± 0.05
D-56	572129	3644471		Calcic	1.5 ± 0.1
D-49	572034	3644696	P08-AB-16	Calcic	1.68 ± 0.05
2009-36	573375	3643289	P09-AB-42	Calcic	1.69 ± 0.04
D-48	572234	3644601		Calcic	1.7 ± 0.1
2009-22	572768	3644227	P08-AB-13	Other	1.79 ± 0.03
2009-23	573501	3643351	P09-AB-38	Calcic	1.8 ± 0.03
D-46	572048	3644953	P08-AB-14	Calcic	1.84 ± 0.03
D-42	572577	3644508		Calcic	1.85 ± 0.1
D-43	572577	3644508		Calcic	1.85 ± 0.1
D-45	572048	3644953		Calcic	1.85 ± 0.1
D-37	573178	3644118		Calcic	1.92 ± 0.06
D-38	573178	3644118		Calcic	1.92 ± 0.06
D-39	573178	3644118	P08-AB-12	Calcic	1.92 ± 0.06
D-35	573660	3643494	P08-AB-11	Calcic	1.94 ± 0.03
3/8/09a	570453	3647406	P09-AB-32	Calcic	2.03 ± 0.04
2009-17	574750	3642488	P09-AB-34	Other	2.11 ± 0.098
2009-11	572352	3645528	-	Other	2.15 ± 0.1
2/16/09a	572446	3645522	P09-AB-28	Calcic	2.15 ± 0.04
2009-16	575075	3642367	P09-AB-33	Calcic	2.1 ± 0.06
D-31	572995	3645404		Calcic	2.2 ± 0.1
D-30	572921	3645385		Calcic	2.25 ± 0.1
D-27	572616	3645624		Calcic	2.25 ± 0.04
D-28	572616	3645624	P08-AB-9	Calcic	2.25 ± 0.04
2009-10	572570	3645740	P09-AB-26	Calcic	2.34 ± 0.02

Appendix A (continued)

	UTM (NAD 83)				
Paleosol	**Northing**	**Easting**	**Sample #**	**Type**	**Age (Ma)**
D-22	572797	3645966	P08-AB-7	Calcic	2.39 ± 0.02
D-20	572584	3646641		Calcic	2.6 ± 0.1
D-21	572626	3646605	P09-AB-12	Calcic	2.6 ± 0.1
D-19	572580	3646685	P08-AB-6	Calcic	2.61 ± 0.1
2009-4	572580	3646685	P09-AB-11	Calcic	2.62 ± 0.1
2009-3	572565	3664810	P09-AB-10	Calcic	2.7 ± 0.09
D-17	572614	3646874	P08-AB-5	Calcic	2.76 ± 0.07
2009-7	577710	3641466	P09-AB-22	Vertic	2.8 ± 0.2
2009-2	572629	3647017	P09-AB-9	Calcic	2.85 ± 0.04
2009-35	578324	3640106	P09-AB-41	Calcic	2.9 ± 0.1
2009-8	578194	3640979	P09-AB-23	Vertic	3 ± 0.2
2009-6	582077	3635946	P09-AB-20	Vertic	3 ± 0.2
D-70	573630	3646976	P08-AB-31	Calcic	3.18 ± 0.06
D-12	573029	3647519	P08-AB-4	Calcic	3.23 ± 0.05
2009-1	572859	3647816	P09-AB-6	Calcic	3.25 ± 0.03
2009-1b	572859	3647816	P09-AB-7	Calcic	3.25 ± 0.03
D-07	572754	3647939		Calcic	3.25 ± 0.1
2009-32	578044	3642962		Vertic	3.3 ± 0.2
2009-33	577956	3643231		Vertic	3.3 ± 0.2
2009-34	577956	3643231		Vertic	3.3 ± 0.2
2009-15	572287	364883	P09-AB-31	Calcic	3.3 ± 0.01
2009-14	572303	3648458		Other	3.31 ± 0.1
2009-19	571644	3649753		Vertic	3.4 ± 0.15
2009-20	572195	3649457	P09-AB-37	Vertic	3.4 ± 0.15
2009-21	572147	3649282		Vertic	3.4 ± 0.15
D-01	573266	3648186	P08-AB-3	Calcic	3.41 ± 0.1
2009-13	573790	3648163		Vertic	3.5 ± 0.1
2009-13b	573790	3648163		Vertic	3.5 ± 0.1
2009-13c	573790	3648163		Vertic	3.5 ± 0.1
D-67	573613	3648535	P08-AB-28	Calcic	3.53 ± 0.1
2009-24	570253	3651313	P09-AB-39	Calcic	3.55 ± 0.15
2009-25	571561	3650403		Vertic	3.55 ± 0.15
2009-26	571667	3650407		Vertic	3.55 ± 0.15
2009-28	576359	3647591		Vertic	3.6 ± 1.5
D-66	574286	3649029	P08-AB-26	Calcic	3.7 ± 0.01
2009-27	573976	3648849		Vertic	3.75 ± 0.15
2009-29	576716	3647197	P09-AB-40	Calcic	3.83 ± 0.01
2009-30	576127	3646967		Vertic	3.9 ± 1.5
2009-31	577081	3647497		Vertic	3.9 ± 1.5

APPENDIX B

MULTIPLE ANALYSES OF FIVE CARBONATE SAMPLES

Sample	Run #	$\delta^{13}C$	$\delta^{18}O$
P08-AB-3	1	-9.06 ± 0.15	-10.4 ± 0.16
	2	-9.02 ± 0.11	-10.16 ± 0.13
	Standard Deviation	0.03	0.17
	Range	0.04	0.12
	Average	**-9.04**	**-10.28**
P08-AB-31	1	-3.36 ± 0.07	-9.74 ± 0.1
	2	-3.18 ± 0.07	-9.46 ± 0.08
	Standard Deviation	0.13	0.20
	Range	0.18	0.28
	Average	**-3.27**	**-9.60**
P08-AB-26	1	-4.1 ± 0.15	-10.45 ± 0.14
	2	-4.29 ± 0.08	-11.19 ± 0.09
	3	-4.42 ± 0.07	-11.56 ± 0.07
	4	-3.82 ± 0.06	-10.71 ± 0.11
	5	-4.51 ± 0.09	-11.21 ± 0.21
	Standard Deviation	0.28	0.44
	Range	.69	1.11
	Average	**-4.23**	**-11.02**
P08-AB-19	1	-3.74 ± 0.07	-8.35 ± 0.08
	2	-3.57 ± 0.04	-8.13 ± 0.05
	Standard Deviation	0.28	0.16
	Range	0.17	0.22
	Average	**-3.65**	**-8.24**
P08-AB-16	1	-3.58 ± 0.16	-10.08 ± 0.15
	2	-3.35 ± 0.06	-9.61 ± 0.01
	Standard Deviation	0.16	0.33
	Range	0.23	0.44
	Average	**-3.46**	**-9.84**

APPENDIX C

MEASURED STRATIGRAPHIC SECTIONS AND MAGNETOSTRATIGRAPHIC SAMPLE LOCATIONS

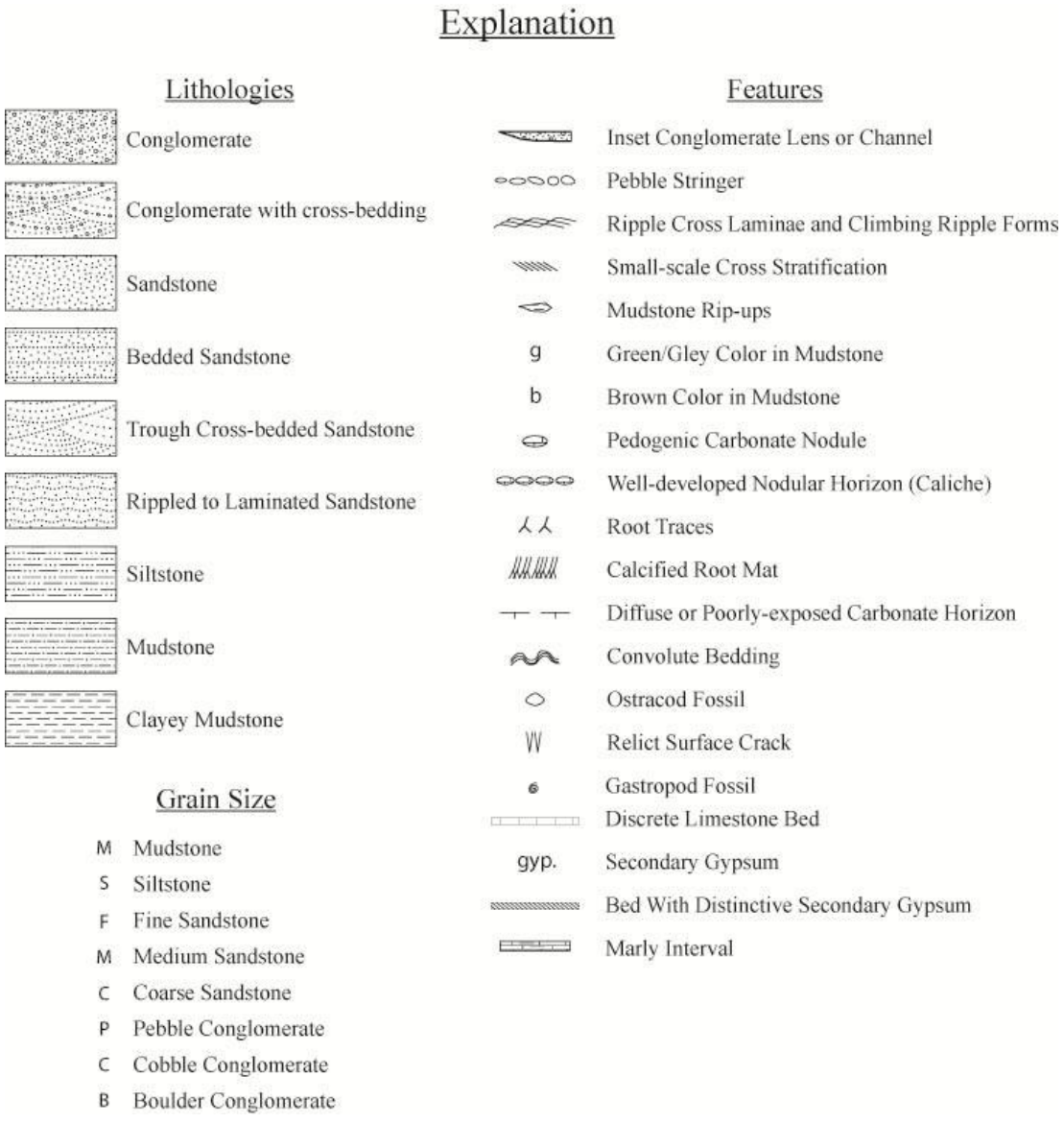

Section 1

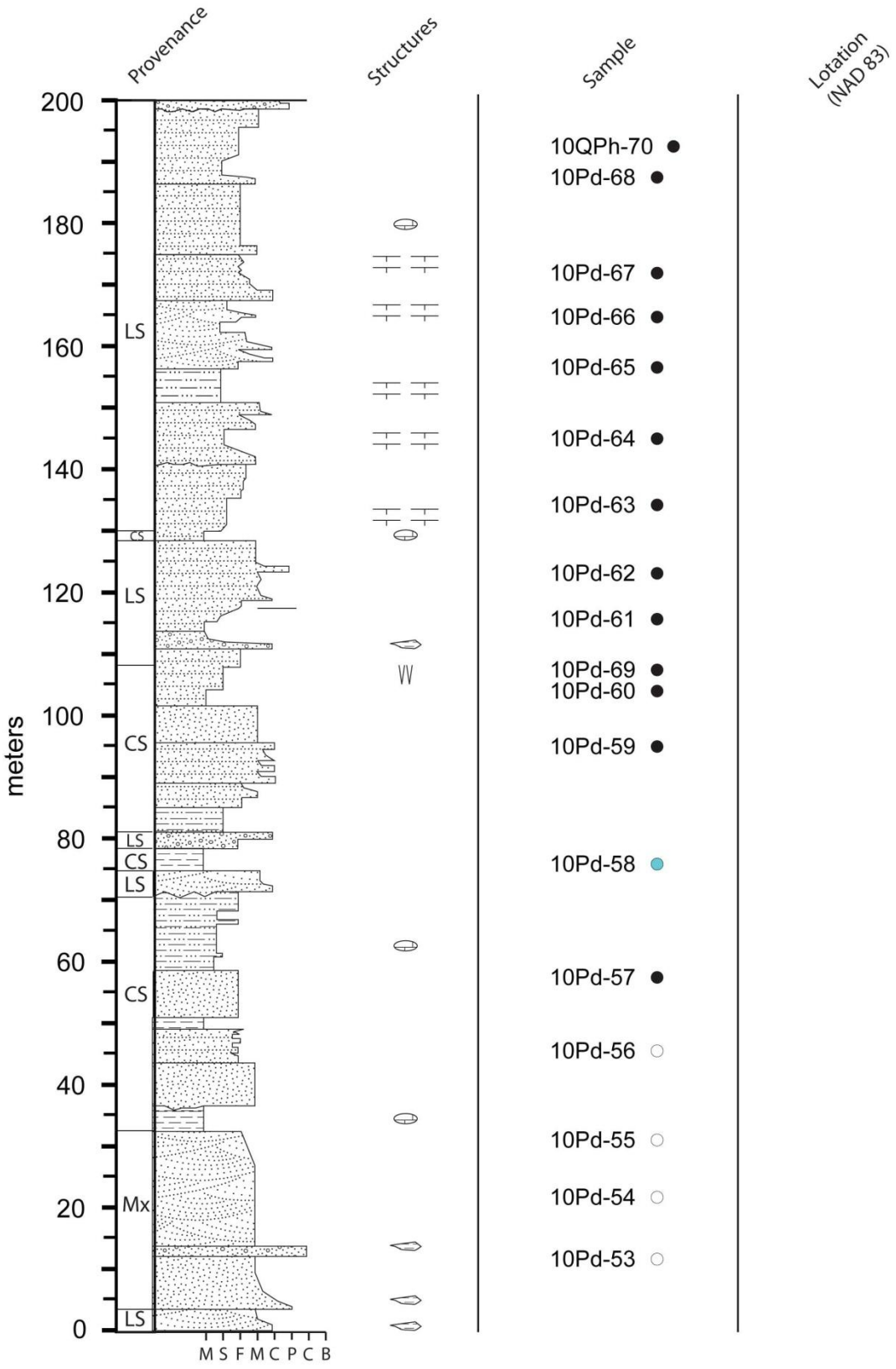
Provenance
Structures
Sample
Lotation (NAD 83)
meters
200
180
160
140
120
100
80
60
40
20
0
LS
CS
LS
CS
LS
CS
LS
CS
LS
Mx
LS
M S F M C P C B
10QPh-70
10Pd-68
10Pd-67
10Pd-66
10Pd-65
10Pd-64
10Pd-63
10Pd-62
10Pd-61
10Pd-69
10Pd-60
10Pd-59
10Pd-58
10Pd-57
10Pd-56
10Pd-55
10Pd-54
10Pd-53

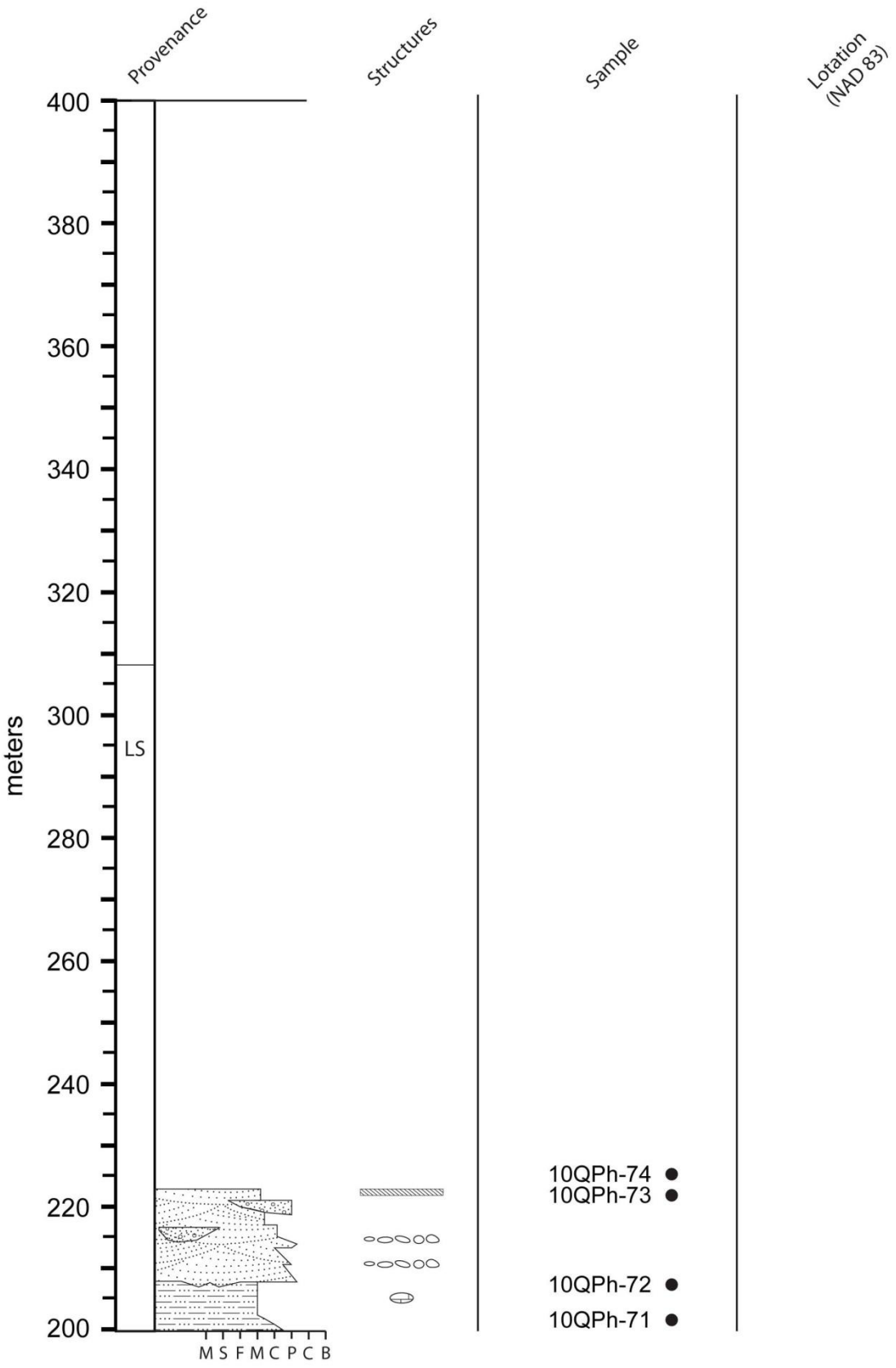
Provenance
Structures
Sample
Lotation (NAD 83)
meters
400
380
360
340
320
300
280
260
240
220
200
LS
M S F M C P C B
10QPh-74
10QPh-73
10QPh-72
10QPh-71

Section 2

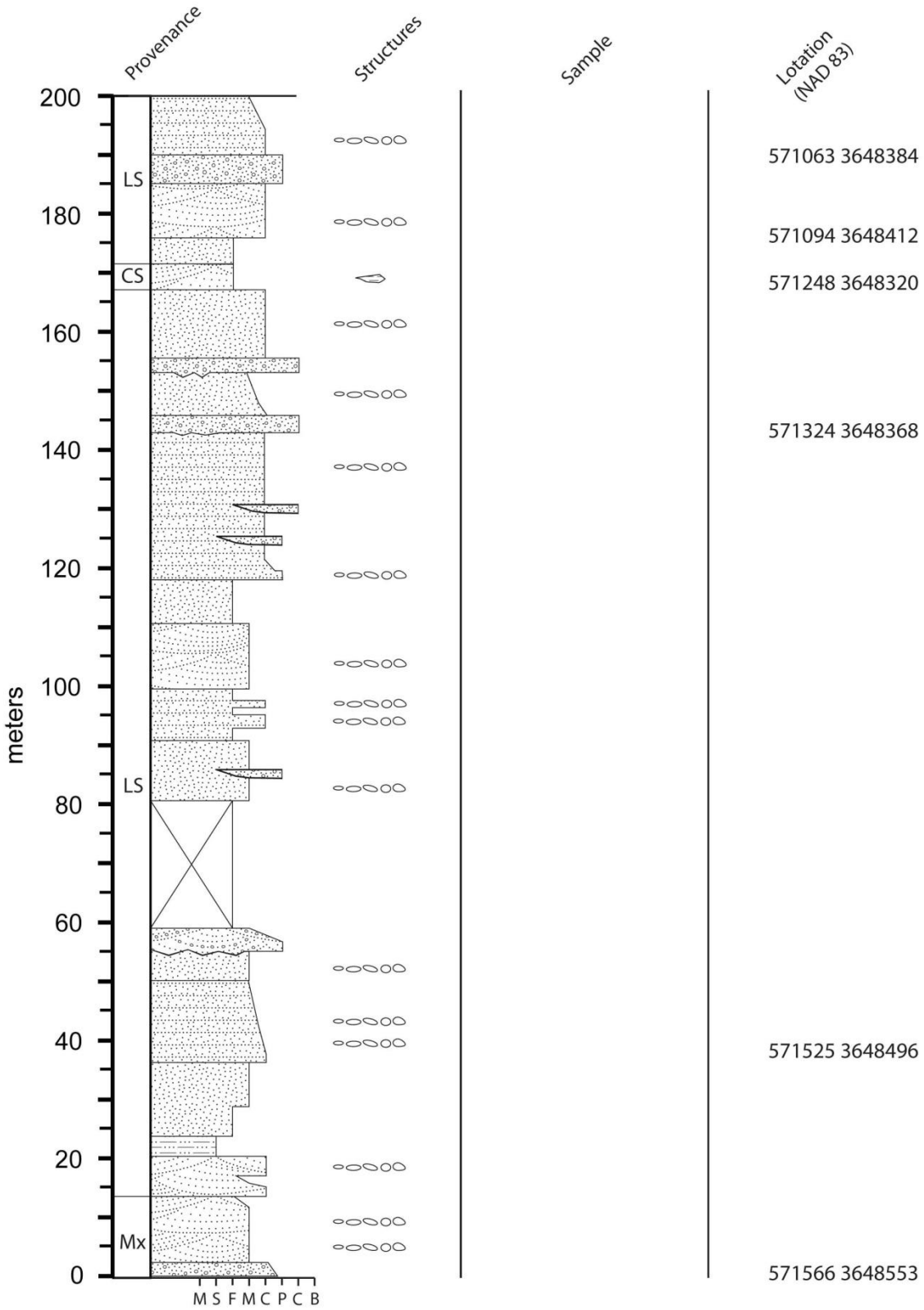
Provenance
Structures
Sample
Lotation (NAD 83)
meters
200
180
160
140
120
100
80
60
40
20
0
LS
CS
LS
Mx
M S F M C P C B
571063 3648384
571094 3648412
571248 3648320
571324 3648368
571525 3648496
571566 3648553

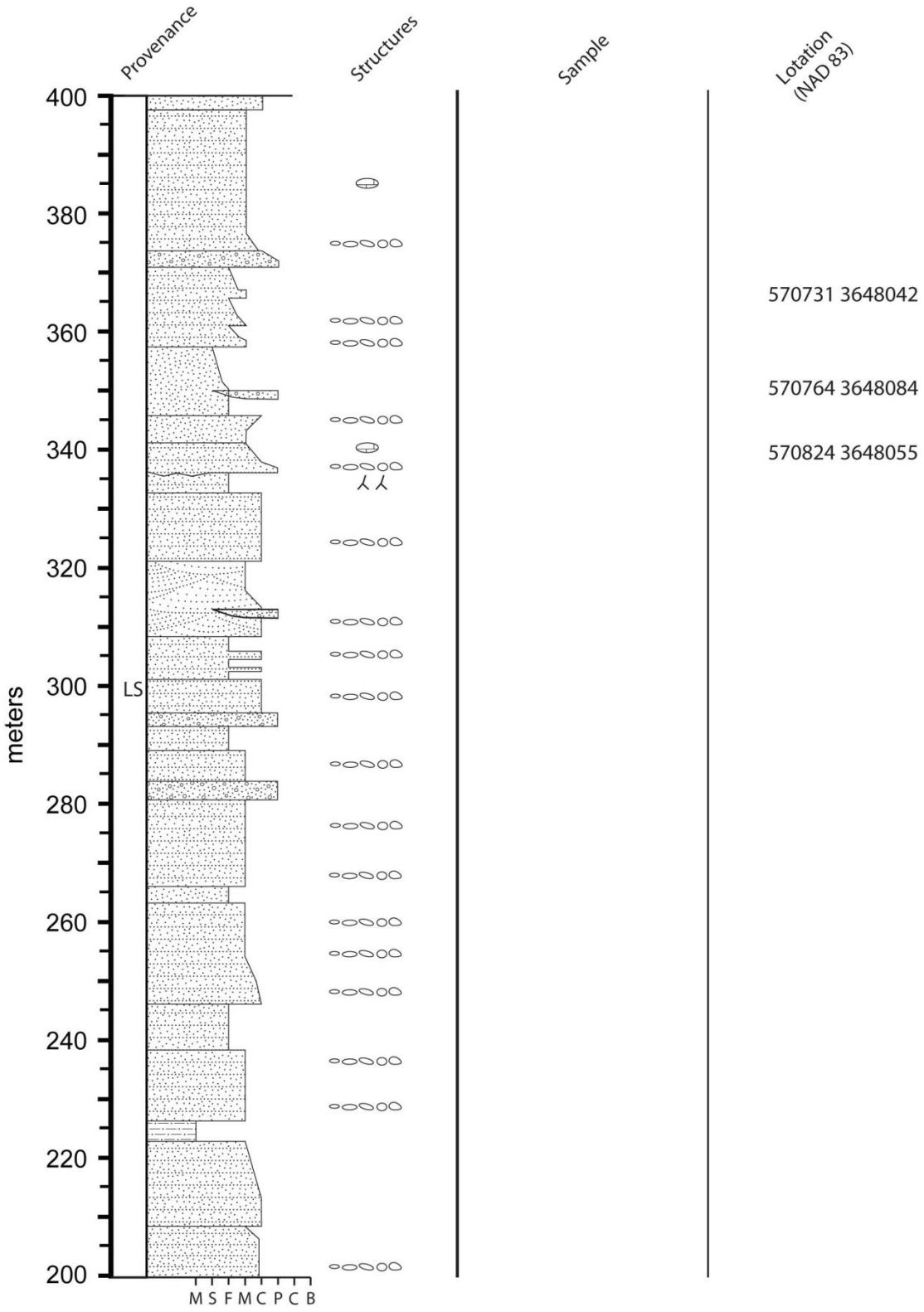
Provenance
Structures
Sample
Lotation (NAD 83)
meters
400
380
360
340
320
300
280
260
240
220
200
LS
M S F M C P C B
570731 3648042
570764 3648084
570824 3648055

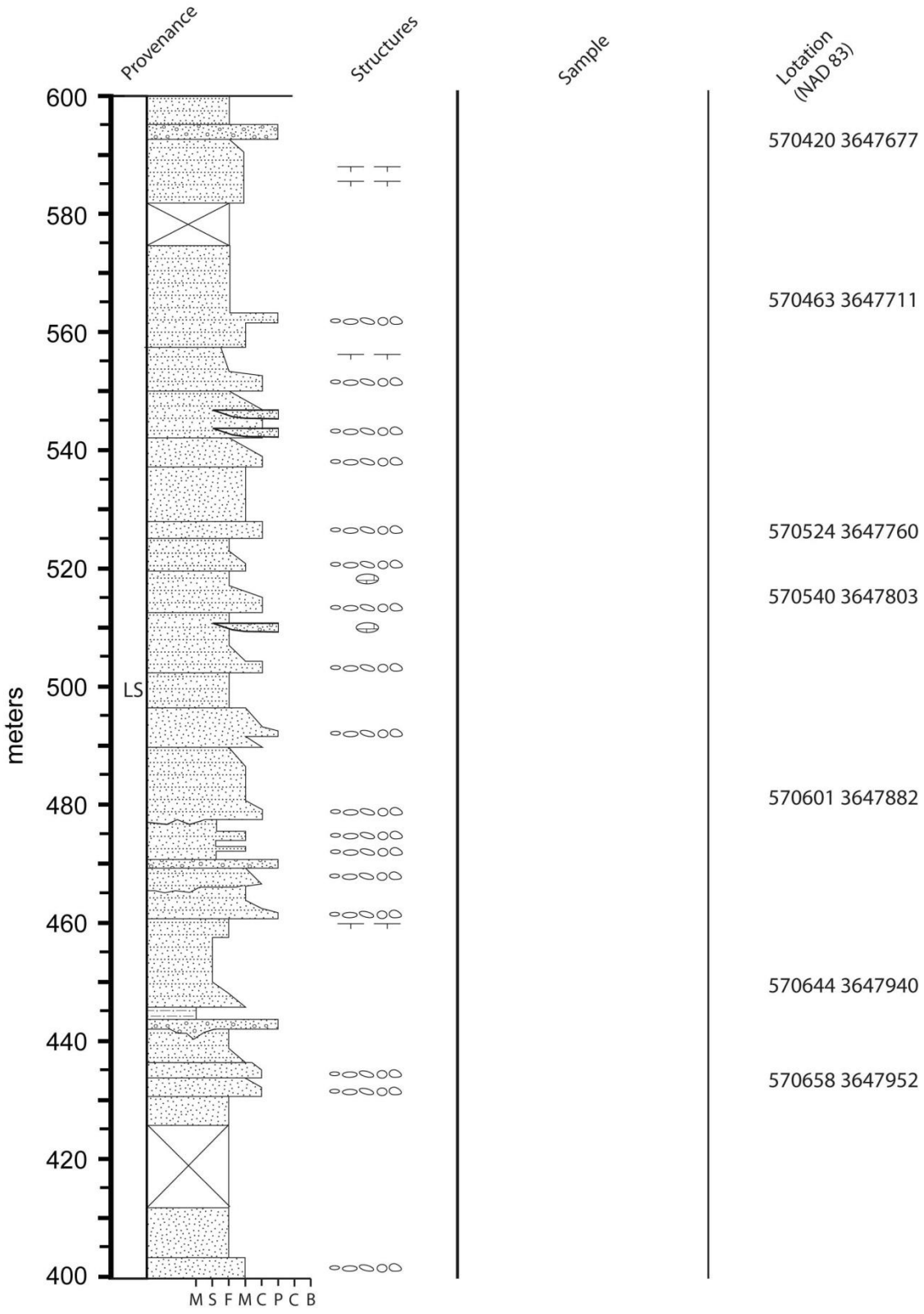
Provenance
Structures
Sample
Lotation (NAD 83)
meters
600
580
560
540
520
500
480
460
440
420
400
LS
M S F M C P C B
570420 3647677
570463 3647711
570524 3647760
570540 3647803
570601 3647882
570644 3647940
570658 3647952

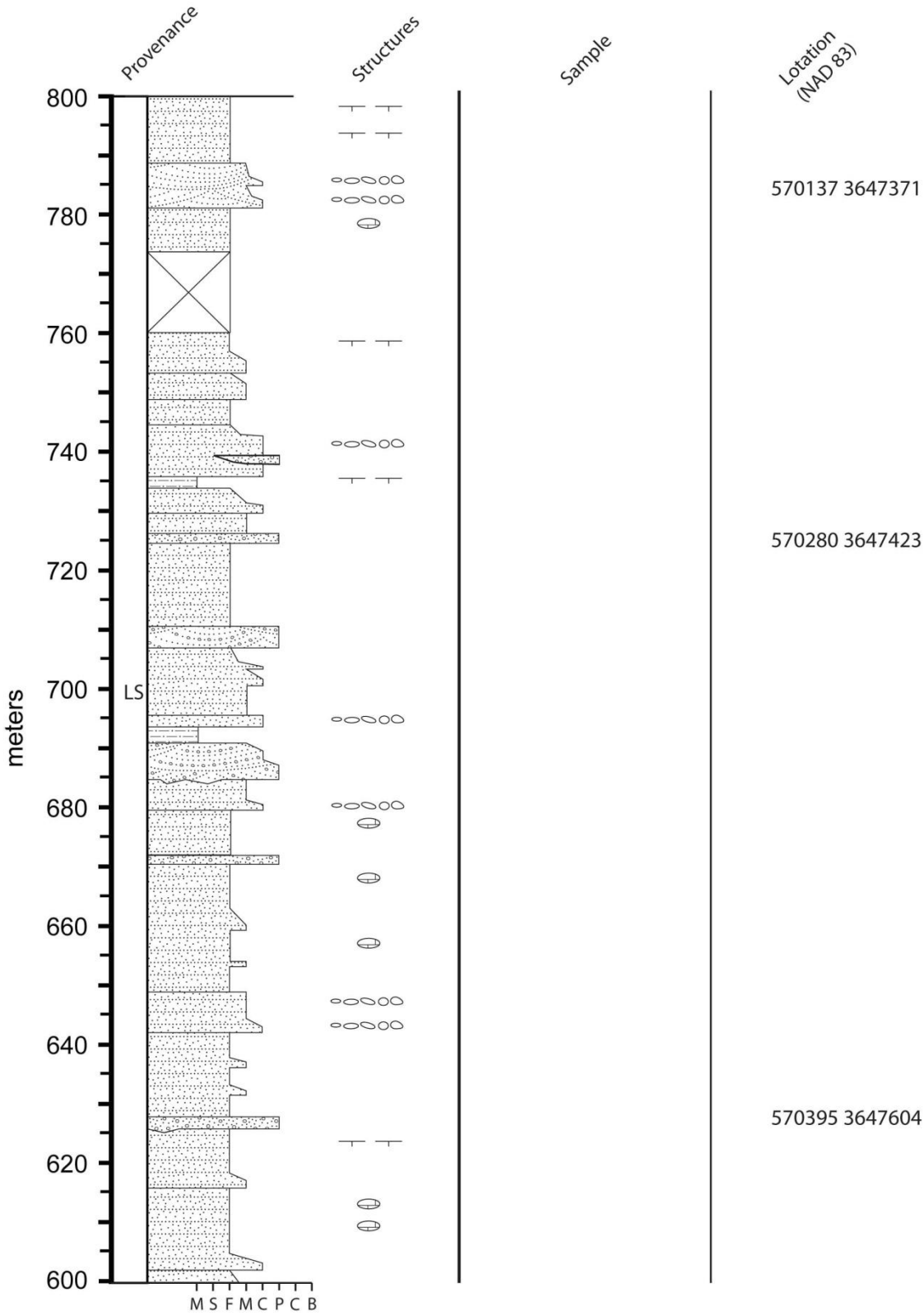
Provenance
Structures
Sample
Lotation (NAD 83)
800
780
760
740
720
700
680
660
640
620
600
meters
LS
M S F M C P C B
570137 3647371
570280 3647423
570395 3647604

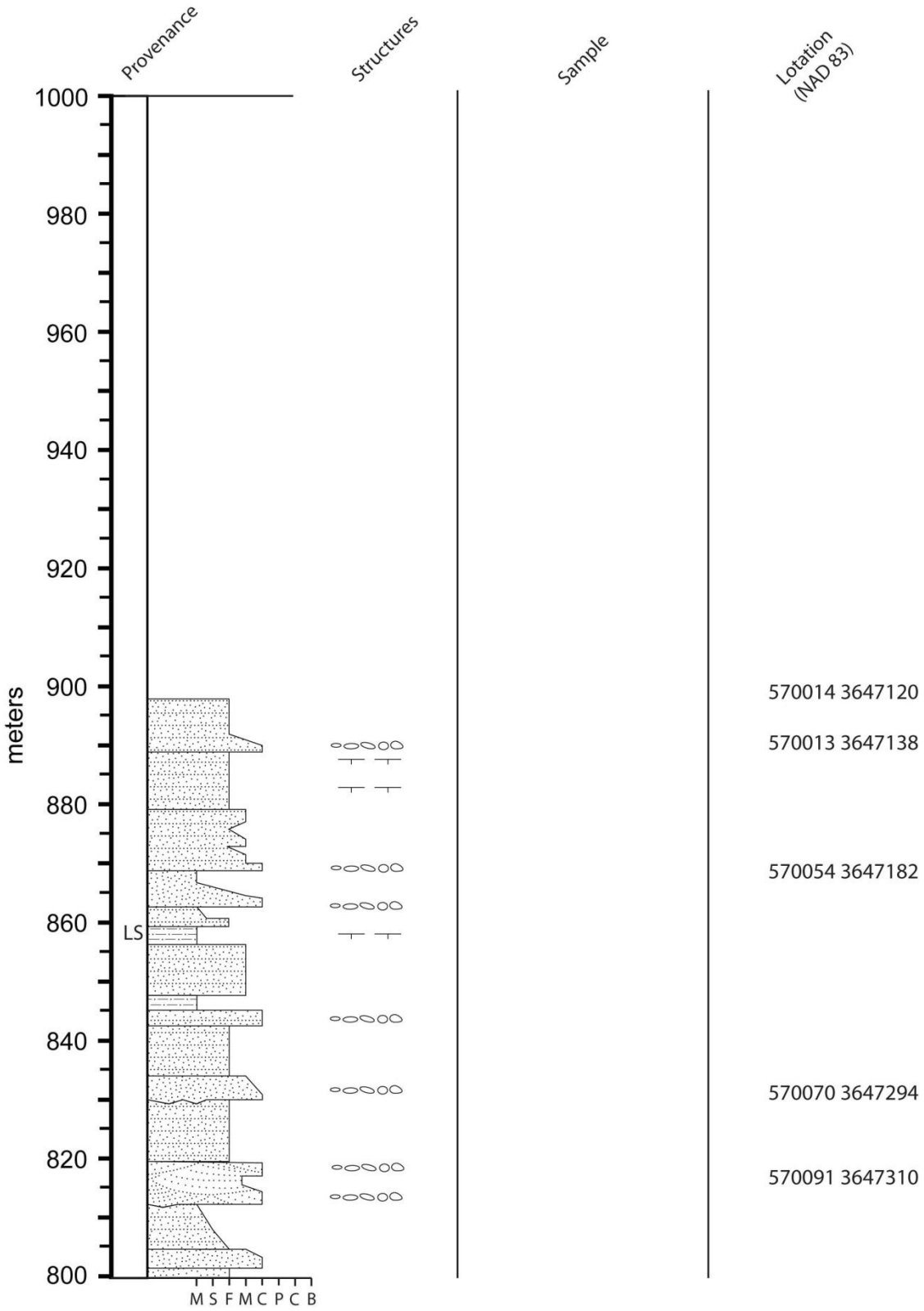
Provenance
Structures
Sample
Lotation (NAD 83)
1000
980
960
940
920
900
880
860
840
820
800
meters
LS
M S F M C P C B
570014 3647120
570013 3647138
570054 3647182
570070 3647294
570091 3647310

Section 3

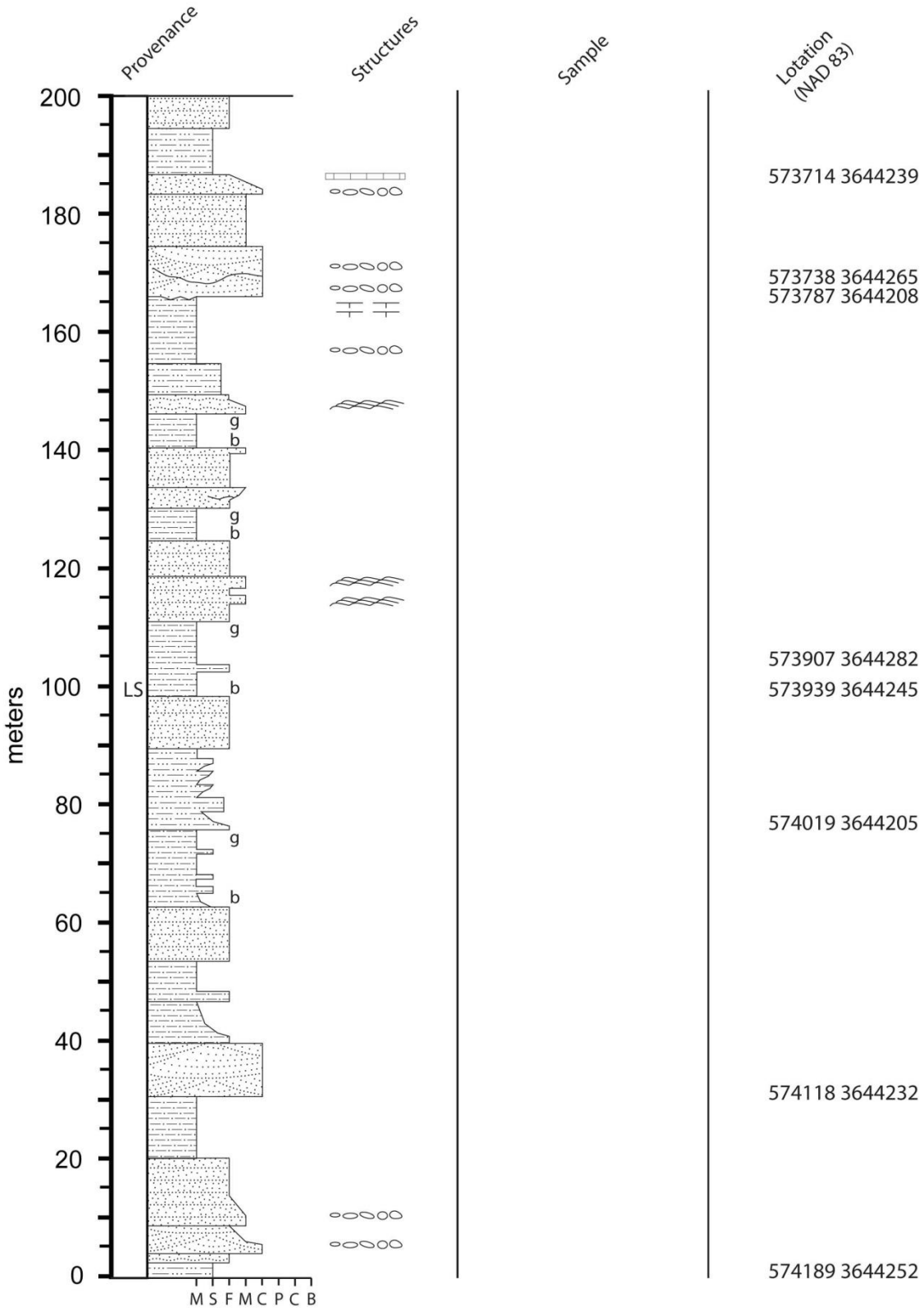
Provenance
Structures
Sample
Lotation (NAD 83)
meters
200
180
160
140
120
100
80
60
40
20
0
LS
g
b
M S F M C P C B
573714 3644239
573738 3644265
573787 3644208
573907 3644282
573939 3644245
574019 3644205
574118 3644232
574189 3644252

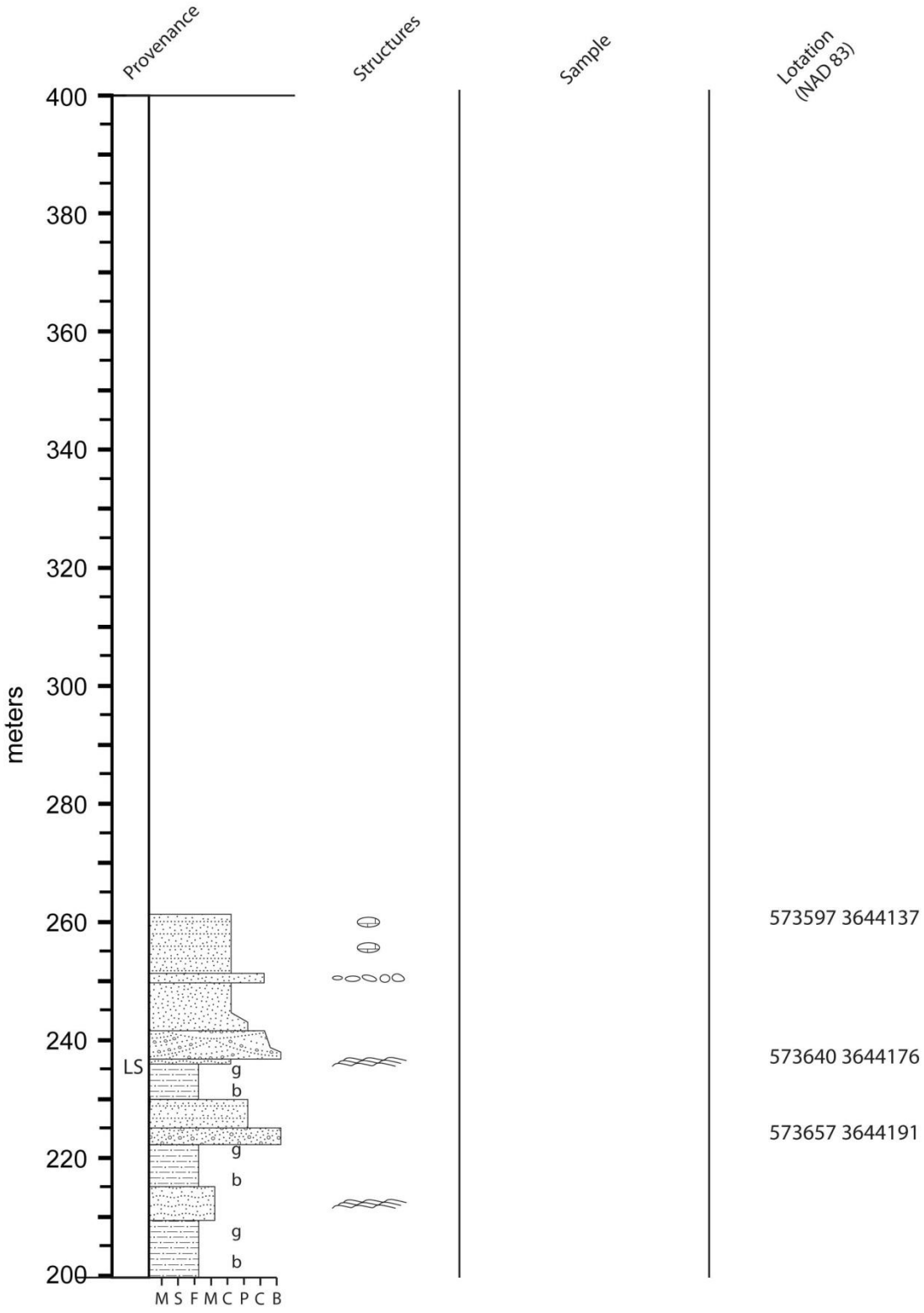
Provenance
Structures
Sample
Lotation (NAD 83)
meters
400
380
360
340
320
300
280
260
240
220
200
LS
g
b
g
b
g
b
M S F M C P C B
573597 3644137
573640 3644176
573657 3644191

Section 4

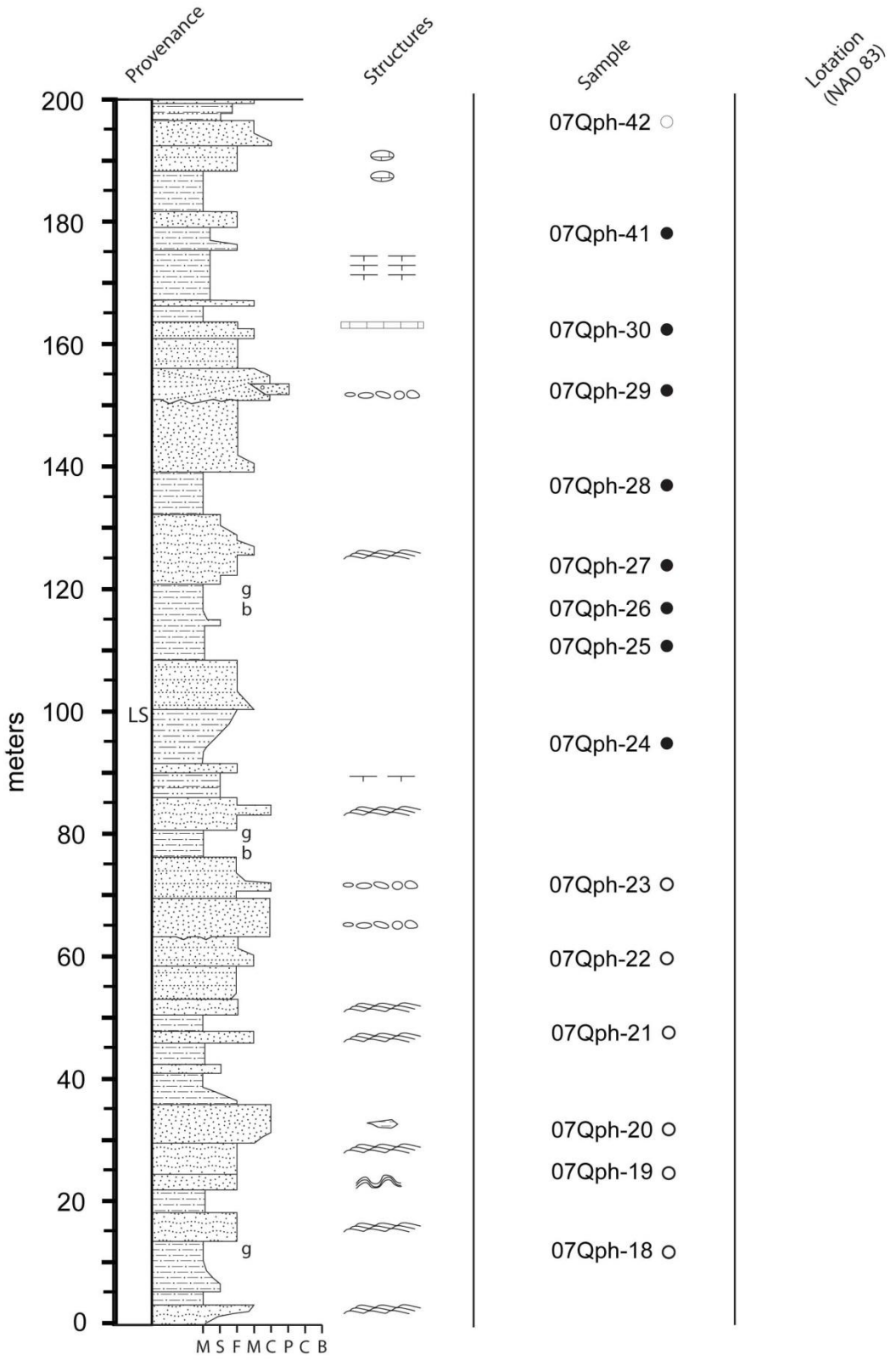
Provenance
Structures
Sample
Lotation (NAD 83)
meters
200
180
160
140
120
100
80
60
40
20
0
LS
g
b
g
b
g
M S F M C P C B
07Qph-42
07Qph-41
07Qph-30
07Qph-29
07Qph-28
07Qph-27
07Qph-26
07Qph-25
07Qph-24
07Qph-23
07Qph-22
07Qph-21
07Qph-20
07Qph-19
07Qph-18

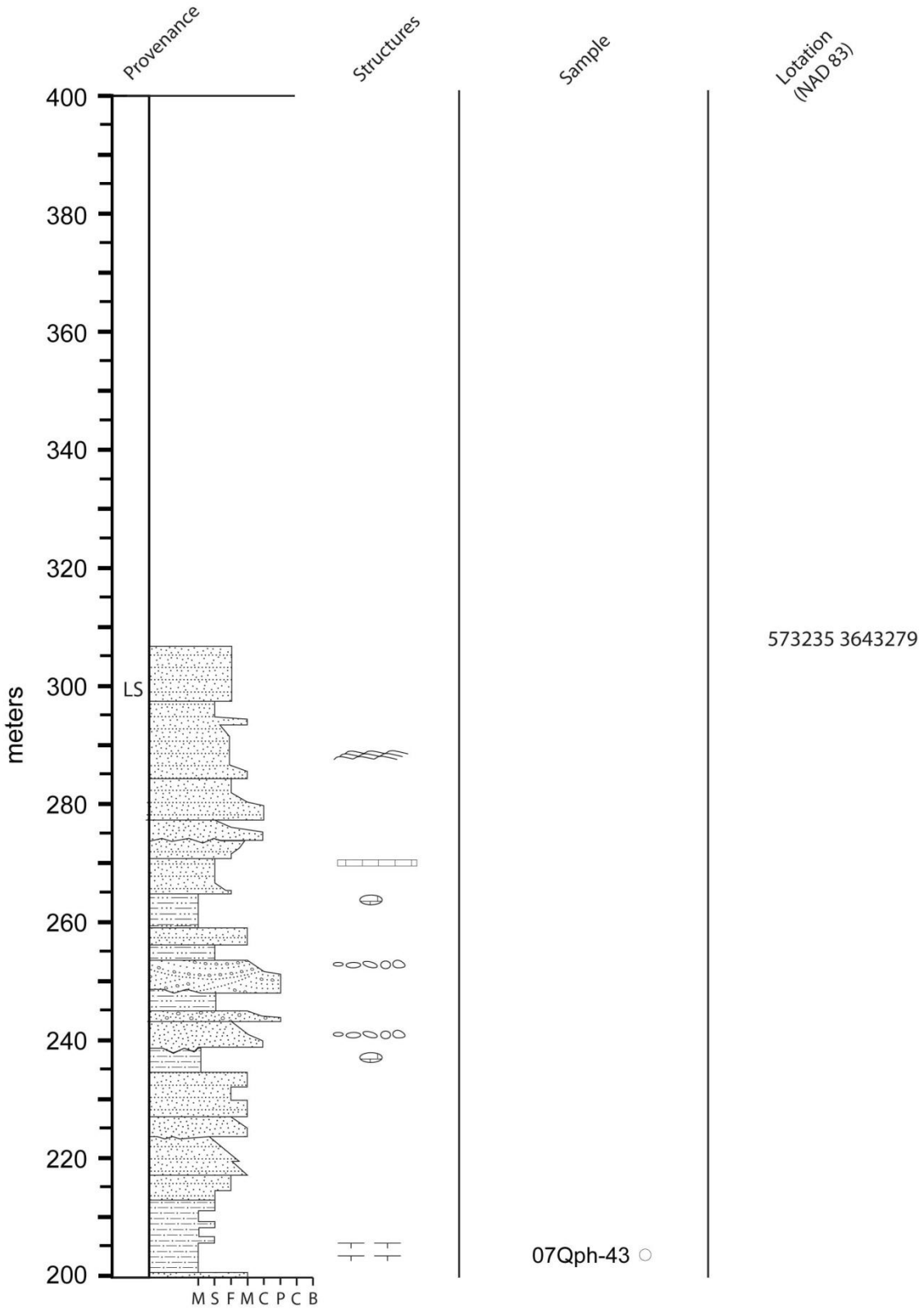
Provenance
Structures
Sample
Lotation (NAD 83)
400
380
360
340
320
300
280
260
240
220
200
meters
LS
M S F M C P C B
573235 3643279
07Qph-43

Section 5

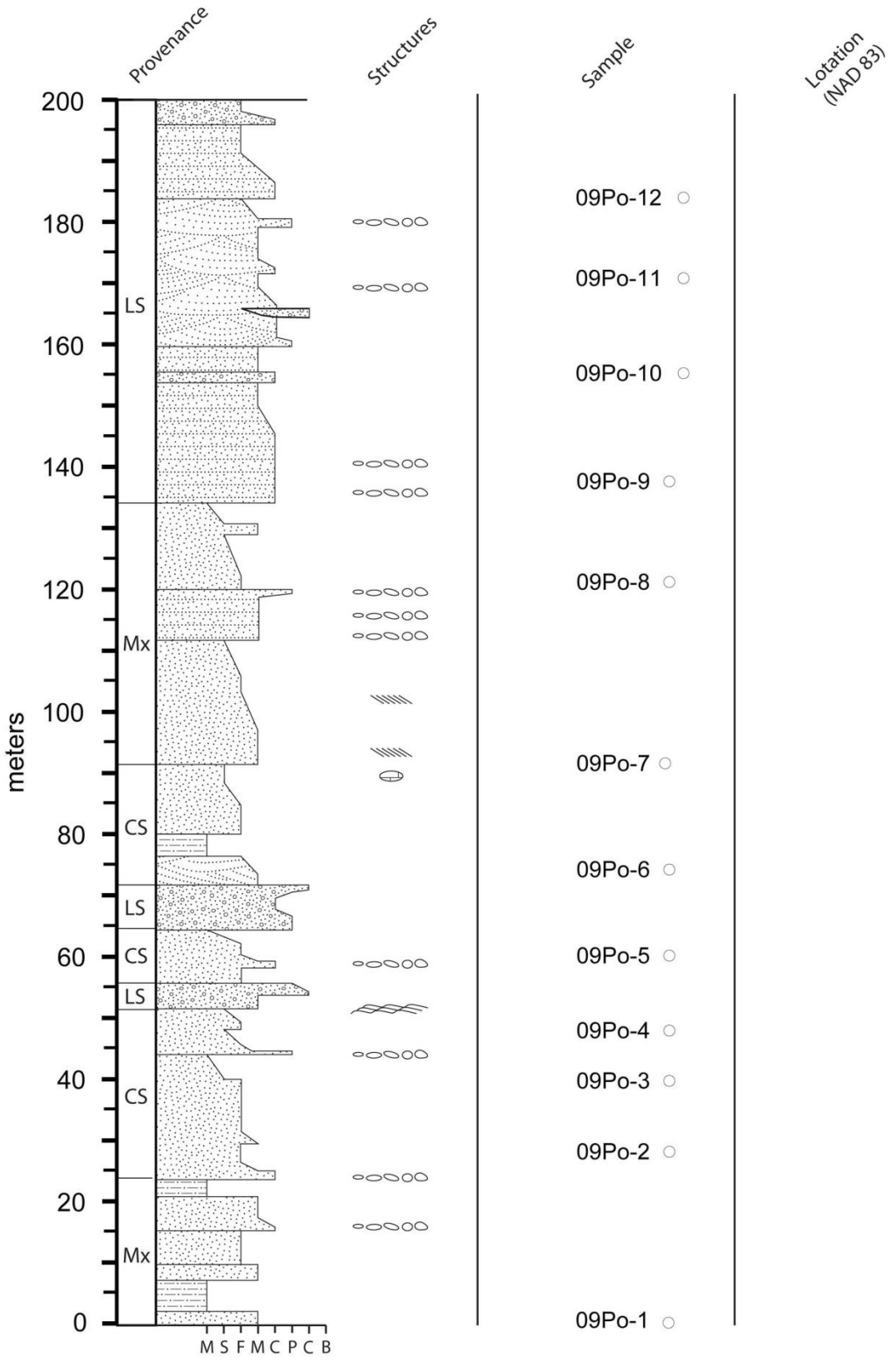
Provenance
Structures
Sample
Lotation (NAD 83)
meters
200
180
160
140
120
100
80
60
40
20
0
LS
Mx
CS
LS
CS
LS
CS
Mx
M S F M C P C B
09Po-12
09Po-11
09Po-10
09Po-9
09Po-8
09Po-7
09Po-6
09Po-5
09Po-4
09Po-3
09Po-2
09Po-1

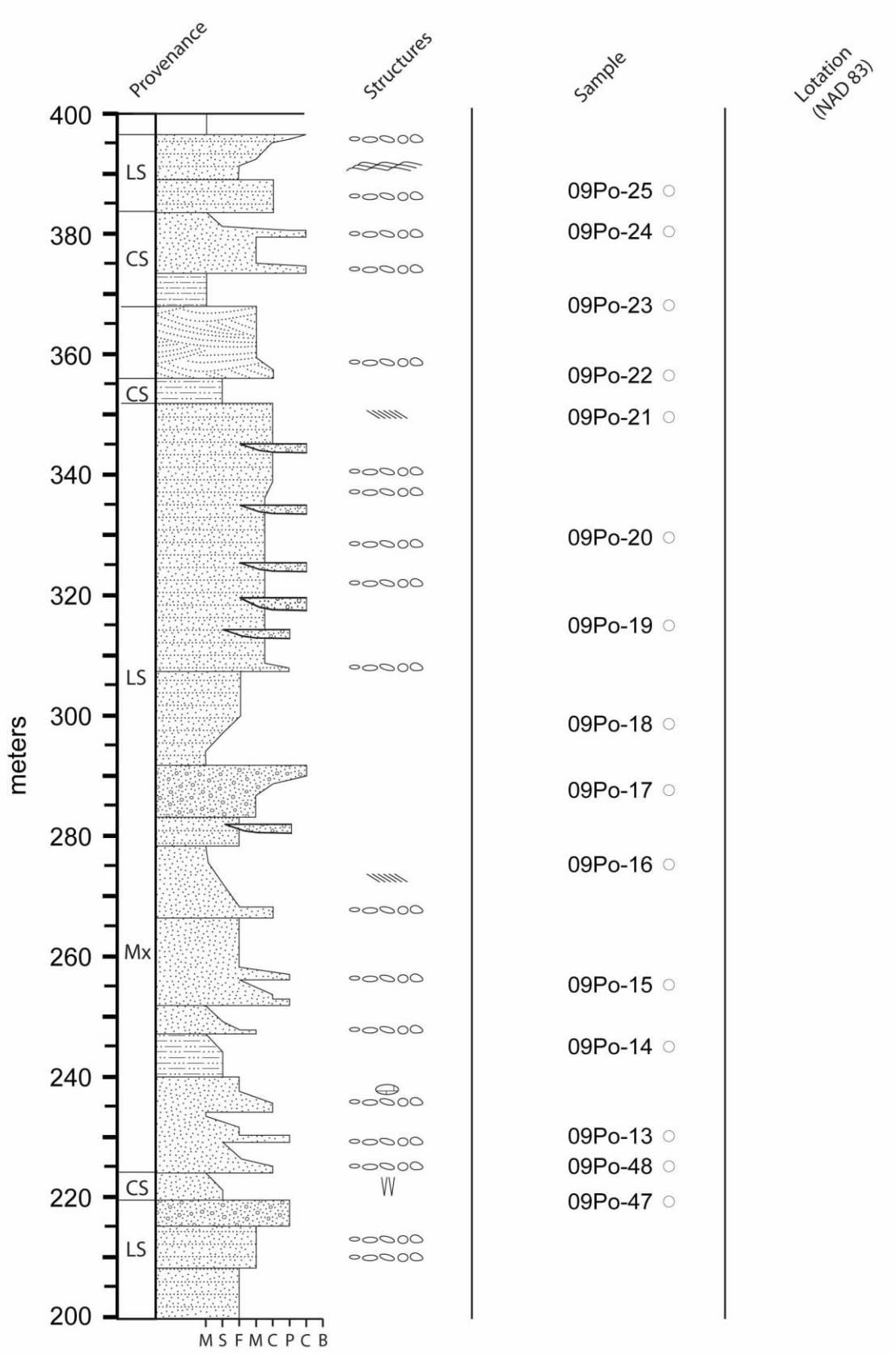
Provenance
Structures
Sample
Lotation (NAD 83)
meters
400
380
360
340
320
300
280
260
240
220
200
LS
CS
CS
LS
Mx
CS
LS
M S F M C P C B
09Po-25
09Po-24
09Po-23
09Po-22
09Po-21
09Po-20
09Po-19
09Po-18
09Po-17
09Po-16
09Po-15
09Po-14
09Po-13
09Po-48
09Po-47

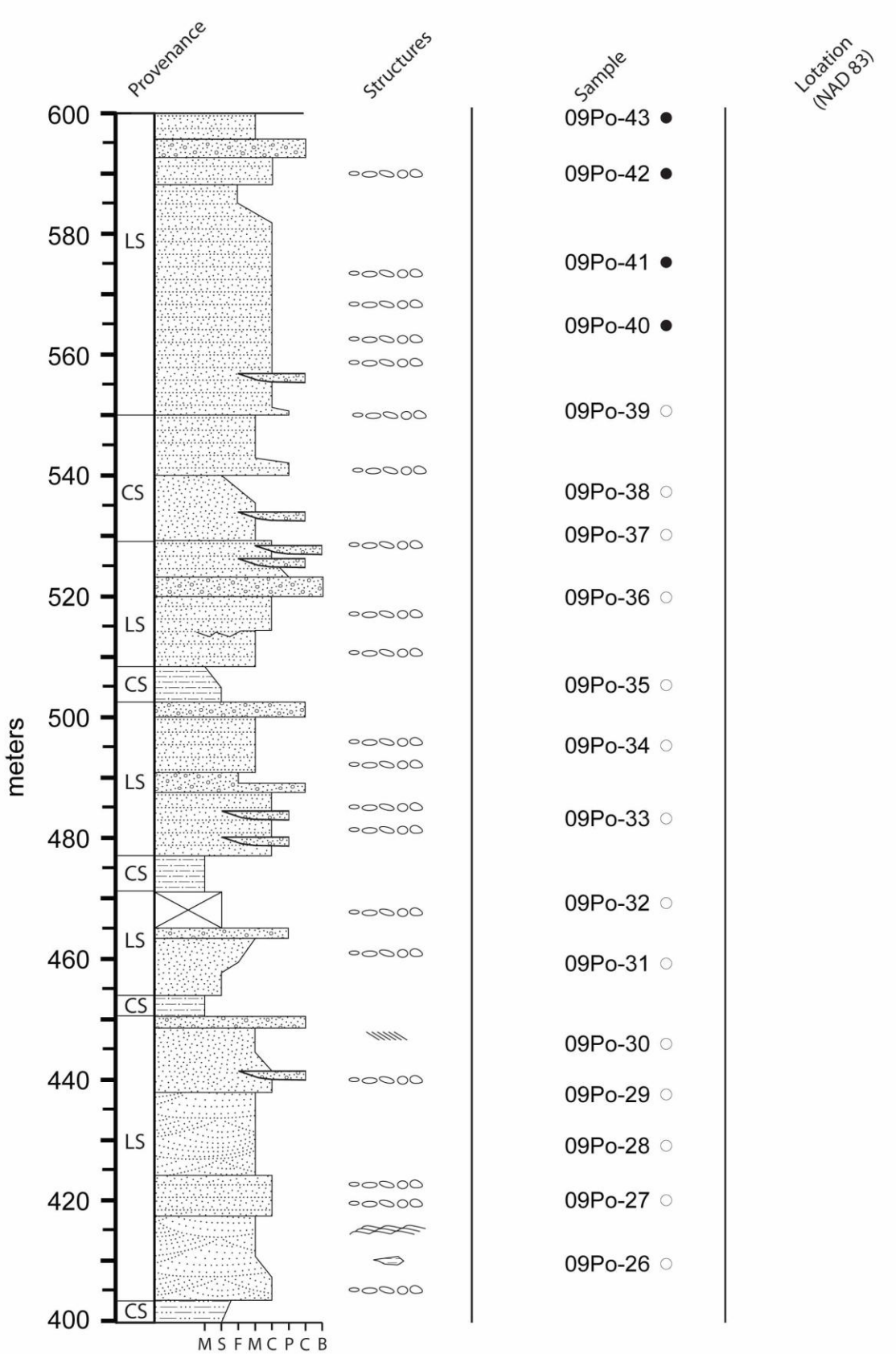
Provenance
Structures
Sample
Lotation (NAD 83)
meters
600
580
560
540
520
500
480
460
440
420
400
LS
CS
LS
CS
LS
CS
LS
CS
LS
CS
09Po-43
09Po-42
09Po-41
09Po-40
09Po-39
09Po-38
09Po-37
09Po-36
09Po-35
09Po-34
09Po-33
09Po-32
09Po-31
09Po-30
09Po-29
09Po-28
09Po-27
09Po-26
M S F M C P C B

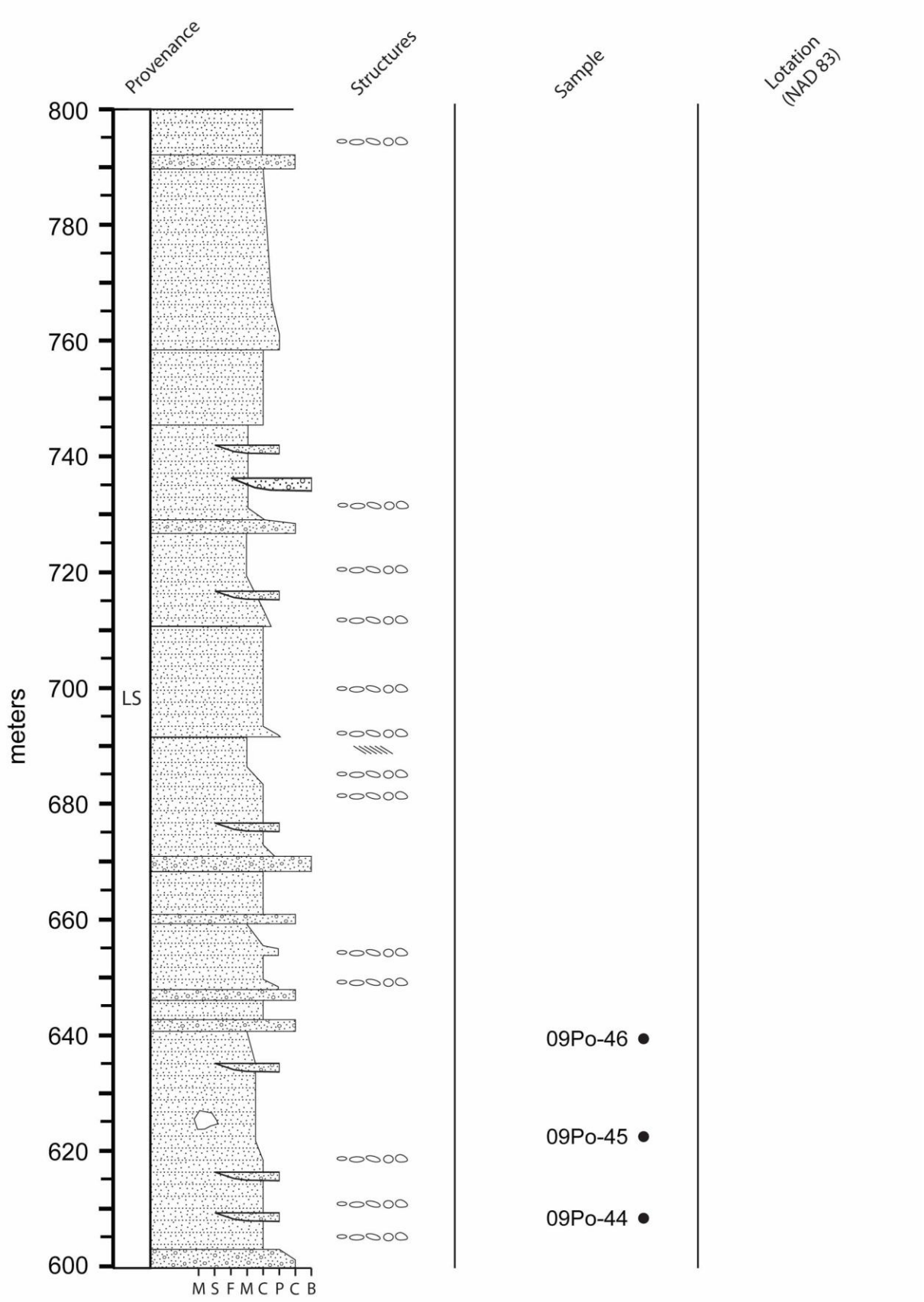
Provenance
Structures
Sample
Lotation (NAD 83)
meters
800
780
760
740
720
700
680
660
640
620
600
LS
M S F M C P C B
09Po-46
09Po-45
09Po-44

Section 6

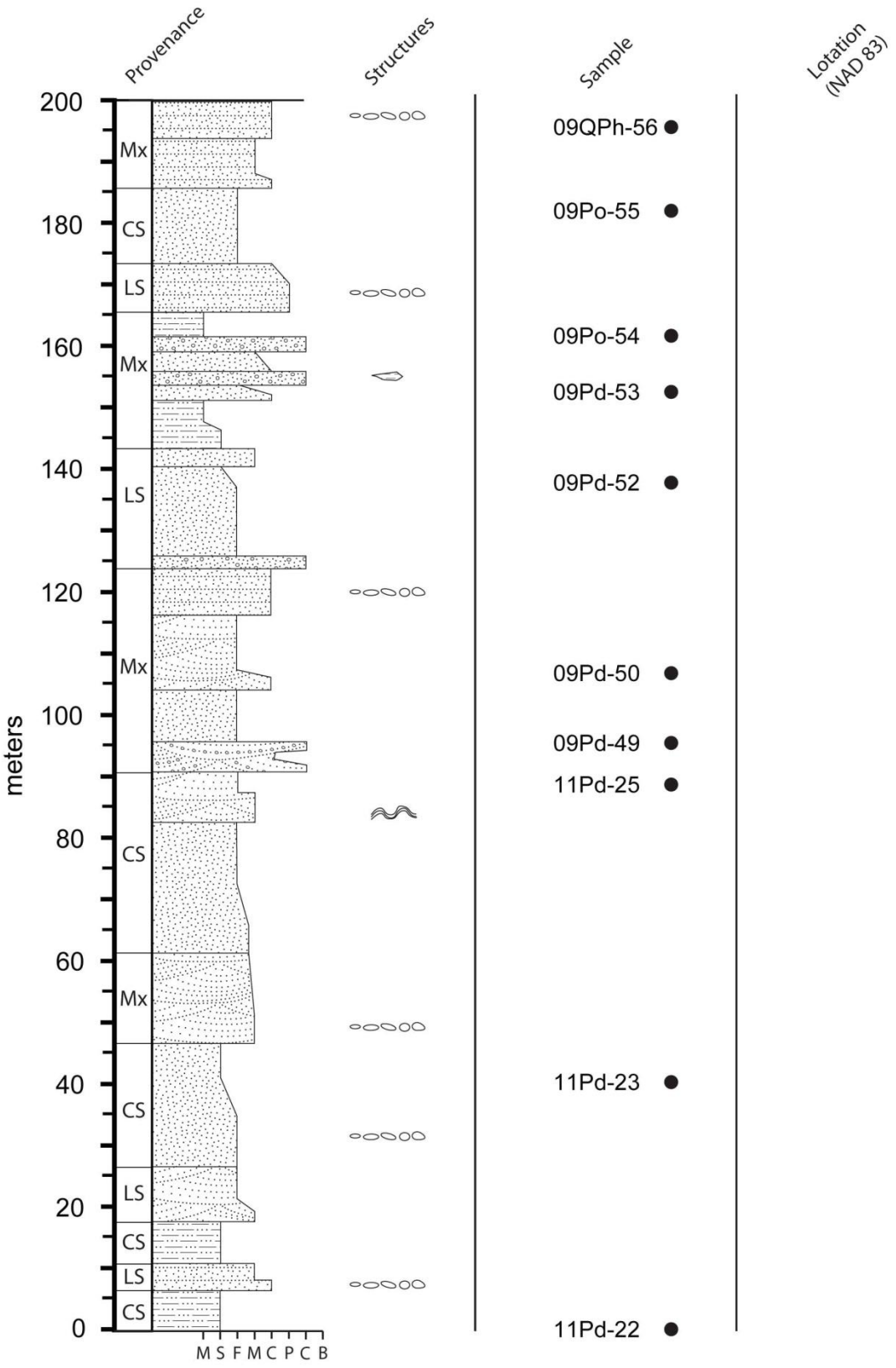
Provenance
Structures
Sample
Lotation (NAD 83)
meters
200
180
160
140
120
100
80
60
40
20
0
Mx
CS
LS
Mx
LS
Mx
CS
Mx
CS
LS
CS
LS
CS
M S F M C P C B
09QPh-56
09Po-55
09Po-54
09Pd-53
09Pd-52
09Pd-50
09Pd-49
11Pd-25
11Pd-23
11Pd-22

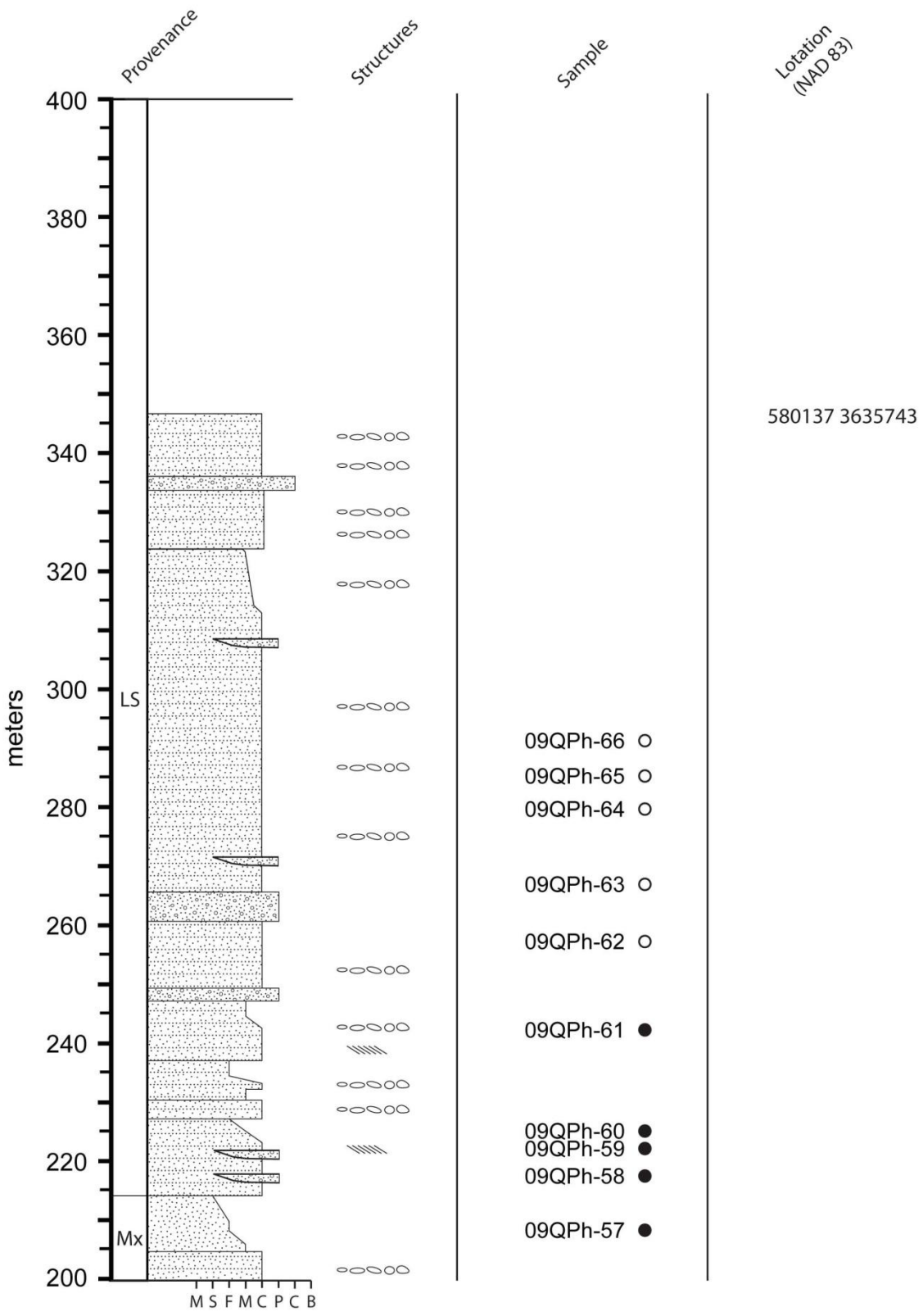
Provenance
Structures
Sample
Lotation (NAD 83)
400
380
360
340
320
300
280
260
240
220
200
meters
LS
Mx
M S F M C P C B
580137 3635743
09QPh-66
09QPh-65
09QPh-64
09QPh-63
09QPh-62
09QPh-61
09QPh-60
09QPh-59
09QPh-58
09QPh-57

Section 7

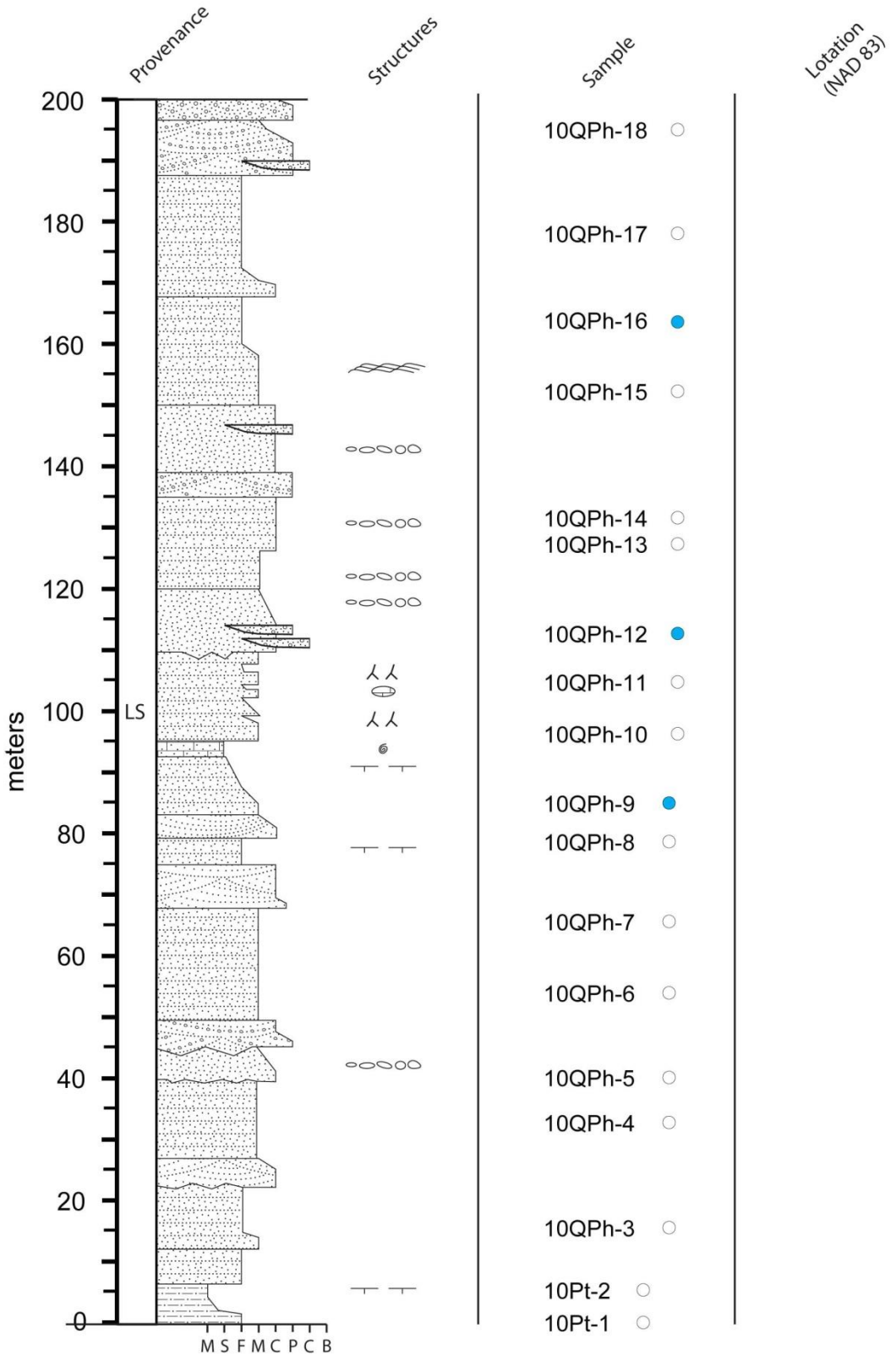
Provenance
Structures
Sample
Lotation (NAD 83)
meters
200
180
160
140
120
100
80
60
40
20
0
LS
M S F M C P C B
10QPh-18
10QPh-17
10QPh-16
10QPh-15
10QPh-14
10QPh-13
10QPh-12
10QPh-11
10QPh-10
10QPh-9
10QPh-8
10QPh-7
10QPh-6
10QPh-5
10QPh-4
10QPh-3
10Pt-2
10Pt-1

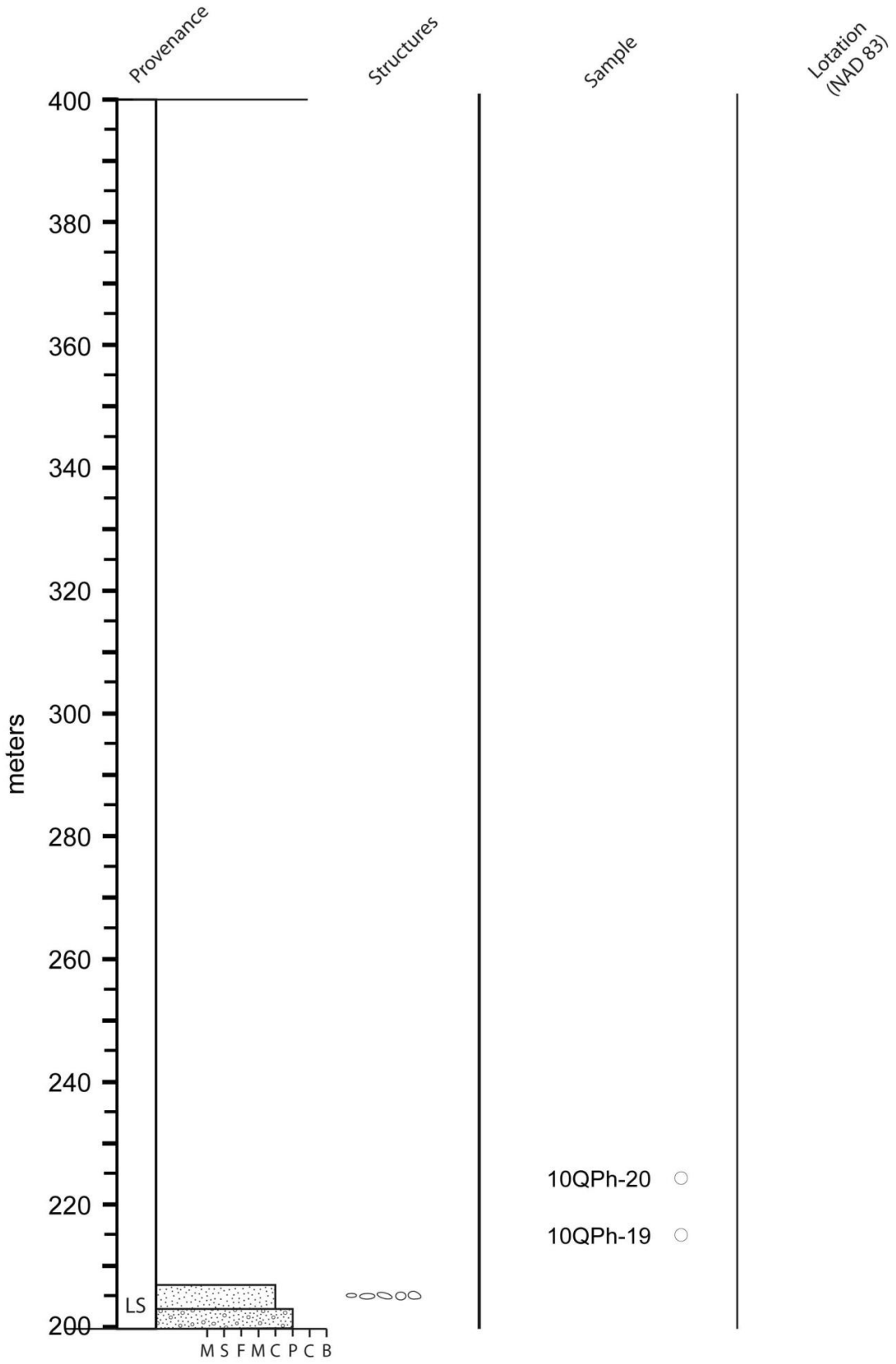
Provenance
Structures
Sample
Lotation (NAD 83)
meters
400
380
360
340
320
300
280
260
240
220
200
LS
M S F M C P C B
10QPh-20
10QPh-19

Section 8

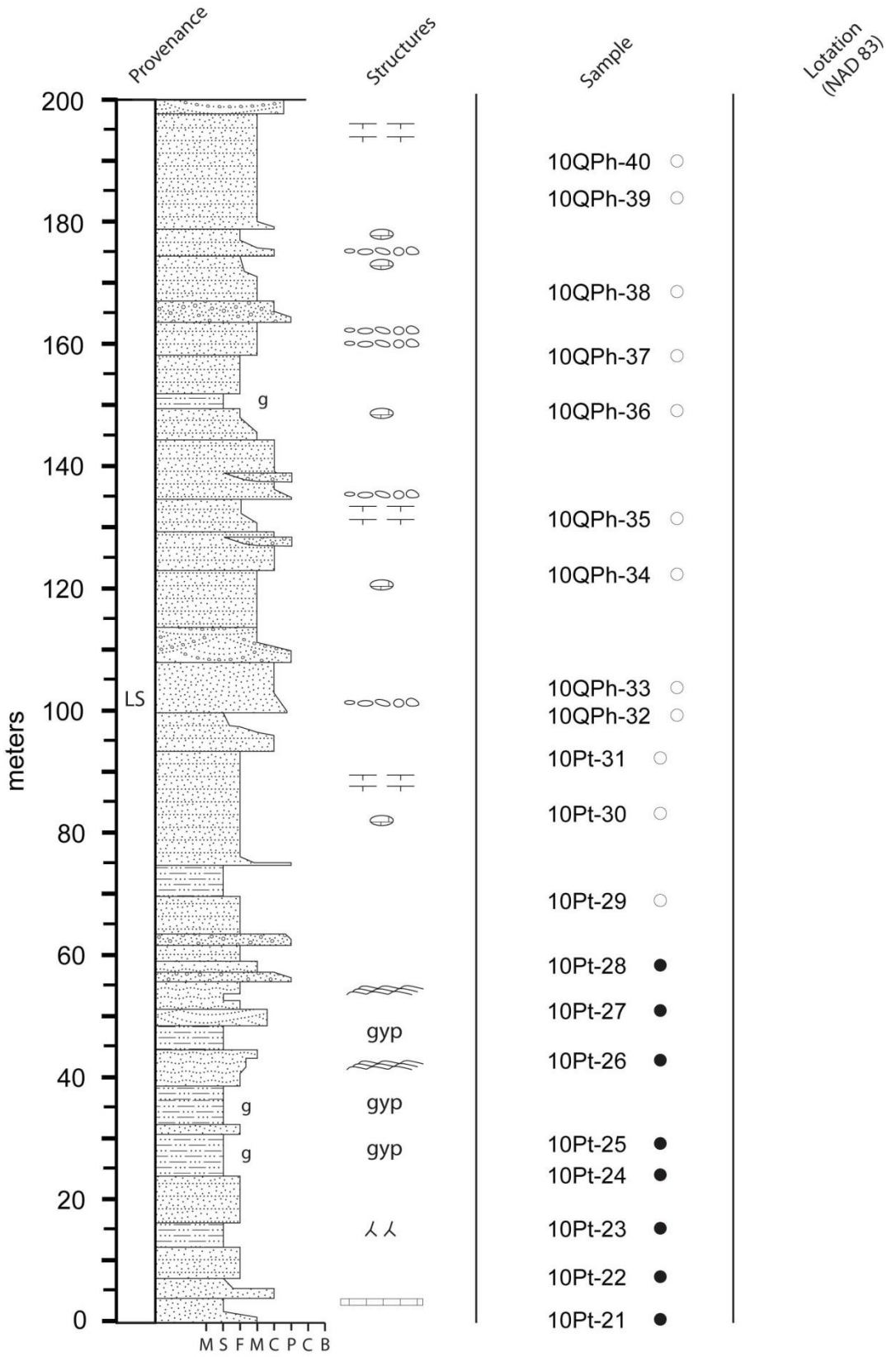
Provenance
Structures
Sample
Lotation (NAD 83)
meters
200
180
160
140
120
100
80
60
40
20
0
LS
g
g
g
gyp
gyp
gyp
10QPh-40
10QPh-39
10QPh-38
10QPh-37
10QPh-36
10QPh-35
10QPh-34
10QPh-33
10QPh-32
10Pt-31
10Pt-30
10Pt-29
10Pt-28
10Pt-27
10Pt-26
10Pt-25
10Pt-24
10Pt-23
10Pt-22
10Pt-21
M S F M C P C B

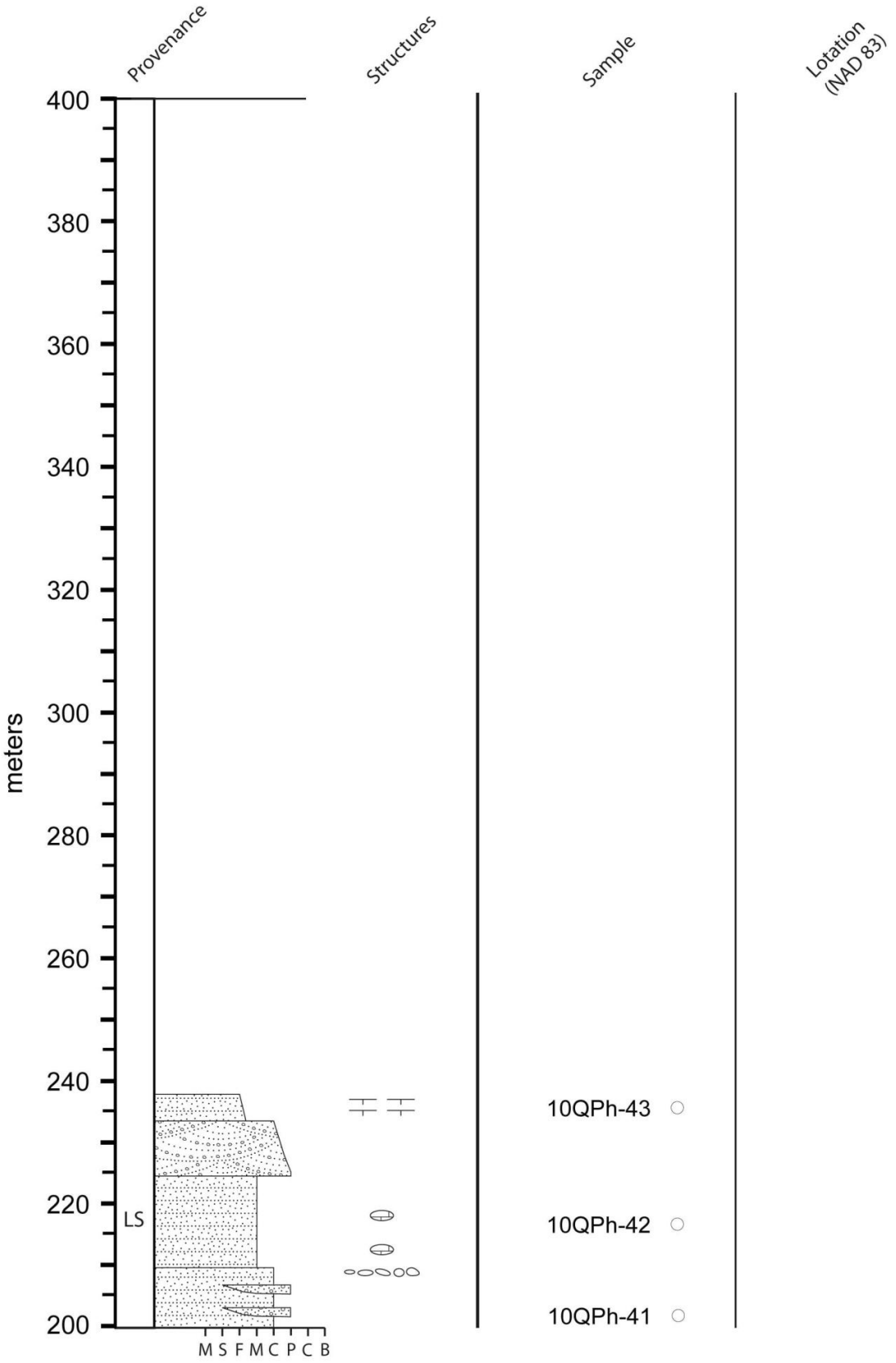
Provenance
Structures
Sample
Lotation (NAD 83)
meters
400
380
360
340
320
300
280
260
240
220
200
LS
M S F M C P C B
10QPh-43
10QPh-42
10QPh-41

Section 9

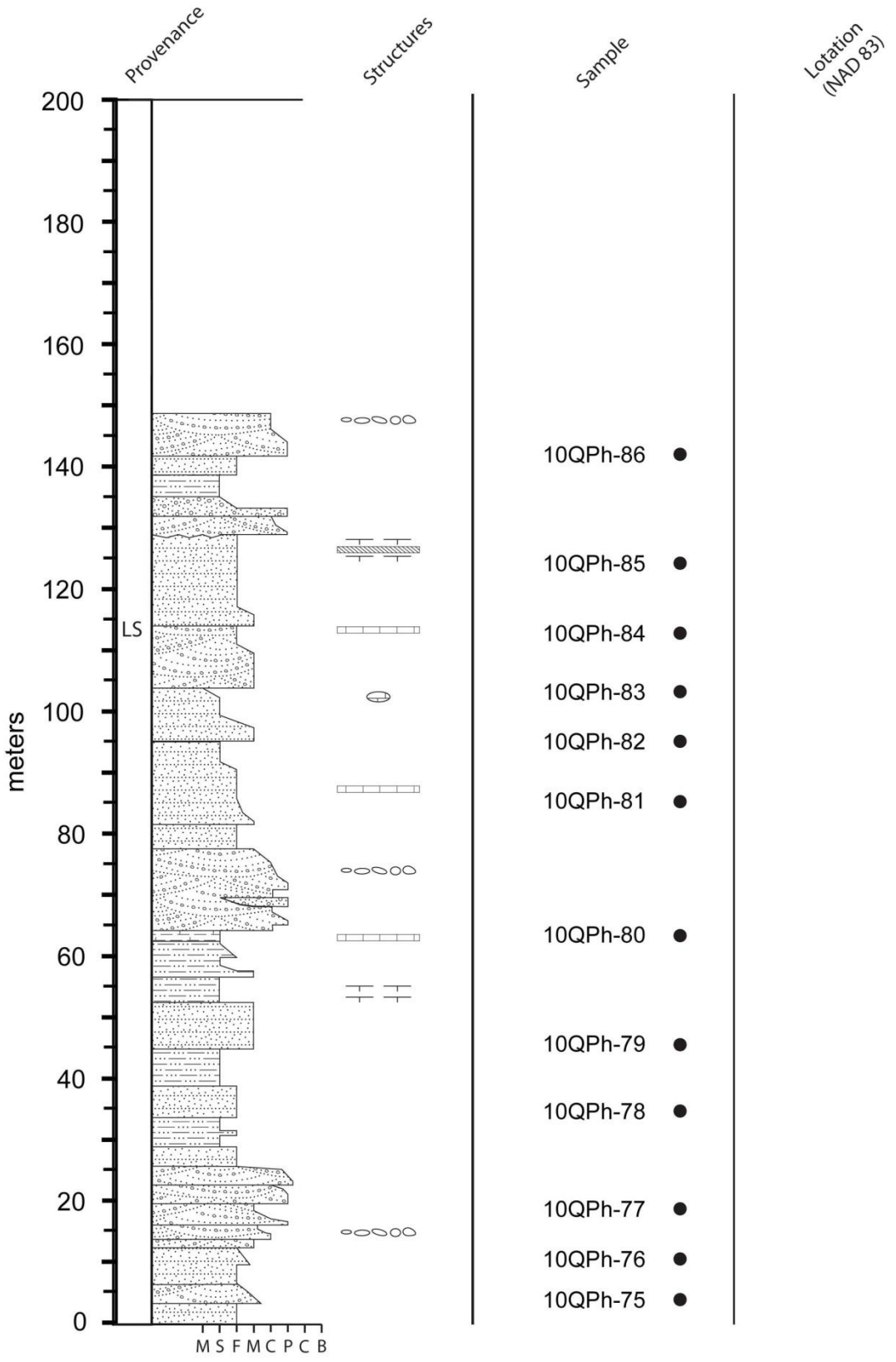
Provenance
Structures
Sample
Lotation (NAD 83)
meters
200
180
160
140
120
100
80
60
40
20
0
LS
M S F M C P C B
10QPh-86
10QPh-85
10QPh-84
10QPh-83
10QPh-82
10QPh-81
10QPh-80
10QPh-79
10QPh-78
10QPh-77
10QPh-76
10QPh-75

Section 10

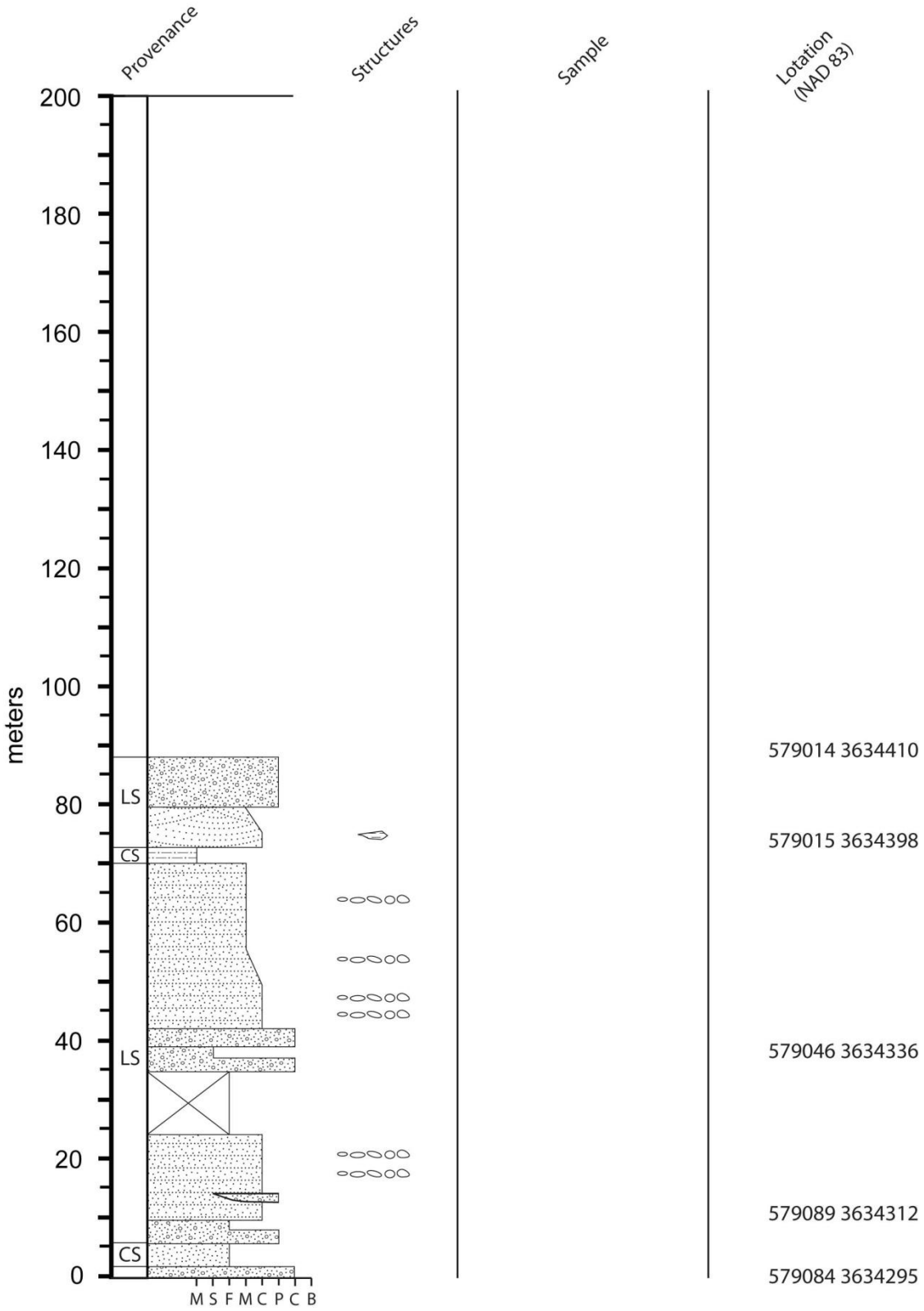
Provenance
Structures
Sample
Lotation (NAD 83)
meters
200
180
160
140
120
100
80
60
40
20
0
LS
CS
LS
CS
M S F M C P C B
579014 3634410
579015 3634398
579046 3634336
579089 3634312
579084 3634295

Section 11

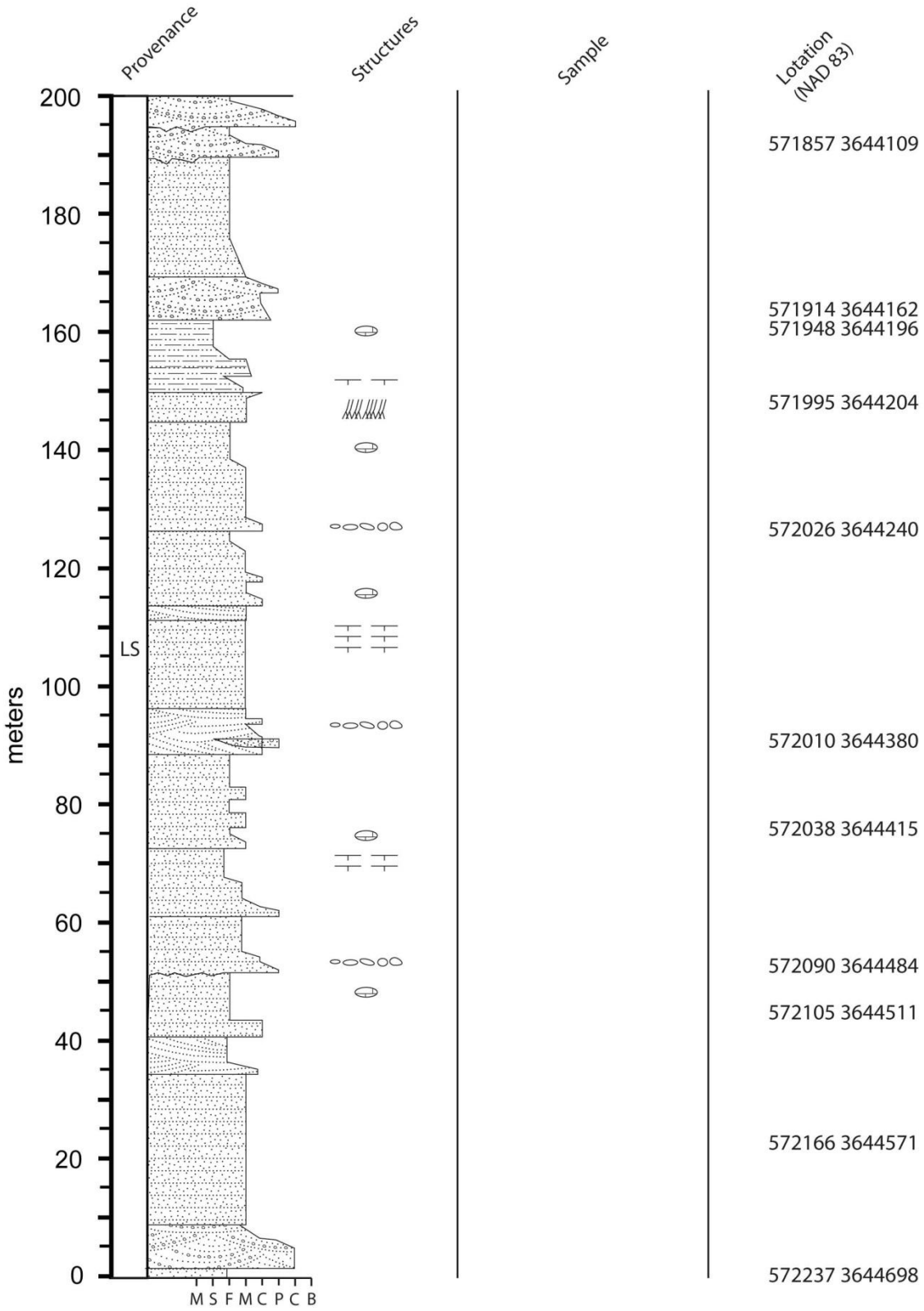
Provenance
Structures
Sample
Lotation (NAD 83)
200
180
160
140
120
100
80
60
40
20
0
meters
LS
M S F M C P C B
571857 3644109
571914 3644162
571948 3644196
571995 3644204
572026 3644240
572010 3644380
572038 3644415
572090 3644484
572105 3644511
572166 3644571
572237 3644698

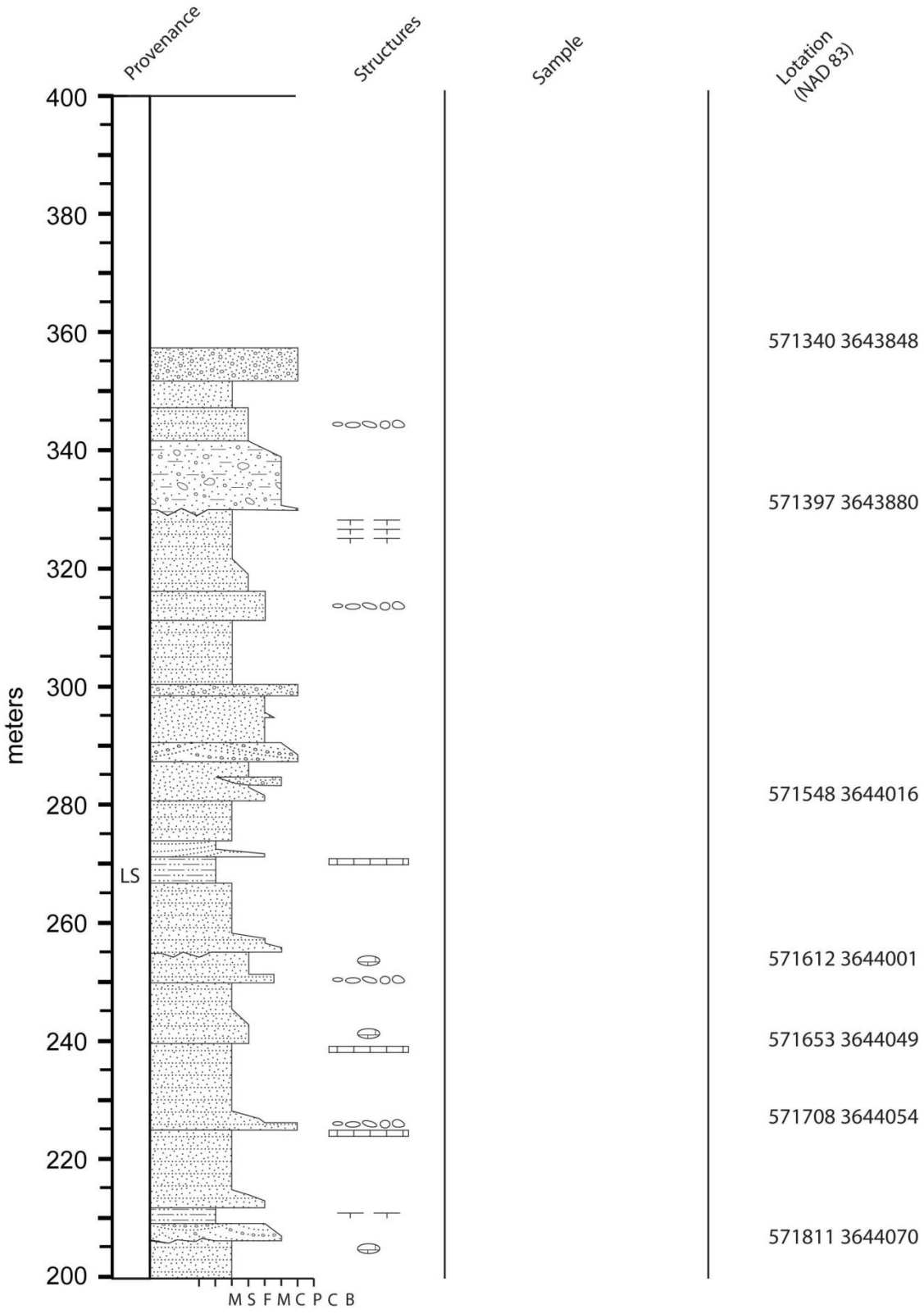
Provenance
Structures
Sample
Lotation (NAD 83)
meters
400
380
360
340
320
300
280
260
240
220
200
LS
M S F M C P C B
571340 3643848
571397 3643880
571548 3644016
571612 3644001
571653 3644049
571708 3644054
571811 3644070

Section 12

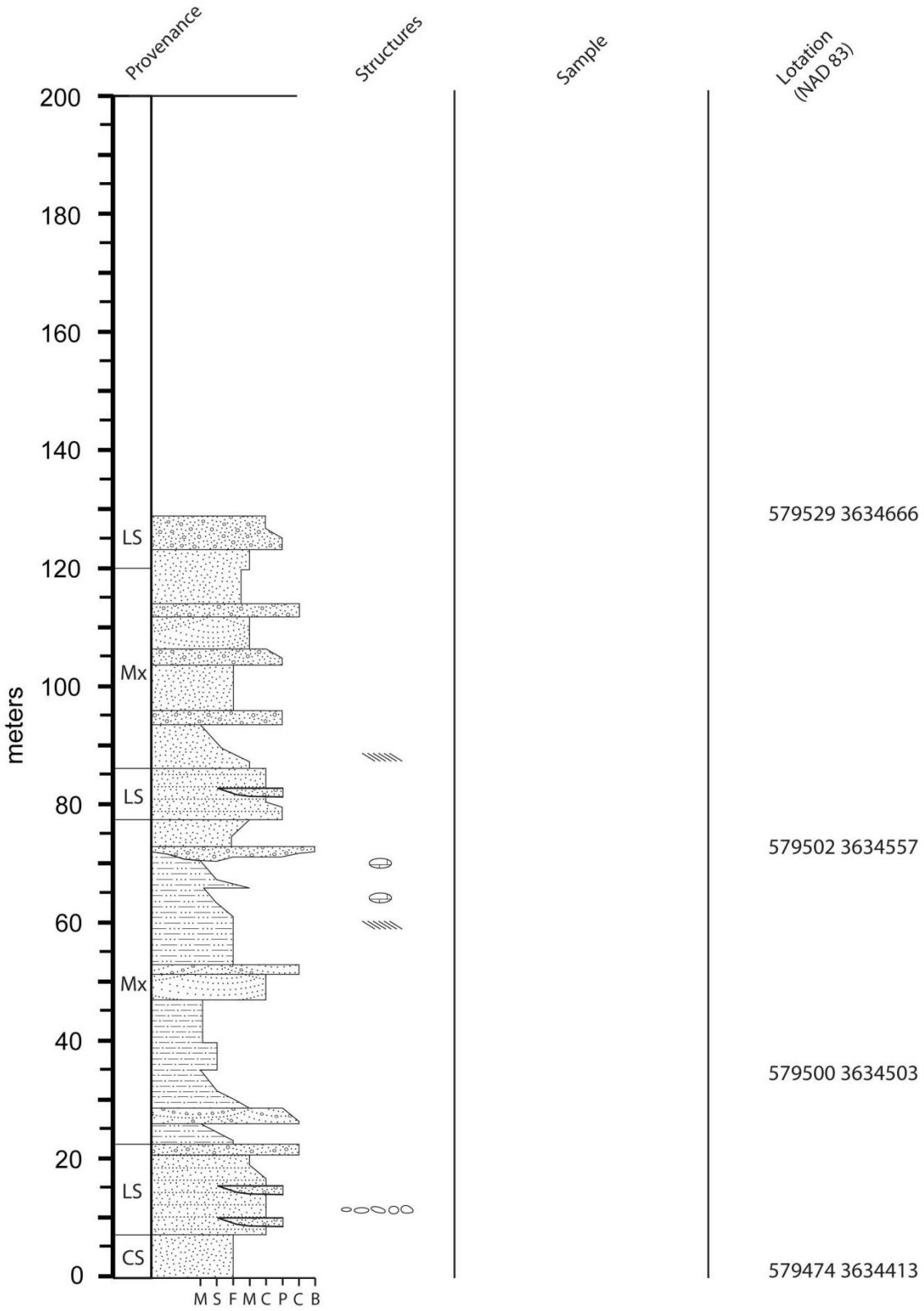
Provenance
Structures
Sample
Lotation (NAD 83)
meters
200
180
160
140
120
100
80
60
40
20
0
LS
Mx
LS
Mx
LS
CS
M S F M C P C B
579529 3634666
579502 3634557
579500 3634503
579474 3634413

Section 13

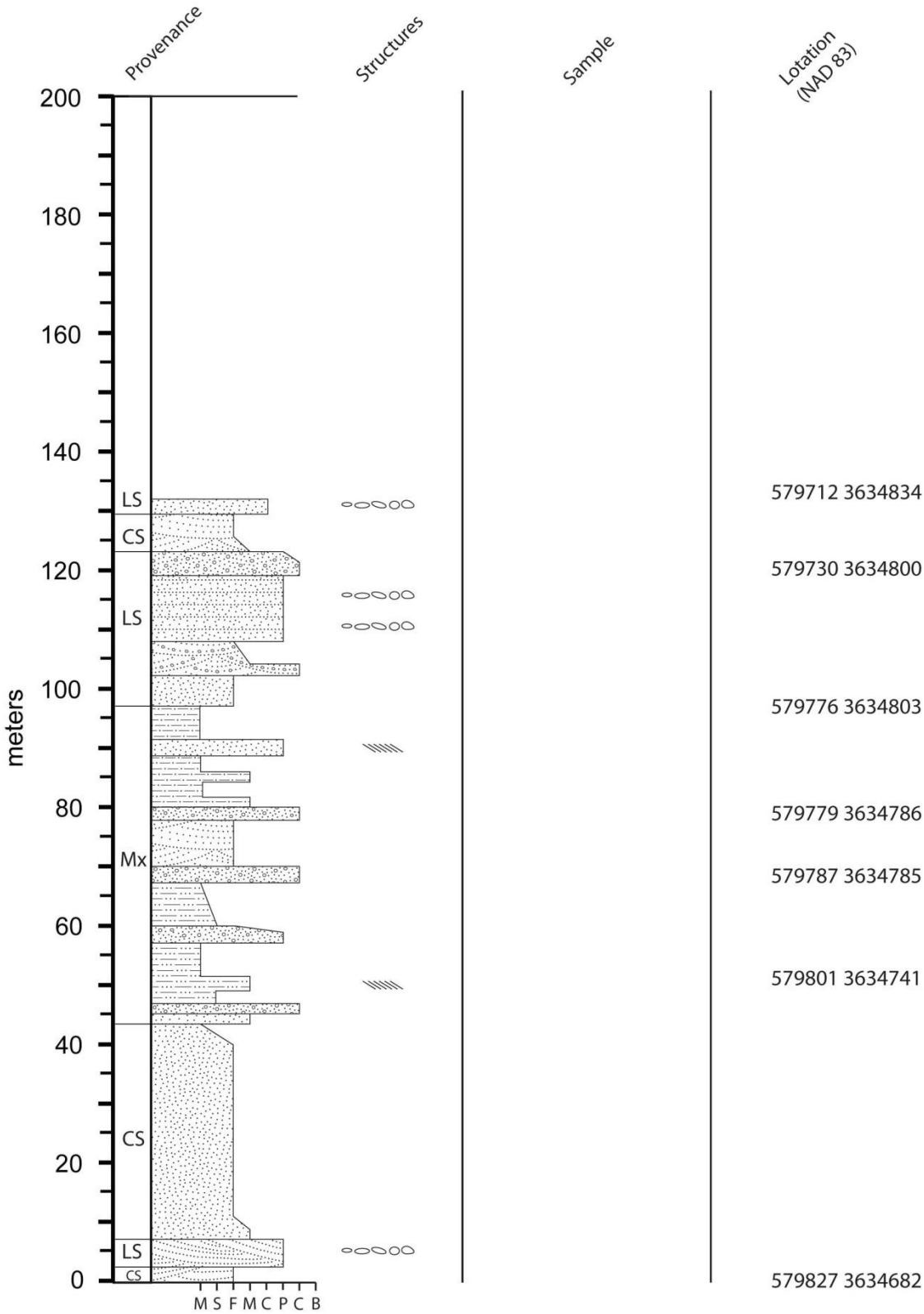
Provenance
Structures
Sample
Lotation (NAD 83)
meters
200
180
160
140
120
100
80
60
40
20
0
LS
CS
LS
Mx
CS
LS
CS
M S F M C P C B
579712 3634834
579730 3634800
579776 3634803
579779 3634786
579787 3634785
579801 3634741
579827 3634682

Section 14

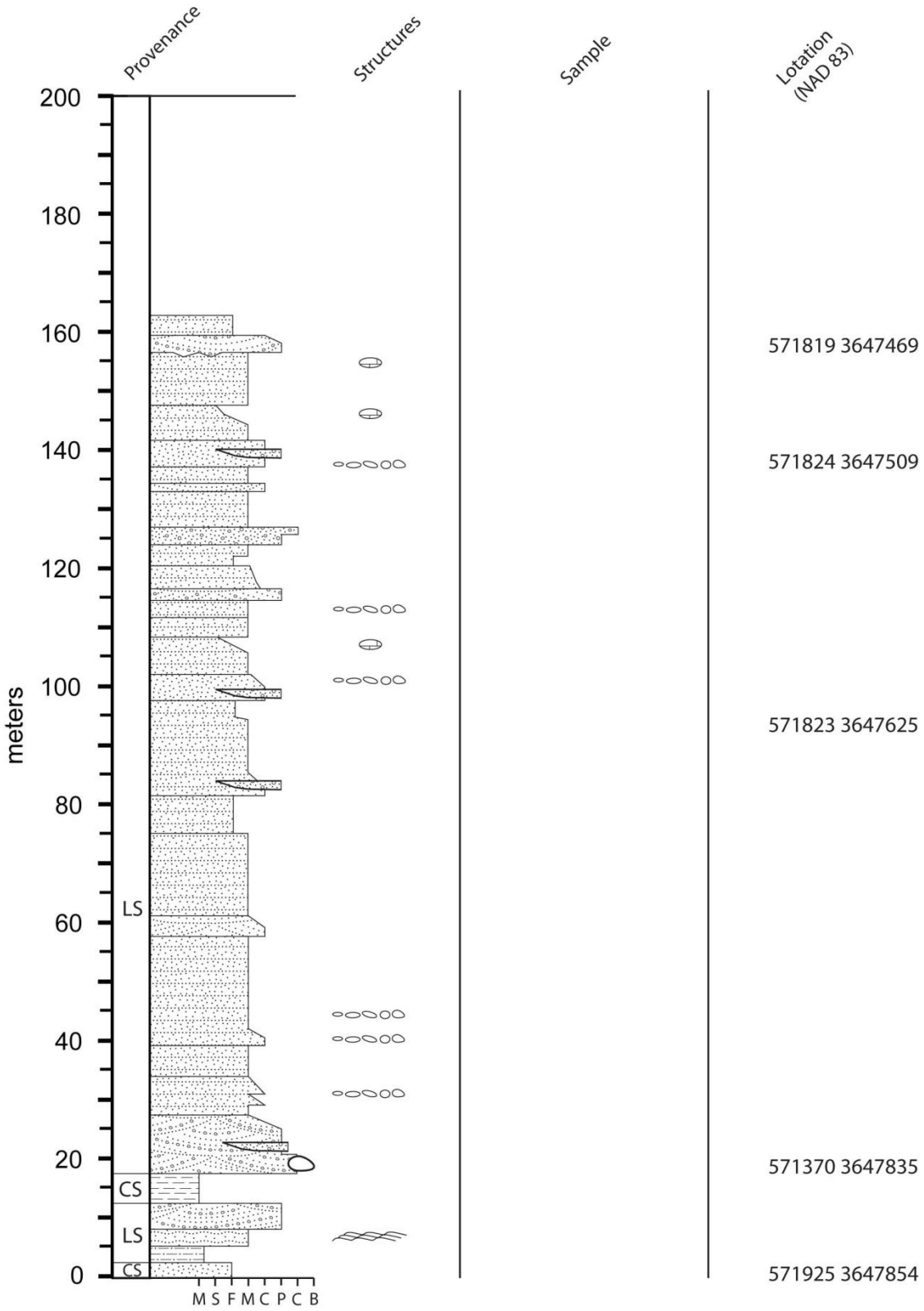
Provenance
Structures
Sample
Lotation (NAD 83)
meters
200
180
160
140
120
100
80
60
40
20
0
LS
CS
LS
CS
M S F M C P C B
571819 3647469
571824 3647509
571823 3647625
571370 3647835
571925 3647854

Section 15

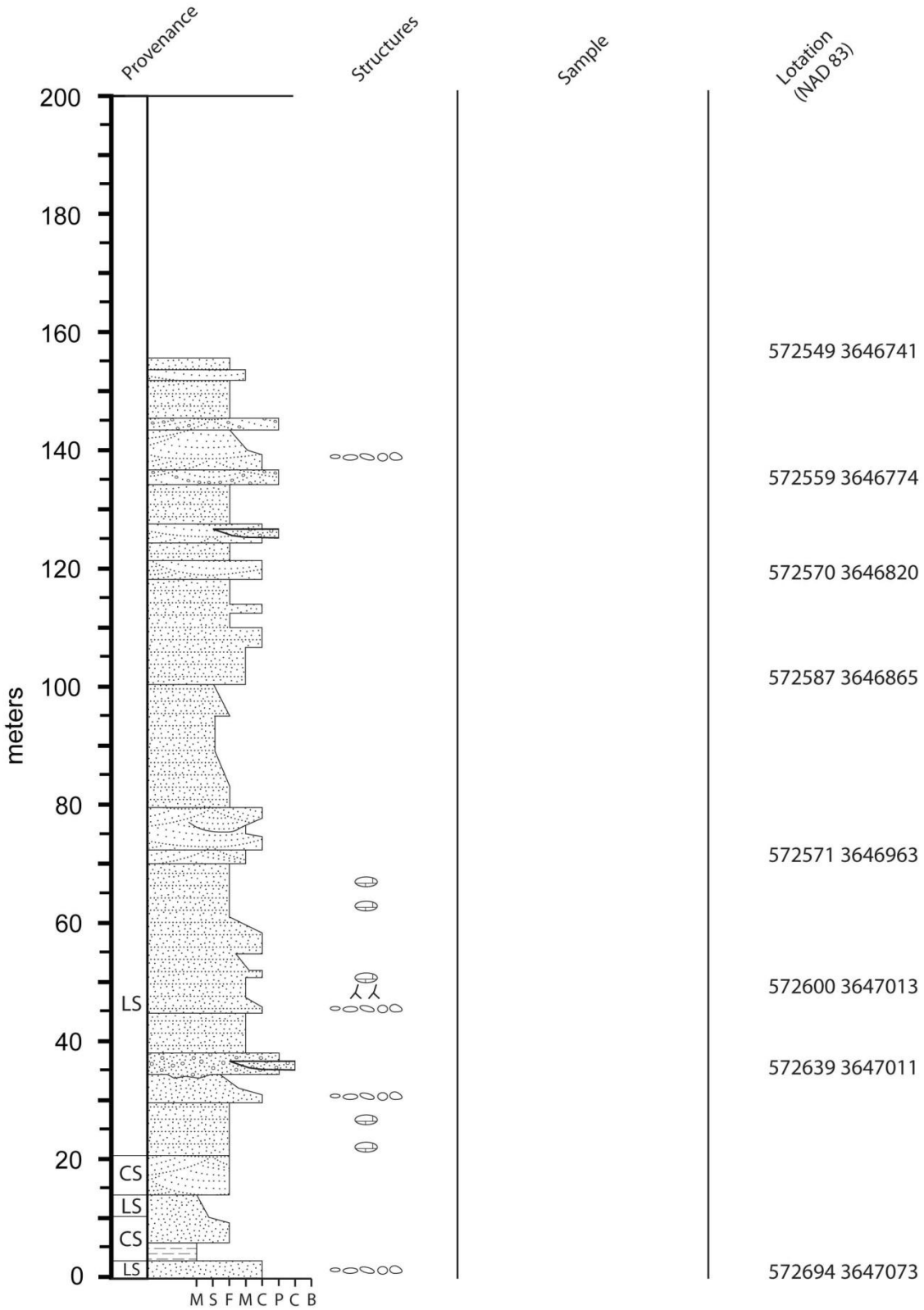
Provenance
Structures
Sample
Lotation (NAD 83)
meters
200
180
160
140
120
100
80
60
40
20
0
LS
CS
LS
CS
LS
M S F M C P C B
572549 3646741
572559 3646774
572570 3646820
572587 3646865
572571 3646963
572600 3647013
572639 3647011
572694 3647073

Section 16

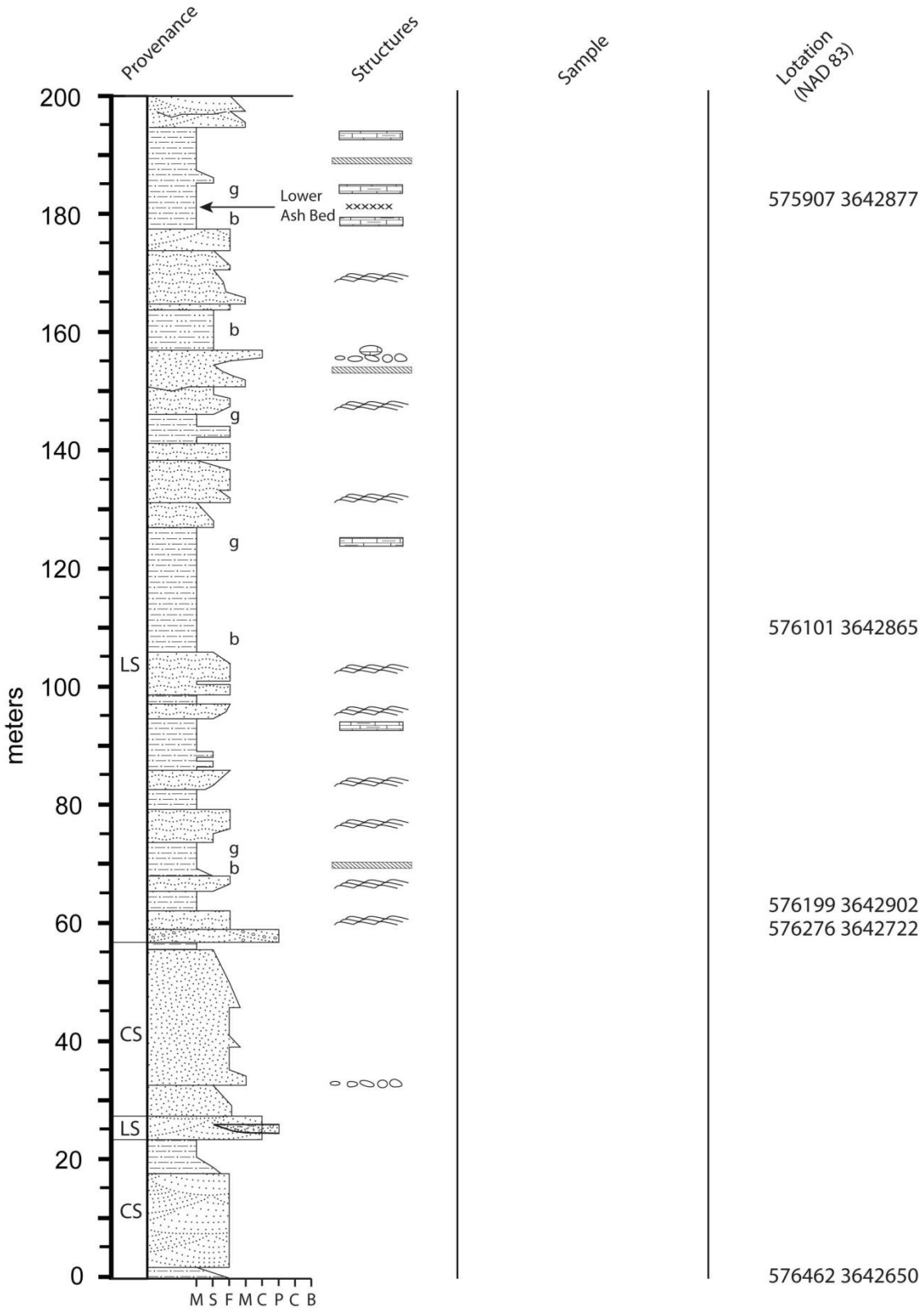
Provenance
Structures
Sample
Lotation (NAD 83)
meters
200
180
160
140
120
100
80
60
40
20
0
g
b
Lower Ash Bed
xxxxxx
LS
CS
LS
CS
M S F M C P C B
575907 3642877
576101 3642865
576199 3642902
576276 3642722
576462 3642650

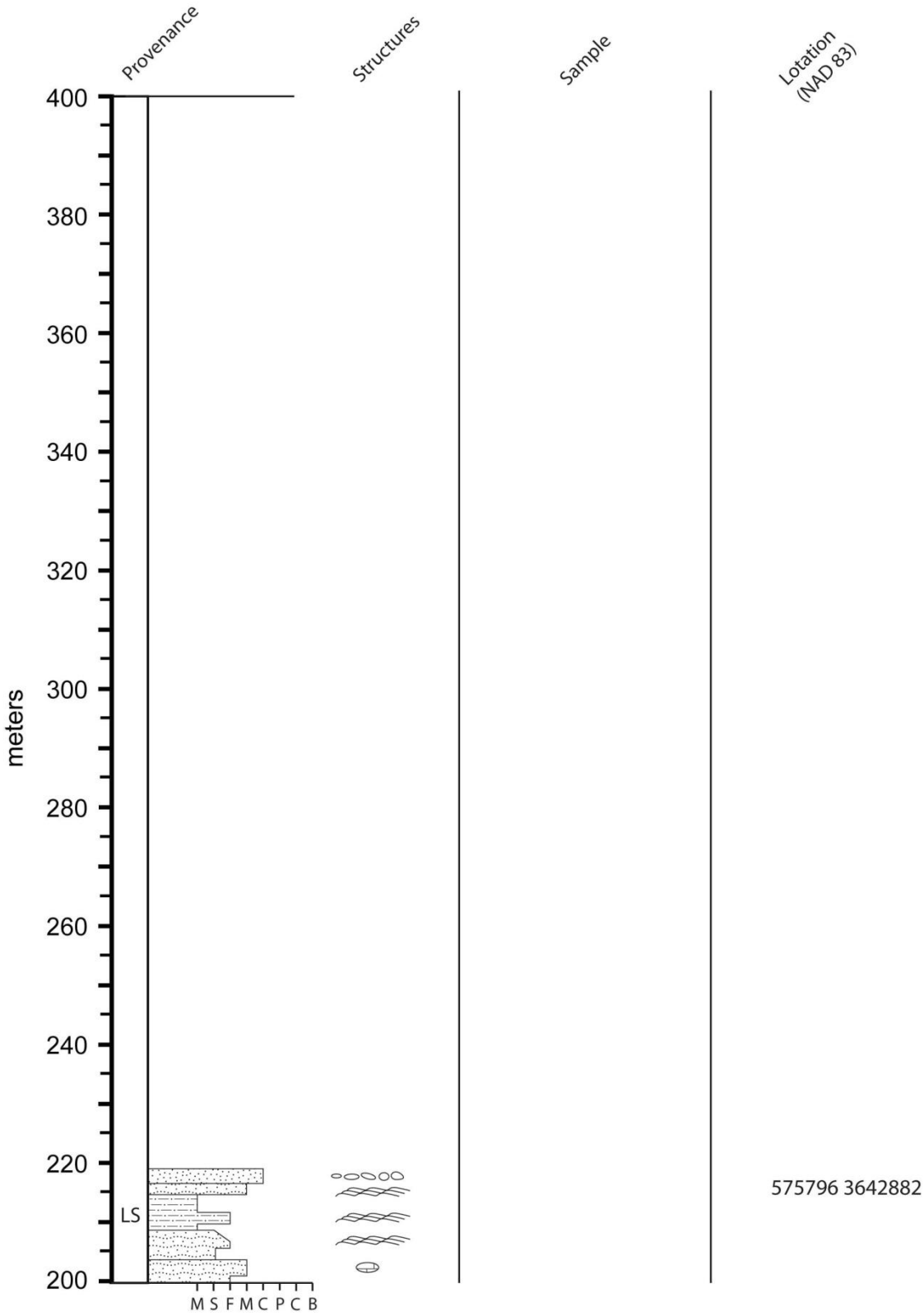
Provenance
Structures
Sample
Lotation (NAD 83)
meters
400
380
360
340
320
300
280
260
240
220
200
LS
M S F M C P C B
575796 3642882

Section 17

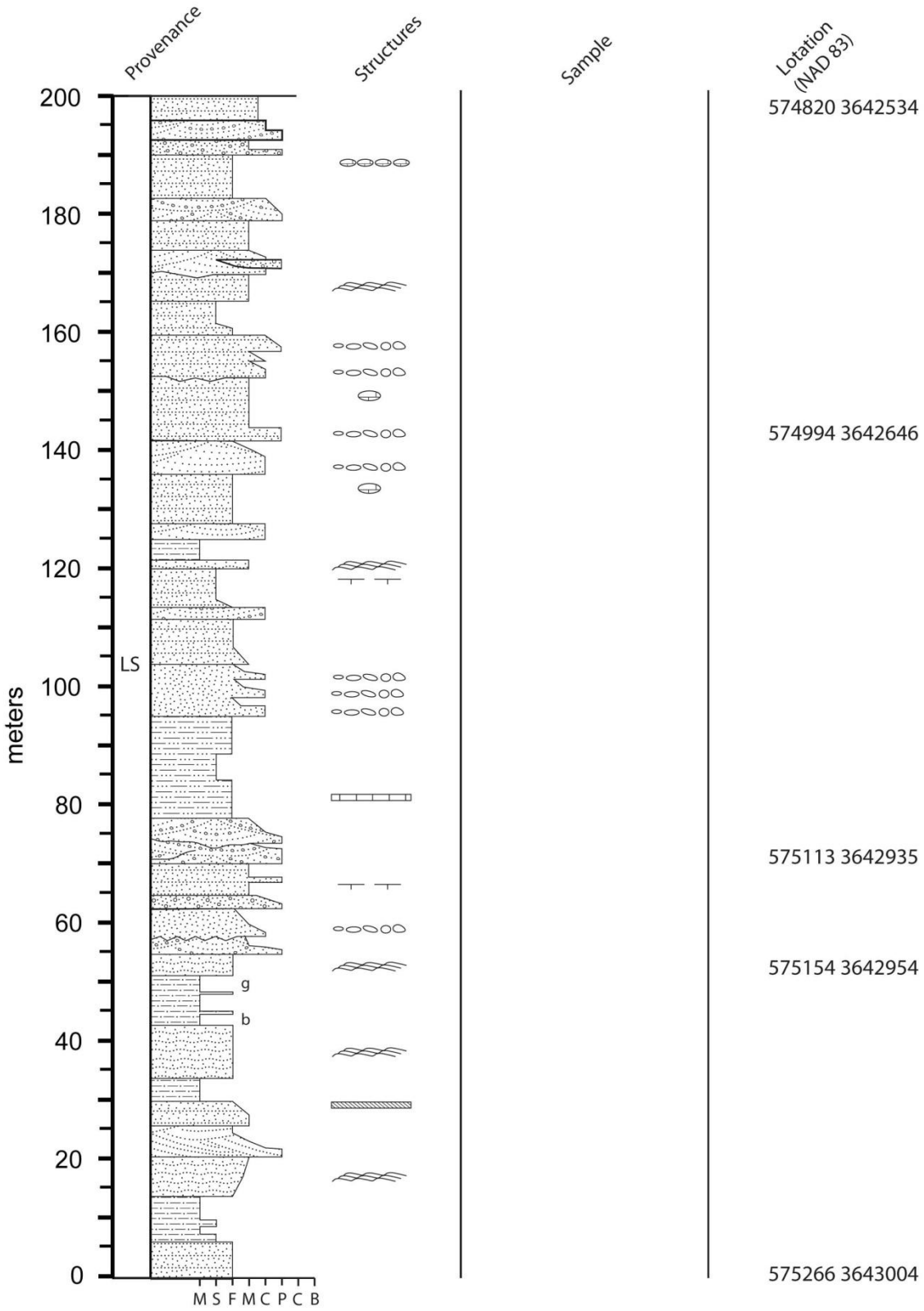
Provenance
Structures
Sample
Lotation (NAD 83)
574820 3642534
574994 3642646
575113 3642935
575154 3642954
575266 3643004
meters
200
180
160
140
120
100
80
60
40
20
0
LS
g
b
M S F M C P C B

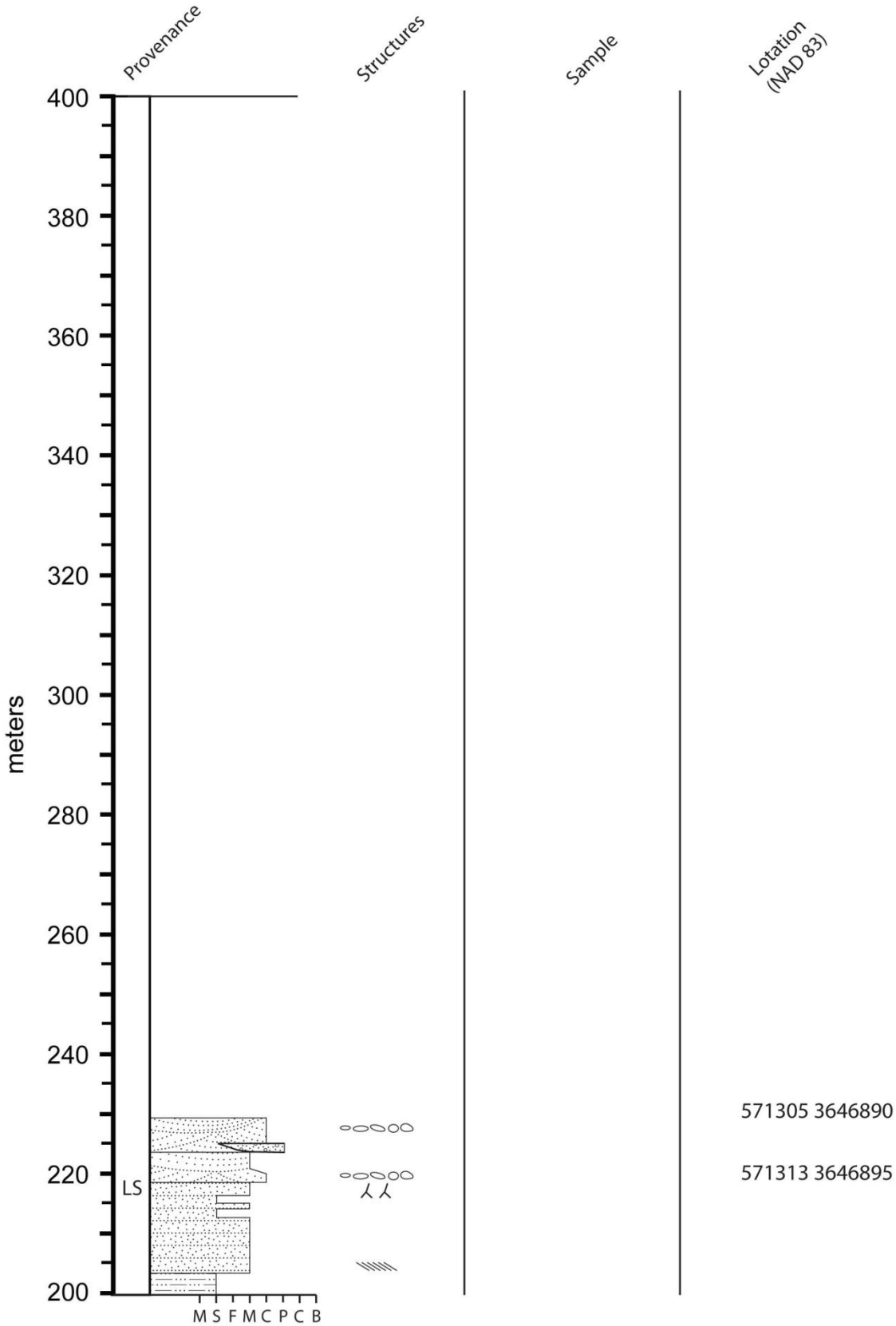
Provenance
Structures
Sample
Lotation (NAD 83)
meters
400
380
360
340
320
300
280
260
240
220
200
LS
M S F M C P C B
571305 3646890
571313 3646895

Section 18

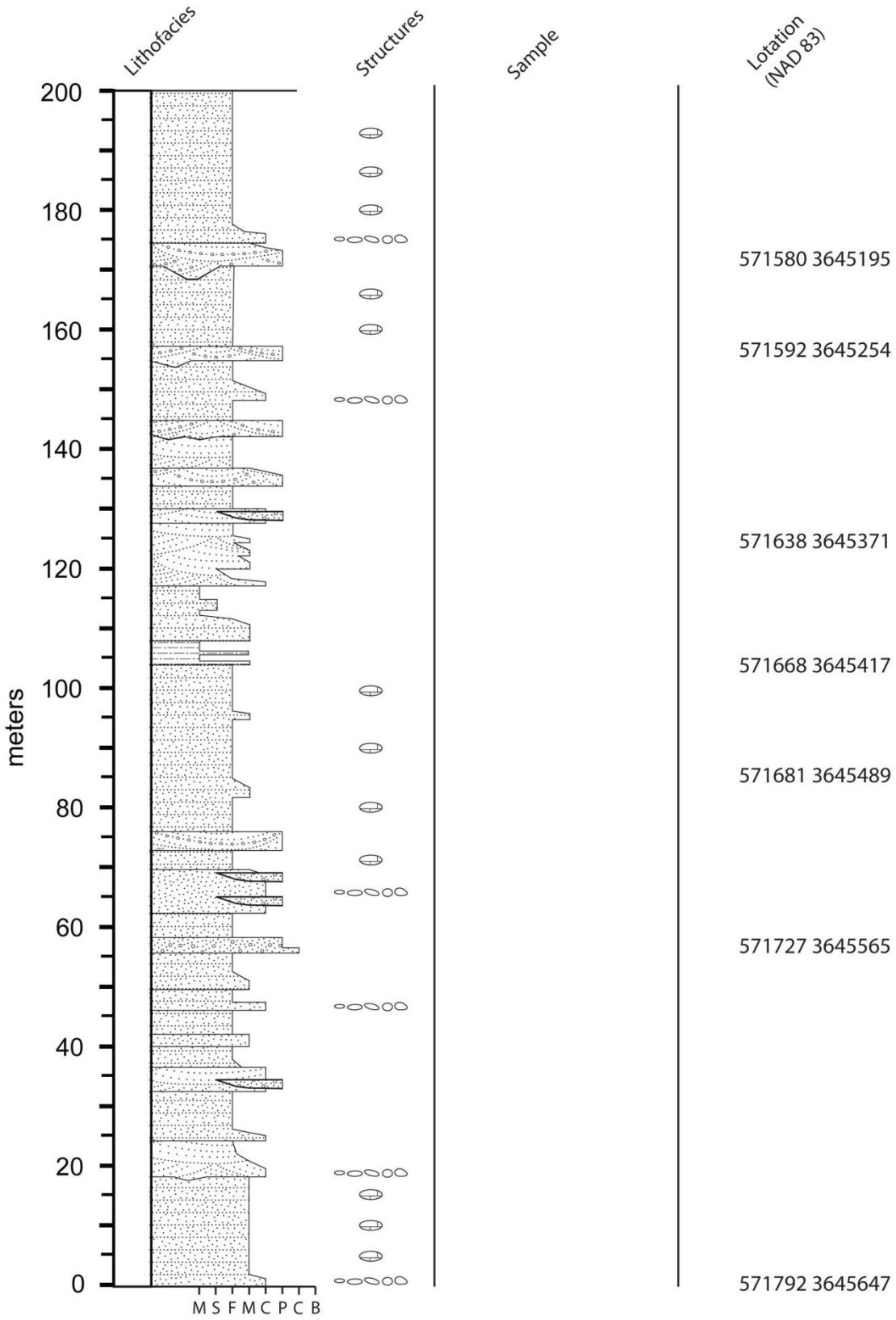
Lithofacies
Structures
Sample
Lotation (NAD 83)
meters
200
180
160
140
120
100
80
60
40
20
0
M S F M C P C B
571580 3645195
571592 3645254
571638 3645371
571668 3645417
571681 3645489
571727 3645565
571792 3645647

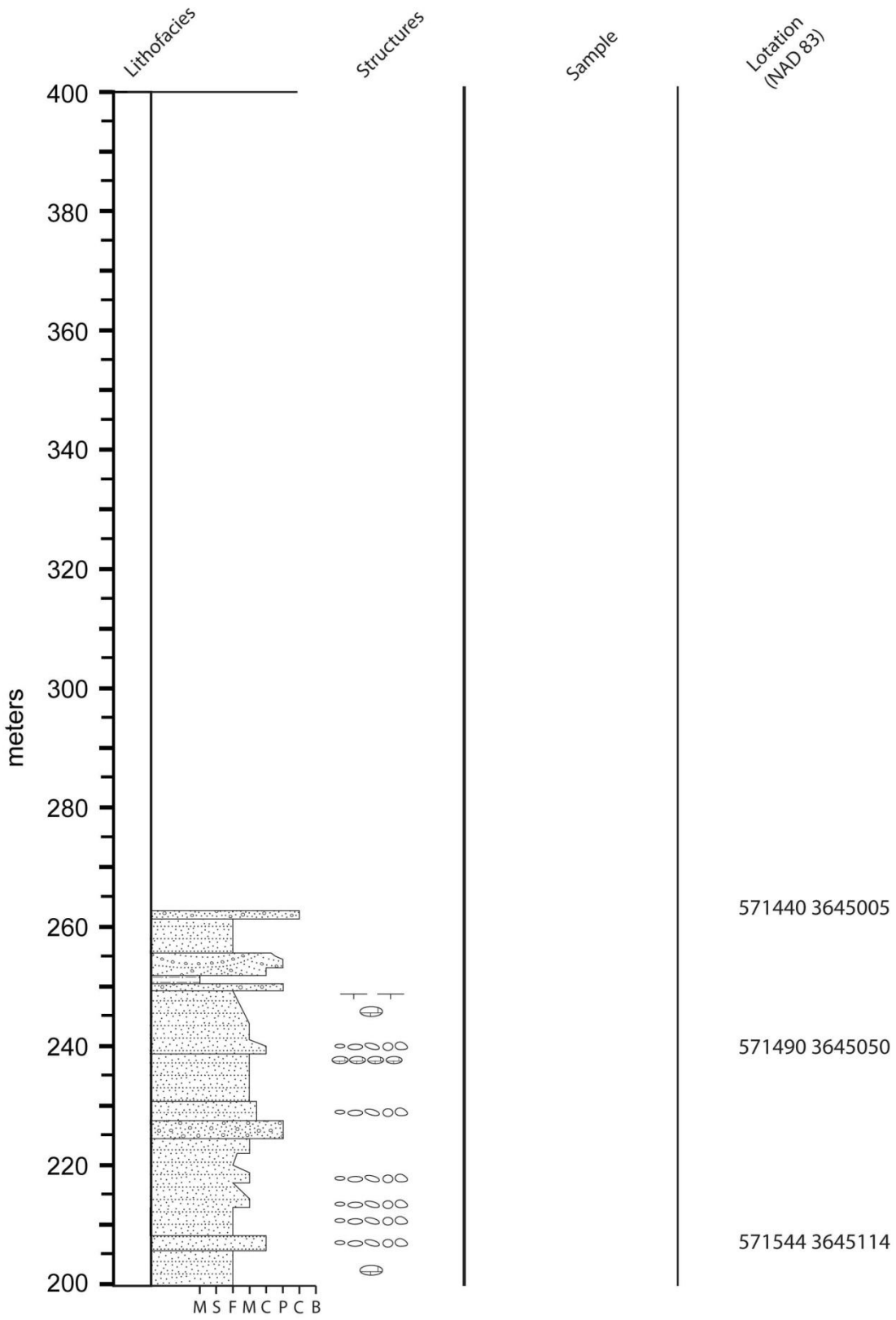
Lithofacies
Structures
Sample
Lotation (NAD 83)
meters
400
380
360
340
320
300
280
260
240
220
200
M S F M C P C B
571440 3645005
571490 3645050
571544 3645114

Section 19

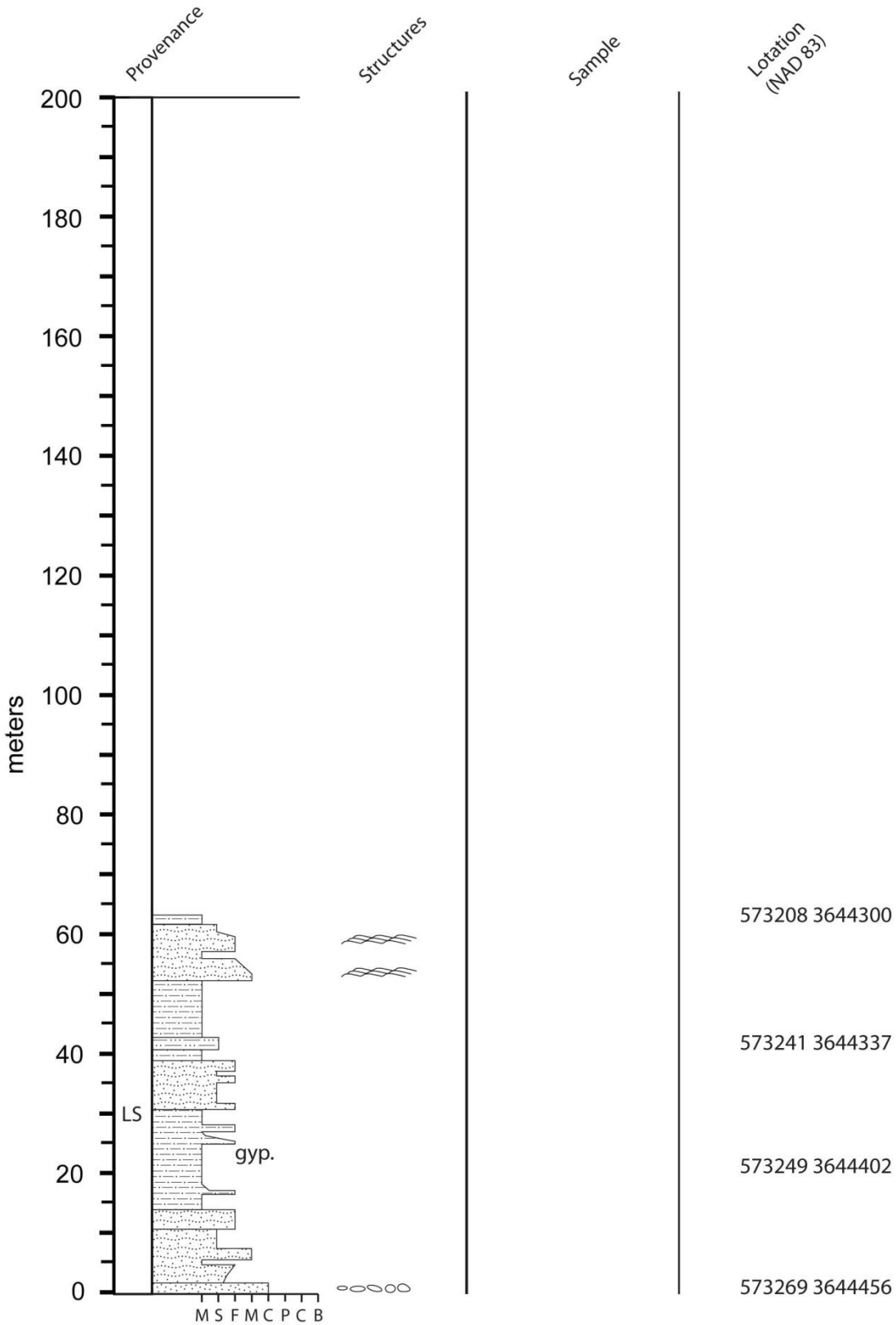
Provenance
Structures
Sample
Lotation (NAD 83)
meters
200
180
160
140
120
100
80
60
40
20
0
LS
gyp.
M S F M C P C B
573208 3644300
573241 3644337
573249 3644402
573269 3644456

Section 20

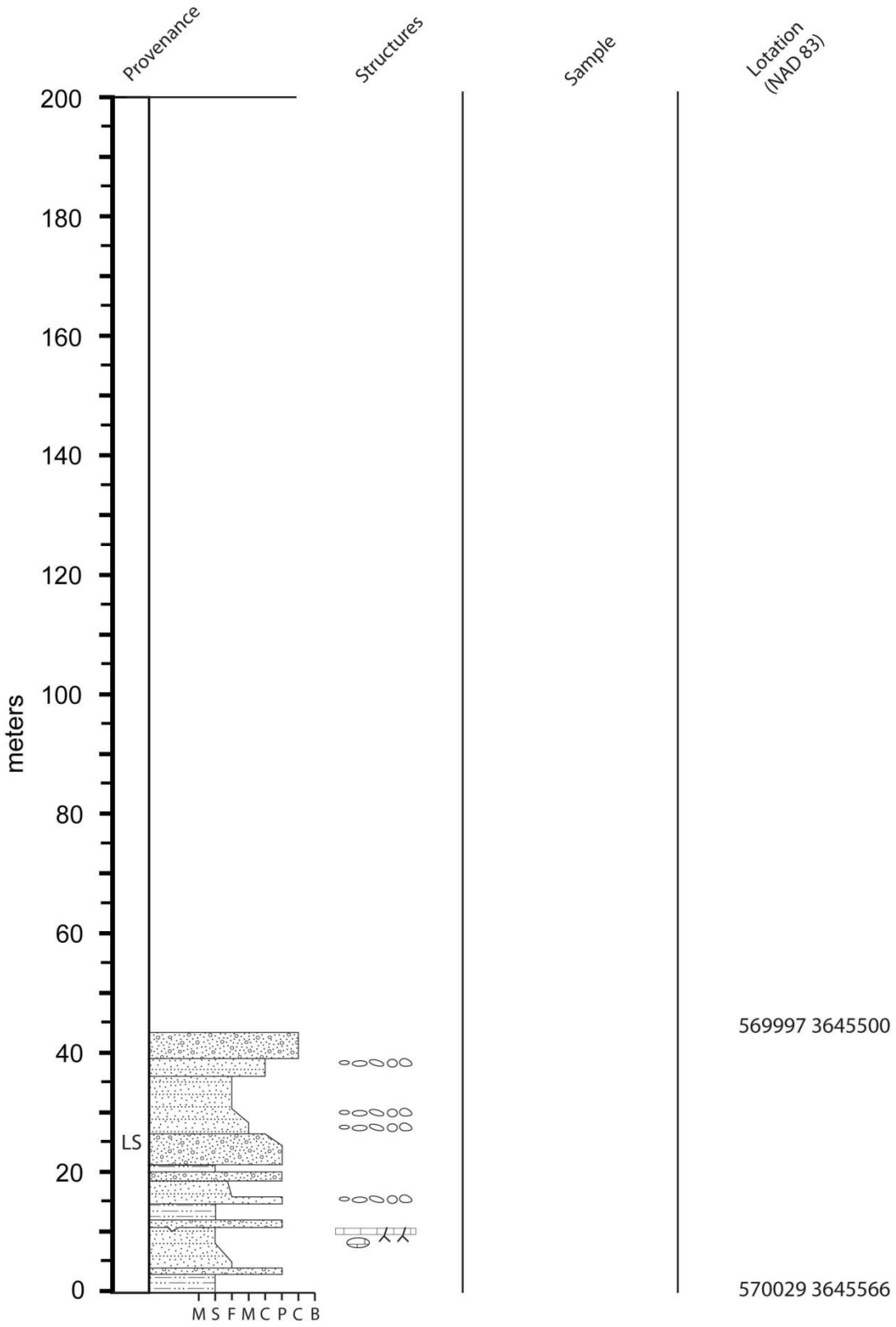
Provenance
Structures
Sample
Lotation (NAD 83)
meters
200
180
160
140
120
100
80
60
40
20
0
LS
M S F M C P C B
569997 3645500
570029 3645566

Section 21

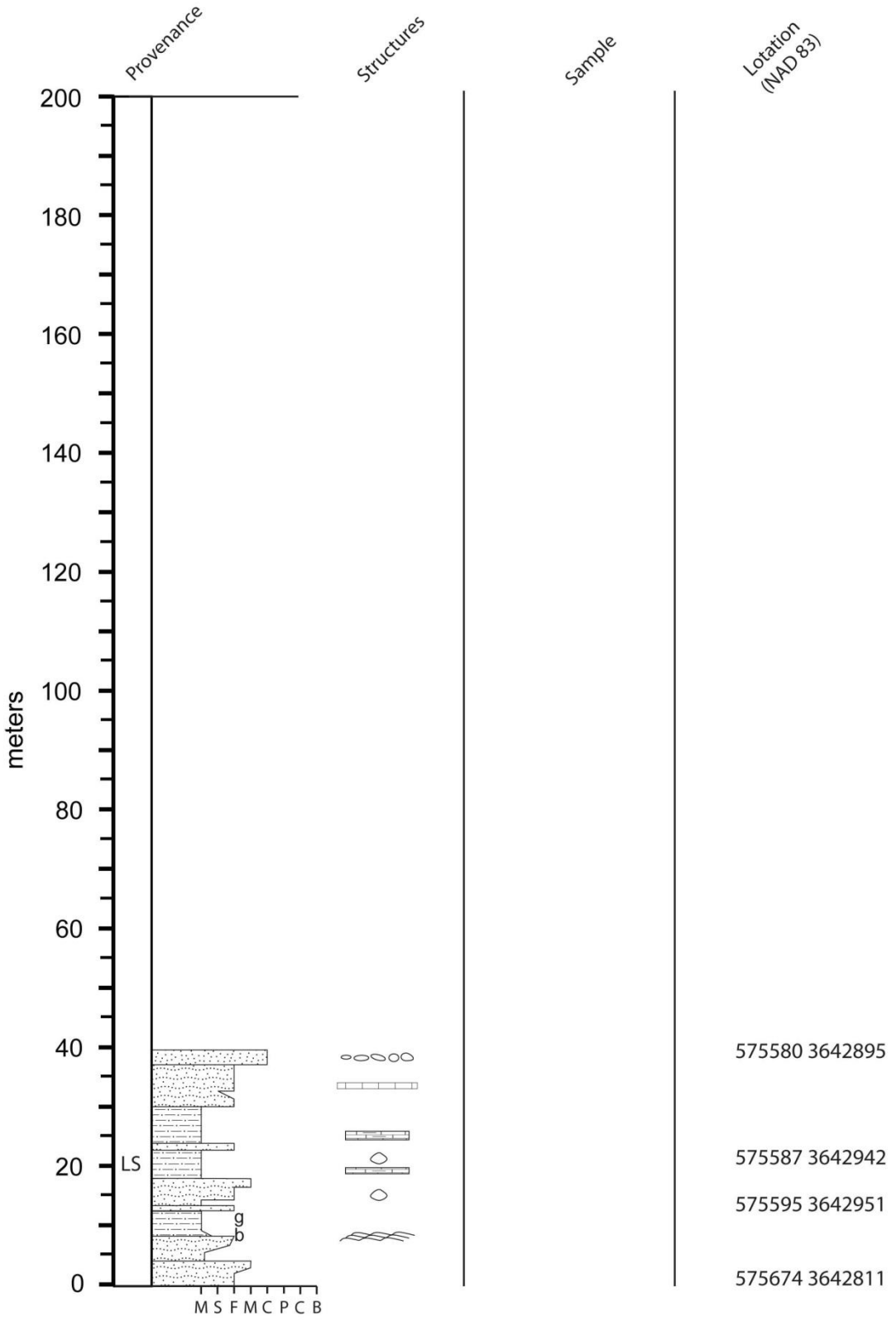
Provenance
Structures
Sample
Lotation (NAD 83)
meters
200
180
160
140
120
100
80
60
40
20
0
LS
g
b
M S F M C P C B
575580 3642895
575587 3642942
575595 3642951
575674 3642811

Section 22

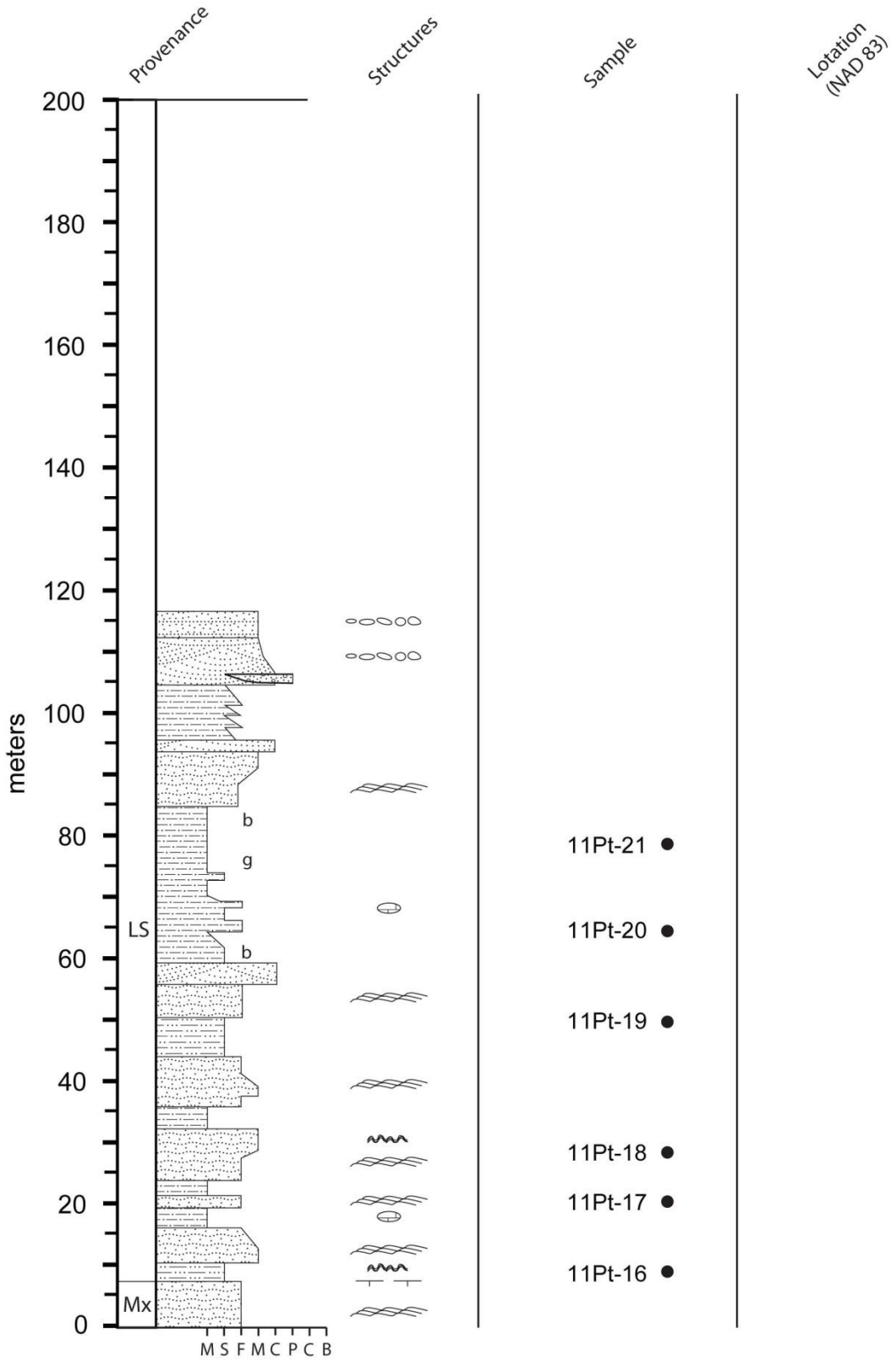
Provenance
Structures
Sample
Lotation (NAD 83)
meters
200
180
160
140
120
100
80
60
40
20
0
b
g
b
LS
Mx
M S F M C P C B
11Pt-21
11Pt-20
11Pt-19
11Pt-18
11Pt-17
11Pt-16

Section 23

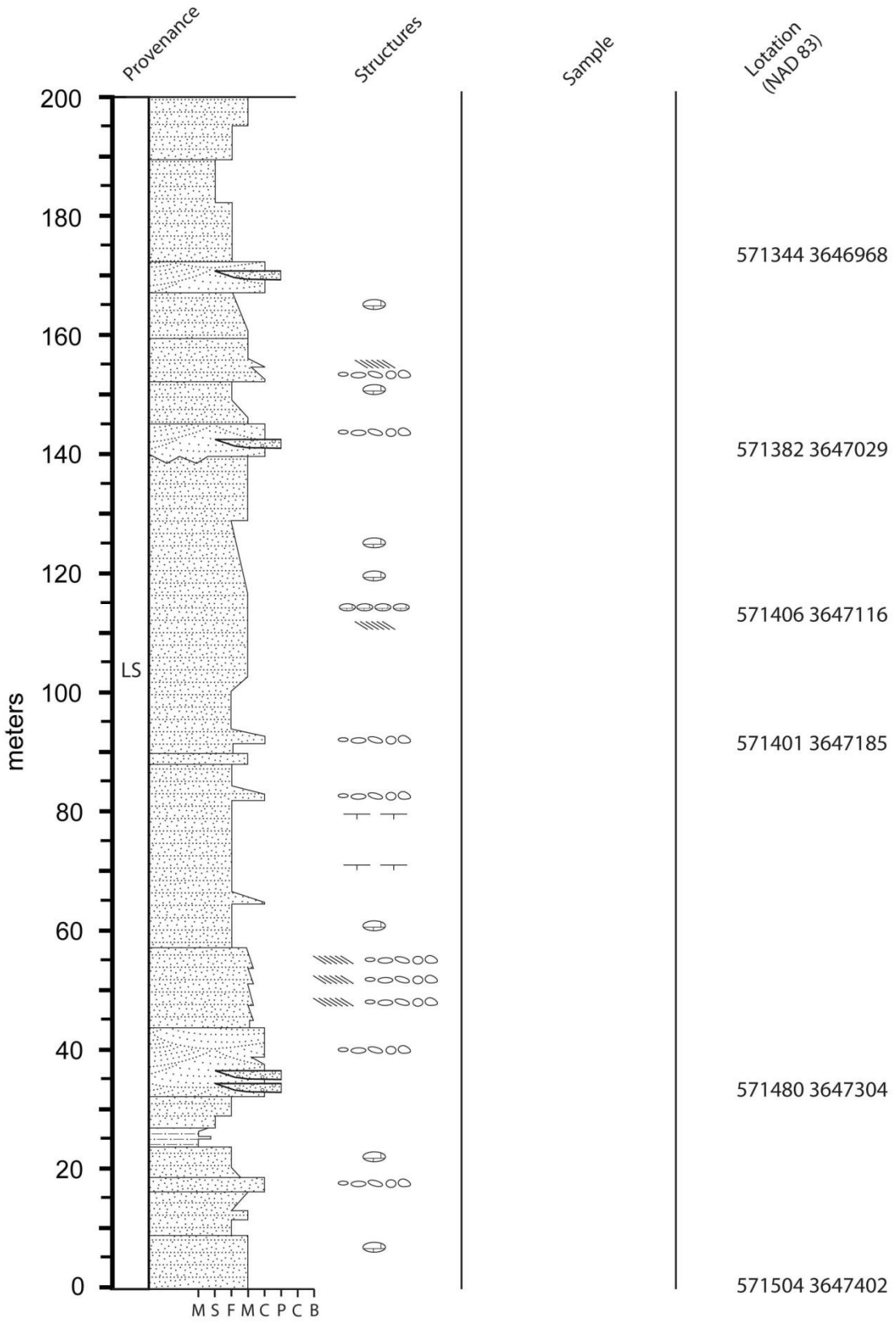
Provenance
Structures
Sample
Lotation (NAD 83)
200
180
160
140
120
100
80
60
40
20
0
meters
LS
M S F M C P C B
571344 3646968
571382 3647029
571406 3647116
571401 3647185
571480 3647304
571504 3647402

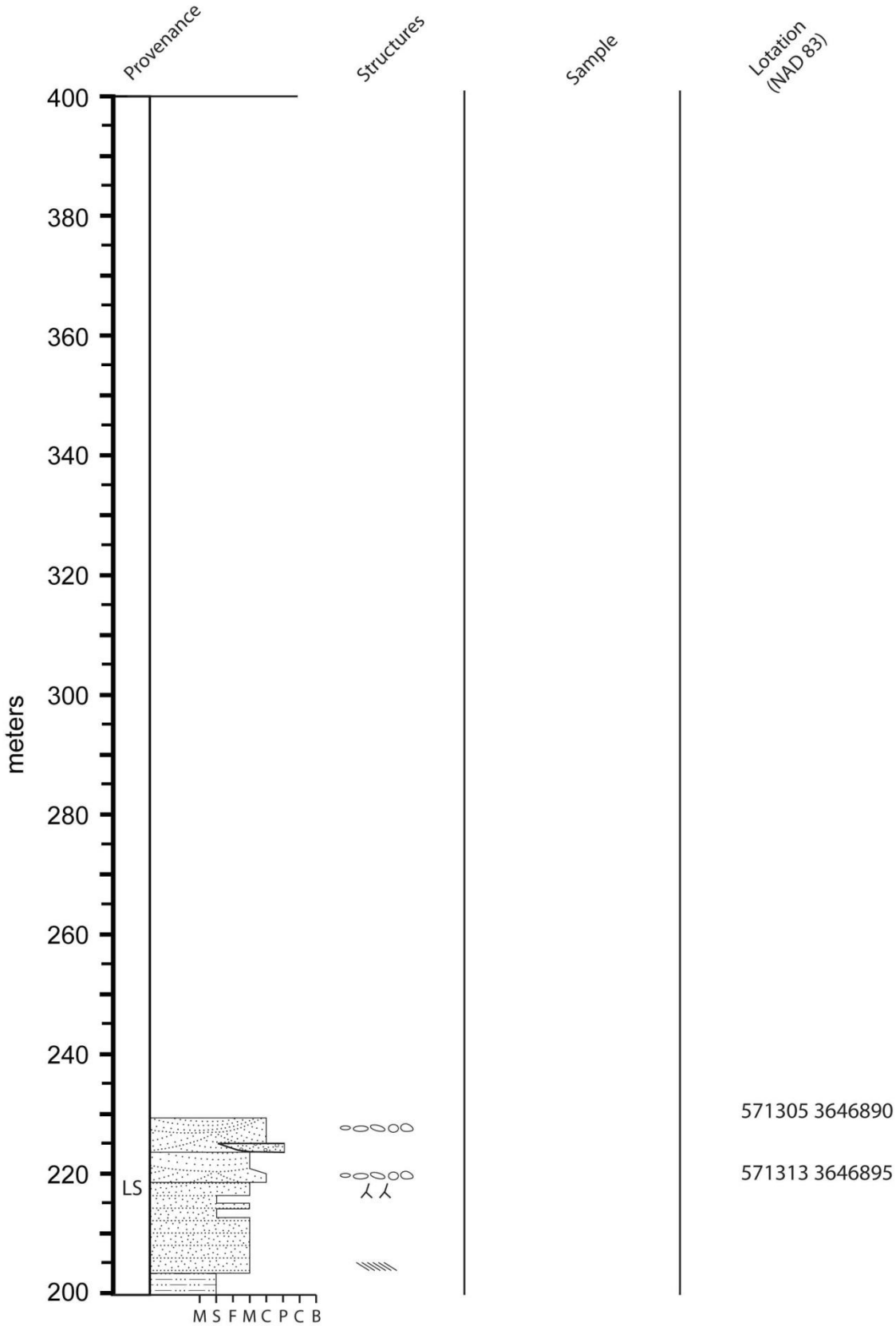
Provenance
Structures
Sample
Lotation (NAD 83)
meters
400
380
360
340
320
300
280
260
240
220
200
LS
M S F M C P C B
571305 3646890
571313 3646895

REFERENCES CITED

CHAPTER II

Abbot, P.L.,Smith, T.E., 1989. Sonora, Mexico, source for the Eocene Poway Conglomerate of southern California. Geology, 17(4): 329-332.

Adams, D.K.,Comrie, A.C., 1997. The North American Monsoon. Bulletin of the American Meteorological Society, 78(10): 2197-2213.

Amundson, R.G., Chadwick, O.A., Sowers, J.M.,Doner, H.E., 1988. Relationship between climate and vegetation and the stable carbon isotope chemistry of soils in the eastern Mojave Desert, Nevada. Quaternary Research, 29: 245-254.

Axelrod, D.I., 1973. History of the Mediterranean ecosystem in California. In: di Castri, F.,,Mooney, H.A. (Eds.), Ecological Studies, Analysis and Synthesis, 7. Springer-Verlag, pp. 225-277.

Axen, G.J.,Fletcher, J.M., 1998. Late Miocene-Pleistocene extensional faulting, Northern Gulf of California, Mexico and Salton Trough, California. International Geology Review, 40(3): 217-244.

Blisniuk, P.M., and Stern, L.A., 2005, Stable isotope paleoaltimetry: a critical review. American J. of Science, 305: 1033-1074.

Breecker, D.O., Sharp, Z.D.,McFadden, L.D., 2009. Seasonal bias in the formation and stable isotopic composition of pedogenic carbonate in modern soils from central New Mexico, USA. Geological Society of America Bulletin, 121(3/4): 630-640.

Brogenski, C.B., 2001. Terrestrial evidence for Plio-Pleistocene climate change in oxygen and carbon isotopic values of Southern California horse teeth, M.S. Thesis, University of California, Davis, Davis, 91 pp.

Carey, D.L., 1976, Forms and processes in the pseudokarst topography of Arroyo Tapiado, Anza-Borrego Desert State Park, San Diego County, California, M.S. Thesis University of California, Los Angeles, Los Angeles, 126 pp.

Cassiliano, M.L., 1994. Biostratigraphy of Blancan and Irvingtonian mammals in the Fish Creek-Vallecito Creek section, Southern California, and a review of the Blancan-Irvingtonian boundary. J. of Vertebrate Paleontology, 19(1): 169-186.

Caudill, M.R., Driese, S.G., Mora, C.J., 1996, Preservation of a paleo-Verisol and an estimate of Late Mississippian paleoprecipitation. J. of Sedimentary Research, 66(1): 58-70.

Cayan, D.R., Dettinger, M.D., Diaz, H.F.,Graham, N.E., 1998. Decadal variability of precipitation over Western North America. J. of Climate, 11(12): 3148-3166.

Cerezo-Mota, R., Cavazos, T., Farfán, L.M., 2006, Numerical simulation of heavy precipitation in northern baja California and southern California. J. of Hydrometeorology, 7: 137-148.

Cerling, T.E., 1984. The stable isotopic composition of modern soil carbonate and its relationship to climate. Earth and Planetary Science Letters, 71(2): 229-240.

Cerling, T.E.,Quade, J., 1993. Stable carbon and oxygen isotopes in soil carbonates, Climate Change in continental isotope records. American Geophysical Union, pp. 217-231.

Cerling, T.E., Quade, J., Wang, Y., Bowman, J.R., 1989. Carbon isotopes in soils and paleosols as ecologic and paleoecologic indicators. Nature, 341: 138-139.

Chamberlain, C.P., Poage, M.A., 2000. Reconstructing the paleotopography of mountain belts from the isotopic compotition of authigenic minerals. Geology, 28(2): 115-118.

Cosma, T.N., 2002a. Late Tertiary climate variations inferred from ostracode data, Anza-Borrego Desert, Southern California, USA, M.S. Thesis, Kent State University, Kent, 108 pp.

Cosma, T.N., 2002b. Uplift of Peninsular Ranges affects terrestrial climate record of enhanced tropical moisture in late Pliocene, Anza-Borrego Desert, California. Geological Society of America Abstracts with Programs, 34(6): 45.

Dekens, P.S., Ravelo, A.C.,, McCarthy, M.D., 2007. Warm upwelling regions in the Pliocene warm period. Paleoceanography, 22.

Dorsey, R.J., Housen, B.A., Janecke, S.U., Fanning, M.,, Spears, A.L.F., 2010. Stratigraphic record of basin development within the San Andreas fault system: Late Cenozoic FIsh Creek-Vallecito basin, Southern California. Gelogical Society of America Bulletin.

Driese, S.G., Mora, C.I., 1993. Physico-chemical environment of pedogenic carbonate formation in Devonian vertic paleosols, central Appalachians, USA. Sedimentology, 40: 199-216.

Dudal, R., Eswaran, H., 1988. Distribution, properties and classification of Vertisols. In: Wilding, L.P., Puentes, R. (Eds.), Vertisols: their distribution, properties, classificationa nd management. Texas A&M Publishing, College Station, pp. 1-22.

Farquhar, G.D., Ehleringer, J.R., Hubick, K.T., 1989. Carbon isotope discrimination and photosynthesis. Annual Review of Plant Physiology and Plant Molecular Biology, 40: 503-537.

Fox, D.L., Koch, P.L., 2003. Tertiary history of C4 biomass in the Great Plains, USA. Geology, 31(9): 809-812. Gensler, P.A., Jefferson, G.T., Roeder, M.A., 2006. The lower fossil vertebrates: fish, amphibians and reptiles. In: Jefferson, G.T., and Lindsay, L. (Eds.), Fossil Treasures of the Anza-Borrego Desert. Sunbelt Publications, Inc., San Diego, pp. 139-146.

Graham, A., 1999. Late Cretaceous and Cenozoic history of North American Vegetation (North of Vegetation). Oxford University Press, 350 pp.

Haug, G.H., Granopolski, A., Sigman, D.M., Rosell-Mele, A., Swann, G.E.A., Tiedemann, R., Jaccard, S.L., Bollman, J., Maslin, M.A., Leng, M.J., Eglington, G., 2005. North Pacific seasonality and the glaciation of North America 2.7 million years ago. Nature, 433: 821-825.

Haug, G.H., Tiedemann, R., Zahn, R., Ravelo, A.C., 2001. Role of Panama uplift on oceanic freshwater balance. Geology, 29(3): 207-210.

Haywood, A.M., Valdes, P.J., 2004. Modelling Pliocene warmth: contribution of atmosphere, oceans and cryosphere. Earth and Planetary Science Letters, 218: 363-377.

Higgins, R.W., Chen, Y., Douglas, A.V., 1999. Interannual variability of the North American warm season precipitation regime. J. of Climate, 12: 653-680.

Higgins, R.W., Yao, Y., Wang, X.L., 1997. Influence of the North American Monsoon system on the U.S. summer precipitation regime. J. of Climate, 10: 2600-2622.

Howard, H.H., 1963. Fossil birds from the Anza-Borrego desert. Los Angeles County Museum Contributions in Science, 73: 1-33.

Hsieh, J.C.C., Chadwick, O.A., Kelly, E.A., Savin, S.M., 1998. Oxygen isotopic composition of soil water: quantifying evaporation and transpiration. Geoderma, 82: 269-293.

Intergovernmental Panel on Climate Change, 2007. Climate change, 2007: the scientific basis. Cambridge University Press, Cambridge, 996 pp.

Jolly, D.W., 2000. Fossil turtles and tortoises of Anza-Borrego Desert State Park, California, M.S. Thesis, Northern Arizona University, Flagstaff, 197 pp.

Kent-Corson, M.L., Sherman, L.S., Mulch, A., Chamberlain, C.P., 2006. Cenozoic topographic and climatic response to changing tectonic boundary conditions in Western North America. Earth and Planetary Science Letters, 252: 453-466.

Kirby, S.M. et al., 2007. Pleistocene Brawley and Ocotillo formations: evidence for initial strike-slip deformation along the San Felipe and San Jacinto fault zones, Southern California. J. of Geology, 115: 43-62.

Kleinert, K., Strecker, M.R., 2001. Climate change in response to orographic barrier uplift: paleosol and stable isotopic evidence from the late Neogene Santa Maria basin, northwestern Argentina. Geological Society of America Bulletin, 113(6): 728-742.

Lewis, J.L., Day, S.M., Magistrale, H., Castro, R.R., Astiz, L., Rebollar, C., Eakins, J., Vernon, F.L., Brune, J.N., 2001. Crustal thickness of the Peninsular Ranges and Gulf Extensional Province in the Californias. J. of Geophysical Research, 106: 13599-13611.

Lewis, J.L., Day, S.M., Magistrale, H., Eakins, J., Vernon, F., 2000. Regional crustal thickness variations of the Peninsular Ranges, California. Geology, 28: 303-306.

Lisiecki, L.E., Raymo, M.E., 2005. A Pliocene-Pleistocene stack of 57 globally distributed benthic $\delta^{18}O$ records. Paleoceanography, 20.

Lutz, A.T., Dorsey, R.J., Housen, B.A., Janecke, S.U., 2006. Stratigraphic record of Pleistocene faulting and basin evolution in the Borrego Badlands, San Jacinto fault zone, Southern California. Geological Society of America Bulletin, 118(11/12): 1377-1397.

Machette, M.N., 1985. Calcic soils of the southwestern United States. In: D.L. Weide (Editor), Soils and Quaternary geology of the southwestern United States. Geological Society of America, pp. 1-22.

Mack, G.H., James, W.C., 1994. Paleoclimate and the global distribution of paleosols. The J. of Geology, 102: 360-366.

Marrs, B., 2006. History of fossil collecting in the Anza-Borrego desert region. In: Jefferson, G.T., Lindsay, L. (Eds.), Fossil Treasures of the Anza-Borrego Desert. Sunbelt Publications, Inc., San Diego, pp. 1-23.

Minnich, R.A., Franco-Vizcaíno, E., Dezzani, R.J., 2000, The El Niño/Southern Oscillation and precipitation variability in Baja California, Mexico. Atmósfera, 13: 1-20.

Mitchell, D.L., Ivanova, D., Rabin, R., Brown, T.J., Redmond, K., 2002. Gulf of California sea surface temperatures and the North American Monsoon: mechanistic implications from observations. J. of Climate, 15: 2261-2281.

Mitchell, V.A., 1976. The regionalization of climate in the Western United States. J. of Applied Meteorology, 15(9): 920-927.

Mo, K.C., Higgins, R.W., 1998. Tropical influence on California precipitation. J. of Climate, 11: 412-430.

Molnar, P., 2010. Deuterium and oxygen isotopes, paleoelevations of the Sierra Nevada, and Cenozoic climate, Geological Society of America Bulletin, 122(7/8): 1106-1115.

Molnar, P., Cane, M.A., 2002. El Niño's tropical climate and teleconnections as a blueprint for pre-Ice Age climates. Paleoceanography, 17(2).

Mueller, K., Kier, G., Rockwell, T., Jones, C.T., 2009. Quaternary rift flank uplift of the Peninsular Ranges in Baja and southern California by removal of mantle lithosphere. Tectonics, 28.

Mundelsee, M., Raymo, M.E., 2005. Slow dynamics of the Northern Hemisphere glaciation. Paleoceanography, 20.

J.Oskin, M., and Stock, J., 2003, Pacific-North America plate motion and opening of the Upper Delfin basin, northern Gulf of California, Mexico. Geological Society of America Bulletin, 115(10): 1173-1190.

Quade, J., Cater, J.M., Ojha, T.P., Adam, J., Harrison, T.M., 1995. Late Miocene environmental change in Nepal and the northern Indian subcontinent: stable isotopic evidence from paleosols. Geological Society of America Bulletin, 107(12): 1381-1397.

Quade, J., Cerling, T.E., Bowman, J.R., 1989. Systematic variations in the carbon and oxygen isotopic composition of pedogenic carbonate along elevation tranxects in the southern Great Basin, USA. Geological Society of America Bulletin, 101(4): 464-475.

Quade, J., Garzione, C., Eiler, J., 2007. Paleoelevation reconstruction using pedogenic carbonates. Reviews in Minerology and Geochemistry, 66: 53-87.

Ravelo, A.C., Andreason, D.H., Lyle, M., Lyle, A.O., Wara, M.W., 2004. Regional climate shifts caused by gradual cooling in the Pliocene epoch. Nature, 429: 263-267.

Raymo, M.E., 1994. The initiation of Northern Hemisphere glaciation. Annual Review of Earth and Planetary Sciences, 22: 353-383.

Raymo, M.E., Grant, B., Horowitx, M., Rau, G.H., 1996. Mid-Pliocene warmth: stronger greenhouse and stronger conveyor. Marine Micropaleontology, 27: 313-326.

Remeika, P., 2006. Ancestral woodlands of the Colorado River delta plain. In: Jefferson, G.T., Lindsay, L. (Eds.), Fossil Treasures of the Anza-Borrego Desert. Sunbelt Publications, Inc., San Diego, pp. 75-88.

Retallack, G.J., 1999. Postapocalyptic greenhouse paleoclimate revealed by earliest Triassic paleosols in the Sydney Basin, Australia. Geological Society of America Bulletin, 111(1): 52-70.

Retallack, G.J., 2005. Pedogenic carbonate proxies for amount and seasonality of precipitation in paleosols. Geology, 33(4): 333-336.

Retallack, G.J., Wynn, J.G., Fremd, T.J., 2004, Glacial-interglacial-sclae paleoclimatic change without large ice sheets in the Oligocene of central Oregon. Geology, 32(4): 297-300.

Sage, R.F., Wedin, D.A., Li, M., 1999, The biogeography of C4 photosynthesis: patterns and controlling factors. In: Sage, R.F., Monson, R.K. (Eds.), C4 Plant Biology.Academic Press, San Diego, pp. 313-376.

Schoenherr, A.A., Burk, J.H., 2007, Colorado Desert vegetation,. In: Barbour, M.G., Keeler-Wolf, T., Schoenherr, A.A. (Eds.), Terrestrial Vegetation fo California, University of California Press, Berkeley, pp. 657-682.

Schrag, D.P., Hampt, G., Murray, D.W., 1996. Pore fluid constraints on the temperature and oxygen isotopic composition of the glacial ocean. Science, 272: 1930-1932.

Sheldon, N.D., Retallack, G.J., 2001, Equation for compaction of paleosols due to burial. Geology, 29(3): 247-250.

Sheldon, N.D., Tabor, N.J., 2009. Quantitative paleoenvironmental and paleoclimatic reconstruction using paleosols. Earth-Science Reveiews, 95: 1-52.

Smith, G.A., Wang, Y., Cerling, T.E., Geissman, J.W., 1993. Comparison of a paleosol carbonate isotope record to other records of Pliocene-early Pleistocene climate in the western United States. Geology, 21: 691-694.

Smith, G.I., 1984. Paleohydraulic regimes in the southwestern Great Basin, 0-3.2 my ago, compared with other long records of "global" climate. Quaternary Research, 22: 1-17.

Spaulding, W.G., 1991. Pluvial climatic episodes in North America and North Africa: types and correlations with global climate. Palaeogeography, Palaeoclimatology, Palaeoecology, 84: 217-227.

Spero, H.L., Brogenski, C.B., Jefferson, G.T., 2003. Initiation of modern Pacific atmospheric circulation at the Plio-Pleistocene boundary recorded in horse teeth enamel geochemistry. Geological Society of America Abstracts with Programs, 35(6): 586.

Soil Survey Staff, 1999. Soil Taxonomy. United States Department of Agriculture Handbook, 436.

Steely, A.N., Janecke, S.U., Dorsey, R.J., Axen, G.J., 2009. Early Pleistocene initiation of the San Felipe fault zone, NW Salton Trough, during reorganization of the San Andreas fault system. Geological Society of America Bulletin, 121: 663-687.

Stevenson, B.A., Kelly, E.F., McDonald, E.V., Busacca, A.J., 2005. The stable carbon isotope composition of soil organic carbon and pedogenic carbonates along a bioclimatic gradient in the Palouse region, Washington State, USA. Geoderma, 124: 37-47.

Sussman, S., Lindsay, L., Spero, H., 2006. Paleoclimates and environmental change in the Anza-Borrego Desert region. In: Jefferson, G.T., Lindsay, L. (Eds.), Fossil Treasures of the Anza-Borrego Desert. Sunbelt Publications, Inc., San Diego, pp. 339-352.

Tipple, B.J., Meyers, S.R., Pagani, M., 2010. Carbon isotope ratio of Cenozoic CO2, a comparative evaluation of available geochemical proxies. Paleoceonagraphy, 25: 11 p.

Van Devender, T.R., 1990, Late Quaternary vegetation and climate of the Sonoran desert, United States and Mexico. In: Betancourt, J.L., Van Devender, T.R., Martin, T.S. (Eds.), Packrat Middens: The Last 40,000 Years of Biotic Change. University of Arizona Press, Tucson, pp. 134-165.

Vaughan, T.W., 1904. A California Tertiary coral reef and its bearing on American recent coral reefs. Science, 19.

Wang, Y., Cerling, T.E., MacFadden, B.J., 1994. Fossil horses and carbon isotopes: new evidence for Cenozoic changes in North America. Palaeogeography, Palaeoclimatology, Palaeoecology, 107: 269-279.

Wara, M.W., Ravelo, A.C., Delaney, M.L., 2005. Permanent El Niño-like conditions during the Pliocene warm period. Science, 309: 758-761.

White, J.A., Wagner, H., Jefferson, G.T., 2006. The small fossil mammals: rodents, rabbits and their relatives. In: Jefferson, G.T., Lindsay, L. (Eds.), Fossil Treasures of the Anza-Borrego Desert. Sunbelt Publications, Inc., San Diego, pp. 235-251.

Wieder, M., Yaalon, D.H., 1974. Effect of matrix composition on carbonate nodule crystallization. Geoderma, 11: 95-121.

Williams, A.E., Rodoni, D.P., 1997, Regional isotope effects and application to hydrologic investigations in southwestern California. Water Resources Research, 33(7): 1721-1729.

Woodhouse, C.A., 1997. Winter climate and atmospheric circulatioon in the Sonoran Desert region, USA. J. of Climatology, 17: 859-873.

Yang, Y., Forsyth, D.W., 2006. Rayleigh wave phase velocities, small-scale convection, and azimuthal anisotropy beneath Southern California. J. of Geophysical Research, 111: 20 p.

Zachos, J., Pagani, M., Sloan, L., Thomas, E., Billups, K., 2001. Trends, rythms, and abberations in global climate 65 Ma to the present. Science, 292: 386-392.

CHAPTER III

Abbott, P. L., Smith, T.E., 1978, Trace-element comparison of clasts in Eocene conglomerates, southwestern California and northwestern Mexico: Journal of Geology, v. 86, p. 753-762.

Allen, P. A., and A. L. Densmore, 2000, Sediment flux from an uplifting fault block: Basin research, v. 12, p. 367-380.

Allen, P. A., and N. Hovius, 1998, Sediment supply from landslide-dominated catchments: implications for basin-margin fans: Basin Research, v. 10, p. 19-35.

Aragón-Arreola, M., and Martín-Barajas, A., 2007, Westward migration of extension in the northern Gulf of California, Mexico: Geology, v. 35, no. 6, p. 571-574.

Armitage, J.J., Duller, R.A., Whittaker, A.C., and Allen, P.A., 2011, Transformation of tectonic and climatic signals from source to sedimentary archive: Nature Geoscience, v. 4, p. 231-235.

Aschoff, J and Steel, R., 2011, Anomalous clastic wedge development during the Sevier-Laramide transition, North American Cordilleran foreland basin, USA: Geological Society of America Bulletin, v. 123, p. 1822-1835.

Axen, G., 1995, Extensional segmentation of the Main Gulf Escarpment, Mexico and United States: Geology, v. 23, p. 515-518.

Axen, G. J., and J. M. Fletcher, 1998, Late Miocene-Pleistocene extensional faulting, Northern Gulf of California, Mexico and Salton Trough, California: International Geology Review, v. 40, p. 217-244.

Blair, T. C., and W. L. Bilodeau, 1988, Development of tectonic cyclothems in rift, pull-apart, and foreland basins: sedimentary response to episodic tectonism: Geology, v. 16, p. 517-520.

Brozović, N., and Burbank, D.W., 2000, Dynamic fluvial systems and gravel progradation in the Himalayan foreland: Geological Society of America Bulletin, v. 112, p. 394-412.

Carroll, A.R., and Bohacs, K.M.,m 1999, Stratigraphic controls of ancient lakes: balancing tectonic and climatic controls: Geology, v. 27, p. 99-102.

Compton, R. R., 1985, Geology in the Field: New York, John Wiley.

Cosma, T.N., 2002, Late Tertiary climate variations inferred from ostracode data, Anza-Borrego Desert, Southern California, USA: M.S. Thesis, Kent State University, Kent, 108 p.

Densmore, A.L., Allen, P.A., and Simpson, G., 2007, Development and response of a coupled catchment fan system under changing tectonic and climatic forcing: Journal of Geophysical Research, v. 112.

Dibblee, T. W., 1954, Geology of the Imperial Valley region, California, *in* R. H. Jahns, ed., Geology of California, California Division of Mines Bulletin, Sacramento, California, California Division of Mines, p. 21-28.

Dibblee, T. W., 1984, Stratigraphy and tectonics of the San Felipe Hills, Borrego Badlands, Superstition Hills , and vicinity, *in* C. A. Rigsby, ed., The Imperial Basin - tectonics, sedimentation and thermal aspects: field trip guidebook, v. 40, Pacific Section, Society of Economic Paleontologists and Mineralogists, p. 31-44.

Dibblee, T. W., ed., 1996, Stratigraphy and tectonics of the Vallecito-Fish Creek Mountains, Vallecito Badlands, Coyote Mountains, and Yuha Desert, southwestern Imperial Basin, v. Annula Field Trip Guide: Santa Ana, South Coast Geological Society, 59-80 p.

Dorsey, R.J., and Becker, U., 1995, Evolution of a large Miocene growth structure in the upper plate of the Whipple detachment fault, north-eastern WHipple Mountains, California: Basin Research, v. 7, p. 151-163.

Dorsey. R.J., and Martín-Barajas, A., 1999, Sedimentation and deformation in a Pliocene-Pleistocene transtensional supradetachment basin, Laguna Salada, north-west Mexico: Basin Research, v. 11, p. 205-221.

Dorsey, R. J., S. U. Janecke, S. M. Kirby, K. A. McDougall, and A. N. Steely, 2005, Pliocene evolution of the lower Colorado River in the Salton Trough: tectonic controls on paleogeography and the regional Borrego Lake, *in* M. C. Reheis, ed., Geologic and biotic perspectives on late Cenozoic drainage history of the southwestern Great Basin andlower Colorado River region: conference abstract. U.S. Geological Survey Open-File Report 2005-1404, p. 13.

Dorsey, R. J., A. Fluette, K. McDougall, B. A. Housen, S. U. Janecke, G. J. Axen, and C. R. Shirvell, 2007, Chronology of Miocene-Pliocene deposits at Split Mountain Gorge, Southern California: a record of regional tectonics and Colorado River evolution: Geology, v. 35, p. 57-60.

Dorsey, R. J., B. A. Housen, S. U. Janecke, C. M. Fanning, and A. L. F. Spears, 2011, Stratigraphic record of basin development within the San Andreas fault system: Late Cenozoic Fish Creek–Vallecito basin, southern California Geological Society of America Bulletin, v. 123 p. 771-793.

Dorsey, R. J., G. Axen, T. Peryam, and M. Kairouz, 2012, Initiation of the southern Elsinore fault at ~1.2 Ma: evidence from the Fish Creek-Vallecito basin, southern California: Tectonics.

Friedman, S.J., and Burbank, D.W., 1995, Rift basins and supradetachment basins: intracontinental end-members: Basin Research, v. 7, p. 109-127.

Friedman, S.J., Davis, G.A., and Fowler, T.K., 1996; Geometry. paleodrainage, and geologic rates from the Miocene Shadow Valley supradetachment basin, eastern Mojave Desert, California: *in* Beratan, K.K., ed., Reconstructing the history of basin and range extension using sedimentology and stratigraphy, Special Paper 303: Boulder, Colorado, Geological Society of America, p. 85-106.

Gangopadhyay, S., and McCabe, G.J., 2010, Predicting regime shifts in flow of the Colorado River: Geophysical Research Letters, v. 37, doi: 10.1029/2010GL044513.

Gastil, G., Krummanacher, D., Minch, J., 1979, The record of Cenozoic volcanism around the Gulf of California: Geological Society of America Bulletin, v. 90, p. 839-587.

Gastil, R. G., Phillips, R.P., Allison, E.C., 1971, Reconnaissance geologic map of the state of Baja California: Geological Society of America.

Grove, M., O. Lovera, and M. Harrison, 2003, Late Cretaceous cooling of the east-central Peninsular Ranges batholoth (33°): relationship to La Posta pluton emplacement, Laramide shallow subduction , and forearc sedimentation, *in* S. E. Johnson, Paterson, S.R., Fletcher, J.M., Girty, G.H., Kimbrough, D.L., Martin-Barajas, A., ed., Tectonic evolution of northwestern Mexico and southwestern USA, Special Paper 374: Boulder, Colorado, Geological Society of America, p. 355-379.

Heller, P. L., and C. Paola, 1992, The large-scale dynamics of grain-size variation in alluvial basins, 2: Application to syntectonic conglomerate: Basin Research, v. 4, p. 91-102.

Horton, B.K., Constenius, K.N. and DeCelles, P.G., 2004, Tectonic control on coarse-grained foreland-basin sequences: an example from the Cordilleran foreland basin, Utah: Geology, v. 32, p. 637-640.

Housen, B.A and Dorsey, R.J., 2010, Magnetostratigraphy and paleomagnetism of the Plio-Pleistocene Arroyo Diablo and Borrego formations in the Borrego Badlands, western Salton Trough, CA. Abstract GP23C-08 presented at 2010 Fall Meeting, AGU, San Francisco, Calif., 13-17 Dec.

Huntington, K. W., A. E. Blythe, and K. V. Hodges, 2006, Climate change and Late Pliocene acceleration of erosion in the Himalaya: Earth and Planetary Science Reviews, v. 252, p. 107-118.

Janecke, S. U., R. J. Dorsey, D. Forand, A. N. Steely, S. M. Kirby, A. T. Lutz, B. A. Housen, B. Belgarde, V. E. Langenheim, and T. M. Rittenour, 2010a, High geologic slip rates since early Pleistocene intiation of the San Jacinto and San Felipe fault zones in the San Andreaws fault system: southern California, USA: Geological Society of America Special Paper 475.

Johnson, N. M., C. B. Officer, N. D. Opdyke, G. D. Woodard, P. K. Zeitler, and E. H. Lindsay, 1983, Rates of late Cenozoic tectonism in the Vallecito-Fish Creek basin, western Imperial Valley, California: Geology, v. 11, p. 664-667.

Kairouz, M. E., 2005, Geology of the Whale Peak region of the Vallecito Mountains: emphasis on the kinematics and timing of the West Salton detachment fault, southern California, University of California, Los Angeles, 156 p.

Kies, R. P., Abbott, P.L., 1983, Rhyolite clast populations and tectonics in the California continental borderland: Journal of Sedimentary Petrology, v. 53, p. 461-475.

Kirby, S. M., S. U. Janecke, R. J. Dorsey, B. A. Housen, V. E. Langenheim, K. A. McDougall, and A. N. Steely, 2007, Pleistocene Brawley and Ocotillo formations: evidence for initial strike-slip deformation along the San Felipe and San Jacinto fault zones, Southern California: Journal of Geology, v. 115, p. 43-62.

Koltermann, C. E., and S. M. Gorelick, 1992, Paleoclimate signature in terrestrial flood deposits: Science, v. 256, p. 1775-1782.

Lampe, C. M., 1988, Geology of the Granite Mountain area: implications of the extent and style of deformation along the southeast portion of the Elsinore Fault, San Diego State University, San Diego, CA, 150 p.

Leeder, M. R., and R. L. Gawthorpe, 1987, Sedimentary models for extensional tilt-block/half-graben basins, *in* M. P. Coward, J. F. Dewey, and P. L. Hancock, eds., Continental Extensional Tectonics, Geological Society Special Publication No. 28: Geological Society Special Publication: London.

Longinotti, N. E., M. E. OSkin, C. J. Deboer, B. A. Housen, T. C. Peryam, and R. J. Dorsey, 2011, 10Be-derived paleo-erosion rates recorded in the Fish Creek-Vallecito basin, California indicate no increase across the Plio-Pleistocene climate transition: American Geophysical Union 2011 Fall Meeting Abstracts.

Lutz, A. T., R. J. Dorsey, B. A. Housen, and S. U. Janecke, 2006, Stratigraphic record of Pleistocene faulting and basin evolution in the Borrego Badlands, San Jacinto fault zone, Southern California: Geological Society of America Bulletin, v. 118, p. 1377-1397.

Mack, G. H., and M. R. Leeder, 1999, Climatic and tectonic controls on alluvial-fan and axial-fluvial sedimentation in the Plio-Pleistocene Palomas half graben, southern Rio Grande rift: Journal of Sedimentary Research, v. 69, p. 635-652.

Mack, G.H., and Stout, D.M., 2005, Unconventional facies distribution of facies in a continental rift basin: the Pliocene-Pleistocene Mangas basin, south-western New Mexico, USA: Sedimentology, v. 52, p. 1187-1205.

Marr, J. G., J. B. Swenson, C. Paola, and V. R. Voller, 2000, A two-diffusion model of fluvial stratigraphy in closed depositional basins: Basin Research, v. 12, p. 381-398.

Martinsen, O.J., Ryseth, A., Hellend-Hansen, W., Flesche, H., Torkildsen, G., and Idil, S., 1999, Stratigraphic base level and fluvial architecture: Ericson Sandstone (Campanian), Rock Springs uplift, SW Wyoming, USA: Sedimentology, v. 46, p. 235-263.

Marzo, M., and Steel, R.J., 2000, Unusual features of sediment-supply-dominated, transgressive-regressive sequences: Paleogene clastic wedges, SE Pyrenean foreland basin, Spain: Sedimentary Geology, v. 138, p. 3-15.

Molnar, P., 2004, Late Cenozoic increase in accumulation rates of terrestrial sediment: how might climate change have affected erosion rates? : Annual Review of Earth and Planetary Sciences, v. 32, p. 67-89.

Nagy, E., and Stock, J., 2000, Structural controls on the continent-ocean transition in the northern Gulf of California: Journal of Geophysical Research, v. 105, p. 16251-16269.

Pacheco, M., Martín-Barajas, A., Elders, W., Espinosa-Cardeña, J.M., Helenes, J., Segura, A., 2006, Stratigraphy and structure of the Altar basin of NW Sonora: implications for the history of the Colorado River delta and the Salton trough: Revista Mexicana de Ciencieas Geológicas, v. 23, p. 1-22.

Parra, M., Mora, A., Jaramillo, C., Torres, V., Zeilinger, G., and Strecker, M.R., 2010 Tectonic controls on Cenozoic foreland basin development in the north-eastern Andes, Columbia: Basin Research, v. 22, p. 874-903.

Paola, C., P. L. Heller, and C. L. Angevine, 1992, The large-scale dynamics of grain-size variation in alluvial basins, 1: Theory: Basin Research, v. 4, p. 73-90.

Peryam, T. C., R. J. Dorsey, and I. Bindeman, 2011, Plio-Pleistocene climate change and timing of Peninsular Ranges uplift in southern California: Evidence from paleosols and stable isotopes in the Fish Creek–Vallecito basin: Palaeogeography, Palaeoclimatology, Palaeoecology, v. 305, p. 65-74.

Peryam, T. C., R. J. Dorsey, M. E. Oskin, K. Blisniuk, and B. A. Housen, 2010, Controls on mid-Pliocene (ca. 2.8 Ma) progradation of coarse detritus in the Fish Creek-Vallecito Basin, southern California: Geological Society of America Abstracts with Programs, v. 42, p. 429.

Reitz, D. T., 1977, Geology of the western and central San Felipe Hills, northwestern Imperial County, California, University of Southern California, Los Angeles, 155 p.

Rogers, T. H., 1966, Geologic map of California: Santa Ana sheet: State of California Division of Mines and Geology.

Smith, G. A., Y. Wang, T. E. Cerling, and J. W. Geissman, 1993, Comparison of a paleosol carbonate isotope record to other records of Pliocene-early Pleistocene climate in the western United States: Geology, v. 21, p. 691-694.

Steely, A. N., S. U. Janecke, R. J. Dorsey, and G. J. Axen, 2009, Early Pleistocene initiation of the San Felipe fault zone, NW Salton Trough, during reorganization of the San Andreas fault system: Geological Society of America Bulletin, v. 121, p. 663-687.

Stock, J., 2000, Realtion of the Puertocitos volcanic province, Baja California, MExico, to development of the plate boundary in the Gulf of California: in Delgado-Granados, H., et al., eds., Cenozoic tectonics and volcanism of Mexico: Geological Society of America Special Paper 334, p. 143-156.

Strand, R. G., 1962, Geologic map of California, San Diego-El Centro sheet: State of California Division of Mines and Geology.

Todd, V. R., 2004, Preliminary Geologic Map of the El Cajon 30' x 60' Quadrangle, Southern California, Version 1.0, United States Geological Survey.

Whipple, K. X., and C. R. Trayler, 1996, Tectonic control of fan size: the importance of spatially-variable subsidence rates: Basin Research, v. 8, p. 351-366.

Winker, C. D., 1987, Neogene stratigraphy of the Fish Creek-Vallecito section, Southern California: implications for early history of the Northern Gulf of California and Colorado Delta, University of Arizona, Tucson, 494 p.

Winker, C. D., and S. M. Kidwell, 1986, Paleocurrent evidence for lateral displacement of the Pliocene Colorado River delta by the San Andreas fault system, southeastern California: Geology, v. 14, p. 788-791.

Winker, C. D., and S. M. Kidwell, 1996, Stratigraphy of a marine rift basin: Neogene of the western Salton Trough, California, *in* P. L. Abbott, and J. D. Cooper, eds., Field conference guidebook and volume for the American Association of Petroleum Geologists annual convention, San Diego, California: Bakersfield, American Association of Petroleum Geologists, p. 295-336.

Woodard, G. D., 1963, The Cenozoic succession of the west Colorado Desert, San Diego and Imperial Counties, southern California, University of California, Berkeley, 173 p.

Zhang, P., P. Molnar, and W. R. Downs, 2001, Increased sedimentation rates and grain sizes 2-4 Myr due to the influence of climate change on erosion rates: Nature, v. 410, p. 891-897.

CHAPTER IV

Angevine, C.L., Heller, P.L., and Paola, C., 1990, Quantitative sedimentary basin modeling: American Association of Petroleum Geologists (AAPG) Short Course Note Series 32, 247 p.

Berger, A., and Loutre, M.F., 1991, Insolation values for the climate of the last 10 million years: Quaternary Science Review, v. 10, no. 4, p. 297-317.

Bloemendal, J., Oldfield, F., and Thompson, R., 1979, Magnetic measurements used to assess sediment influx at Llyn Goddionduon: Nature, v. 280, p. 50-53.

Brogenski, C.B., 2001, Terrestrial evidence for Plio-Pleistocene climate change in oxygen and carbon isotopic values of southern California horse teeth: M.S. Thesis, University of California, Davis, Davis, 91 p.

Bull, W.B., and Schick, A.P., 1979, Impact of climatic change on an arid watershed: Nahal Yael, southern Israel: Quaternary Research, no. 11, p. 153-171.

Carroll, A.R., and Bohacs, K.M., 1999, Stratigraphic controls of ancient lakes: balancing tectonic and climatic controls: Geology, v. 27, p. 99-102.

Cayan, D.R., Dettinger, M.D., Diaz, H.F., and Mora, C.J., 1998, Decadal variability of precipitation over western North America: Journal of Climate, v. 19, no. 1., p. 169-186.

Chapin, C.E., 2008, Interplay of oceanographic and paleoclimate events with tectonism during middle to late Miocene sedimentation across the southwestern USA: Geosphere, v. 4, p. 976-991.

Clinkenbeard, J.P. and Walawender, M.J., 1989, Mineralogy of the La Posta pluton: implications for the origin of zoned plutons in the eastern Peninsular Ranges batholith, southern and Baja California: American Mineralogist, v. 74, p. 1258-1269.

Clift, P. D., 2006, Controls on the erosion of Cenozoic Asia and the flux of clastic sediment to the ocean: Earth and Planetary Science Letters, v. 241, p. 571-580.

Cosma, T.N., 2002a. Late Tertiary climate variations inferred from ostracode data, Anza-Borrego Desert, Southern California: USA, M.S. Thesis, Kent State University, Kent, 108 p.

Cosma, T.N., 2002b. Uplift of Peninsular Ranges affects terrestrial climate record of enhanced tropical moisture in late Pliocene, Anza-Borrego Desert, California: Geological Society of America Abstracts with Programs, 34(6): 45.

Daubechies, I., 1990, The wavelet transform time-frequency localization and signal analysis: IEEE Transactions of Information Theory, v. 36, p. 961-1004.

Day, R., Fuller, M., and Schmidt, V.A., 1977, Hysteresis properties of titanomagnetites: grain-size and compositional dependence: Physics of Earth and Planetary Interiors, v. 13, p. 260-267.

Dearing, J., 1999, Environmental magnetic susceptibility: using the Bartington MS2 system (second edition): Chi Publishing, England, 54 p.

Deboer, C., Block rotation and magnetostratigraphy of the Fish Creek-Vallecito basin, Salton Trough, CA: M.S. Thesis, Western Washington University, 107 p.

Dekens, P.S., Ravelo, A.C., and McCarthy, M.D., 2007, Warm upwelling regions in the Pliocene warm period: Paleoceanography, v. 22, doi: 10.1029/2006PA001394.

Dibble, T.W., 1954, Geology of the Imperial Valley region, California: California Division of Mines Bulletin 170, p. 21-28.

Dibblee, T. W., 1984, Stratigraphy and tectonics of the San Felipe Hills, Borrego Badlands, Superstition Hills , and vicinity, *in* C. A. Rigsby, ed., The Imperial Basin - tectonics, sedimentation and thermal aspects: Field Trip Guidebook, v. 40, Pacific Section, Society of Economic Paleontologists and Mineralogists, p. 31-44.

Dorsey, R. J., Janecke, S.U., Kirby,S.M., McDougall, K.A., and Steely, A.N., 2005, Pliocene evolution of the lower Colorado River in the Salton Trough: tectonic controls on paleogeography and the regional Borrego Lake, *in* M. C. Reheis, ed., Geologic and biotic perspectives on late Cenozoic drainage history of the southwestern Great Basin and lower Colorado River region: conference abstract. U.S. Geological Survey Open-File Report 2005-1404, p. 13.

Dorsey, R. J., Housen, B.A. Janecke, S.U., Fanning, C.M., and Spears, A.L.F., 2011, Stratigraphic record of basin development within the San Andreas fault system: Late Cenozoic Fish Creek–Vallecito basin, southern California Geological Society of America Bulletin, v. 123, p. 771-793.

Dorsey, R.J., Fluette, A., McDougall, K.A., Housen, B.A., Janecke, S.U., Axen, G.J., and Shirvell, C.R., 2007, Chronology of Miocene-Pliocene deposits at Split Mountain Gorge, Southern California: a record of regional tectonics and Colorado River evolution: Geology, v. 35, p. 57-60.

Dorsey, R. J., Axen,G.J., Peryam, T.C., and Kairouz, M., 2012, Initiation of the southern Elsinore fault at ~1.2 Ma: evidence from the Fish Creek-Vallecito basin, southern California: Tectonics, doi: 10.1029/2011TC003009.

Dosseto, A., Hesse, P.P., Maher, K., and Turner, S., 2010, Climatic and vegetation control on sediment dynamics during the last glacial cycle: Geology, v. 38, no. 5, p. 395-398.

Dunlop, D.J., 2002, Theory and application of the Day plot (Mrs/Ms versus Hcr/Hc) 1. Theoretical curves and tests using titanomagnetite data: Journal of Geophysical Research, v. 107, no. B3. Doi:10.1029/2001JB000486.

Enzel, Y., Amit, R., Grodek, T., Ayalon, A., Lekach, J., Porat, N., Bierman, P., Blum, J.D., and Erel, Y., 2012, Late Quaternary weathering, erosion, and deposition in Nahal Yale, Israel: an "impact of climatic change on an arid watershed"?: Geological Society of America Bulletin, v. 5/6, p. 705-722, doi: 10.1130/B30538.1.

Esner, J.B. and Tsonis, A.A., 1991, Do bidecadal oscillations exist in the global temperature record?: Nature, v. 353, p. 551-553.

Federov, A.V., Dekens, P.S., McCarthy, M., Ravelo, A.C., deMenocal, P.B., Barreiro, M., Pacanowski, R.C., and Philander, S.G., 2006, The Pliocene paradox (mechanisms for a permanent El Niño: Science, v. 312, p. 1485-1489.

Forester, R.M., 1991, Pliocene-climate history of the western United States derived from lacustrine ostracodes: Quaternary Science Reviews, v. 10, p. 133-146.

Gangopadhyay, S., and McCabe, G.J., 2010, Predicting regime shifts in flow of the Colorado River: Geophysical Research Letters, v. 37, doi: 10.1029/2010GL044513.

Geiss, C.E., and Zanner, C.W., 2006, How abundant is pedogenic magnetite? Abundance and grain size estimate for loessic soils based on rock magnetic analyses: Journal of Geophysical Research, v. 111, doi:10.1029/2006JB004564.

Gensler, P.A., Jefferson, G.T., and Roeder, M.A., 2006, The lower fossil vertebrates: fish, amphibians and reptiles, *in* Jefferson, G.T., and Lindsay, L., eds., Fossil Treasures of the Anza-Borrego Desert: Sunbelt Publications, Inc., San Diego, p. 139-146.

Ghil, M., Allen, M.R., Dettinger, M.D., Ide, K., Kondrashov, D., Mann, M.E., Robertson, A.W., Saunders, A., Tian, Y., Varadi, F., and Yiou, P., 2002, Advanced spectral methods for climatic time series: Review of Geophysics, v. 40, no. 1, doi:10.1029/2001RG000092.

Haug, G.H., Tiedemann, R., Zahn, R., Ravelo, A.C., 2001. Role of Panama uplift on oceanic freshwater balance: Geology, v. 29, no. 3, p. 207–210.

Haug, G.H., Granopolski, A., Sigman, D.M., Rosell-Mele, A., Swann, G.E.A., Tiedemann, R.,Jaccard, S.L., Bollman, J., Maslin, M.A., Leng, M.J., Eglington, G., 2005, North Pacific seasonality and the glaciation of North America 2.7 million years ago: Nature 433, p. 821–825.

House, P.K., Pearthree, P.A., Howard, K.A., Bell, J.W., Perkins, M.E., Faulds, J.E., and Brock, A.L., 2005, Birth of the lower Colorado River—stratigraphic and geomorphic evidence for its inception near the conjunction of Nevada, Arizona and California, *in* Pedersen, J., and Dehler, C.M., eds., Interior western United States: Geological Society of America Field Guide 6, p. 357-387.

Housen, B.A and Dorsey, R.J., 2010, Magnetostratigraphy and paleomagnetism of the Plio-Pleistocene Arroyo Diablo and Borrego formations in the Borrego Badlands, western Salton Trough, CA: American Geophysical Union Fall Meeting Abstracts, GP23C-08.

Hudson, I.L., and Keatley, M.R., 2010, Singular spectrum analysis: climatic niche identification: Phenological Research, doi:10.1007/978-90-481-335-2_18.

Huntington, K. W., A. E. Blythe, and K. V. Hodges, 2006, Climate change and Late Pliocene acceleration of erosion in the Himalaya: Earth and Planetary Science Reviews, v. 252, p. 107-118.

Johnson, C.L., and Graham, S.A., 2004, Sedimentology and reservoir architecture of a synrift lacustrine delta, southeastern Mongolia: Journal of Sedimentary Research, v. 74, no. 6, p. 770-785.

Kaiser, G., 1994, A friendly guide to wavelets: Birkhäuser, 300 p.

Kirby, S. M., Janecke,S.U., Dorsey, R.J., Housen, B.A., Langenheim, V.E., McDougall, K.A. and Steely, A.N., 2007, Pleistocene Brawley and Ocotillo formations: evidence for initial strike-slip deformation along the San Felipe and San Jacinto fault zones, Southern California: Journal of Geology, v. 115, p. 43-62.

Kleiven, H.F., Jansen, E., Fronval, T., and Smith, T.M., 2002, Intensification of northern hemisphere glaciations in the curcum Atlantic region (3.5-2.4 Ma) – ice-rafted detritus evidence: Palaeogeography, Palaeoclimatology, Palaeoecology, v. 184, no. 3-4, p. 213-223.

Kruiver, P.R., Dekkers, M.J., and Heslop, D., 2001, Quantification of magnetic coercivity components by the analysis of acquisition curves of isothermal remanent magnetisation: Earth and Planetary Science Letters, v. 189, p. 269-276.

Lawrence, K.T., Liu, Z., and Herbert, T.D., 2006, Evolution of the eastern tropical Pacific through Plio-Pleistocene glaciation: Science, v. 312, p. 79-83.

Leeder, M.R., Harris, T., and Kirkby, M.J., Sediment supply and climate change: implications for basin stratigraphy: Basin research, v. 10, p. 7-18.

Lisiecki, L.E., and Raymo, M.E., 2005. A Pliocene-Pleistocene stack of 57 globally distributed benthic δ18O records: Paleoceanography 20.

Longinotti, N.E., Oskin, M.E., DeBoer, C.J., Housen, B.A., Peryam, T.C., and Dorsey, R.J., 2011, ^{10}Be-derived paleo-erosion rates recorded in the Fish Creek-Vallecito basin, California indicate no increase across the Plio-Pleistocene climate transition: American Geophysical Union Fall Meeting Abstracts, A792.

Lutz, A. T., Dorsey, R.J., Housen, B.A. and Janecke, S.U., 2006, Stratigraphic record of Pleistocene faulting and basin evolution in the Borrego Badlands, San Jacinto fault zone, Southern California: Geological Society of America Bulletin, v. 118, p. 1377-1397.

Mack, G.H., and Stout, D.M., 2005, Unconventional facies distribution of facies in a continental rift basin: the Pliocene-Pleistocene Mangas basin, south-western New Mexico, USA: Sedimentology, v. 52, p. 1187-1205.

Maher, B.A., and Taylor, R.M., 1988, Formation of ultrafine-grained magnetite in soils: Nature, v. 336, p. 368-370.

Mann, M.E., and Lees, J.M., 1996, Robust estimation of background noise and signal detection in climatic time series: Climate Change, v. 33, p. 409-445.

Maslin, M.A., Li, X.S., Loutre, M.F., and Berger, A., 1998, The contribution of orbital forcing to the progressive intensification of northern hemisphere glaciation: Quaternary Science Reviews, v. 17, p. 411-426.

McDonald, E.V., McFadden, L.D., and Wells, S.G., 2003, Regional response of alluvial fans to the Pleistocene-Holocene climatic transition, Mojave desert, California. *in* Enzel, Y., Wells, S.G., and Lancaster, N., eds. Paleoenvironments and paleohydrology of the Mojave and southern Great Basin deserts: Boulder, Geological Society of America Special Paper 368, p. 189-205.

Meko, D.M., Woodhouse, C.A., Baisan, C.A., Knight, T., Lukas, J.L., Hughes, M.K., and Salzer, M.W., 2007, Medieval drought in the upper Colorado River basin: Geophysical Research Letters, v. 34, doi: 10.1029/2007GL029988.

Meyers, S.R., Sageman, B.B., and Pagani, M., 2008, Resolving Milankovitch: consideration of signal and noise: American Journal of Science, v. 308, p. 770-786, doi:10.2475/06.2008.02.

Minnich, R.A., Franco-Viscaíno, E., and Dezzani, R.J., 2000, The El Niño-Southern Oscillation and precipitation variability in Baja California, Mexico: Atmósfera, v. 13, p. 1-20.

Mo, K.C., and Higgins, R.W., 1998, Tropical influence on California precipitation: Journal of Climate, v. 11, p. 412-430.

Molnar, P., 2004, Late Cenozoic increase in accumulation rates of terrestrial sediment: how might climate change have affected erosion rates?: Annual Review of Earth and Planetary Sciences, v. 32, p. 67-89.

Mundelsee, M., and Raymo, M.E., 2005, Slow dynamics of the northern hemisphere glaciation: Paleoceonography, v. 20, doi: 10.1029/2005PA001153.

Oldfield, F., 2007, Sources of fine-grained magnetic minerals in sediments: a problem revisited: The Holocene, p. 1265-1271, doi:10.1177/0959683607085135.

Pederson, J., Smith, G., and Pazzaglia, F., 2001, Comparing the modern, Quaternary and Neogene records of climate-controlled hillslope sedimentation in southeast Nevada: Geological Society of America Bulletin, v. 113, no. 3, p. 305-319.

Percival, D.B., and Walden, A.T., 1993, Spectral analysis for physical applications: Cambridge, Cambridge University Press, 583 p.

Peryam, T.C., Dorsey, R.J., and Bindeman, I., 2011, Plio-Pleistocene climate change and timing of Peninsular Ranges uplift in southern California: evidence from paleosols and stable isotopes in the Fish Creek-Vallecito basin: Palaeogeography, Palaeoclimatology, Palaeoecology, v. 305, p. 65-74, doi: 10.1016/j.palaeo.2011.02.014.

Peryam, T.C., Dorsey, R.J., DeBoer, C., and Housen, B.A., 2012, Controls on Pliocene sedimentation and basin reorganization in the Fish Creek-Vallectio basin, southern California: *in preparation.*

Ravelo, A.C., Andreason, D.H., Lyle, M., Lyle, A.O., and Wara, M.W., 2004. Regional climate shifts caused by gradual cooling in the Pliocene epoch: Nature 429, p. 263–267.

Raymo, M.E., 1994, The initiation of northern hemisphere glaciation: Annual Review of Earth and Planetary Sciences, v. 22, p. 353-383, doi: 10.1146/annure.ea.22.050194.002033.

Raymo, M.E., and Nisancioglu, K., 2003, The 41 kyr world: Milankovitch's other unsolved mystery: Paleoceonography, v. 18, no. 1, doi: 10.1029/2002PA000791.

Remeika, P., 2006, Ancestral woodlands of the Colorado River delta plain, *in* Jefferson, G.T., and Lindsay, L., eds., Fossil Treasures of the Anza-Borrego Desert: Sunbelt Publications, Inc., San Diego, p. 75-88.

Retallack, G.J., 1991, Untangling the effects of burial alteration and ancient soil formation: Annual Review of Earth and Planetary Science, v. 19, p. 183-206.

Reyes, S. and Mejía-Trejo, A., 1991, Tropical perturbations in the eastern Pacific and the precipitation field over northwestern Mexico in relation to the ENSO phenomenon: International Journal of Climatology, v. 11, p. 515-528.

Robinson, D.J., and France, D.E., 1994, Discrimination of remanence-carrying minerals in mixtures, using isothermal remanent magnetization acquisition curves: Physics of the Earth and Planetary Interiors, v. 82, p. 223-234.

Sclater, J.G., and Christie, P.A.F., 1980, Continental stretching: an explanation of the post-Mid-Cretaceous subsidence of the central North Sea Basin: Journal of Geophysical Research, v. 85, no. B7, p. 3711-3789.

Shun, T., and Duffy, C., 1999, Low-frequency oscillations in precipitation, temperature and run-off on a west-facing mountain front: a hydrologic interpretation: Water Resource Research, v. 35, p. 191-201.

Smith, G., I., Paleohydrologic regimes in the southwestern Great Basin, 0-3.2 my ago, compared with other long records of "global" climate: Quaternary Research, v. 22, p. 1-17.

Spencer, K.E., Peters, L., McIntosh, W.C., and Patchett, P.J., 2001, $^{40}Ar/^{39}Ar$ geochronology of the Hualapai Limestone and Bouse Formation and implications for the age of the lower Colorado River, *in* Young, R.A., and Spamer, E.E., eds., Colorado River: Origin and evolution: Grand Canyon, Arizona, Grand Canyon Association, p. 89-92.

Tarbet, L.A., and Holman, W.H., 1944, Stratigraphy and micropaleontology of the west side of the Imperial Valley, California: American Association of Petroleum Geologists Bulletin, v. 28, DOI: 10.1306/3D9336FE-16B1-11D7-8645000102C1865D.

Tauxe, L., Mullender, T.A.T., and Pick, T., 1996, Potbellies, wasp-waists, and superparamagnetism in magnetic hysteresis: Journal of Geophysical Research, v. 101, no. B1, p. 571-583.

Tauxe, L., Bertram, H.N., and Seberino, C., 2002, Physical interpretation of hysteresis loops: micromagnetic modeling of fine particle magnetite: Geochemistry Geophysics Geosystems, v. 3, no. 10, doi: 10.1029/2001GC000241.

Thompson, R., Battarbee, R.W., O'Sullivan, P.E., and Oldfield, F., 1975, Magnetic susceptibility of lake sediments: Limnology and Oceanography, v. 20, no. 5, p. 687-698.

Thompson, R.S., 1991, Pliocene environments and climates in the western United States: Quaternary Science Reviews, v. 10, p. 115-132.

Todd, V. R., 2004, Preliminary Geologic Map of the El Cajon 30' x 60' Quadrangle, Southern California, Version 1.0: United States Geological Survey.

Torence, C., and Compo, G.P., 1998, A practical guide to wavelet analysis: Bulletin of the American Meteorological Society, v. 79, p. 61-78.

Trenberth, K., 2005, Uncertainty in hurricanes and global warming: Science, v. 308, p. 1753-1754.

Tucker, G.E., and Slingerland, R., 1997, Drainage basin response to climate change: Water Resources Research, v. 33, no. 8, p. 2031-2047.

Vautard, R., and Ghil, M., 1989, Singular spectrum analysis in nonlinear dynamics, with applications to paleoclimatic time series: Physica D, v. 35, p. 395-424.

Vautard, R., Yiou, P., and Ghil, M., 1992, Singular spectrum analysis: a toolkit for short noisy chaotic signals: Physica D, v. 58, p. 95-126.

Wara, M.W., Ravelo, A.C., and Delaney, M.L., 2005, Permanent El Niño-like conditions during the Pliocene warm period: Science, v. 309, p. 758-761.

Weedon, G., 2003, Time-series analysis and cyclostratigraphy: examining stratigraphic records of environmental cycles: Cambridge, Cambridge University Press, 259 p.

Willinbring, J. K., and F. von Blanckenburg, 2010, Long-term stability of global erosion rates and weathering during late-Cenozoic cooling: Nature, v. 465, p. 211-214.

Zachos, J., Pagani, M., Sloan, L., Thomas, E., Billups, K., 2001. Trends, rhythms, and aberrations in global climate 65 Ma to the present: Science 292, 386–392.

Zhang, P., Molnar, P. and Downs, W.R., 2001, Increased sedimentation rates and grain sizes 2-4 Myr due to the influence of climate change on erosion rates: Nature, v. 410, p. 891-897.